

79-FM-5
(Supersedes 72-FM-190)

JSC-14675
(Supersedes MSC-07222)

Onboard Navigation Systems Characteristics

(NASA-TM-79944) ONBOARD NAVIGATION SYSTEMS N79-21121
CHARACTERISTICS (NASA) 310 p HC A14/MF A01
CSCL 17G

Unclas
G3/17 24245

Mission Planning and Analysis Division

March 1979



National Aeronautics and
Space Administration

Lyndon B. Johnson Space Center
Houston, Texas



DISTRIBUTION FOR 79-FM-5, CHANGE

JM6/Technical Library (2)
 JM61/Center Data Mgmt. (3)
 CF/H. Draughon
 N. Hutchinson
 C. Parker
 CF3/M. Collins
 J. T. Chapman
 J. Ferguson
 M. Lancaster
 CG5/C. Deiterich
 EH2/D. Dyer
 M. Contella
 EH6/C. Manry
 A. Turley
 EH13/C. Price
 FE/C. H. Woodling
 FM/E. C. Lineberry
 FM2/R. Becker
 M. Jenness
 FM4/C. Graves
 D. Heath
 FM6/E. McHenry
 R. Hinson
 FM8/E. Schiesser
 A. Actkinson
 A. Bond
 J. Blucker
 B. F. Cockrell
 G. deVezin
 R. Eckelkamp
 C. Halliman
 E. Henry
 M. Montez
 P. T. Pixley (2)
 R. Pocklington
 S. Richardson
 R. T. Savely (9)
 R. Stokes
 J. Thibodeau
 R. Osburn (2)
 FM14/Report Control Files (25)
 B. Woodland
 S. Cole
 The Analytic Sciences Corp./
 Harold Jones (3)
 6 Jacob Way
 Reading, MA 01867
 CSC/Houston/M30/E. Brownd
 R. Khare
 G. Johnson
 B. Schumacher

CSDL/MS23/R. A. Larson
 CSDL/MS63/M. Landey
 D. McKern
 CSDL/MS73/E. S. Muller (3)
 B. A. Kriegsman
 P. Kachmar
 IBM/MC56/R. Evans
 IBM/MC62/T. Green.
 L. Roberts
 A. Yao
 IBM/MC65/G. Smith
 J. H. Chaun
 H. Otten
 IBM/MC91/C. Choe
 W. Madden
 Intermetrics
 2750 Bellflower Blvd.
 Long Beach, CA 90815
 Intermetrics
 1506 E. Broadway Suite. 100
 Pearland, TX 77581.
 Intermetrics
 701 Concord Ave.
 Cambridge, MA 02138/Clark Neely
 Ray Morth
 LEC/Houston/B11/B. Hodges
 LEC/Houston/B12/J. M. Parks
 LEC/Houston/Floyd Brake
 KSC/VE-GED-1/C. A. Whitesides
 MDTSCO/1100 NASA Rd. 1/W. E. Wedlake
 R. Peterson (2)
 M. Rasmussen
 J. J. Ewell
 D. Lukaszewski (10)
 R. Spier
 W. Hayes
 NASA Hdqs./MHE-7/R. V. Murad
 P. E. Baynes
 Ray Falz
 P. O. Box 179
 Mail Stop SH6 8600
 Denver, CO 80201

N79-211,21#

79FM5

JSC-14675

NASA-JM-79944

CHANGE SHEET

JSC INTERNAL NOTE NO. 79-FM-5
DATED March 1979

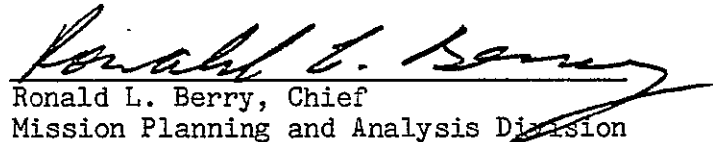
ONBOARD NAVIGATION SYSTEMS CHARACTERISTIC:

By Mathematical Physics Branch, JSC; and
McDonnell Douglas Technical Services Co.

Change 3
September 1980



Emil R. Schiesser, Chief
Mathematical Physics Branch



Ronald L. Berry, Chief
Mission Planning and Analysis Division

NOTE: An asterisk in the margin indicates the area of change.

After the attached enclosures, which are replacement/additional pages, have been inserted, place this CHANGE SHEET between the cover and title page and write on the cover, "CHANGE 3 inserted."

1. Replace pages

9-7/9-8 with 9-7/9-7a and 9-7b/9-8
9-15/9-16

2. Add pages

9-16a/9-16b

CHANGE HISTORY FOR JSC IN 79-FM-5

Change no.	Date	Description
1	Sept. 1979	The changes reflected on page 1 of this change sheet are the result of additions to software.
2	May 1980	The changes reflected on page 1 of this change sheet are the result of additions to software.
3	Sept. 1980	The changes reflected on page 1 of this change sheet are the result of changes to the Tacan RF-link model, thus affecting the models for the onboard Tacan antenna gain pattern as well as the gain pattern for the ground stations.

79FM5

JSC-14675

CHANGE SHEET

JSC INTERNAL NOTE NO. 79-FM-5
DATED March 1979

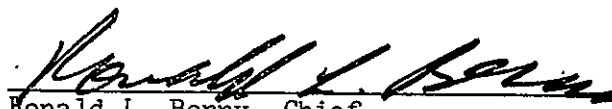
ONBOARD NAVIGATION SYSTEMS CHARACTERISTICS

By Mathematical Physics Branch, JSC; and
McDonnell Douglas Technical Services Company

Change 2
June 1980



Emil R. Schiesser, Chief
Mathematical Physics Branch


Ronald L. Berry, Chief
Mission Planning and Analysis Division

NOTE: An asterisk in the margin indicates the area of change.

After the attached enclosures, which are replacement/additional pages, have been inserted, place this CHANGE SHEET between the cover and title page and write on the cover, "CHANGE 2 inserted."

1. Replace pages

9-11/9-12
9-13/9-14

CONTENTS

Section		Page
1.0	<u>INTRODUCTION</u>	1-1
1.1	REFERENCES	1-2
2.0	<u>INERTIAL MEASUREMENT UNIT</u>	2-1
2.1	GENERAL DESCRIPTION	2-1
2.2	SIMULATION APPROACH	2-3
2.3	ERROR MODELS	2-11
2.3.1	<u>Gyro Error Model - Block 6</u>	2-11
2.3.2	<u>Platform Initial Misalignment - Block 7</u>	2-12
2.3.3	<u>Accelerometer Error Model - Block 10</u>	2-16
2.3.4	<u>IMU Case to Navigation Base Mounting Misalignment - Block 12</u>	2-17
2.3.5	<u>Gimbal Angle Nonorthogonality Errors - Block 12</u>	2-18
2.3.6	<u>Resolver Error Model - Block 12</u>	2-20
2.4	ERROR SOURCE VALUES	2-21
2.4.1	<u>IMU Locations</u>	2-21
2.4.2	<u>Gyro Error Values (1σ)</u>	2-21
2.4.3	<u>Initial Misalignment Error Values (1σ)</u>	2-23
2.4.4	<u>Accelerometer Error Values (1σ)</u>	2-25
2.4.5	<u>IMU Case Error Values (1σ)</u>	2-26
2.4.6	<u>Gimbal Nonorthogonalities (γ, μ, ϵ)</u>	2-26
2.4.7	<u>Resolver and A/D Converter Error Values (1σ)</u>	2-27
2.5	REFERENCES	2-28
3.0	<u>BODY MOUNTED SENSORS</u>	3-1
3.1	GENERAL DESCRIPTION	3-1
3.2	SIMULATION APPROACH	3-2
3.3	ERROR MODELS	3-6
3.3.1	<u>Accelerometer Assembly Error Model - Block 5</u>	3-6
3.3.2	<u>Rate Gyro Assembly Error Model - Block 6</u>	3-7
3.4	ERROR SOURCE VALUES	3-9
3.4.1	<u>Accelerometer Assembly</u>	3-9
3.4.2	<u>Rate Gyro Assembly</u>	3-10
3.4.3	<u>Body Mounted Sensor Locations</u>	3-10

Section	Page
3.5	REFERENCES 3-12
4.0	<u>BAROMETRIC ALTIMETER</u> 4-1
4.1	GENERAL DESCRIPTION 4-1
4.2	SIMULATION APPROACH 4-1
4.3	ERROR MODEL 4-5
4.4	REFERENCES 4-8
5.0	<u>STAR TRACKER</u> 5-1
5.1	GENERAL DESCRIPTION 5-1
5.1.1	<u>Star Tracker Operating Characteristics</u> 5-3
5.1.2	<u>Star Tracker Operating Constraints</u> 5-5
5.1.3	<u>Star Tracker Hardware/Software System Operation</u> 5-7
5.2	SIMULATION APPROACH 5-11
5.3	ERROR MODEL 5-18
5.4	ERROR SOURCES AND CONSTRAINT VALUES 5-22
5.5	REFERENCES 5-25
6.0	<u>CREW OPTICAL ALINEMENT SIGHT</u> 6-1
6.1	GENERAL DESCRIPTION 6-1
6.2	SIMULATION APPROACH 6-3
6.2.1	<u>COAS Model</u> 6-3
6.2.2	<u>Onboard COAS Software</u> 6-6
6.3	ERROR MODEL 6-11
6.3.1	<u>Sighting Error</u> 6-11
6.3.2	<u>Structural Instability Error</u> 6-12
6.4	ERROR SOURCES AND CONSTRAINT VALUES 6-14
6.5	REFERENCES 6-15
7.0	<u>RENDEZVOUS RADAR</u> 7-1
7.1	GENERAL DESCRIPTION 7-1

Section	Page
7.2	SIMULATION APPROACH 7-3
7.3	ERROR MODEL 7-10
7.4	ERROR SOURCES AND CONSTRAINT VALUES 7-12
7.5	REFERENCES 7-17
8.0	<u>RADAR ALTIMETER</u> 8-1
8.1	GENERAL DESCRIPTION 8-1
8.2	SIMULATION APPROACH 8-2
8.3	ERROR MODEL 8-3
8.4	ERROR SOURCE VALUES 8-5
8.5	REFERENCES 8-6
9.0	<u>TACAN</u> 9-1
9.1	GENERAL DESCRIPTION 9-1
9.2	SIMULATION APPROACH 9-3
9.3	ERROR MODELS 9-12
9.3.1	<u>Range Error Model - Block 4</u> 9-12
9.3.2	<u>Bearing Error Model - Block 8</u> 9-13
9.4	ERROR SOURCE VALUES 9-15
9.4.1	<u>Orbiter Antenna Pointing Directions</u> 9-15
9.4.2	<u>Orbiter Antenna Gain Pattern</u> 9-15
9.4.3	<u>Ground Station Antenna Gain</u> 9-16
9.4.4	<u>Range Error Values</u> 9-16
9.4.5	<u>Bearing Error Values</u> 9-17
9.5	REFERENCES 9-19
10.0	<u>MSBLS</u> 10-1
10.1	GENERAL DESCRIPTION 10-1
10.2	SIMULATION APPROACH 10-3
10.2.1	<u>Block Diagram Description</u> 10-3
10.2.2	<u>Geometric Observables Computation</u> 10-5

Section	Page
10.3	SUBSYSTEM MODELING FORMULATIONS 10-8
10.3.1	<u>Coverage Check</u> 10-8
10.3.2	<u>RF Lockon Check</u> 10-9
10.3.3	<u>Data Validity</u> 10-12
10.3.4	<u>Error Modeling</u> 10-12
10.3.5	<u>Special Notes</u> 10-17
10.4	MSBLS MODEL VALUES 10-19
10.4.1	<u>Geometric Observable Values</u> 10-19
10.4.2	<u>Coverage Check Values</u> 10-19
10.4.3	<u>RF Parameter Values</u> 10-19
10.4.4	<u>MSBLS Error Model Values</u> 10-22
10.5	REFERENCES 10-29
	<u>APPENDIX A - REVIEW OF CONCEPTS</u> A-1
	<u>APPENDIX B - ENVIRONMENT PHENOMENOLOGY AND MODELING ERRORS</u> B-1
	<u>APPENDIX C - SUBROUTINE LISTINGS AND DESCRIPTIONS</u> C-1

TABLES

Table		Page
4-I	BAROMETRIC ALTIMETER ERROR MODEL (1-sigma)	4-7
5-I	STAR TRACKER MISALINEMENT AND STAR SIGHTING ERRORS	5-23
5-II	IDEAL NAVIGATION BASE TO STAR TRACKER TRANSFORMATIONS	5-24
7-I	RADAR PARAMETER MEASUREMENT LIMITS	7-13
7-II	RADAR PARAMETER ALLOWABLE MEASUREMENT ERRORS	7-14
B.2-I	GRAVITY MODEL COEFFICIENTS	B-9
B.3-I	DENSITY MODEL - 1962 STANDARD ATMOSPHERE	B-23
B.3-II	SEASONAL DENSITY MODEL - JANUARY 60° N AND JULY 60° N	B-24
B.3-III	SEASONAL DENSITY MODEL - JANUARY 30° N AND JULY 30° N	B-25
B.3-IV	SEASONAL DENSITY MODEL - APRIL 30° N	B-26
B.3-V	$3\sigma \Delta\delta/\delta$ VERSUS ALTITUDE FOR ENCLOSED ATMOSPHERES	B-27
B.3-VI	ORBITS USED IN PREDICTION EXPERIMENTS	B-28
B.3-VII	POSITION DEPENDENCE ON DENSITY MODEL	B-29
B.7-I	SCHEDULED VENTS	B-58
B.7-II	CONTINGENCY VENTS	B-62
B.7-III	FAILURE VENTS	B-63
B.7-IV	RCS AND OMS PRESSURE RELIEF VENTS	B-65
B.11-I	CONVERSION FACTORS	B-81
B.11-II	EARTH'S ANGULAR ROTATIONAL VELOCITY WITH RESPECT TO A PRECESSING EQUINOX (ω_p) AND INERTIAL EQUINOX (ω_I) VERSUS YEAR	B-84

FIGURES

Figure		Page
2-1	Inertial measurement unit component diagram	2-2
2-2	Inertial measurement unit simulation functional block diagram	2-4
3-1	Body mounted sensors orientation	3-1
3-2	Body mounted sensors simulation block diagram	3-3
4-1	Altitude above an ellipsoidal Earth	4-2
4-2	Barometric altimeter simulation block diagram	4-3
5-1	Star tracker mounting geometry	5-2
5-2	Star tracker scan geometry	5-4
5-3	Star tracker simulation functional block diagram	5-13
5-4	Star tracker coordinate system	5-17
6-1	COAS sighting functional block diagram	6-4
6-2	COAS calibration functional block diagram	6-8
7-1	Rendezvous radar model functional block diagram	7-4
7-2	Orbiter body coordinate system and rendezvous radar coordinate system	7-6
7-3	Rendezvous radar parameter geometry	7-7
7-4	Three-sigma random range error	7-15
7-5	Range bias error	7-16
9-1	TACAN simulation functional block diagram	9-5
10-1	MSBLS subsystem model functional block diagram	10-4
A-1	Equiprobability ellipse	A-21
A-2	Likelihood of occurrence for multidimensional Stochastic variables	A-34
A-3	Accuracy of empirically-derived variances	A-35

Figure		Page
B-1	Drag altitude pseudomeasurement block diagram	B-34
B-2	Refraction of electromagnetic waves by a slab atmosphere . .	B-42
B-3	Suggested algorithm for computing refraction corrections for the Space Shuttle	B-47
B-4	Locations of onorbit vents	B-57
B-5	Recent behavior of TAI-UTC	B-78

ACRONYMS

AA	accelerometer assembly
ADI	altitude director indicator
ADS	air data subsystem
ADTA	air data transducer assembly
AIL	Airborne Instrumentation Laboratory
ALT	approach and landing test
AMDB	Advanced Mission Design Branch
APU	auxiliary power unit
ASTP	Apollo-Soyuz Test Project
AVVI	attitude vertical velocity indicator
Az	azimuth
BIH	Bureau International de l'Heure
BITE	Built-in test equipment
B-M	Babb-Mueller
CCIR	International Radio Consultant Committee
COAS	crew optical alinement sight
COESA	Committee on Extension to the Standard Atmosphere
CRT	cathode ray tube
DME	distance measuring equipment
DSCS	Defense Satellite Communication System
EAFB	Edwards Air Force Base
ECAC	Electromagnetic Compatibility Analysis Center
ECI	Earth-centered inertial coordinate system
ECLSS	environmental control and life support system
ECRV	exponentially correlated random variable

EL elevation
EM electromagnetic
ET ephemeris time
ETR eastern test range
FCP fuel cell powerplant
GMT Greenwich mean time
GPC general purpose computer
HOPE Houston operations predictor/estimator
IMU inertial measurement unit
JSC Johnson Space Center
KSC Kennedy Space Center
LED light-emitting diode
LHS left-hand side
LLTD launch/landing trajectory determination processor
LORAN long-range navigation
LOS line of sight
LPS launch processing system
MCC Mission Control Center
MET mission elapsed time
MPS main propulsion subsystem
MSBLS microwave scanning beam landing system
MTU master timing unit
M50 mean of 1950 coordinate system
NASA National Aeronautics and Space Administration
NBS National Bureau of Standards
ODP orbit determination processor

OFT orbital flight test

OMS orbital maneuvering subsystem

OV-101 Orbiter vehicle-101, Enterprise

PCM pulse code modulation

PLB payload bay

PRSD power reactant supply and distribution (network)

RA radar altimeter

RCS reaction control system

RF radio frequency

RGA rate gyro assembly

RHS right-hand side

RMS root mean square

RSS root sum square

RTLS return-to-launch site

SAMTEC Space and Missile Technical Evaluation Center

SMCC Shuttle Mission Control Center

SOP subsystem operating programs

STDN Spaceflight Tracking and Data Network

SVDS space vehicle dynamics simulation

TACAN tactical air navigation

TAI international atomic time

USB unified S-band

USNO United States Naval Observatory

UT universal time

UTC universal coordinated time

UTO observed universal time

WBTH water boiler thermal control hydraulics

..

1.0 INTRODUCTION

This document describes the Space Shuttle onboard navigation systems characteristics. Its purpose is to serve as a standard source of equations and numerical data for use in error analyses and mission simulations related to Space Shuttle development.

The sensor characteristics described in this document are used for Shuttle onboard navigation performance assessment. Complete models are not always used for such studies, depending on the analyses to be performed, the capabilities of the computer programs, and the availability of computer resources.

This document is not a control document. Controlling documents include the Shuttle Operational Data Book (refs. 1-1 and 1-2), the Coordinate Systems for the Space Shuttle Program (ref. 1-3), and the Space Shuttle Astrodynamical Constants (ref. 1-4) software configuration controlled input loads and trajectory design input data baseline.

This document will be revised periodically. Suggestions for these revisions should be brought to the attention of R. T. Savely, FM8, at NASA/JSC.

1.1 REFERENCES

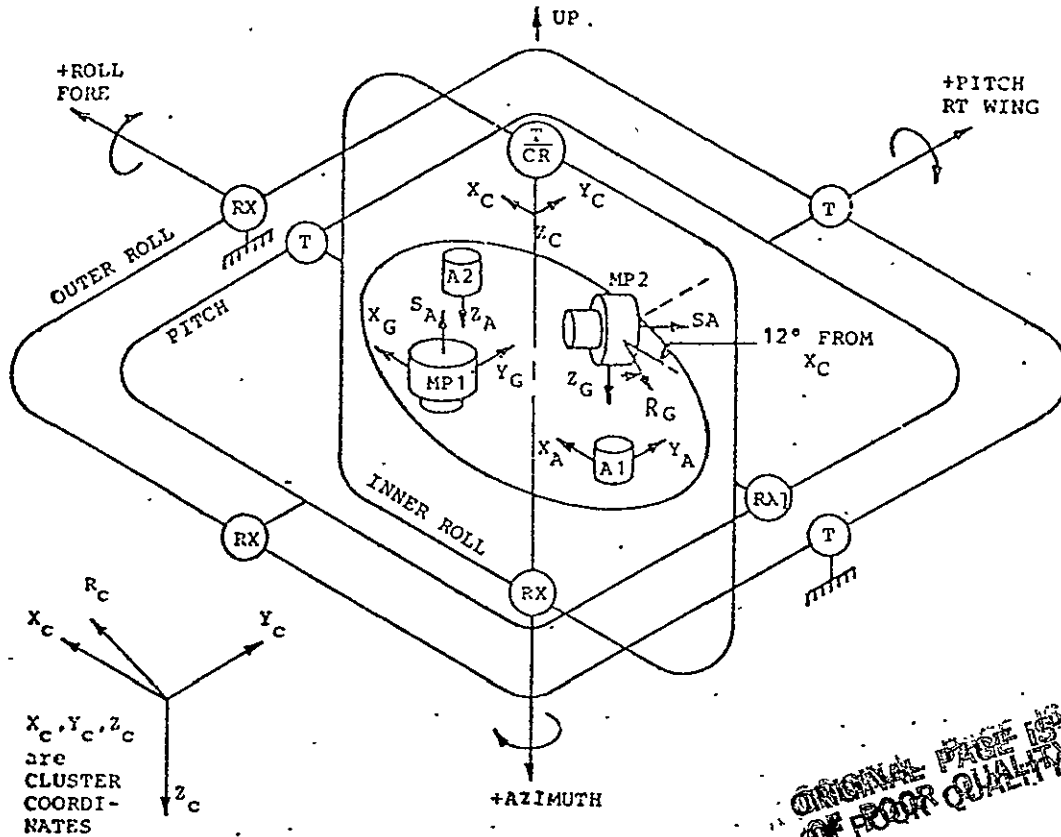
- 1-1 Operational Data Branch: Shuttle Operational Data Book, Vol. I, Shuttle Systems Performance and Constraints Data, 79 amendments. JSC-08934, Oct. 1976.
- 1-2 Operational Data Branch: Shuttle Operational Data Book, Vol. II, Mission Mass Properties. JSC-08934, Sept. 1975.
- 1-3 Cockrell, B. F.; and Williamson, J. B.: Space Shuttle Astrodynamical Constants. JSC IN 78-FM-32, June 1978.
- 1-4 Coordinate Systems for the Space Shuttle Program. NASA TMS-58153, JSC-09084, Oct. 1974.

2.0 INERTIAL MEASUREMENT UNIT

2.1 GENERAL DESCRIPTION

The inertial measurement unit (IMU) used on the Space Shuttle provides an inertially-fixed stable platform. Mounted on the platform are accelerometers that measure nongravitational accelerations and rate-integrating gyroscopes, which drive the gimbals. The platform is suspended by four gimbals to provide all-attitude rotational isolation of the platform from vehicle motion. The gimbals are read by gimbal angle resolvers, which yield body attitude information with respect to inertial space (fig. 2-1). The outputs of the IMU (inertial accelerations and body attitude with respect to inertial space) are used by navigation and guidance for estimating position and velocity.

The alinement of the platform to a desired orientation is performed by first determining the present orientation and then accurately torquing the platform to the desired alinement. In-flight alinement is accomplished by optical sightings on stars using either the star tracker (sec. 5.0) or crew optical alinement sight (COAS) (sec. 6.0). Prelaunch alinement is performed by gyro compassing/leveling in which the gyros and accelerometers are used to orient the platform with respect to Earth rate and local gravity vectors.



x_c, y_c, z_c
are
CLUSTER
COORDI-
NATES

Notes: X_G =X Gyro I.A.

Y_G =Y Gyro I.A.

Z_G =Z Gyro I.A.

R_G =Redundant Gyro I.A.

X_A =X Accel Sens. Axis

Y_A =Y Accel Sens. Axis

Z_A =Z Accel Sens. Axis

T Gimbal Torquer

RX=Gimbal Angle Resolver (1x/8x)

CR=Gyro Coordinate Resolver

RX1=Single Speed (8x) Resolver (Redundant Roll)

VERTICAL GYRO

AZIMUTH GYRO

DUAL AXIS ACCEL.

SINGLE AXIS ACCEL.

Figure 2-1.- Inertial measurement unit component diagram.

2.2 SIMULATION APPROACH

The IMU provides a measurement of the nongravitational acceleration applied to the IMU in the form of delta-velocity outputs, $\Delta\tilde{V}_p$, from a set of three orthogonally-mounted accelerometers. A measurement of the vehicle attitude is provided by the platform gimbal angles, $\tilde{\Theta}$, which define the orientation of the vehicle with respect to the inertial orientation of the platform.

An environment simulation provides the true vehicle acceleration, \underline{a}_I , in a reference inertial coordinate system and a set of Euler angles, $\underline{\beta}$, which define the vehicle attitude relative to the reference system. Vehicle rate data may also be supplied by the environment, but we have chosen to derive the body rate within the IMU model.

Figure 2-2 presents a block diagram for an IMU simulation. The functions of each block are as follows:

- a. Block 1 - computes the vehicle orientation matrix T_{BI} .

$$T_{BI} = F(\underline{\beta})$$

where $F(\underline{\beta})$ is the transformation matrix that represents the rotation from reference inertial space to body coordinates defined by the Euler angle set $\{$

- b. Block 2 - the inertial acceleration, \underline{a}_I , is transformed to body coordinates.

$$\underline{a}_B = T_{BI}\underline{a}_I$$

where T_{BI} is computed in block 1.

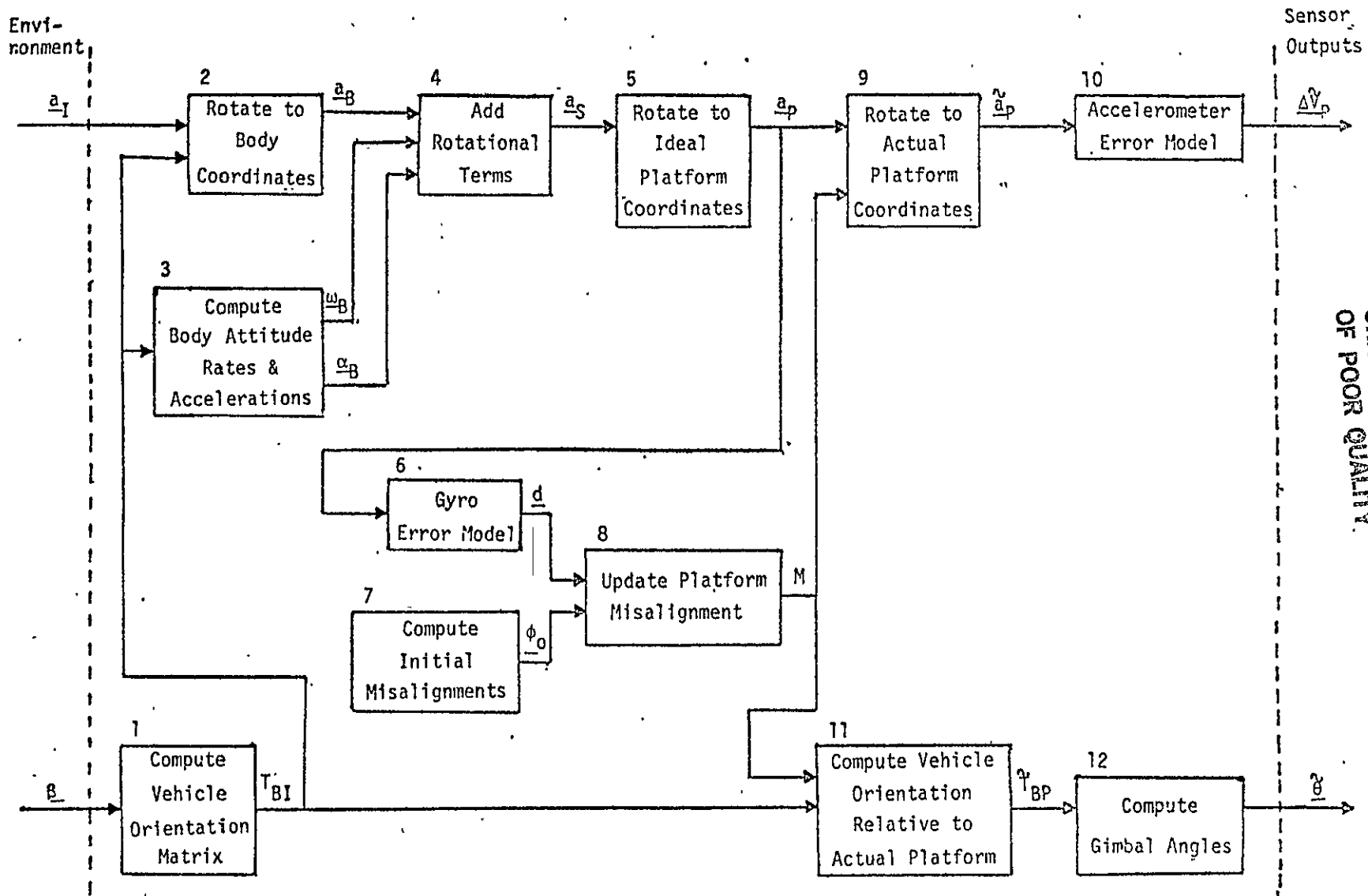


Figure 2-2.- Inertial measurement unit simulation functional block diagram.

2-4

ORIGINAL PAGE IS
OF POOR QUALITY.

- c. Block 3 - computes the average body attitude rate vector and the average body attitude acceleration vector over the time interval Δt . The change in body attitude is given by

$$R = (T_{BI})_t (T_{BI})^T_{t - \Delta t}$$

The average body attitude rate vector, $\underline{\omega}_B$, is computed for the eigenaxis rotation defined by R ,

$$\underline{\omega}_B = \frac{1}{2\Delta t} \begin{pmatrix} R_{23} - R_{32} \\ R_{31} - R_{13} \\ R_{12} - R_{21} \end{pmatrix}$$

assuming small attitude changes, $\sin(|\omega|\Delta t) \approx |\omega|\Delta t$.

The average attitude acceleration vector is given by

$$\underline{\alpha}_B = ((\underline{\omega}_B)_t - (\underline{\omega}_B)_{t - \Delta t}) / \Delta t$$

- d. Block 4 - computes the sensed acceleration, \underline{a}_S , by adding rotational terms.

$$\underline{a}_S = \underline{a}_B + \underline{\omega}_B \times (\underline{\omega}_B \times \underline{r}) + \underline{\alpha}_B \times \underline{r}$$

where \underline{a}_B was calculated in block 2, $\underline{\omega}_B$ and $\underline{\alpha}_B$ were calculated in block 3, and \underline{r} is the position vector of the IMU with respect to the center of gravity of the vehicle in body coordinates.

- e. Block 5 - expresses the sensed acceleration in ideal platform coordinates.

$$\underline{a}_p = (T_{PI})(T_{BI})^T \underline{a}_S$$

where \underline{a}_s was calculated in block 4, T_{BI} was calculated in block 1, and T_{PI} is the transformation from reference inertial coordinates to ideal platform coordinates.

- f. Block 6 - computes the platform drift vector, \underline{d} , using the gyro error model equations presented in section 2.3.1.
- g. Block 7 - computes the platform initial misalignment error vector, $\underline{\phi}_0$, for either in-flight or prelaunch alignment using the equations presented in section 2.3.2.
- h. Block 8 - updates the platform misalignment matrix, M . The platform misalignment matrix is the rotation from ideal platform to actual platform coordinates. The change in M due to gyro drift, \underline{d} , over time interval Δt is given by

$$M_t = RM_t - \Delta t$$

where R is the transformation matrix for the eigenaxis rotation about the drift vector \underline{d} , assuming \underline{d} is constant over the time interval Δt .

$$R = I + (1 - \cos \delta) U^2 / d_m^2 - (\sin \delta) U / d_m$$

where d_m is the drift rate magnitude, $|\underline{d}|$,

I is the identity matrix

$$\delta = d_m \Delta t \text{ (eigenaxis incremental drift angle)}$$

$$U = \begin{bmatrix} 0 & -d_z & d_y \\ d_z & 0 & -d_x \\ -d_y & d_x & 0 \end{bmatrix}$$

The initial misalignment matrix is formed from the misalignment error vector, $\underline{\phi}_0$, computed in block 7 as follows:

$$M_0 = I + (1 - \cos\phi)V^2/\phi^2 - (\sin\phi)V/\phi$$

where ϕ is the misalignment vector magnitude, $|\underline{\phi}_0|$

$$V = \begin{bmatrix} 0 & -\phi_{oz} & \phi_{oy} \\ \phi_{oz} & 0 & -\phi_{ox} \\ -\phi_{oy} & \phi_{ox} & 0 \end{bmatrix}$$

- .. Block 9 - transforms the sensed acceleration from reference platform coordinates to actual platform coordinates.

$$\tilde{\underline{a}}_p = M\underline{a}_p$$

where \underline{a}_p was computed in block 5 and M was computed in block 8.

- j. Block 10 - generates the simulated sensed delta-velocity vector $\underline{\Delta\tilde{V}}_p$.

$$\underline{\Delta\tilde{V}}_p = (\tilde{\underline{a}}_p + \underline{\Delta a}) \Delta t$$

Where $\underline{\Delta\tilde{V}}_p$ is the accelerometer output before quantization

$\underline{\Delta a}$ is the accelerometer error (sec. 2.3.3)

Δt is the time interval between accelerometer samples

$\tilde{\underline{a}}_p$ is computed by block 9 and assumed to be constant over time interval Δt .

Nondestructive quantization of the accelerometer data is performed in the following manner:

$$\underline{V}_t = \underline{V}_{t-\Delta t} + \underline{\Delta V}_p$$

$$\underline{\widetilde{\Delta V}}_p = q(\underline{V}_t) - q(\underline{V}_{t-\Delta t})$$

where \underline{V}_t is the accumulated delta-velocity vector at time t , generated by summing the nonquantized accelerometer outputs over the simulation interval

$q()$ is the quantization operator that truncates the argument to the least significant bit value for the specific accelerometer being simulated

$\underline{\widetilde{\Delta V}}_p$ is the quantized accelerometer output vector.

Block 11 - computes vehicle orientation relative to the actual platform.

$$\widetilde{T}_{BP} = T_{BI} T_{PI} T_M^T$$

where M is the misalignment matrix computed in block 8

T_{BI} is the rotation matrix computed in block 1

T_{PI} is the transformation from reference inertial to ideal platform coordinates.

- Block 12 - computes a set of gimbal angles, $\widetilde{\Theta}$, from the IMU case orientation with respect to the actual platform:

$$\widetilde{T}_{CP} = T_{CN} T_{NB} \widetilde{T}_{BP}$$

where \tilde{T}_{BP} was calculated in block 11, T_{NB} is the transformation from the body to navigation base coordinates (10.6° nav. base tilt):

$$T_{NB} = \begin{bmatrix} \cos 10.6^\circ & 0 & +\sin 10.6^\circ \\ 0 & 1 & 0 \\ -\sin 10.6^\circ & 0 & \cos 10.6^\circ \end{bmatrix},$$

and T_{CN} is the IMU case mounting misalignment with respect to the navigation base matrix given by the equations in section 2.3.4.

The platform is stabilized in an inertial orientation by the gyro output signals that drive torque motors on the azimuth, inner roll, and pitch gimbals. The outer roll gimbal receives its control signal from the inner roll resolver (the pick-off mounted between the inner roll and pitch gimbals). This control loop maintains perpendicularity between the inner roll and pitch gimbals, and the inner roll gimbal angle at zero degrees.

The gimbal angle sequence defining the rotation from platform coordinates to vehicle coordinates is azimuth (θ_A), inner roll (δ), pitch (θ_P), and outer roll (θ_R). Since the outer roll gimbal control loop maintains the inner roll gimbal angle (δ) at zero degrees, the vehicle attitude relative to the platform is defined by the Euler angle sequence θ_A , θ_P , θ_R .

Let

$$\underline{\theta} = \begin{pmatrix} \theta_A \\ \theta_P \\ \theta_R \end{pmatrix}$$

Then the case orientation matrix, \tilde{T}_{CP} , is related to the gimbal angle set $\underline{\theta}$ by the equations given in section 2.3.5 that model the effects of gimbal nonorthogonalities.

The gimbal angles, $\hat{\underline{\theta}}$, are read by gimbal angle resolvers, and the result is quantized:

$$\underline{\theta} = q(\hat{\underline{\theta}} + \underline{\Delta\theta})$$

where $\hat{\underline{\theta}}$ are the gimbal angles resulting from nonorthogonalities (sec. 2.3.5)

$\underline{\Delta\theta}$ are the gimbal angle resolver errors (sec. 2.3.6)

$q()$ is the quantization operator that truncates the argument to the least significant bit value for the specific resolver being simulated.

2.3 ERROR MODELS

The mathematical models for accelerometers and gyros presented below are single-degree-of-freedom models. Two-degrees-of-freedom models can be constructed from these single-axis models by appropriate choice of error parameter values to model any cross-coupling or correlation exhibited by the two-degrees-of-freedom sensors.

2.3.1 Gyro Error Model - Block 6

Error in the gyro output can be modeled by bias drift, acceleration-sensitive (mass unbalance) drift, and acceleration-squared-sensitive (anisoclastic) drift. A mathematical error model for a rate-integrating gyro is given by the equation:

$$d = r + \mu + \underline{h}^T \underline{\tilde{a}}_s + \underline{\tilde{a}}_s^T G \underline{\tilde{a}}_s$$

where d is the total gyro drift rate

r is the bias drift

μ is the random drift

$\underline{H} \underline{a}_p = \underline{\tilde{a}}_s = \begin{pmatrix} \tilde{a}_i \\ \tilde{a}_s \\ \tilde{a}_o \end{pmatrix}$ is the acceleration vector in sensor input (i), spin (s), output (o) axis coordinates. \underline{a}_p is calculated in block 5. H is the transformation matrix from reference platform coordinates to sensor coordinates for the particular gyro.

$\underline{h} = \begin{pmatrix} h_i \\ h_s \\ h_o \end{pmatrix}$ is a vector of g-sensitive drift coefficients for acceleration along the input, spin, and output axes.

$$G = \begin{bmatrix} g_{ii} & g_{is} & g_{io} \\ 0 & g_{ss} & g_{so} \\ 0 & 0 & g_{oo} \end{bmatrix}$$
 is a matrix of g-squared sensitive drift coefficients for products of accelerations along the input, spin, and output axes.

2.3.2 Platform Initial Misalignment - Block 7

The generation of ϕ_0 is dependent on the alinement technique and the sensors used in the alinement measurements. The simulation of an in-flight alinement using the star tracker (or COAS) and a prelaunch alinement using gyrocompassing and accelerometer leveling are presented here.

2.3.2.1 In-flight Alinement

The outputs from the star tracker (sec. 5.0) and the COAS (sec. 6.0) are measured line-of-sight (LOS) vectors to a pair of selected stars in actual platform coordinates. These LOS vectors are combined with the stored LOS vectors in reference inertial coordinates to form the transformation matrix from actual platform to reference inertial coordinates as follows (ref. 2-1).

Let \underline{I}_{S1} and \underline{I}_{S2} be the stored LOS unit vectors in reference inertial coordinates. Define

$$\underline{I}_1 = \underline{I}_{S1}$$

$$\underline{I}_2 = \text{UNIT} (\underline{I}_{S1} \times \underline{I}_{S2})$$

$$\underline{I}_3 = \text{UNIT} (\underline{I}_1 \times \underline{I}_2)$$

where UNIT() is an operator that normalizes a vector. The transformation from star coordinates to reference inertial coordinates is given by

$$T_{IS} = (\underline{I}_1 : \underline{I}_2 : \underline{I}_3)$$

Let $\tilde{\underline{I}}_{S1}$ and $\tilde{\underline{I}}_{S2}$ be the measured LOS unit vectors in actual platform coordinates. Define

$$\begin{aligned}\tilde{\underline{I}}_1 &= \tilde{\underline{I}}_{S1} \\ \tilde{\underline{I}}_2 &= \text{UNIT} (\tilde{\underline{I}}_{S1} \times \tilde{\underline{I}}_{S2}) \\ \tilde{\underline{I}}_3 &= \text{UNIT} (\tilde{\underline{I}}_1 \times \tilde{\underline{I}}_2)\end{aligned}$$

The transformation from actual platform to star coordinates is given by:

$$\tilde{T}_{SP} = (\tilde{\underline{I}}_1 : \tilde{\underline{I}}_2 : \tilde{\underline{I}}_3)$$

Thus, the transformation from actual platform to reference inertial coordinates is

$$\tilde{T}_{IP} = T_{IS} \tilde{T}_{SP} \quad ;$$

and the misalignment matrix, M_o , is given by

$$M_o = \tilde{T}_{IP}^T T_{IP}$$

where T_{IP} is the transformation from ideal platform to reference inertial coordinates used in block 5. ϕ_o is computed from the off-diagonal elements of M_o as follows.

$$\phi_o = \begin{pmatrix} M_o(2,3) \\ -M_o(1,3) \\ M_o(1,2) \end{pmatrix}$$

If the misalignments are too large the crew has several options for realignment and calibration of the IMU's. The nominal platform misalignment errors following in-flight star tracker realignment are presented in section 2.4.3.

2.3.2.2 Prelaunch Alinement

For prelaunch alinement the IMU's are driven to a specified orientation, T_{DN} ; the desired platform orientation with respect to the navigation base. The specified orientation for IMU-1 is chosen such that IMU-1 X-platform axis is along the Up direction and tilted 0.4 degrees toward South, Y is pointed East, and Z is pointed North and tilted 0.4 degrees above the local horizontal plane when the Shuttle is at the launch tower. IMU-2 and IMU-3 are related to IMU-1 by the skewing matrix, M_{PJP1} , which describes the transformation from IMU-1 to IMU-2 and IMU-1 to IMU-3 for $J = 2$ and $J = 3$, respectively. M_{PJP1} for launch is given in section 2.4.3. Also listed are the gimbal angles that the three IMU's will nominally display at platform release.

Use of gyrocompassing and accelerometer leveling determine the actual platform orientation with respect to the North-West-Up coordinates at the time of platform release, \tilde{T}_{NWUP} . The error inherent in this transformation is due to the accelerometers and gyros that are used to determine the local-vertical and the Earth-rate vectors. Knowledge of the time of platform release, the Greenwich hour angle, and the geodetic latitude and longitude will yield the transformation from North-West-Up coordinates at the launch site to the reference inertial coordinates, T_{INWU} . The transformation from actual platform to reference inertial can now be calculated as

$$\tilde{T}_{IP} = T_{INWU} \tilde{T}_{NWUP}$$

Comparison of this transformation with the ideal platform to reference inertial transformation yields the misalignment matrix, M_o ,

$$M_o = \tilde{T}_{IP}^T T_{IP} = \tilde{T}_{NWUP}^T T_{NWUP}$$

Since accelerometer and gyro outputs are used to define the platform orientation with respect to the North-West-Up coordinates, the initial alinement errors, ϕ_o , which are used to define M_o , are highly correlated to the instrument errors.

$$\underline{\phi}_o = (\phi_{on} \ \phi_{ow} \ \phi_{ou})^T$$

where $\phi_{ou} = \phi_u + d_U t_{GCA}$

$$\phi_{on} = \phi_N + Z_N$$

$$\phi_{ow} = \phi_W + Z_W$$

ϕ_u , ϕ_N , ϕ_W are zero-mean random errors with a Gaussian distribution. Section 2.4.3 gives the 1σ values. d_U is defined below. t_{GCA} is the time from completion of gyro-compass alinement to platform release (nominally 10 minutes). Z_N and Z_W are the north and west components of the accelerometer instrument biases (sec. 2.3.3) divided by the magnitude of the local gravity vector, g .

$$\begin{pmatrix} Z_N \\ Z_W \\ Z_U \end{pmatrix} = \frac{1}{g} T_{NWUP} \begin{pmatrix} b_x \\ b_y \\ b_z \end{pmatrix}$$

From platform release to 12 seconds before lift-off, fine-tune gyro torquing, which compensates for the known acceleration environment, is performed. The drift for this time period affects IMU misalignments as

$$\underline{\phi}_o = \underline{\phi}_o + \underline{d}_o t$$

where t is the time from platform release and

\underline{d}_o is the fine-tune gyro torquing compensation drift rate in North-West-Up coordinates

$$\underline{d}_0 = (d_N \ d_W \ d_U)^T$$

where 1σ values for d_N and d_W are given in section 2.4.3. The drift rate about the azimuth does not have the fine-tune compensation and is therefore given by the projection of the platform drift rate vector, \underline{d} , calculated in section 2.3.1, into the azimuth (up) direction via T_{NWUP} . After lift-off minus 12 seconds the platform misalignment is updated as shown in block 8.

2.3.3 Accelerometer Error Model - Block 10

Errors in the accelerometer output can be modeled by bias shift, scale factor error, input axis misalignment, and scale factor nonlinearity. A mathematical model for the acceleration measurement error is given by the equation

$$\Delta a = b + \eta + \underline{k}^T \underline{\tilde{a}}_s + m (\tilde{a}_i)^2 + k_a |\tilde{a}_i|$$

where Δa is the acceleration measurement error

b is the accelerometer bias

η is the accelerometer noise

$$\underline{k} = \begin{pmatrix} k_i \\ \gamma_j \\ \gamma_k \end{pmatrix} \text{ is a vector of scale factor error } (k_i) \text{ and input axis misalignments } (\gamma_j, \gamma_k).$$

$$\underline{H} \underline{\tilde{a}}_p = \underline{\tilde{a}}_s = \begin{pmatrix} \tilde{a}_i \\ \tilde{a}_j \\ \tilde{a}_k \end{pmatrix} \text{ is the acceleration vector in sensor } (i,j,k) \text{ axis coordinates. } \underline{\tilde{a}}_p \text{ is calculated in block 9. } H \text{ is the transformation matrix from actual platform to sensor coordinates for the particular accelerometer.}$$

\tilde{a}_i is the acceleration component along the sensor input axis.

\tilde{a}_j, \tilde{a}_k are the acceleration components along orthogonal axes perpendicular to the input axis.

m is the scale factor nonlinearity.

k_a is the scale factor asymmetry error.

The error model parameters are assumed to be independent random variables with zero-mean Gaussian distributions.

2.3.4 IMU Case to Navigation Base Mounting Misalignment - Block 12

The IMU case to navigation base mounting misalignment is a function of not only the accuracy of the case installation, but also the stiffness of the navigation base itself. Let \underline{C} be a vector of the IMU case misalignments with respect to the navigation base. The transformation from navigation base to the IMU case is given by

$$T_{CN} = I + (1 - \cos C) \frac{U^2}{C^2} - (\sin C) \frac{U}{C}$$

where I is the 3 x 3 identity matrix

$C = |\underline{C}|$, the magnitude of the IMU case misalignment vector

$$U = \begin{bmatrix} 0 & -C_z & C_y \\ C_z & 0 & -C_x \\ -C_y & C_x & 0 \end{bmatrix}$$

The error model parameters are assumed to be independent random variables with zero-mean Gaussian distributions.

2.3.5 Gimbal Angle Nonorthogonality Errors.- Block 12

The following discussion is derived entirely from reference 2-2. Let θ_A , θ_p , θ_R represent the inner, middle, and outer gimbal angles; δ , the inner roll gimbal angle

γ = the small angle misalignment of the azimuth axis towards the inner roll axis

μ = the small angle misalignment of the inner roll axis towards the pitch axis

ϵ = the small angle misalignment of the pitch axis towards the outer roll axis

The outer roll axis of rotation is defined along the X case axis. Any misalignment of the outer roll axis to the IMU case can be included in the IMU case to navigation base misalignment (sec. 2.3.5).

The transformation from actual platform to IMU case coordinates can be written as a series of seven single axis transformations

$$\tilde{T}_{CP} = R_X(\theta_R)R_Z(\epsilon)R_Y(\theta_p)R_Z(\mu)R_X(\delta)R_Y(\gamma)R_Z(\theta_A)$$

where:

$$R_Z(\theta) = \begin{bmatrix} c\theta & s\theta & 0 \\ -s\theta & c\theta & 0 \\ 0 & 0 & 1 \end{bmatrix}$$

$$R_Y(\theta) = \begin{bmatrix} C\theta & 0 & -S\theta \\ 0 & 1 & 0 \\ S\theta & 0 & C\theta \end{bmatrix}$$

$$R_X(\theta) = \begin{bmatrix} 1 & 0 & 0 \\ 0 & C\theta & S\theta \\ 0 & -S\theta & C\theta \end{bmatrix}$$

and $S\theta = \sin \theta$ and $C\theta = \cos \theta$.

Equating the above matrix, after multiplication of the seven rotation matrices using small angle approximations for γ , μ , ϵ , and δ and neglecting second-order terms, with the matrix

$$\tilde{T}_{CP} = \tilde{T}_{CN} T_{NB} \tilde{T}_{BP} = N$$

calculated in block 12, leads to the following iterative solution.

$$\hat{\theta}_A = \tan^{-1} \left(\frac{N(1,2) - \epsilon C\theta_A - \delta C\theta_A S\theta_p}{N(1,1) - \epsilon S\theta_A - \delta S\theta_A S\theta_p} \right) - \mu$$

$$\hat{\theta}_p = \sin^{-1} (-N(1,3)) - \gamma$$

$$\hat{\theta}_R = \tan^{-1} \left(\frac{N(2,3) - \epsilon S\theta_p C\theta_R - \delta C\theta_R}{N(3,3) + \epsilon S\theta_p S\theta_R + \delta S\theta_R} \right)$$

As an initial estimate of the real gimbal angles, use

$$\theta_A = \tan^{-1} N(1,2)/N(1,1)$$

$$\theta_p = \sin^{-1} -N(1,3) - \gamma$$

$$\theta_R = \tan^{-1} N(2,3)/N(3,3)$$

$$\delta = 0$$

The error model parameters are assumed to be independent random variables with nonzero-mean Gaussian distributions. The azimuth and pitch nonorthogonalities (γ and μ) are compensated for in the IMU SOP by adding γ to the pitch resolver readout (θ_p) and by adding μ to the yaw resolver readout (θ_γ). The outer roll nonorthogonality (ϵ) is measured in Hanger Cal B and is compensated for in the attitude processor onboard software module. Values for the range of the means and the errors in calibration are given in section 2.4.6.

2.3.6 Resolver Error Model - Block 12

Gimbal angle resolver errors can be categorized as those caused by bias shift and sinusoidal resolver errors. A mathematical model for the gimbal angle resolver error is given by the equation:

$$\Delta\theta = B_\theta + \eta_\theta + \sum_{n=1}^N A_{\theta n} \sin(n\hat{\theta} + \phi_n)$$

where $\Delta\theta$ is the total resolver error

B_θ is the resolver bias

η_θ is the resolver random noise

$A_{\theta n}$ is the sinusoidal bias for multiplicative speed n

ϕ_n is the random phase error for multiplicative speed n

$\hat{\theta}$ is the gimbal angle component ($\hat{\theta}_A$, δ , $\hat{\theta}_p$, or $\hat{\theta}_R$) resulting from nonorthogonalities, as computed in section 2.3.5.

The error model parameters are assumed to be random independent variables with zero-mean Gaussian distributions, except for the phase angle errors, ϕ_n , which have zero-mean uniform distributions.

2.4 ERROR SOURCE VALUES

The Space Shuttle contains three Singer-Kearfott IMU's. Each IMU contains two two-degrees-of-freedom Gyroflex gyros and one single-axis accelerometer and one dual-axis accelerometer.

2.4.1 IMU Locations

The location of the three IMU's are given below in Orbiter structural body coordinates with units of inches

<u>IMU</u>	<u>X_o</u>	<u>Y_o</u>	<u>Z_o</u>
1	419.187	-13.75	422.0
2	419.187	0	422.0
3	419.187	13.75	422.0

To determine the locations in body coordinates, the center of mass of the Orbiter for the particular flight must be expressed in Orbiter structural body coordinates and subtracted from the IMU locations listed above. The following transformation matrix, T_{BO} , applied to the resultant difference vector will give the IMU locations in body coordinates.

$$T_{BO} = \begin{bmatrix} -1 & 0 & 0 \\ 0 & 1 & 0 \\ 0 & 0 & -1 \end{bmatrix}$$

2.4.2 Gyro Error Values (1σ)

Bias drift (r) - all axes

0.015 deg/hr for 17 hours after preflight alinement and calibration

0.022 deg/hr for 17 hours after
each onorbit calibration

0.035 deg/hr thereafter

g-sensitive drift - input and output axes

(h_i, h_o)

- spin axis (h_s)

0.025 deg/hr/g

0 deg/hr/g

g^2 -sensitive drift - off-diagonal terms

(g_{is}, g_{io}, g_{so})

- diagonal terms

(g_{ii}, g_{oo}, g_{ss})

0.025 deg/hr/ g^2

0 deg/hr/ g^2

Transformation matrix for X-axis gyro

$$H_X = \begin{bmatrix} 1 & 0 & 0 \\ 0 & 0 & -1 \\ 0 & -1 & 0 \end{bmatrix}$$

Transformation matrix for Y-axis gyro

$$H_Y = \begin{bmatrix} 0 & 1 & 0 \\ 1 & 0 & 0 \\ 0 & 0 & -1 \end{bmatrix}$$

Transformation matrix for Z-axis gyro

$$H_Z = \begin{bmatrix} 0 & 0 & 1 \\ -\sin 12^\circ & \cos 12^\circ & 0 \\ \cos 12^\circ & \sin 12^\circ & 0 \end{bmatrix}$$

2.4.3 Initial Misalignment Error Values (1σ)

2.4.3.1 In-flight Alinement in Navigation Base Coordinates

ϕ_{ox}	71.2	$\widehat{\text{sec}}$
ϕ_{oy}	72.4	$\widehat{\text{sec}}$
ϕ_{oz}	71.1	$\widehat{\text{sec}}$

The following is the RSS of:

Star tracker bias pointing error, all axes		$60/\sqrt{2}$	$\widehat{\text{sec}}$
Star tracker random error (21 measurement average), all axes		$10.6/\sqrt{21}$	$\widehat{\text{sec}}$
Star tracker to IMU case misalignment, X-, Y-axis		32.2	$\widehat{\text{sec}}$
IMU case to platform bias error	}	Z-axis	29.2 $\widehat{\text{sec}}$
		X-axis	47.1 $\widehat{\text{sec}}$
		Y-axis	49.0 $\widehat{\text{sec}}$
		Z-axis	49.0 $\widehat{\text{sec}}$

The following is the RSS of:

Outer roll to case gimbal nonorthogonality, Y- and Z-axes	20	$\widehat{\text{sec}}$
Resolver bias, Y- and Z-axes	49.0	$\widehat{\text{sec}}$
X-axis	42.1	$\widehat{\text{sec}}$
Outer roll to pitch gimbal nonorthogonality, Y- and Z-axes	$30/\sqrt{2}$	$\widehat{\text{sec}}$

The star tracker to IMU case misalignment is the RSS of:

Star tracker to mounting pads, all axes	20	$\widehat{\text{sec}}$
Mounting pad to nav. base, all axes	5	$\widehat{\text{sec}}$
Thermal nav. base bending, X- and Y-axes	41/3	$\widehat{\text{sec}}$
Nav. base to mounting pads, all axes	5	$\widehat{\text{sec}}$
Mounting pad to IMU case, all axes	20	$\widehat{\text{sec}}$

2.4.3.2 Prelaunch Alinement in NWU Coordinates (1σ)

$$\begin{array}{rcl} \phi_N, \phi_W & & 8.7 \text{ sec} \\ \phi_U & & 60 \text{ sec} \end{array}$$

fine-tune gyro torquing compensation drift rates

$$d_N, d_W \quad .0094 \text{ sec/sec}$$

Completion of gyrocompassing nominally occurs 600 seconds before platform release. Accelerometer leveling is completed at platform release, and lift-off nominally occurs 20 minutes after platform release (not including the possibility of a 10-minute and/or a 20-minute hold).

IMU gimbal angles at platform release

IMU	Roll (deg)	Pitch (deg)	Yaw (deg)
1	0.0000	349.0000	0.0000
2	334.4069	44.3269	309.7792
3	296.2381	25.5850	350.4931

$$T_{DN} \text{ (IMU1)} = \begin{bmatrix} 0.9816272 & 0 & -0.1908089 \\ 0 & 1 & 0 \\ .1908089 & 0 & .9816272 \end{bmatrix}$$

$$T_{DN} \text{ (IMU2)} = \begin{bmatrix} 0.6451763 & -0.2079225 & 0.7351977 \\ -.3090204 & .8090255 & .4999842 \\ -.6987517 & -.5497691 & .4577118 \end{bmatrix}$$

$$T_{DN} (IMU3) = \begin{bmatrix} 0.3987524 & 0.8531113 & 0.3364485 \\ -.8090132 & .5000085 & -.3090127 \\ -.4318494 & -.1489717 & .8895581 \end{bmatrix}$$

$$T_{P2P1} = T_{DN}(IMU2) T_{DN}(IMU1)^T; T_{P3P1} = T_{DN}(IMU3) T_{DN}(IMU1)^T$$

2.4.4 Accelerometer Error Values (1σ)

Bias (b) - all axes	50 μg
Noise (η) - all axes	5 μg
Scale factor (k_i) - all axes	40 PPM for 17 hours after preflight alignment and calibration 100 PPM thereafter
Input axis alinement (γ_j, γ_k) - all axes	15 $\widehat{\text{sec}}$
Scale factor nonlinearity	0 g^{-1}
Scale factor asymmetry	40 PPM
Quantization	1 cm/sec

Transformation matrix for X-axis accelerometer

$$H_X = \begin{bmatrix} 1 & 0 & 0 \\ 0 & 1 & 0 \\ 0 & 0 & 1 \end{bmatrix}$$

Transformation matrix for Y-axis accelerometer

$$H_y = \begin{bmatrix} 0 & 1 & 0 \\ 1 & 0 & 0 \\ 0 & 0 & 1 \end{bmatrix}$$

Transformation matrix for Z-axis accelerometer

$$H_Z = \begin{bmatrix} 0 & 0 & 1 \\ 0 & 1 & 0 \\ 1 & 0 & 0 \end{bmatrix}$$

2.4.5 IMU Case Error Values (1σ)

IMU case to navigation base misalignment (C_X, C_Y, C_Z)

These are the RSS of the following error sources

IMU case to mounting pads - all axes	20 $\widehat{\text{sec}}$
Mounting pads to nav. base - all axes	5 $\widehat{\text{sec}}$
Nav. base bending (static loads) - X, Y axes	
Ascent	$5/\sqrt{2}$ $\widehat{\text{sec}}$
Onorbit	0 $\widehat{\text{sec}}$
Entry	$4/\sqrt{2}$ $\widehat{\text{sec}}$
Nav. base bending (thermal) - X, Y axes	
Onorbit only	$41/3\sqrt{2}$ $\widehat{\text{sec}}$
Outer-roll to case gimbal nonorthogonality - Y, Z axes	20 $\widehat{\text{sec}}$

2.4.6 Gimbal Nonorthogonalities (γ, μ, ϵ)

Range of means (γ, μ, ϵ)	± 413 $\widehat{\text{sec}}$
Error in calibration (ϵ) - 1σ	30 $\widehat{\text{sec}}$
Error in calibration (γ, μ) - 1σ	0 $\widehat{\text{sec}}$

2.4.7 Resolver and A/D Converter Error Values (1σ)

Resolver bias (B_{θ})	30 $\widehat{\text{sec}}$
Random noise (η_{θ})	12 $\widehat{\text{sec}}$
Sinusoidal bias	
First harmonic ($A_{\theta 1}$)	7.6 $\widehat{\text{sec}}$
Eighth harmonic ($A_{\theta 8}$)	19.0 $\widehat{\text{sec}}$
Ninth harmonic ($A_{\theta 9}$)	4.2 $\widehat{\text{sec}}$
Sixteenth harmonic ($A_{\theta 16}$)	20.0 $\widehat{\text{sec}}$
Random phase error (ϕ_n)	$-180^{\circ} \leq \phi_n \leq 180^{\circ}$
Quantization	20.0 $\widehat{\text{sec}}$

ORIGINAL PAGE IS
OF POOR QUALITY.

2.5 REFERENCES

- 2-1 Space Shuttle Orbital Flight Test Level C Functional Subsystem Software Requirements; Guidance, Navigation, and Control, Part E, Subsystem Operating Programs, Inertial Measurement Unit. Rockwell International SD76-SH-0013, December 15, 1978.
- 2-2 Rasmussen, M. C.: IMU Error Model Update; Gimbal Nonorthogonalities. MDTSCO TM 1.4-MPB-1391, October 31, 1978.
- 2-3 Shuttle Operational Data Book, Vol. I, Shuttle Systems Performance and Constraints Data. JSC-08934, vol. I, rev. A, Oct. 1976.
- 2-4 Pietz, K.: Initial Conditions for Ascent Simulations. MDTSCO TM 1.4-MPB-1104, March 22, 1978.
- 2-5 Collins, C. J.: IMUFDI/SNAP Updates. MDTSCO TM 1.4-MPB-1095, March 14, 1978.
- 2-6 Davis, L. D.: Coordinate Systems for the Space Shuttle Program. NASA TMX-58153, JSC-09084, Oct. 1974.
- 2-7 Pietz, K.: IMU Error Model Update; Prelaunch IMU Pointing Errors. MDTSCO TM 1.4-MPB-1385, October 19, 1978.

3.0 BODY MOUNTED SENSORS

3.1 GENERAL DESCRIPTION

Body mounted sensors consist of rate gyro assemblies (RGA) and accelerometer assemblies (AA). The RGA contains three rate gyros that are mounted to the vehicle frame with the input axes forming an orthogonal triad (fig. 3-1). The outputs from the RGA provide a measurement of vehicle attitude rate used to update the onboard estimate of vehicle inertial attitude. The AA contains normal and lateral accelerometers mounted to the vehicle frame (fig. 3-1). The outputs from the AA provide a measurement of the nongravitational accelerations applied to the vehicle. The AA outputs are used by Flight Control to provide load relief during the high dynamic pressure region of the ascent phase and steering commands to the entry phase digital autopilot to conform to a selected g-profile trajectory.

~~PRECEDING PAGE BLANK NOT FILLED~~

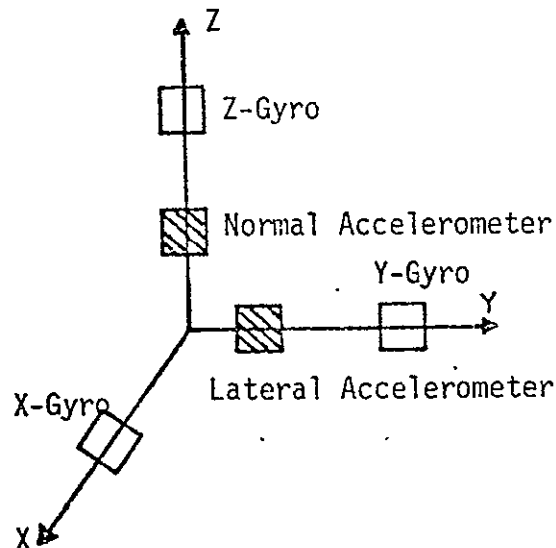


Figure 3-1.- Body mounted sensors orientation.

3.2 SIMULATION APPROACH

The body mounted sensors provide measurements of the normal and lateral nongravitational body accelerations, \tilde{a}_n ($n = 1, 2$), and measurements of the body attitude rates, $\tilde{\omega}_n$ ($n = 1, 2, 3$).

An environment simulation is assumed to provide the true vehicle acceleration, \underline{a}_I , in a reference inertial coordinate system and a set of Euler angles, $\underline{\beta}$, which define the vehicle attitude relative to the reference system. Vehicle rate data may also be supplied by the environment, but the assumption made here is that the rate must be computed within the simulation.

Figure 3.2 presents a block diagram for a body mounted sensors simulation. The functions of each block are as follows.

- a. Block 1 - computes the vehicle orientation matrix T_{BI} .

$$T_{BI} = F(\underline{\beta})$$

where $F(\underline{\beta})$ is the transformation matrix that represents the rotation defined by the Euler angle set $\underline{\beta}$.

- b. Block 2 - the inertial reference acceleration, \underline{a}_I , is transformed to body coordinates.

$$\underline{a}_B = T_{BI} \underline{a}_I$$

where T_{BI} is computed in block 1.

- c. Block 3 - computes the average body attitude rate vector and the average body attitude acceleration vector over the time interval Δt . The change in body attitude is given by

$$R = (T_{BI})_t (T_{BI})_{t-\Delta t}^T$$

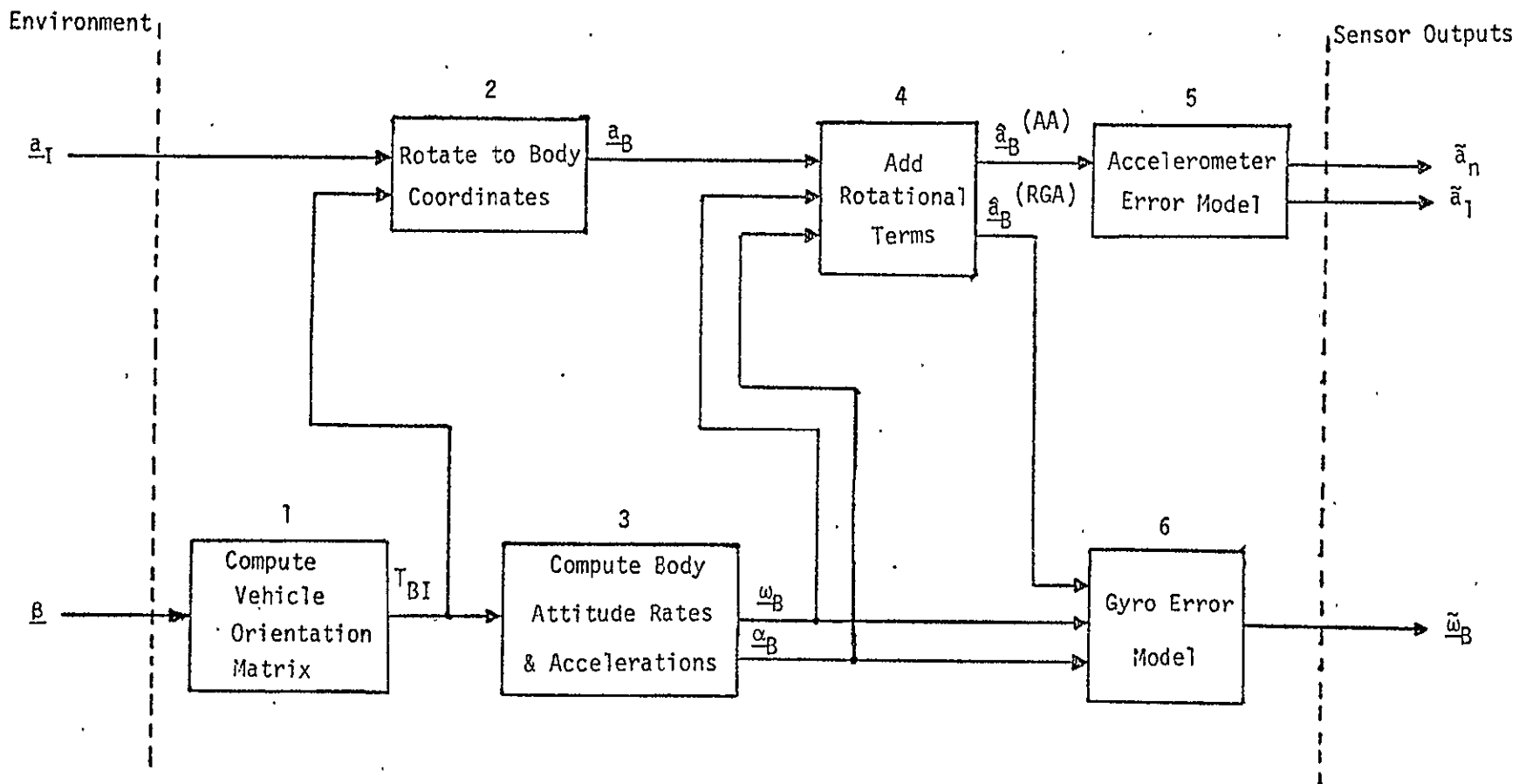


Figure 3-2.- Body mounted sensors simulation block diagram.

The average body attitude rate vector, $\underline{\omega}_B$, is computed for the eigenaxis rotation defined by R.

$$\underline{\omega}_B = \frac{1}{2\Delta t} \begin{pmatrix} R_{23} - R_{32} \\ R_{31} - R_{13} \\ R_{12} - R_{21} \end{pmatrix}$$

assuming minor attitude changes, $\sin(|\underline{\omega}_B|\Delta t) \approx |\underline{\omega}_B|\Delta t$.

The average attitude acceleration vector is given by

$$\underline{\alpha}_B = ((\omega_B)_t - (\omega_B)_{t-\Delta t}) / \Delta t$$

- d. Block 4 - computes noninertial acceleration by adding rotational terms.

$$\hat{\underline{a}}_B = \underline{a}_B + \underline{\omega}_B \times (\underline{\omega}_B \times \underline{r}) + \underline{\alpha}_B \times \underline{r}$$

where \underline{a}_B was calculated in block 2, $\underline{\omega}_B$ and $\underline{\alpha}_B$ were calculated in block 3, and \underline{r} is the position vector of either the rate gyro assembly ($\underline{r}^{(RGA)}$) and the acceleration is denoted by $\underline{a}_B^{(RGA)}$ or the accelerometer assembly ($\underline{r}^{(AA)}$) and the acceleration is denoted by $\underline{a}_B^{(AA)}$ with respect to the center of gravity of the vehicle.

- e. Block 5 - generates the simulated nongravitational acceleration sensed by the accelerometer assembly.

$$\hat{\underline{a}}_n = q (\hat{\underline{a}}_n^{(AA)} + \Delta a_n)$$

$$\hat{\underline{a}}_1 = q (\hat{\underline{a}}_1^{(AA)} + \Delta a_1)$$

where $\hat{\underline{a}}_n^{(AA)}$ and $\hat{\underline{a}}_1^{(AA)}$ are the respective z- and y-components of the body acceleration, $\hat{\underline{a}}_B^{(AA)}$, computed in block 4, Δa_n and

Δa_1 are the normal and lateral accelerometer errors (sec. 3.3.1) and $q ()$ is the quantization operator that truncates the argument to the least significant bit value for the specific accelerometer being simulated.

- . Block 6 - computes the simulated rate gyro output

$$\omega_B = q (\hat{\omega}_B + \Delta\omega_B)$$

where $\hat{\omega}_B$ are the body attitude rates computed in block 3, $\Delta\omega_B$ are the rate gyro errors (sec. 3.3.2), and $q ()$ is the quantization operator similar to the one in block 5.

3.3 ERROR MODELS

3.3.1 Accelerometer Assembly Error Model - Block 5

Single-axis accelerometer errors can be categorized as those caused by bias, random noise, scale factor error, and input axis misalignment. A mathematical model for the normal accelerometer is given by the equation

$$\Delta a_n = b_n + \eta_n + \underline{k}_n^T \hat{\underline{a}}_B^{(AA)}$$

where Δa_n is the normal accelerometer measurement error

b_n is the normal accelerometer bias

η_n is the normal accelerometer noise

$$\underline{k}_n = \begin{pmatrix} \gamma_{nx} \\ \gamma_{ny} \\ k_z \end{pmatrix} \quad \text{is a vector of longitudinal and lateral misalignments } (\gamma_{nx}, \gamma_{ny}) \text{ and scale factor error } (k_z).$$

$\hat{\underline{a}}_B^{(AA)}$ is the acceleration vector of the accelerometer assembly in body coordinates (x, y, z - longitudinal, lateral, normal).

The lateral accelerometer model is given by the equation

$$\Delta a_l = b_l + \eta_l + \underline{k}_l^T \hat{\underline{a}}_B^{(AA)}$$

where Δa_l is the lateral accelerometer measurement error

b_l is the lateral accelerometer bias

η_l is the lateral accelerometer noise

$$\underline{k}_l = \begin{pmatrix} \gamma_{lx} \\ k_y \\ \gamma_{ly} \end{pmatrix} \quad \text{is a vector of longitudinal and normal misalignments } (\gamma_{lx}, \gamma_{ly}) \text{ and scale factor error } (k_y)$$

$\hat{a}_B^{(AA)}$ is the acceleration vector of the accelerometer assembly in body coordinates.

The error model parameters are assumed to be independent random variables with zero-mean Gaussian distribution.

3.3.2 Rate Gyro Assembly Error Model - Block 6

Single-degree-of-freedom rate gyro errors can be categorized as those caused by bias drift, random drift, linear acceleration sensitive drift, angular acceleration sensitive drift, scale factor error, and input axis misalignments. A mathematical model for the rate gyro measurement error is given by the equation

$$\Delta\omega_B = r + \eta + h\hat{a}_B^{(RGA)} + g\alpha_B + \underline{k}^T\hat{\omega}_B$$

where $\Delta\omega_B$ is the total rate measurement error for a given axis (x,y,z - roll, pitch, yaw)

r is the bias drift rate

η is the random noise drift rate

h is the g-sensitive drift rate

$\hat{a}_B^{(RGA)}$ is the linear acceleration component for the rate gyro assembly along the given axis

g is the angular acceleration sensitive drift rate

α_B is the angular acceleration component along the given axis

$$\underline{k} = \begin{pmatrix} k_i \\ \gamma_j \\ \gamma_k \end{pmatrix}$$

is a vector of scale factor error (k_i) and input axis misalignments (γ_j, γ_k)

$\hat{\omega}_B$ is the body attitude rate vector

The error model parameters are assumed to be independent random variables with zero-mean Gaussian distribution.

3.4 ERROR SOURCE VALUES

3.4.1 Accelerometer Assembly

The accelerometer assembly is composed of two Honeywell single-axis accelerometers (model No. 326) mounted orthogonal to each other. Four of these packages are then attached to the vehicle at the locations specified in section 3.4.3. References 3-1 through 3-3 provide the following error source values.

Accelerometer errors (1 σ)

Bias - normal (b_n)	8333 μg
- lateral (b_l)	5000 μg
Random noise - both axes (η_n, η_l)	3333 μg
Scale factor - normal (k_z)	0.833 percent
- lateral (k_y)	1.0 percent
Input axis misalignments (all axes)	0.22 $^\circ$
This is the resultant of:	
Input axis to case misalignment	0.12 $^\circ$
Case-to-body misalignment	0.18 $^\circ$
Quantization - normal	7800 μg
- lateral	2000 μg

3.4.2 Rate Gyro Assembly

The rate gyro assembly is composed of three Northrup single degree-of-freedom rate gyros (model No. G-6). Four assemblies are attached to the vehicle at the locations specified in section 3.4.3. References 3-1 through 3-3 provide the following error source values.

Rate Gyro Errors (1σ)

Bias - all axes (r)	.05 deg/sec
Noise - yaw and pitch (η_y, η_z)	.01667 deg/sec
- roll (η_x)	.03333 deg/sec
Linear acceleration sensitivity - all axes (h)	0.01667 deg/sec/g
Angular acceleration sensitivity - all axes (g)	0.001 deg/sec/deg/sec ²
Scale factor - all axes (k)	1.7 percent
Input axis misalignment - all axes	0.248°
Quantization - pitch and yaw	0.039 deg/sec
- roll	0.078 deg/sec

3.4.3 Body Mounted Sensor Locations

The locations of the four accelerometer assemblies and the four rate gyro assemblies are given below in Orbiter structural body coordinates with units of inches.

	<u>X_o</u>	<u>Y_o</u>	<u>Z_o</u>
AA1	382.8	-6.8	398.2
AA2	381.7	5.6	406.4
AA3	381.7	11.6	406.4
AA4	382.8	-12.8	398.2
RGA1	1307	-100	353
RGA2	1307	100	353
RGA3	1307	-13	295
RGA4	1307	-21	101

To determine the locations in body coordinates, the center of mass of the Orbiter for the particular flight must be expressed in Orbiter structural body coordinates and subtracted from the sensor locations listed above.

The following transformation matrix, T, applied to the resultant difference vector will give the sensor locations in body coordinates.

$$T = \begin{bmatrix} -1 & 0 & -0 \\ 0 & 1 & 0 \\ 0 & 0 & -1 \end{bmatrix}$$

3.5 REFERENCES

- 3-1 Space Shuttle Flight Control System Data Book, Vol. I, Integrated Vehicle. Rockwell International SD73-SH-0097-1E, Nov. 1976.
- 3-2 Shuttle Operational Data Book, Vol. I, Shuttle Systems Performance and Constraints Data. JSC-08934, vol. I, rev. A., Oct. 1976.
- 3-3 Honeywell Ascent FCS Status Review. Paper presented Nov. 1976.
- 3-4 Davis, L. D.: Coordinate Systems for the Space Shuttle Program. NASA TMX-58153, JSC-09084, Oct. 1974.
- 3-5 Rasmussen, M. C.: Rate Gyro Error Model for Use in the IMUFDI Simulation Program. MDTSCO T.M.1.4-MPB-432, Nov. 11, 1976.

4.0 BAROMETRIC ALTIMETER

4.1 GENERAL DESCRIPTION

A barometric altimeter is a device that is used to determine the ambient atmospheric pressure around a vehicle. Use of an atmosphere model then allows pressure to be related to vehicle altitude through a pressure/altitude algorithm. The device itself only measures pressure, and the transformation to altitude is performed within the onboard software. Barometric altimeters are generally restricted to altitudes of less than 100 000 feet.

4.2 SIMULATION APPROACH

The basic data type for simulation of a barometric altimeter is the geometric altitude. The geometric altitude is the altitude (h) above the ellipsoidal Earth (fig. 4-1). Figure 4-2 presents a block diagram for the barometric altimeter simulation. A functional description of each block is as follows.

- a. Block 1 - calculates the geometric altitude (h) for input to the baro error model block as follows (ref. 4-1).

$$h = (1-R_E(1-e)/\sqrt{Z_{EF}^2 + (1-e)^2 R_{XY}^2})(Z_{EF}^2 + (1-e)^2 R_{XY}^2)/\sqrt{Z_{EF}^2 + (1-e)^4 R_{XY}^2}$$

where

R_E = equatorial radius of the Earth

e = Earth flattening

~~PRECEDING PAGE BLANK NOT FILMED~~

ORIGINAL PAGE IS
OF POOR QUALITY

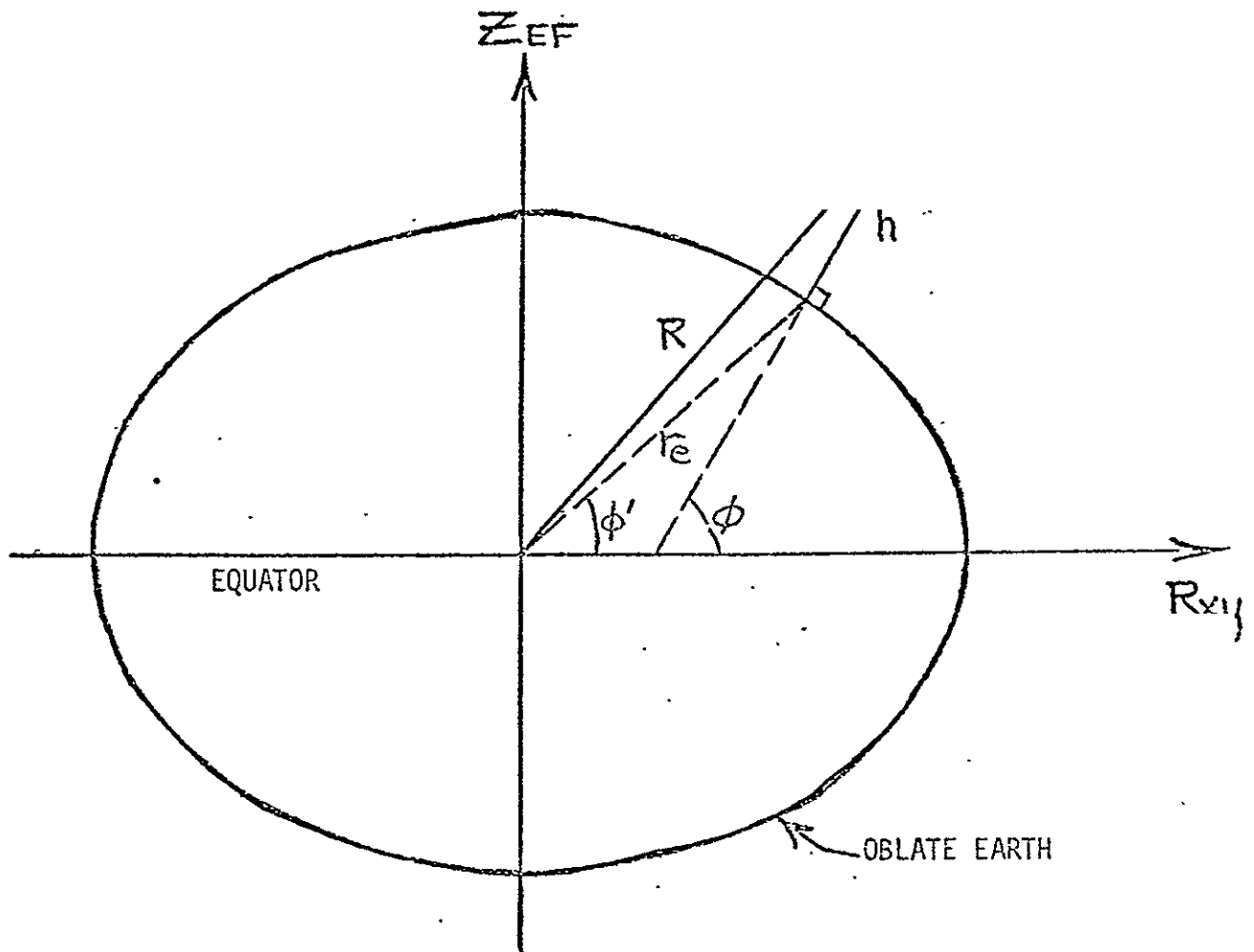


Figure 4-1.- Altitude above an ellipsoidal Earth.

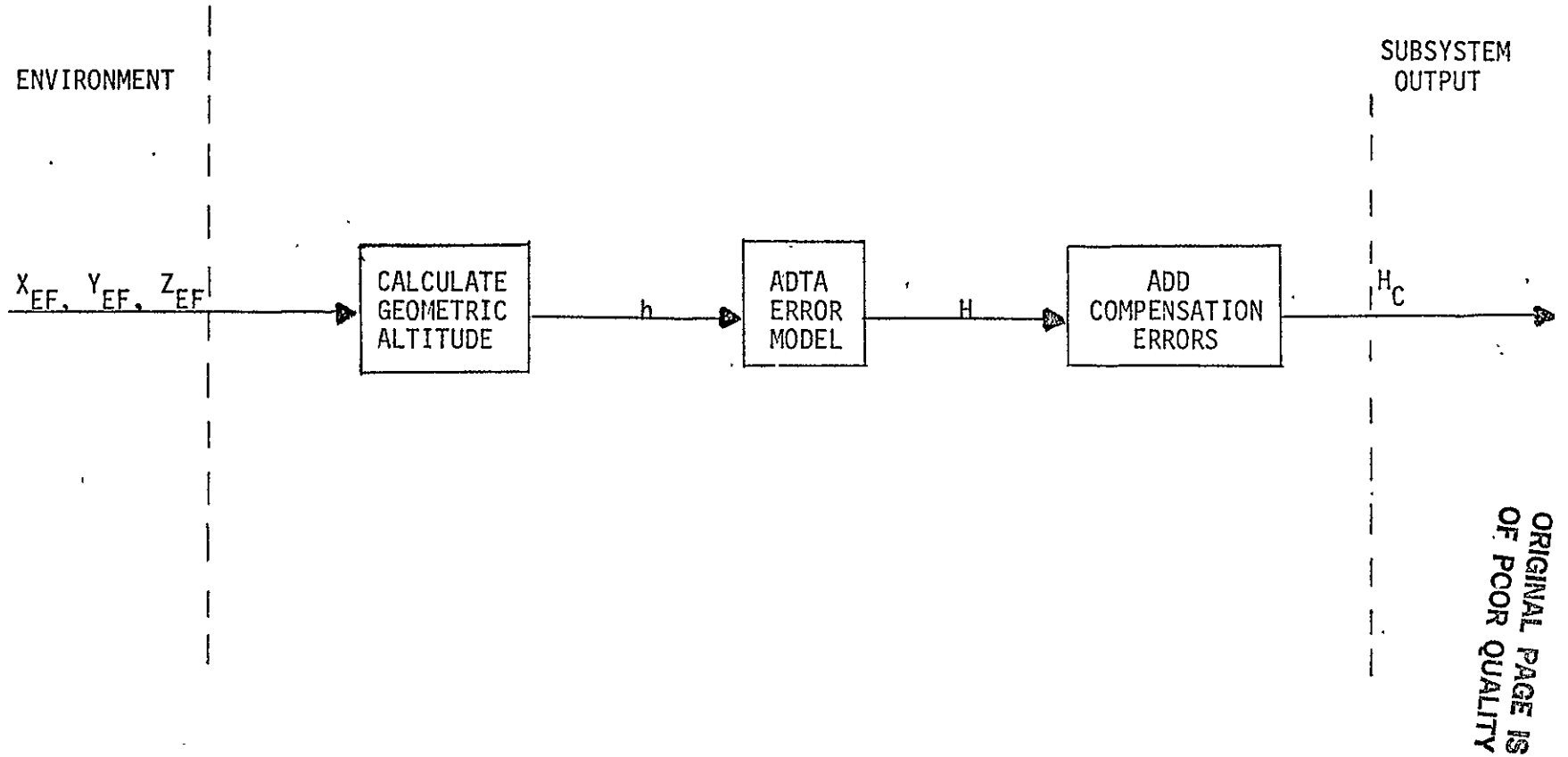


Figure 4-2.- Barometric altimeter simulation block diagram.

ORIGINAL PAGE IS
OF POOR QUALITY

Z_{EF} = Z - component of vehicle position in an Earth-fixed coordinate system

$$R^2_{XY} = X^2_{EF} + Y^2_{EF}$$

- b. Block 2 - computes a corrupted geometric altitude by modifying the output of block 1 with the following error sources (ref. 4-2).

$$H = h + \Delta H_{BE} + \Delta H_{RE}$$

where

ΔH_{BE} = Bias error

ΔH_{RE} = Random error in the air data transducer assembly (ADTA)

- c. Block 3 - compensates the corrupted altitude (H) from block 2 by adding a correction term for nonstandard atmosphere error (ΔH_{SF}) or subtracts a barometric pressure update error (ΔH_{LSBP}), depending on whether the corrupted altitude is above or below a specified altitude. The following equations represent this procedure.

If $H > ALT_{SPEC}$

Then: $H_C = H + \Delta H_{SF}$

Else: $H_C = H - \Delta H_{LSBP}$

where

ALT_{SPEC} = specified altitude

H = corrupted geometric altitude calculated in block 2

ΔH_{SF} = Nonstandard atmosphere error

ΔH_{LSBP} = barometric pressure update error

4.3 ERROR MODEL

The environment baro altimeter error model presented in reference 4-2 identifies the following four error sources.

- a. Bias error - a bias error due to the imperfect measurement of pressure by the barometer (ADTA).
- b. Barometric pressure update error - Uncertainty in the landing site barometric pressure, which is used to update the vehicle's barometric pressure shortly before landing.
- c. Scale factor error - an error due to the difference in average pressure at a particular location not agreeing with the average pressures shown in the 1962 Standard Atmosphere (ref. 4-4).
- d. Random error - A Gaussian noise inherent in the ADTA.

The one-sigma values for the baro altimeter error model are presented in table 4-I. The bias error, uncertainty in the landing site barometric pressure, and scale factor error comprise the correlated error, while the noise error comprises the uncorrelated error that is added to the barometer's measurements.

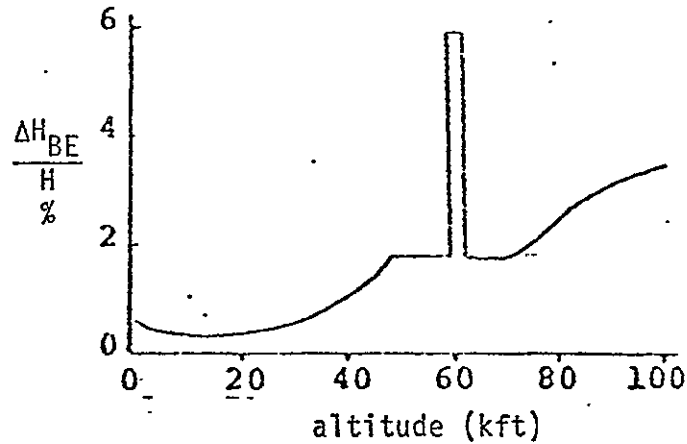
The bias error plot in table 4-I was constructed from a simulation of an OFT-1 trajectory to EAFB (Edwards Air Force Base). The uncertainty in the landing site barometric pressure and scale factor error are modeled as ECRV's (exponential correlated random variable) with time constants of $\tau = \infty$ and $\tau = 1000$ sec, respectively. The uncorrelated error is also modeled as an ECRV with a time constant of $\tau = 0$, which implies a true random error.

The specified altitude (ALT_{SPEC}) for adjusting the compensation errors in block 3 is given as 5000 feet.

TABLE 4-I.- BAROMETRIC ALTIMETER ERROR MODEL (1-sigma)

Correlated error

(1) Bias error



(2) Barometric pressure update error

$\Delta H_{LSBP} = 20 \text{ ft } (\tau = \infty)$ vehicle is updated with the landing site
pressure shortly before landing

(3) Scale factor error related to density reference

$\Delta H_{SF} = 3.5\% \text{ of altitude } (\tau = 1000 \text{ sec})$
using the 1962 standard atmosphere model in
the filter

(4) Instrument Noise $\Delta H_{RE} = 2.3 \exp (H/23000) \text{ ft } (\tau = 0)$

4.4 REFERENCES

- 4-1 Lear, W. M.: A Prototype, Real-Time Navigation Program for Multi-Phase Missions. TRW Report 17618-6003-TO-00, December 1, 1971.
- 4-2 Kriegsman, B. A.; and Tao, Y. C.: Baro-Altitude Related Navigation Problems. The Charles Stark Draper Laboratory, Inc. Shuttle Memo No. 10E-77-68, December 15, 1977.
- 4-3 Watson, et al.: ATDA SOP and RM. Orbiter Software Change Request #12416, February 3, 1978.
- 4-4 U.S. Committee on Extension to the Standard Atmosphere: U.S. Standard Atmosphere, 1962. Government Printing Office (Wash., D.C.), 1962.

5.0 STAR TRACKER

5.1 GENERAL DESCRIPTION

The Shuttle star tracker is a strapped-down, wide field-of-view image-dissector, electro-optical searching and tracking device. The star tracker is used to obtain precise angular measurements on stars or Sun-illuminated targets of small angular image diameter. There are two star trackers mounted on an extension of the Shuttle navigation base (fig. 5-1). The -Z star tracker points in the approximate direction of the Shuttle -Z body axis, while the -Y star tracker centerline is approximately 10.5 degrees forward of the Orbiter -Y body axis. The star tracker instrument consists of both the actual star tracker and a light shade. The light shade enables the tracking of targets that are relatively close to the Sun, Moon, or the sunlit Earth's horizon. The star tracker has the capability to search for, acquire, and track the 153 brightest stars or sunlit targets of 3 to -7 magnitude at any location within its 10 x 10 degree square field of view.

The two star trackers, under onboard computer software control, will track stars for the purpose of IMU platform realignment. Since the IMU inertial platform drifts from a true inertial attitude its orientation must be periodically determined in order to make corrections. Using star tracker measurement data for two stars, and the known star positions, the IMU inertial platform orientation with respect to the mean of 1950 (M50) coordinate system can be computed using deterministic methods. The accumulated IMU error due to drift can then be removed by torquing the IMU platform back to its original position. The star trackers can also be used to track a sunlit rendezvous vehicle. In this case

~~PRECEDING PAGE BLANK NOT FILLED~~

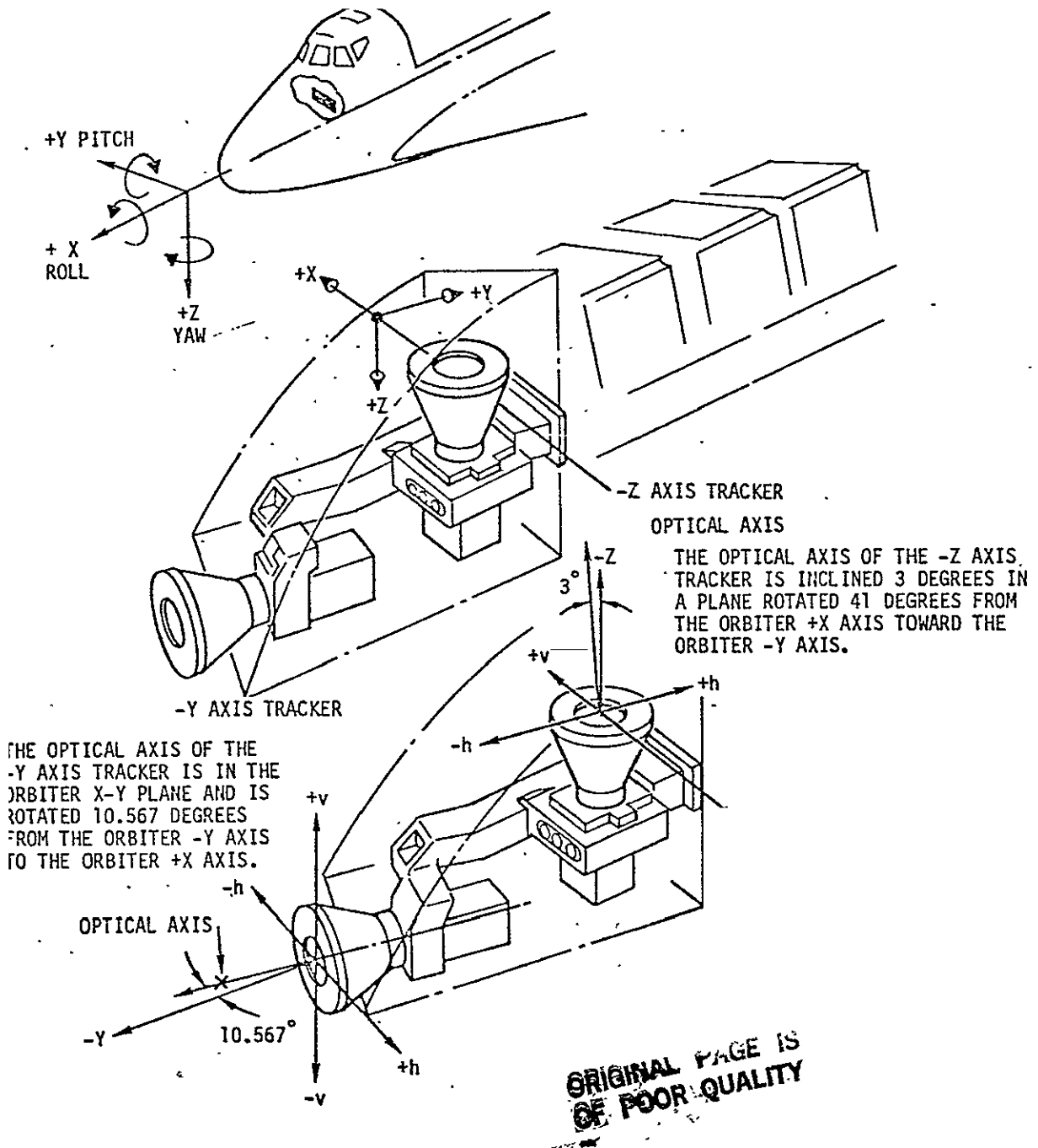


Figure 5-1.- Star tracker mounting geometry.

the star tracker measured angular position data is incorporated into the rendezvous navigation filter for use in relative state estimation.

5.1.1 Star Tracker Operating Characteristics

The Shuttle star tracker contains the following three modes of operation:

- a. Automatic scan mode
- b. Offset scan mode
- c. Self test mode

In the automatic scan mode (the default mode when the star tracker is first turned on), the star tracker scans the entire 10- x 10-degree field of view from top to bottom repeatedly. The search scheme (fig. 5-2) is a left-to-right, right-to-left, top-down raster scan. If a target encountered in the search has a magnitude greater than the currently commanded sensitivity threshold setting, the target will be acquired and the track scan will begin. The track scan is a cruciform pattern centered on the position of the target in the field of view (fig. 5-2). If the target is moving the track scan will follow it, remaining centered on the target. During the track scan, the measured horizontal and vertical components of the position of the target, and the measured target magnitude, are output by the tracker at a 25-Hz rate. The target will continue to be tracked until either it leaves the star tracker field of view or a break track command is sent to the tracker. In either case the star tracker will return to the auto scan mode and search the remainder of the field of view.

When the star tracker is commanded to the offset scan mode it will search a reduced 1- x 1-degree field of view centered at a position in the full field of

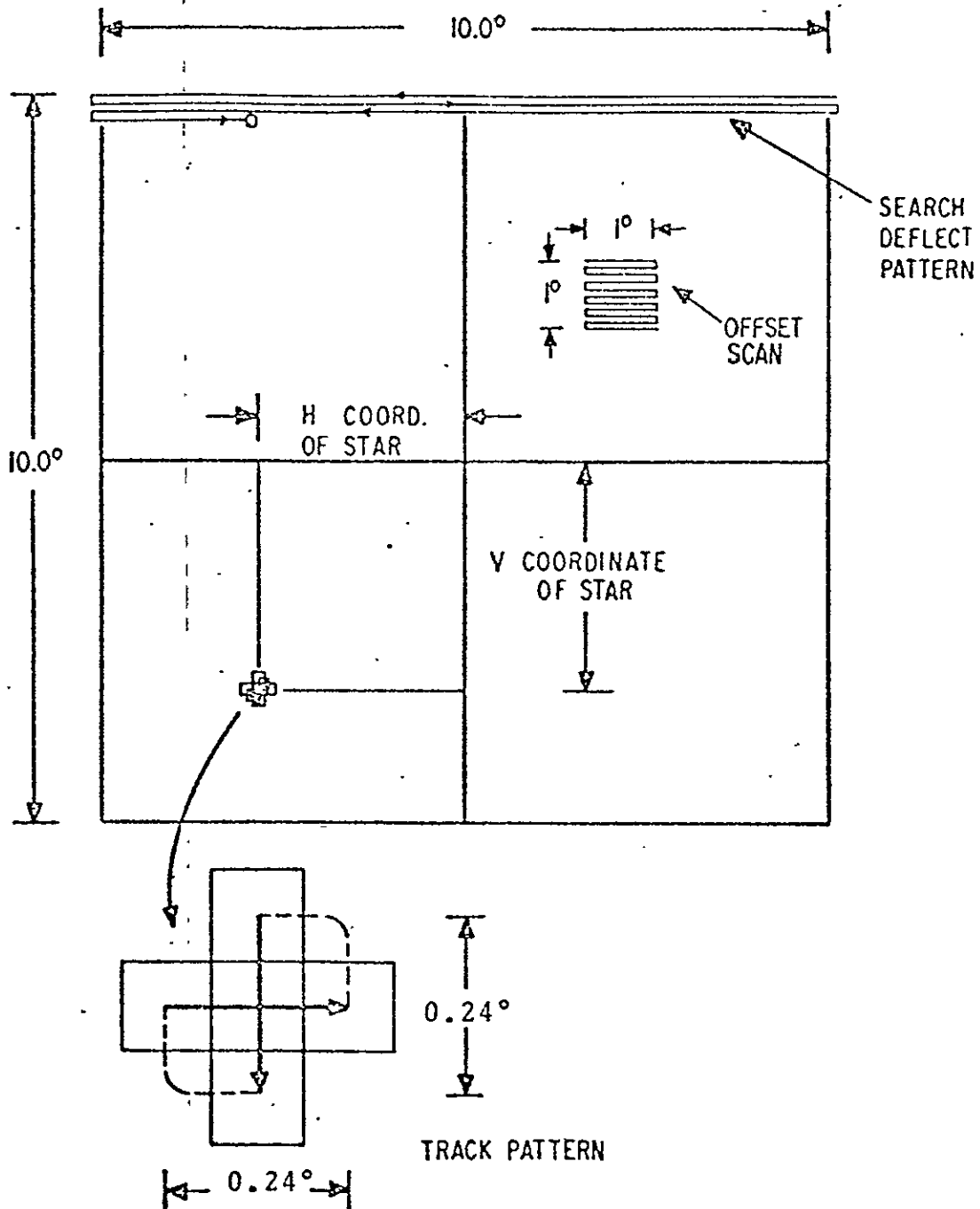


Figure 5-2.- Star tracker scan geometry.

view defined by a pair of commanded offset coordinates. The reduced field-of-view search is also a top-down raster scan similar to the auto scan search. When a target is acquired in the offset mode it will be tracked until either a break track is commanded or the target moves outside of the full 10- x 10-degree field of view. In either case the star tracker will return to the originally commanded offset coordinates and resume the reduced field-of-view scan.

The star tracker can also be commanded to a self-test mode. When this mode is commanded the star tracker searches for and tracks an LED source that is reflected into the star tracker field of view near the edge via a small aluminized spot on the star tracker protective window. The measured offset angles and magnitude of the simulated star are compared with prestored values to determine whether the star tracker operational accuracy conforms with requirements.

5.1.2 Star Tracker Operating Constraints

The following list briefly summarizes the various star tracker specifications and operating constraints.

a. Field of view dimensions

Auto scan - 10 x 10 degrees

Offset scan - 1 x 1 degrees

b. Field of view search time

Auto scan - 10 seconds

Offset scan - 1 second

c. Target intensity limits

Minimum intensity - 3.0 magnitude

Maximum intensity - 7.0 magnitude

- d. Target image diameter must be no greater than 8 arc minutes.
- e. The star tracker does not have the capability to track either star of a pair that have an absolute magnitude difference greater than one and an angular separation less than one-half degree.
- f. The star tracker will acquire and maintain accurate tracking of stars for Orbiter angular rates of up to 0.2 deg/sec and will maintain lockon with reduced accuracy at rates of up to 0.5 deg/sec.
- g. Bright source avoidance angles
 For acquisition and accurate tracking of stars or targets the minimum separation angles between the star tracker boresight axis and the three possible sources of intense light are as follows:
- | | |
|---------------------|-----|
| (1) Center of Sun | 30° |
| (2) Center of Moon | 8° |
| (3) Earth's horizon | 20° |
- h. Sensitivity threshold levels
 The star tracker will not acquire stars or targets having intensities that are less than the currently commanded sensitivity threshold level. The four crew commandable threshold levels correspond to star magnitudes of 3.0, 2.4, 2.0, and 1.0.
- i. Offset command angle quantization
 The reduced field-of-view offset command angles have a granularity of one-third degree.

j. Warm-up time

Star tracker performance requirements are met within 15 minutes after power on.

k. Accuracy requirements

(1) Angular data 30 arc sec noise (1σ)

30 arc set bias (1σ)

(2) Intensity error ± 0.6 magnitude

(a detailed angular data error budget is presented in sec. 5.4)

5.1.3 Star Tracker Hardware/Software System Operation

The Shuttle onboard star tracker computer software accumulates star tracker angular measurement data for each star tracked and converts it into an average measured unit line-of-sight vector expressed in IMU platform coordinates. Two star line-of-sight vectors with adequate separation are required by the IMU on-orbit alinement software for the purpose of realinement of each IMU platform.

Nominal star tracker operation assumes the execution of a vehicle attitude rate by the crew. As each star tracker field of view sweeps across the celestial sphere, the software selects stars of opportunity for tracking. Stars are selected from a navigation star catalog based on an estimated star tracker line of sight. The estimated star tracker line of sight is computed based upon a reasonably well known IMU inertial platform attitude with respect to the celestial sphere. Prior to star selection software checks are performed to determine whether either star tracker is occulted by the Earth, Sun, or Moon. If it is determined that a star is visible in either star tracker field of view, the star tracker is commanded by the software to search a reduced 1- x 1-degree field of view centered at the estimated position of the star in the star tracker full

field of view. If a star is acquired a sequence of 21 measured star tracker output angles are accumulated at a 6.25-Hz rate and then used to compute the average measured horizontal and vertical offset angles of the star. Simultaneously a sequence of 21 IMU gimbal angles are accumulated and averaged. Twenty-one samples are accumulated because this number of samples is the smallest number that yields the minimum average time lag between sensor output and the software read. The time lag is a result of the asynchronous operation of the star tracker and the software. The measured star tracker and IMU data are then converted to a unit line-of-sight vector in IMU coordinates by the following equations.

- a. First, compute the navigation base to IMU cluster transformation matrix using the following average IMU gimbal angles:

AZ = average azimuth gimbal angle

IR = average inner roll gimbal angle

P = average pitch gimbal angle

OR = average outer roll gimbal angle

SAZ = sin AZ

CAZ = cos AZ

SIR = sin IR

CIR = cos IR

SP = sin P

CP = cos P

SOR = sin OR

COR = cos OR

$$(TNBPC) = \begin{bmatrix} CAZ & -SAZ & 0 \\ SAZ & CAZ & 0 \\ 0 & 0 & 1 \end{bmatrix} \begin{bmatrix} 1 & 0 & 0 \\ 0 & CIR & -SIR \\ 0 & SIR & CIR \end{bmatrix} \begin{bmatrix} CP & 0 & SP \\ 0 & 1 & 0 \\ -SP & 0 & CP \end{bmatrix} X$$

$$\begin{bmatrix} 1 & -DP & 0 \\ DP & 1 & 0 \\ 0 & 0 & 1 \end{bmatrix} \begin{bmatrix} 1 & 0 & 0 \\ 0 & COR & -SOR \\ 0 & SOR & COR \end{bmatrix} \quad (TNBRL)$$

DP = the nonorthogonality between the outer roll and pitch axes
(constant)

(TNBRL) = navigation base to IMU roll axis transformation (constant)

- b. Compute the observed star line-of-sight vector in IMU platform coordinates as follows:

$$\underline{S} = (TNBPC) (TNBST)^T \text{ UNIT} \begin{pmatrix} -\tan V \\ \tan H \\ 1 \end{pmatrix}$$

V = average measured vertical offset angle

H = average measured horizontal offset angles

(TNBST) = navigation base to star tracker transformation

- c. Correct the observed line of sight for stellar aberration

$$\underline{COR} = \left\{ \underline{v} + S (TECLM50) \begin{pmatrix} -\sin G \\ \cos G \\ 0 \end{pmatrix} \right\} / c$$

TECLM50 = ecliptic to mean of 1950 coordinate transformation

\underline{v} = vehicle velocity vector in M50 coordinates

G = mean longitude of the Sun at the current time

S = Earth's orbital speed

c. = speed of light

$$\underline{S} = \text{unit} \left(\underline{S} - (TCM50)^T \underline{COR} \right)$$

(TCM50) = present IMU cluster to M50 transformation matrix

A measured unit star line-of-sight vector in IMU platform coordinates is computed for each operating IMU. The star tracker software, in addition to accumulating star tracker measurements and computing the equivalent line-of-sight data, also performs data reasonableness checks for each star and optimum data selection operations. When adequate measurement data have been gathered for two stars an IMU realignment can be performed by the IMU onorbit alinement software.

For the purpose of rendezvous vehicle tracking initial acquisition of the rendezvous target is accomplished by a crew maneuver of the Orbiter to center the target in the selected star tracker field of view and execution of the star tracker software to command an offset mode search for the target. The onboard rendezvous navigation software then accepts average measured star tracker output angles from the star tracker software every 15 seconds for incorporation into the rendezvous navigation filter.

5.2 SIMULATION APPROACH

The diagram in figure 5-3 illustrates the method used in the simulation of the star tracker hardware. It is assumed that the following eight inputs are available from an environment simulation.

- a. (TIB) = mean of 1950 to vehicle body transformation
- b. (TBN) = vehicle body to navigation base transformation
- c. (TNS)_{ideal} = ideal navigation base to star tracker transformation
(one per star tracker)
- d. (TEI) = ecliptic to mean of 1950 transformation
- e. Q = navigation base to star tracker misalignment quaternion
(one per star tracker)
- f. STAR_N = unit line of sight vector of the Nth Shuttle navigation star in mean-of-1950 coordinates
- g. TARGET = relative rendezvous target line of sight vector in mean-of-1950 coordinates
- h. GAMMA = mean longitude of the Sun relative to the mean equinox of date.

If simulated sensor outputs for a star are desired, the first step is to adjust the line of sight of the star to simulate the effect of stellar aberration (fig. 5-3, block 1). These phenomena result in a shift in the observed line of sight of a star due to the relative difference between the velocity of the observer and the velocity of the light from the star. The apparent shift is in the direction of the velocity of the observer. If the rendezvous vehicle is being

tracked this step need not be performed. The following computations are used to simulate the effect of stellar aberration.

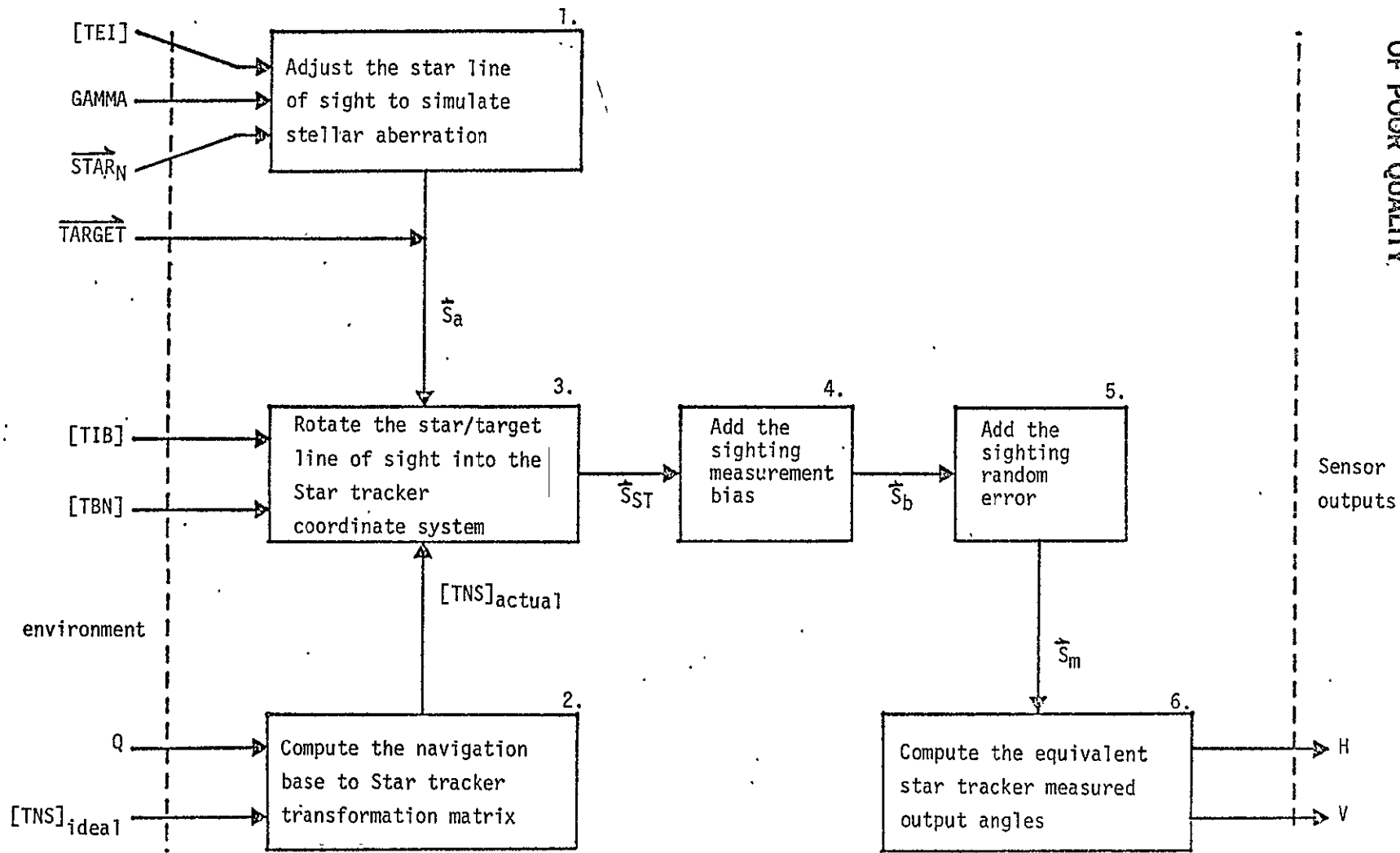


Figure 5-3.- Star tracker simulation functional block diagram.

ORIGINAL PAGE IS
OF POOR QUALITY

- a. Compute a unit vector parallel to the Earth's velocity vector in ecliptic coordinates.

$$\underline{u} = \begin{pmatrix} -\sin (\text{GAMMA}) \\ \cos (\text{GAMMA}) \\ 0 \end{pmatrix}$$

GAMMA = mean longitude of Sun at current environment time

- b. Compute the aberration correction vector

$$\underline{cor} = \{ \underline{v} + S(\text{TEI}) \underline{u} \} / c$$

(TEI) = mean of 1950 to ecliptic transformation

v = vehicle velocity vector in mean of 1950 coordinates

S = Earth's orbital speed

c = speed of light

- c. Add the correction vector to the star line of sight

$$\underline{S}_a = \text{UNIT} (\underline{STAR}_N + \underline{cor})$$

Before adding error to the adjusted star line of sight or the target line of sight it must be transformed into the appropriate star tracker coordinate system. The onboard navigation software uses an ideal navigation base to star tracker transformation; however, the actual, or simulated, transformation will be in error by an amount defined by the input navigation base to star tracker misalignment quaternion, Q. Q is defined as

$$Q = (Q_0, \underline{Q})$$

$$Q_0 = \cos \omega/2$$

$$|\underline{Q}| = \sin \omega/2$$

unit (\underline{Q}) = direction of misalignment error

ω = magnitude of misalignment error

The two sources of misalignment error, ω , for the star tracker are the navigation base to star tracker misalignment and internal star tracker bias. The value to be used for ω , therefore, is the RSS of the magnitudes of these two errors. The actual navigation base to star tracker transformation is computed in block 2 of figure 5.3 by the following equation.

$$(\text{TNS})_{\text{actual}} = \begin{bmatrix} 1-2(Q_2^2 + Q_3^2) & 2(Q_1Q_2 - Q_0Q_3) & 2(Q_1Q_3 + Q_0Q_2) \\ 2(Q_2Q_1 + Q_0Q_3) & 1-2(Q_3^2 + Q_1^2) & 2(Q_2Q_3 - Q_0Q_1) \\ 2(Q_3Q_1 - Q_0Q_2) & 2(Q_3Q_2 + Q_0Q_1) & 1-2(Q_1^2 + Q_2^2) \end{bmatrix} (\text{TNS})_{\text{ideal}}$$

$(\text{TNS})_{\text{ideal}}$ = ideal navigation base to star tracker transformation
(one per star tracker)

$(\text{TNS})_{\text{actual}}$ = actual simulated navigation base to star tracker transformation
(one per star tracker)

For a single mission simulation the navigation base to star tracker misalignment, Q , will be constant; therefore, the transformation $(\text{TNS})_{\text{actual}}$ need only be computed once.

The apparent star or target line of sight can now be rotated into the appropriate star tracker coordinated system (block 3).

$$\underline{S}_{\text{ST}} = (\text{TNS})_{\text{actual}} (\text{TBN}) (\text{TIB}) \underline{S}_a$$

(TBN) = vehicle body to navigation base transformation

(TIB) = mean of 1950 to vehicle body transformation

The error model (block 4 and block 5) computes and adds errors to the star line of sight yielding a measured star line of sight in star tracker coordinates, \underline{S}_I

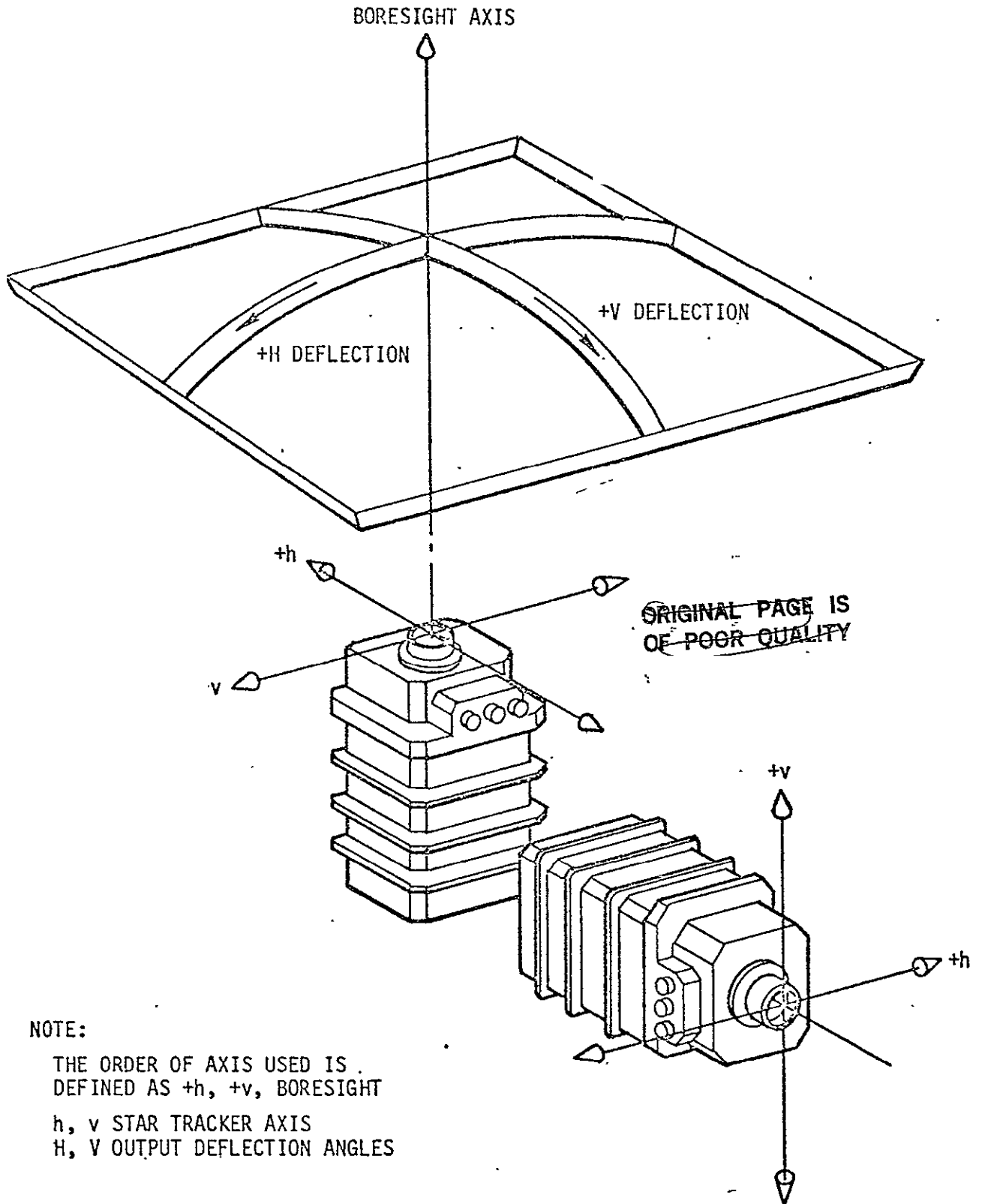
The following equations are then used to compute the equivalent star tracker output angles for the measured line of sight (block 6).

$$H = \tan^{-1}(S_{m2}/S_{m3})$$

$$V = \tan^{-1}(-S_{m1}/S_{m3})$$

These equations are derived from the relation between the star tracker measured output angles, H and V, and the three star tracker coordinate system axes, h,

ORIGINAL PAGE IS
OF POOR QUALITY



NOTE:

THE ORDER OF AXIS USED IS
DEFINED AS +h, +v, BORESIGHT
h, v STAR TRACKER AXIS
H, V OUTPUT DEFLECTION ANGLES

Figure 5-4.- Star tracker coordinate system.

5.3 ERROR MODEL

The star tracker error model computes simulated measured star tracker output angles by adding errors to the line of sight of the object being tracked. This error model is also designed to be used in conjunction with the star tracker data accumulation software (sec. 5.1.2).

The sources of star tracker error can be divided into two groups. The first group contains errors that will be referred to as the random errors. These errors appear randomly distributed when sampled at a high frequency or at the star tracker software data sampling rate of 6.25 Hz. The sources of these errors include:

- a. Noise
- b. Digital resolution
- c. Variations in input voltage

The remaining star tracker errors remain fairly constant over the period of time required for the star tracker software to accumulate 21 sightings on 1 particular star. These errors, although random, change noticeably only over long periods of time and for different stars. For a set of 21 sightings on 1 star for a period of 3.36 seconds these errors would not change significantly between each individual sighting. The sources of these bias errors include:

- a. Variations in star intensity
- b. Variations in temperature
- c. Earth's magnetic field
- d. Time lag
- e. Mechanical stability

- f. Lens stability
- g. Calibration
- h. Long-term drift of electronic components

This model adds just two errors to each star sighting: one being the RSS of all the random errors and the other the RSS of all the bias errors. The random error is recomputed and changed for each individual star sighting; while the bias is computed once for each set of 21 star sightings and added to each individual sighting of that set.

This model adds the errors to a line-of-sight vector by rotating it in a parallel plane by an amount equal to the error. The amount of rotation is computed from a normally distributed random number, the direction of rotation is determined by a uniformly distributed random number, and the actual rotation is performed by vector quaternion multiplication. This method of adding on the error assumes that the random error is both Gaussian in distribution and isotropic.

The following is a detailed description of the computations used in blocks 4 and 5 of figure 5-3.

- a. If this is the first sighting of the 21 sightings, compute the bias error and construct the bias error quaternion for this set of sightings; otherwise, proceed to step 2.

- (1) Construct the bias quaternion so that it is perpendicular to the actual line of sight and parallel to the Y-Z plane.

$$\underline{V} = \text{UNIT} (\underline{S}_{\text{ST}} \times \underline{i})$$

- (2) Compute the direction of the bias quaternion and rotate it about the actual line of sight by an amount equal to the computed direction.

$$\underline{R} = (R_0, \underline{R})$$

$$R_0 = \cos C\pi/2$$

$$\underline{R} = (\sin C\pi/2) \underline{S}_{ST}$$

C = random uniformly distributed number

A value for C is supplied by a uniform distribution random number generator such that $0 \leq C \leq 1$; therefore, $0 \leq C\pi \leq \pi$.

$$\underline{V} = \underline{R} * \underline{V} \underline{R}$$

- (3) Compute the magnitude of the bias quaternion.

$$QB = (QB_0, \underline{QB})$$

$$QB_0 = \cos (E * BIAS/2)$$

$$\underline{QB} = \{ \sin (E * BIAS/2) \} \underline{V}$$

BIAS = RSS of the star tracker 1σ bias errors

E = random normally distributed number

The value of E is supplied by a normal distribution random number generator such that $-3 \leq E \leq +3$; therefore,

$$-3 * BIAS \leq E * BIAS \leq +3 * BIAS.$$

4. Add the bias for this set of sightings to the actual line of sight (block 4, fig. 5-3).

$$\underline{S}_b = QB * \underline{S}_{ST} QB$$

5. Compute the random error quaternion for this individual sighting.

- (1) Construct the random error quaternion so that it is perpendicular to the vector \underline{S}_b and parallel to the X-Y plane.

$$\underline{V} = \text{UNIT} (\underline{S}_b \times \underline{i})$$

- (2) Compute the direction of the random error quaternion and rotate it about the line of sight \underline{S}_b by an amount equal to the computed direction.

$$R = (R_o, \underline{R})$$

$$R_o = \cos C\pi/2$$

$$\underline{R} = (\sin C\pi/2) \underline{S}_b$$

C = random uniformly distributed number

$$\underline{V} = R * \underline{S}_b R$$

- (3) Compute the magnitude of and form the random error quaternion.

$$QE = (QE_o, \underline{QE})$$

$$QE_o = \cos (E * \text{ERROR}/2)$$

$$\underline{QE} = \{\sin (E * \text{ERROR}/2)\} \underline{V}$$

ERROR = RSS of the 10 star tracker random errors

E = random normally distributed number

- i. Add the random error for this sighting (block 5).

$$\underline{S}_m = QE * \underline{S}_b QE$$

The vector \underline{S}_m points in the simulated star tracker sensed direction of the star or target being tracked. This line-of-sight vector is converted into the equivalent star tracker output angles in block 6 using the appropriate equations presented in section 5.2.

5.4 ERROR SOURCES AND CONSTRAINT VALUES

The star tracker bias error is listed in table 5-I. This error is modeled by the nonvarying star tracker to navigation base misalignment quaternion. The star tracker measurement random error sources and the measurement bias sources are also listed in table 5-I. Table 5-II gives representative values for $(TNS)_{ideal}$, which are the I_LOAD navigation base to star tracker transformations.

TABLE 5-I.- STAR TRACKER MISALIGNMENT AND STAR SIGHTING ERRORS

Star tracker alignment uncertainty (1σ)		
Star tracker to navigation base misalignment	ω_x	22.8 $\widehat{\text{sec}}$
	ω_y	22.8 $\widehat{\text{sec}}$
	ω_z	20.6 $\widehat{\text{sec}}$
Star sighting errors (2-axis, 1σ)		
Random star position errors (ERROR)	-	15.0 $\widehat{\text{sec}}$
Star sighting biases (BIAS)		60.0 $\widehat{\text{sec}}$

TABLE 5-II.- IDEAL NAVIGATION BASE TO STAR TRACKER TRANSFORMATIONS

Ideal navigation base to -Z star tracker transformation

<u>Component</u>	<u>Values</u>
1,1	-0.0056491
1,2	.9994101
1,3	-.0338744
2,1	.9894338
2,2	.0006786
2,3	-.1449833
3,1	-.1448747
3,2	-.0343355
3,3	-.9888540

Ideal navigation base to -Y star tracker transformation

<u>Component</u>	<u>Values</u>
1,1	-0.9662658
1,2	-.1833851
1,3	.1808317
2,1	-.1839513
2,2	.0000000
2,3	-.9829353
3,1	.1802558
3,2	-.9830411
3,3	-.0337339

5.5 REFERENCES

- 5-1 Star Tracker Subsystem Operating Program. Rockwell International (Downey), July 1, 1977.
- 5-2 Kotrc, V. L.: Star Tracker, Space Shuttle Orbital Vehicle BBRC Model No. SE030A. Ball Brothers Research Corporation, September 11, 1975.
- 5-3 Space Shuttle Star Tracker/Light Shade Preliminary Design Review. Ball Brothers Research Corporation, October 7, 1975.
- 5-4 Corson, R. W.: Star Tracker Hardware Math Model. MDTSCO-HAD WP #E914-8A/B-020, February 25, 1977.
- 5-5 Lui, O. Y; and Blucker, T. J.: Shuttle Star Tracker Math Model. JSC IN 74-FM-39, May 31, 1974.

6.0 CREW OPTICAL ALINEMENT SIGHT

6.1 GENERAL DESCRIPTION

The Shuttle crew optical alinement sight (COAS) is an optical sighting instrument that will be used to provide both backup IMU platform alinement and rendezvous vehicle tracking capability. Since the operation of the Shuttle star trackers requires a reasonably well known IMU reference, the COAS will be used when the orientation of all three IMU platforms is unknown. The COAS must also be used in the event of double star tracker failure. The COAS instrument can be mounted in two different locations. When mounted at the forward windows its line of sight is in the +X body axis direction, and when installed at the rendezvous window it points in the direction of the Shuttle -Z body axis.

To use the COAS for the purpose of IMU alinement, the crewman must first execute the COAS sighting software via a keyboard entry item. The crewman also inputs the identification number of the star to be sighted and the identity of the COAS instrument being used. He then maneuvers the vehicle so that the selected star is centered in the reticle of the appropriate COAS instrument. When the crewman is satisfied that the star is sufficiently centered he takes a mark by depressing a hardware mark button (ADI attitude reference button). When the mark is taken, the onboard Shuttle software computes a line-of-sight vector to the star in IMU platform coordinates based on the calibrated COAS pointing direction and IMU attitude information. After sighting data have been taken for two stars the orientation of the IMU platform with respect to the M50 coordinate system can be determined.

Rendezvous vehicle tracking using the COAS is performed in a similar manner. In this case, however, a pair of COAS calibration angles and vehicle body attitude

~~PRECEDING PAGE BLANK NOT FILMED~~

information at mark time are provided for incorporation into the onboard rendezvous navigation filter for use in relative state estimation.

Before the COAS instrument can be used for star or target sighting, its pointing direction in both navigation base and body coordinates must be accurately determined or calibrated. This must be done while the IMU is accurately aligned. The crewman executes the COAS calibration software and inputs the COAS instrument identity and the identity of the star to be sighted. When the mark is taken on the selected star the onboard Shuttle software computes a line of sight for the COAS in both navigation base and body coordinates, based on the known IMU reference and the known position of the star. The COAS calibration will nominally be performed for each COAS instrument as soon as is practical after orbital insertion. This ensures that the COAS is calibrated before any possible IMU or star tracker failures. Furthermore, the quality of the IMU alignment is maximum at this time.

6.2 SIMULATION APPROACH

The functional block diagram in figure 6-1 illustrates the method used in the simulation of the COAS instrument. The diagram describes not only the functions performed by the COAS error model but also those functions performed by an IMU model and onboard flight software. (Note that the COAS model alone is not sufficient for generating simulated COAS measurements since the model merely defines the body attitude at mark time.) In the following subsections the COAS model and the onboard software will be discussed separately. The IMU model is described in section 2.0.

6.2.1 COAS Model

- a. S, the unit line-of-sight vector of the star to be sighted in M50 coordinates
- b. T, the unit line-of-sight vector of the rendezvous target in M50 coordinates
- c. C, the actual COAS unit line-of-sight vector in the vehicle body coordinates (one per COAS mounting location)
- d. (TEI), the ecliptic-to-M50 transformation matrix at the time of the sighting mark
- e. GAMMA, the longitude of the Sun at the sighting mark time

If simulated measurements for a star are desired, the first step is to adjust the line of sight of the star to simulate the effect of stellar aberration (fig. 6-1, block 1). These phenomena result in a shift in the observed line of sight of a star due to the relative differences between the velocity of the observer

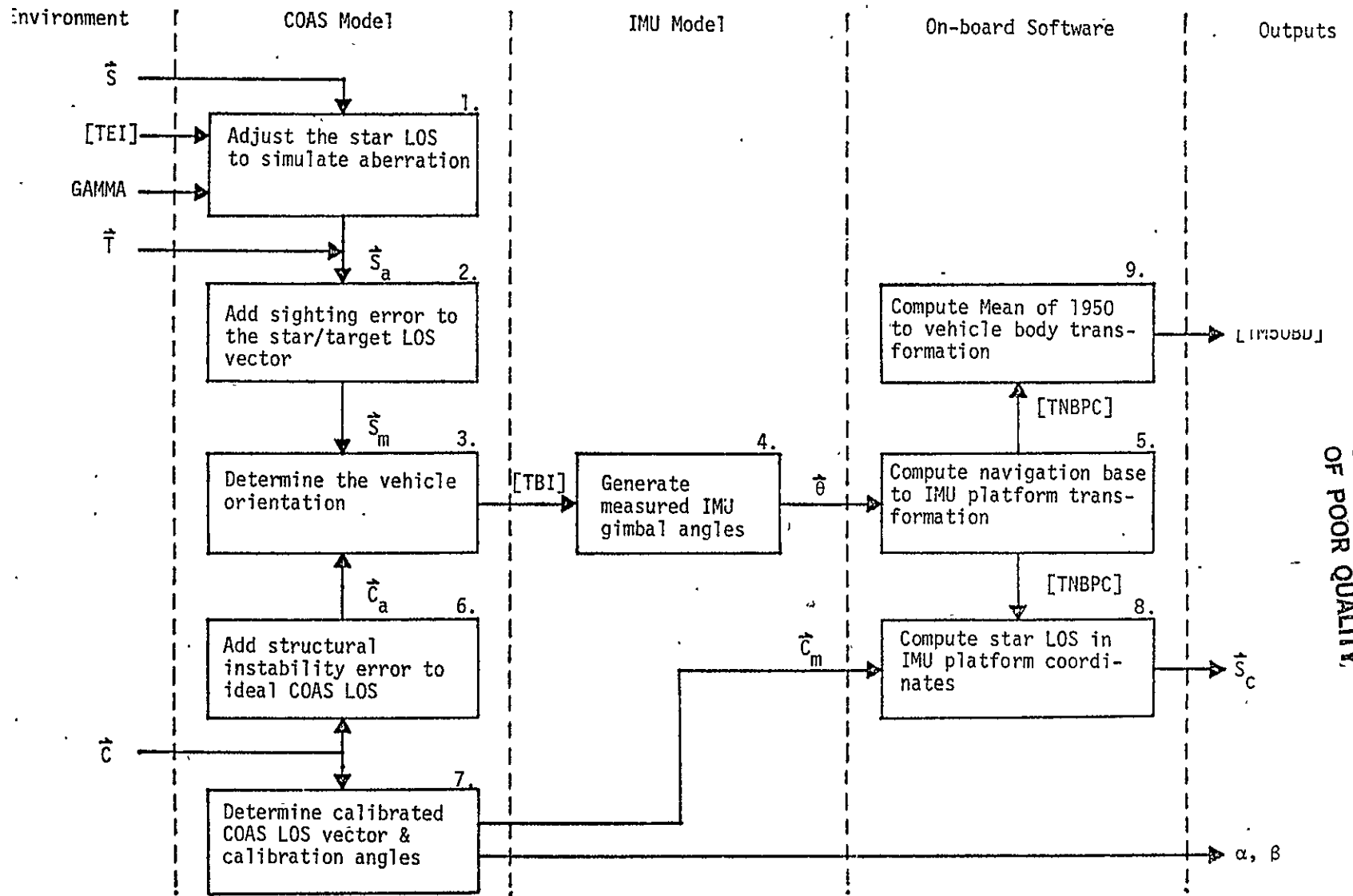


Figure 6-1.- COAS sighting functional block diagram.

6-4

ORIGINAL PAGE IS
OF POOR QUALITY.

and the velocity of the light from the star. The apparent shift is in the direction of the velocity of the observer. If the rendezvous vehicle is being sighted this step need not be performed.

The equations necessary for computing and adding the aberration correction are presented in section 5.2. The error model (block 2) then computes and adds error to the star or target line of sight yielding a measured star line of sight in M50 coordinates, \underline{S}_m .

In order to generate IMU gimbal angles at the mark time the vehicle body orientation must be determined at that time (block 3). This involves a vehicle maneuver to align the COAS instrument with the measured star line of sight. The maneuver can be simulated as a body rotation about a single axis until the measured star line of sight is colinear with the actual COAS pointing direction vector. The two line-of-sight vectors are first rotated into a common coordinate frame.

$$\underline{S}_B = (TIB) \underline{S}_m$$

\underline{S}_B = measured star line of sight in body coordinates

(TIB) = M50 to vehicle body transformation matrix at mark time

$$\underline{C}_B = (TBN)^T \underline{C}_a$$

\underline{C}_B = actual COAS pointing direction vector in body coordinates

(TBN) = actual vehicle body to navigation base transformation

\underline{C}_a = actual COAS pointing direction vector in navigation base coordinates computed from the ideal COAS line of sight by the error model (block 6)

The axis of rotation is perpendicular to both \underline{S}_B and \underline{C}_B .

$$\underline{R} = \text{UNIT} (\underline{C}_B \times \underline{S}_B)$$

R = unit vector parallel to the axis of rotation

The M50 to vehicle body transformation at the sighting mark time is, therefore,

$$(TIB) = (\underline{C}_B \ : \ \underline{R} \ : \ (\underline{C}_B \times \underline{R})) (\underline{S}_B \ : \ \underline{R} \ : \ (\underline{S}_B \times \underline{R}))^T (TIB)$$

With the M50 to vehicle body transformation matrix at mark time, IMU gimbal angles can be generated by using the IMU model (sec. 2.0, block 4).

The calibrated COAS line of sight and the COAS calibration angles must also be generated for Shuttle software use (block 7, fig. 6-1). The computations performed in block 7 need only be executed once per single mission simulation to model the COAS calibration error. The simplest and most straightforward method for modeling the calibration error is to actually simulate the COAS calibration process. This is accomplished by using the COAS model and the onboard calibration software (fig. 6-2).

6.2.2 Onboard COAS Software

The previous section described how the COAS model produces a definition of body attitude at mark time and the simulated COAS calibrated line of sight. The body attitude information, in conjunction with the IMU model (sec. 2.0), can be used to generate simulated measured IMU gimbal angles. This section will describe how the IMU and calibration data are used by the onboard software to produce measurement parameters that can be used by either IMU alinement or rendezvous navigation simulations.

Simulated IMU gimbal angles are used to compute the navigation base to IMU platform transformation at the mark time. The direction of the COAS line of sight in navigation base coordinates will have been previously determined for each COAS location; therefore, a line-of-sight vector to the star in IMU coordinates can be computed (block 8, fig. 6-1).

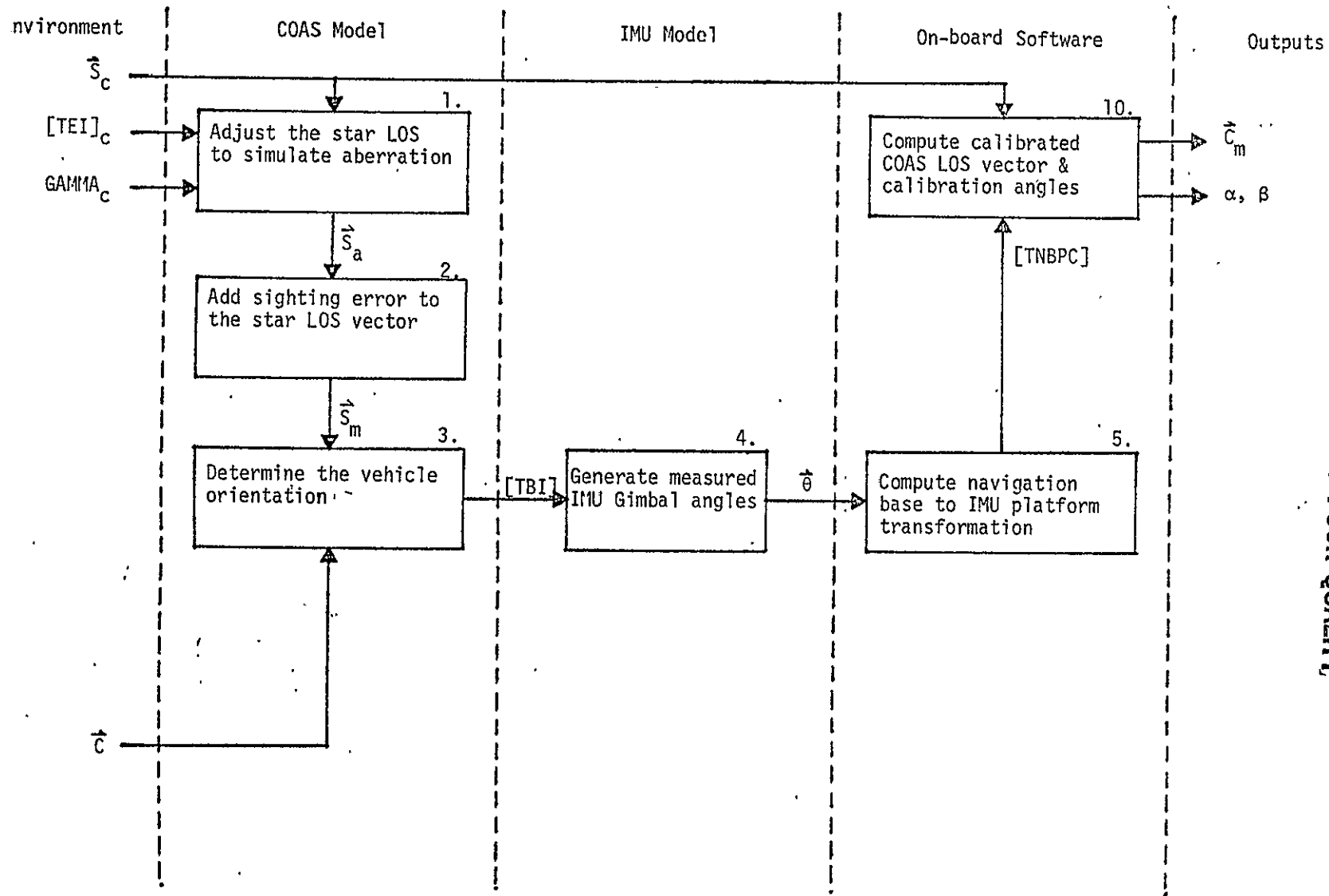


Figure 6-2.- COAS calibration functional block diagram.

6-8

C-2

ORIGINAL PAGE IS
OF POOR QUALITY

$$\underline{S}_C = (TNBPC)\underline{C}_m$$

\underline{S}_C = measured star line-of-sight vector in IMU platform coordinates

$(TNBPC)$ = navigation base to IMU cluster transformation matrix at mark time

\underline{C}_m = calibrated COAS line-of-sight vector in navigation base coordinates

The navigation base to IMU cluster transformation matrix at mark time is computed by the equation for $(TNBPC)$ (sec. 5.1.3-a, block 5, fig. 6-1); however, in this case the IMU gimbal angles at mark time are used rather than averaged gimbal angles.

In order to simulate rendezvous sighting data the gimbal angle information is used to compute an equivalent mean of 1950 to vehicle body transformation (block 9, fig. 6-1).

$$(TM50BD) = (TNBBD)\{(TCM50) (TNBPC)\}^T$$

$(TNBPC)$ = Navigation base to selected IMU cluster transformation matrix at mark time

$(TCM50)$ = IMU cluster to mean of 1950 reference transformation (constant)

$(TNBBD)$ = Navigation base to vehicle body coordinate transformation (constant)

$(TM50BD)$ = Mean of 1950 to vehicle body transformation.

The navigation base to selected IMU cluster transformation matrix at mark time is computed by the equation for $(TNBPC)$ (sec. 5.1.3-a) using the IMU gimbal angles at mark time instead of averaged gimbal angles. The mean of 1950 to vehicle body transformation matrix, a pair of COAS calibration angles in body

coordinates, and the COAS identity can then be provided for incorporation into the rendezvous navigation filter for use in relative state estimation.

One final software task is the computation of the aforementioned COAS calibration angles and the calibrated COAS unit line-of-sight vector. The calibrated COAS unit line-of-sight vector in navigation base coordinates is computed in block 10 of figure 6-2.

$$\underline{C}_m = (\text{TNBPC})^T (\text{TCM50})^T \underline{S}_c$$

\underline{S}_c = selected star unit line-of-sight vector in M50 coordinates

(TCM50) = IMU cluster to M50 reference transformation matrix

(TNBPC) = navigation base to IMU transformation matrix

\underline{C}_m = calibrated COAS line of sight in navigation base coordinates

The navigation base to selected IMU cluster transformation matrix at mark time is computed by the equation for (TNBPC) (sec. 5.1.3-a) using the IMU gimbal angles at mark time in place of averaged gimbal angles. COAS calibration angles in vehicle body coordinates are also computed for the rendezvous navigation filter (block 10, fig. 6-2).

$$\underline{C}_e = (\text{TNB}) \underline{C}_m$$

(TNB) = navigation base to vehicle body transformation

$$\alpha_{-z} = -\tan^{-1} (C_{e2}/-C_{e3})$$

$$\beta_{-z} = \tan^{-1} (C_{e1}/C_{e3})$$

$$\alpha_{+x} = \tan^{-1} (C_{e2}/C_{e1})$$

$$\beta_{+x} = -\tan^{-1} (C_{e3}/C_{e1})$$

6.3 ERROR MODEL

6.3.1 Sighting Error

The COAS instrument sighting error model generates a simulated measured line-of-sight vector by adding error to the apparent star or target line of sight. This model adds error to a line of sight by rotating it in a parallel plane by an amount equal to the error. The amount of rotation is computed from a normally distributed random number, the direction of rotation is determined by a uniformly distributed random number, and the actual rotation is performed by vector quaternion multiplication. This method of adding on the error assumes that the random error is both Gaussian in distribution and isotropic.

The following is a detailed description of the computations used in block 2 of figure 6-1.

a. Compute the random error quaternion for this sighting.

- (1) Construct the error quaternion so that it is perpendicular to the vector \underline{S}_a and parallel to the X - Y plane.

$$\underline{V} = \text{UNIT} (\underline{S}_a \times \underline{i})$$

- (2) Compute the direction of the error quaternion and rotate it about the line of sight \underline{S}_a by an amount equal to the computed direction.

$$R \equiv (R_0, \underline{R})$$

$$R_0 = \cos d\pi/2$$

$$\underline{R} = (\sin d\pi/2) \underline{S}_a$$

$d \equiv$ random uniformly distributed number

A value for d is supplied by a uniform distribution random number generator such that $0 < d < 1$; therefore, $0 < d\pi < \pi$.

$$\underline{V} = R * \underline{V} R$$

(3) Compute the magnitude of and form the error quaternion.

$$Q \equiv (Q_0, \underline{Q})$$

$$Q_0 = \cos (e * \text{ERROR}_0 / 2)$$

$$\underline{Q} = \{ \sin(e * \text{ERROR}_0 / 2) \} \underline{V}$$

$\text{ERROR}_0 \equiv 1\sigma$ COAS instrument random error

$e \equiv$ random normally distributed number

The number, e , is supplied by a normal distribution random number generator such that $-3 < e < +3$; therefore,

$$-3 * \text{ERROR}_0 < e * \text{ERROR}_0 < +3 * \text{ERROR}_0.$$

b. Add the random error for this sighting

$$\underline{S}_m = Q * \underline{S}_a Q$$

The vector \underline{S}_m points in the simulated measured direction of the star or target being sighted.

6.3.2 Structural Instability Error

After the COAS has been calibrated, its line of sight in body coordinates will change due to random structural instabilities. This COAS mounting uncertainty is modeled using the same method that is used for adding the sighting error to a star line of sight. The following is a brief description of the computations performed in block 6 of figure 6-1.

a. Compute the COAS mounting uncertainty error quaternion.

- (1) Construct the error quaternion so that it is perpendicular to the vector \underline{C} and parallel to the body X-Y plane.

$$\underline{V} = \text{UNIT} (\underline{C} \times \underline{i})$$

- (2) Compute the direction of the error quaternion and rotate it about the ideal COAS line of sight, \underline{C} , by an amount equal to the computed direction.

$$R \equiv (R_0, \underline{R})$$

$$R_0 = \cos d\pi/2$$

$$\underline{R} = (\sin d\pi/2) \underline{C}$$

$d \equiv$ random uniformly distributed number

$$\underline{V} = R * \underline{V} R$$

- (3) Compute the magnitude of and form the error quaternion.

$$Q \equiv (Q_0, \underline{Q})$$

$$Q_0 = \cos (e * \text{ERROR}_1/2)$$

$$\underline{Q} = \sin (e * \text{ERROR}_1/2) \underline{V}$$

$\text{ERROR}_1 \equiv 1 \sigma$ COAS mounting uncertainty due to random structural instabilities

$e \equiv$ random normally distributed number

b. Add the error to the ideal COAS line of sight vector.

$$\underline{C}_a = Q * \underline{C} Q$$

The vector \underline{C}_a defines the actual pointing directions of the COAS instrument in vehicle body coordinates.

6.4 ERROR SOURCES AND CONSTRAINT VALUES

The sources of COAS measurement error are listed below.

- a. COAS sighting error
- b. COAS calibration error
- c. COAS mounting uncertainty
- d. IMU error
- e. IMU mounting uncertainty

The IMU errors are a subject of the IMU model description presented in section 2.0. Of the remaining three, two of them are modeled by the algorithms described in section 6.3. These two sources, the sighting error and the mounting uncertainty, have the following 1 sigma values (ref. 6-3).

$$\text{COAS sighting error} \equiv \text{ERROR}_0 = 110 \widehat{\text{sec}}$$

$$\text{COAS mounting uncertainty} \equiv \text{ERROR}_1 = 76 \widehat{\text{sec}}$$

As stated previously the calibration error can be modeled by actually performing a simulated COAS calibration (note that the calibration error is, therefore, a function of all of the following error sources):

- a. COAS sighting error
- b. Random IMU error
- c. IMU error due to drift
- d. IMU mounting misalignment error

6.5 REFERENCES

- 6-1 Corson, R. W.: Shuttle Star Tracker Subsystem Operating Program Crew Optical Alignment Sight (COAS) Simulation. JSC IN 76-FM-41, June 18, 1976.
- 6-2 Star Tracker Subsystem Operating Program. Rockwell International (Downey) July 1, 1977.
- 6-3 Holloway, T. W.: On-Orbit Flight Techniques Meeting #27 Minutes. NASA Memorandum CA5-78-48, August 31, 1978.

7.0 RENDEZVOUS RADAR

7.1 GENERAL DESCRIPTION

The Ku-band radar/communication system is a dual-purpose Orbiter subsystem that is used during orbital operations. It functions as either a wideband communications system for data interchange with the ground or as a rendezvous radar to detect and track detached payloads or other spacecraft before or during rendezvous maneuvers. The functions of communications and radar are not available simultaneously.

The rendezvous radar provides automatic target detection, acquisition, and tracking. It is a target location and parameter estimation device that assists the navigation filter in reducing target location uncertainties during rendezvous maneuvers. The targets are Earth-orbiting satellites that are stabilized in three axes. The radar tracks a target automatically and supplies range, range rate, radar shaft (roll) and trunnion (pitch) angles, and inertial angle rates to both the navigation filter and the crew displays. All output parameters are provided simultaneously during the tracking phase. External assistance and operator intervention are normally required only for functions that initiate the radar search operation.

Upon the initiation of search, the radar performs automatic search about a direction (vector) furnished to the radar by the GPC and indicates that search is in progress for a maximum of 1 minute. If target detection occurs, the search program stops, the search indication is removed, and the radar indicates that detection has occurred.

~~PRECEDING PAGE BLANK NOT FILLED~~

The radar operates in two main modes: passive (no transponder on target vehicle) and cooperative (transponder operating). The range of the unit is enhanced by a factor of 25 when in the cooperative mode, as well as increased measurement limits, while the error characteristics remain essentially the same.

7.2 SIMULATION APPROACH

The functional block diagram in figure 7-1 illustrates the method used in the simulation of the rendezvous radar hardware. It is assumed that the following five inputs are available from an environment simulation.

- a. R_S = Shuttle Orbiter position vector in M50 coordinates
- b. V_S = Shuttle Orbiter velocity vector in M50 coordinates
- c. R_R = rendezvous vehicle position vector in M50 coordinates
- d. V_R = rendezvous vehicle velocity vector in M50 coordinates
- e. (TIB) = M50 to Shuttle vehicle body transformation matrix

The following discussion summarizes the computations performed in each of the blocks in the radar model functional block diagram (fig. 7-1).

- a. Block 1 - compute the Shuttle relative position and velocity vectors of the rendezvous vehicle in the mean of 1950 coordinate system.

$$\underline{R} = \underline{R}_R - \underline{R}_S \qquad \underline{V} = \underline{V}_R - \underline{V}_S \quad \text{---}$$

\underline{R} = rendezvous vehicle position vector relative to the Shuttle in M50 coordinates

\underline{V} = Shuttle-relative rendezvous vehicle velocity vector in M50 coordinates

- b. Block 2 - compute the mean of 1950 to radar sensor coordinate transformation, (TIS).

$$(TIS) = (TBS) (TIB)$$

(TBS) = Shuttle body to radar sensor coordinate transformation

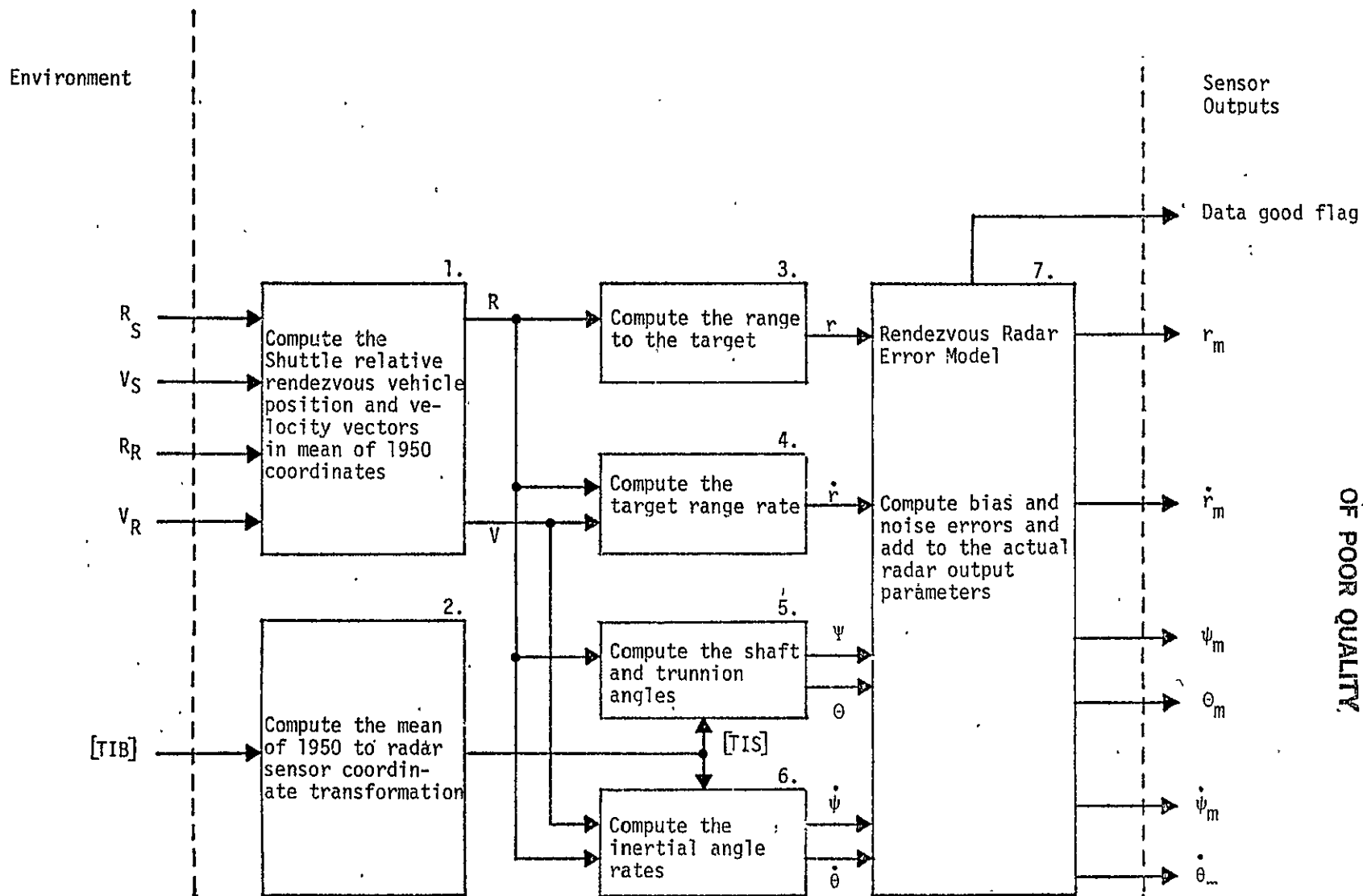


Figure 7-1.- Rendezvous radar model functional block diagram.

The rendezvous radar coordinate system is oriented with respect to the Shuttle body as illustrated in figure 7-2, and the body to radar sensor transformation matrix is defined as

$$(TBS) = \begin{bmatrix} 0 & 0 & -1 \\ 0 & 1 & 0 \\ 1 & 0 & 0 \end{bmatrix}$$

c. Block 3 - compute the target range, r .

$$r = |\underline{R}|$$

d. Block 4 - compute the target range rate, \dot{r} . The range rate is the component of \underline{V} that is parallel to \underline{R} ; therefore,

$$\dot{r} = (\underline{R} \cdot \underline{V})/r$$

Extract the directions of the radar sensor system coordinate axis, X, Y, and Z, from the M50 to sensor transformation.

$$\begin{pmatrix} X \\ Y \\ Z \end{pmatrix} = (TIS)^T$$

Compute the component of the range vector, \underline{R} , that is perpendicular to the radar shaft axis (fig. 7.3).

$$\underline{P} = \underline{R} - \underline{Z} (\underline{Z} \cdot \underline{R})$$

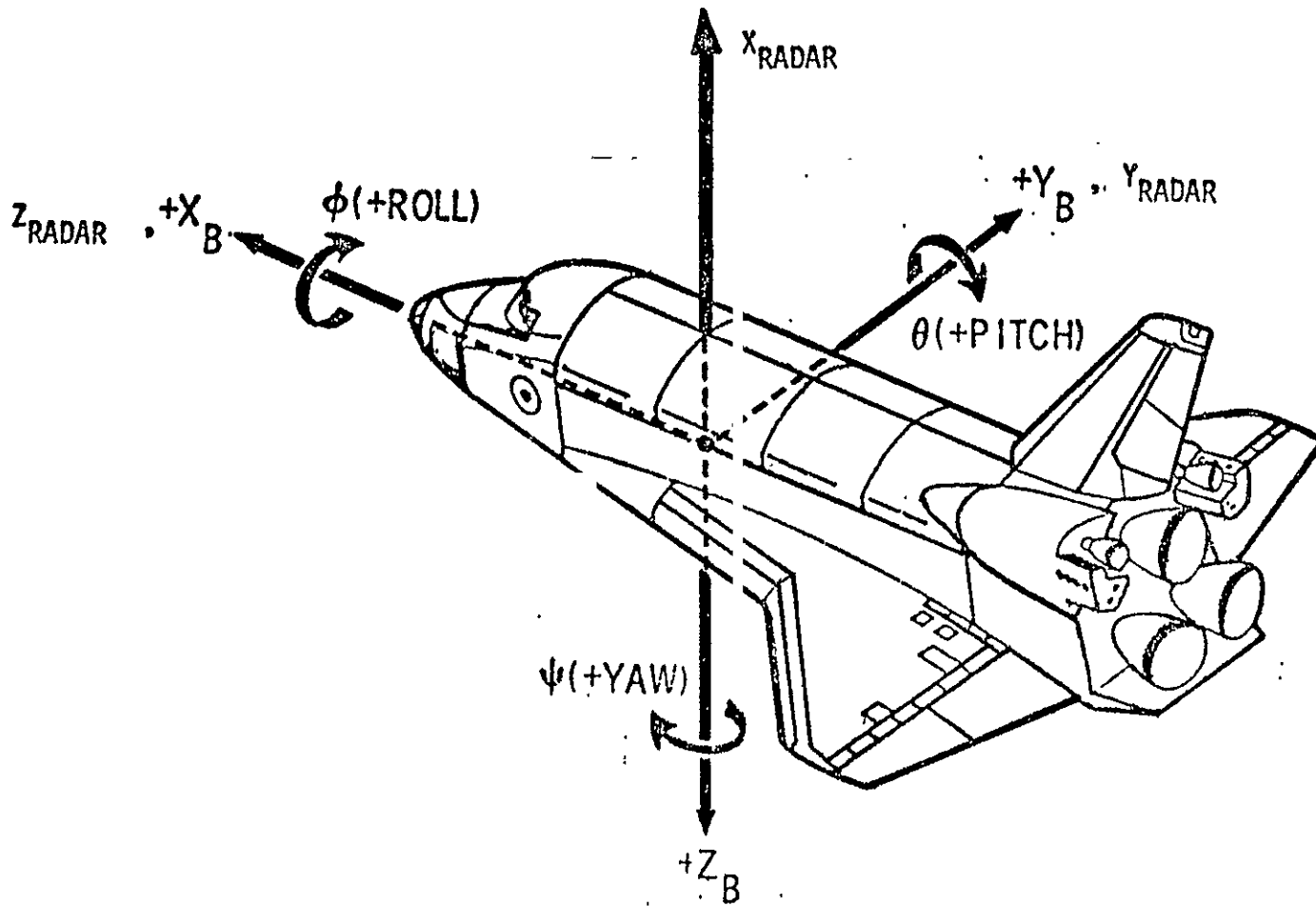
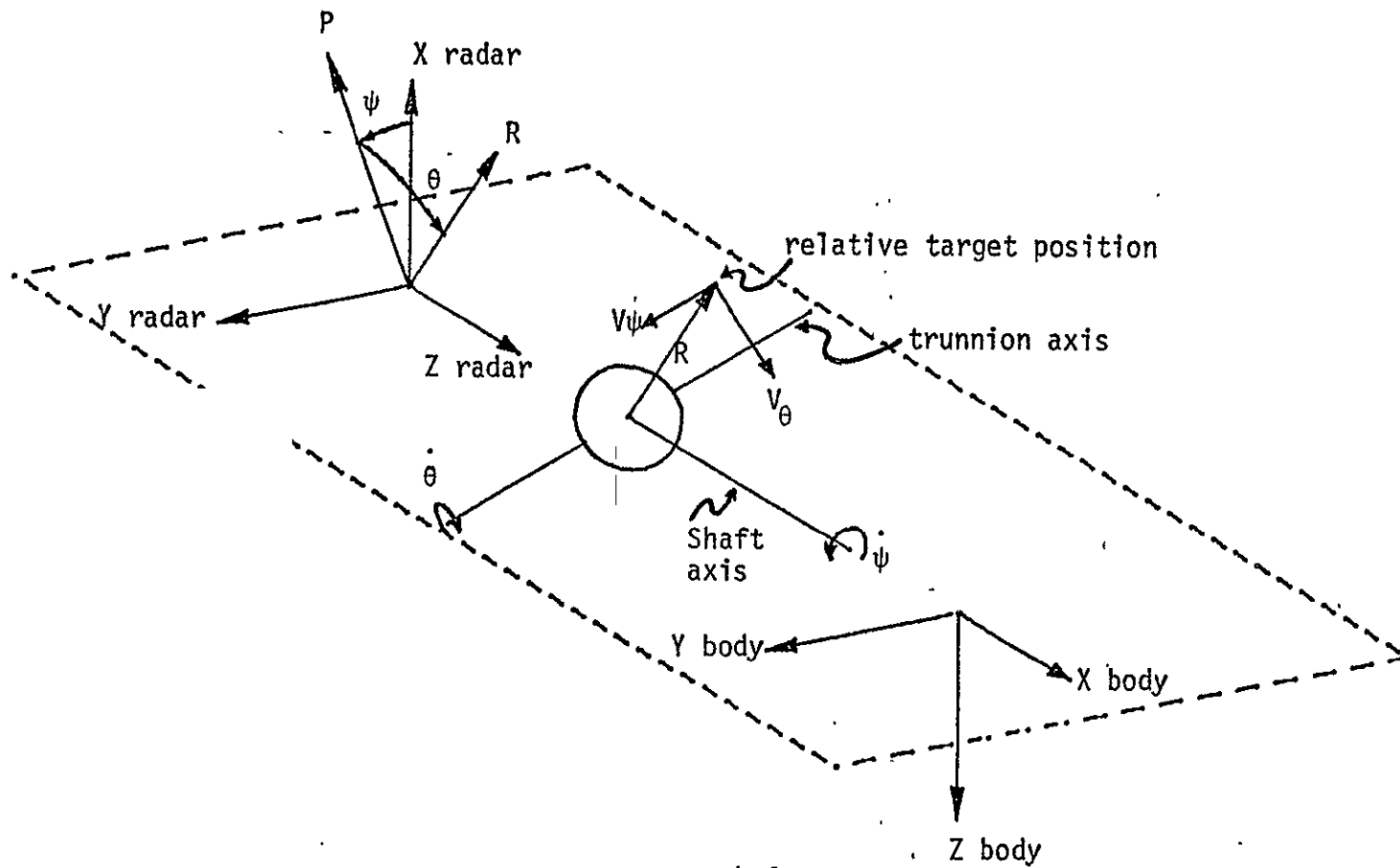


Figure 7-2.- Orbiter body coordinate system and rendezvous radar coordinate system.

ORIGINAL PAGE IS
OF POOR QUALITY



ORIGINAL PAGE IS
OF POOR QUALITY

Figure 7-3.- Rendezvous radar parameter geometry.

- e. Block 5 - compute the shaft angle, Ψ , and the trunnion angle, Θ . The tangent of the shaft angle is simply the component of the range vector parallel to the sensor Y-axis divided by the component of the range vector parallel to the sensor X-axis; therefore,

$$\Psi = \tan^{-1} \{ (\underline{R} \cdot \underline{Y}) / (\underline{R} \cdot \underline{X}) \}$$

Similarly, the tangent of the trunnion angle is the component of the range vector parallel to the sensor Z-axis divided by the component of the range vector parallel to the perpendicular, \underline{P} .

$$\Theta = \tan^{-1} \{ |\underline{P}| (\underline{R} \cdot \underline{Z}) / (\underline{R} \cdot \underline{P}) \}$$

- f. Block 6 - compute the inertial roll rate, $\dot{\Psi}$, and the inertial pitch rate, $\dot{\Theta}$. The roll rate is equivalent to the component of the relative velocity vector perpendicular to both \underline{R} and \underline{Z} divided by the length of the perpendicular \underline{P} .

$$\dot{\Psi} = \{ \underline{V} \cdot (\underline{Z} \times \underline{R}) \} / (\underline{P} \cdot \underline{P})$$

Similarly, the pitch rate is equal to the component of the velocity vector that is perpendicular to both the range vector and the trunnion axis divided by the magnitude of the range; therefore,

$$\dot{\Theta} = \underline{V} \cdot \{ \underline{R} \times (\underline{Z} \times \underline{R}) \} / (\underline{R} \cdot \underline{R} |\underline{P}|)$$

g. Block 7 - Rendezvous radar error model. Once the measurements have been computed they must be tested to ensure that they are realistic with respect to the limits of the instrument. If any measurement is bad (i.e., violates the constraints listed in table 7-I), then all measurements are bad and the output data good flag is set to low or zero. This occurs with the rendezvous radar since all measurements depend on having lock on the target. The ideal radar output parameters are then corrupted using the equations in section 7.3.

7.3 ERROR MODEL

The computation of errors is divided into two parts. At the beginning of each phase (and only then) the random bias for each measurement type is computed. The form of this computation is

$$\text{RANDOM NUMBER} * 1\text{-SIGMA BIAS} = \text{RANDOM BIAS}$$

where the random number is Gaussian with zero mean and standard deviation of 1.

The noise is computed every pass through the model, and follows the same formula:

$$\text{RANDOM NUMBER} * 1\text{-SIGMA NOISE} = \text{RANDOM NOISE}$$

The 1-sigma values of noise and bias are selected and/or computed according to the requirements shown in table 7-II.

The data shown are the current requirements. All 1-sigma values are constant over the measurement interval except range noise, which is range dependent.

Depending on whether the range is greater or less than a predetermined "gate" value, the range noise is either a percentage of the range or a fixed value, whichever is greater.

The noise and bias are added to each ideal rendezvous radar output to simulate the corrupted measurement.

$$q_m^i = q^i + \beta^i + \eta^i$$

$$q_m^i = i^{\text{th}} \text{ measured radar output parameter}$$

q^i = i^{th} actual radar parameter

β^i = bias for i^{th} radar measurement parameter

η^i = computed noise on the i^{th} radar measurement parameter

7.4 ERROR SOURCES AND CONSTRAINT VALUES

The radar parameter measurement limit requirements for the Orbiter rendezvous radar are listed in table 7-I. These limits are functions of both hardware and physical limitations. The maximum range is a function of energy output and thus is constrained by the size, weight, and power requirements of the unit. The minimum range is due to secondary reflections caused by echoes from the primary vehicle. The angle and angle rate constraints are due to limits on gimbal travel, travel rates during tracking, and time constraints placed on the acquisition of the target during the acquisition mode. (It should be noted that the angle rate constraint is tested by components, not by root sum squared, since the azimuth and elevation angle gimbals are independent.) Range rate is constrained by the pulsing frequency of the radar (rate at which it receives and processes information).

The radar parameter measurement error requirements are presented in table 7-II.

TABLE 7-I.- RADAR PARAMETER MEASUREMENT LIMITS

Parameter	Passive mode	Active mode
LOS range	100 ft (30 m) to 10 n. mi. (19 km)	100 ft (30 m) to 300 n. mi. (560 km)
LOS range rate	148 ft/sec (45 m/sec) closing, 75 ft/sec (23 m/sec) opening	1500 ft/sec (457 m/sec) closing, 300 ft/sec (91 m/sec) opening ^a
LOS pitch angle (relative to Orbiter minus-Z axis) ^b	Plus or minus 30 deg	Plus or minus 30 deg
LOS roll angle (relative to Orbiter minus-Z axis) ^b	Same as pitch	Same as pitch
Pitch inertial angle rate	Plus or minus 20 mr/sec	Plus or minus 20 mr/sec
Roll inertial angle	Same as pitch	Same as pitch

^aThe LOS range rate limits versus range shall be as follows:

1500 ft/sec closing, 300 ft/sec opening at 300 n. mi.
700 ft/sec closing, 300 ft/sec opening at 200 n. mi.
300 ft/sec closing, 300 ft/sec opening at 100 n. mi.
200 ft/sec closing, 300 ft/sec opening at 50 n. mi.
148 ft/sec closing, 75 ft/sec opening at 10 n. mi. to 100 ft.

^bAngle measurements capability shall be maintained over the full coverage capability of the antenna with accuracy degraded to levels no less than the equivalent of communication angle measurement accuracy.

TABLE 7-II.- RADAR PARAMETER ALLOWABLE MEASUREMENT ERRORS

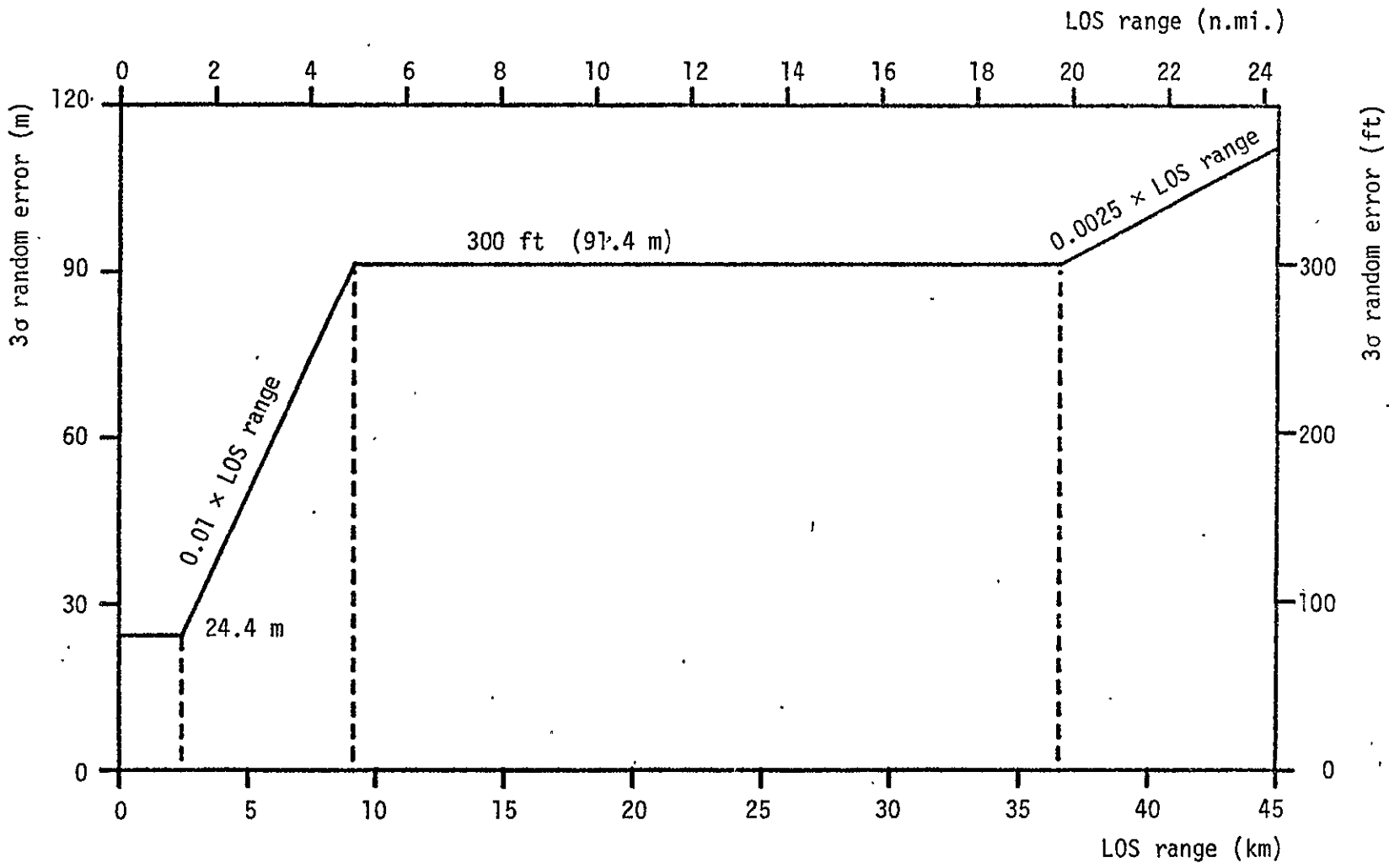
Parameter	Random error (3σ)	Bias error (3σ)
LOS range	a	c
LOS range rate	1 ft/sec (0.3 m/sec) or 1 percent of range rate, whichever is greater	± 1 ft/sec (0.3 m/sec)
LOS pitch angle	8 mrad (0.458 deg)	± 3 deg ^d
LOS roll angle	8 mrad (0.458 deg)	± 3 deg ^d
Pitch inertial angle rate ^b	0.14 mrad/sec (0.008 deg/sec)	± 0.14 mrad/sec (0.008 deg/sec)
Roll inertial angle ^b	0.14 mrad/sec (0.008 deg/sec)	± 0.14 mrad/sec (0.008 deg/sec)

^aSee figure 7-4.

^bNot including target effects.

^cSee figure 7.5.

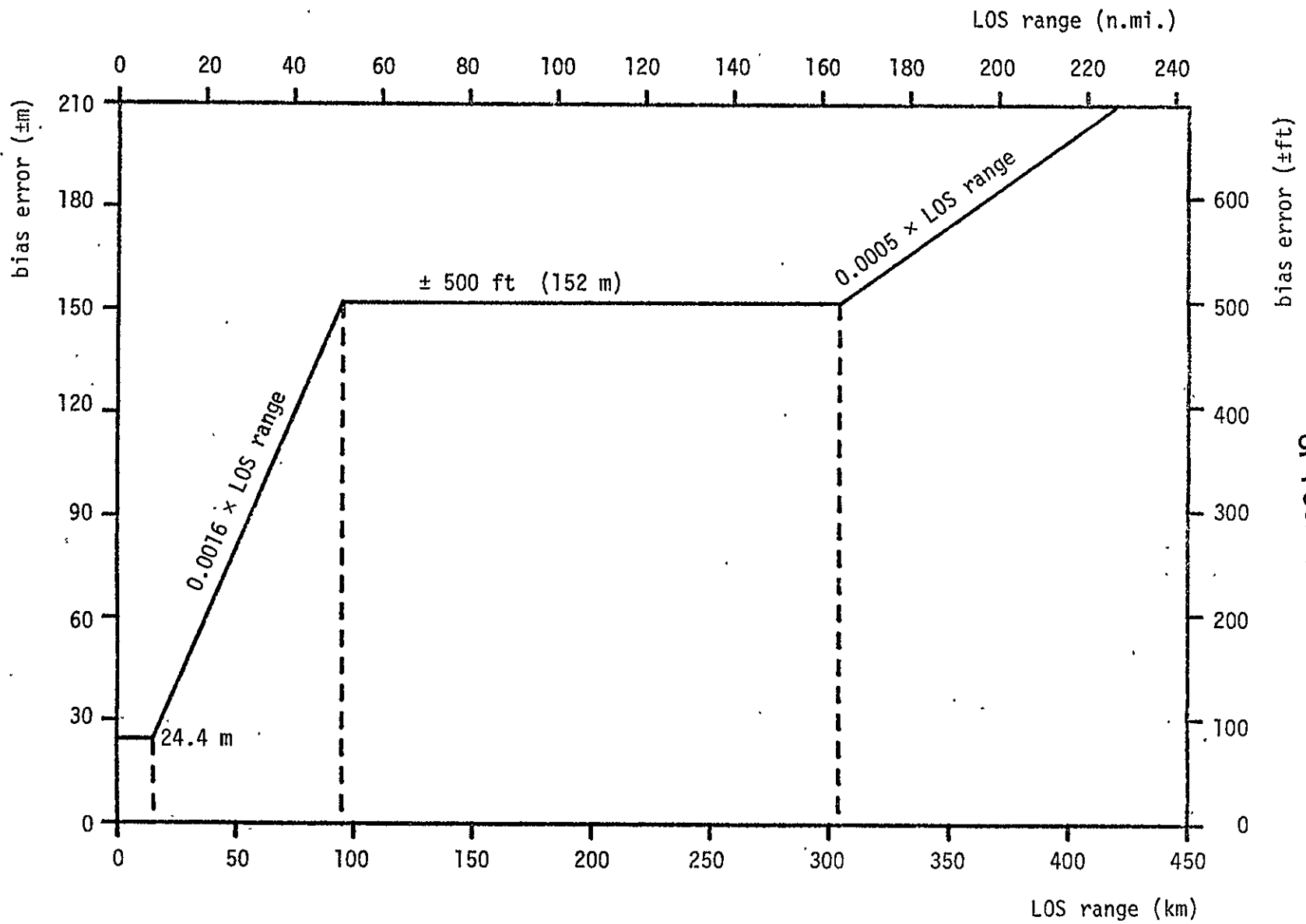
^dIncludes 2-degree requirement value plus a structural uncertainty of 1 degree.



ORIGINAL PAGE IS
OF POOR QUALITY

79FMS

Figure 7-4.- Three-sigma random range error.



ORIGINAL PAGE IS
OF POOR QUALITY

Figure 7-5.- Range bias error.

7.5 REFERENCES

- 7-1 Rendezvous Radar Subsystem Operating Program. Rockwell International (Downey), July 1, 1977.
- 7-2 Wissinger, D. B.: Proposed Design of Orbiter Rendezvous Radar Sensor Model for Use in the Space Vehicle Dynamics Simulation (SVDS) Program. MDTSCO-HAD WP#E914-9A-016, April 16, 1976.
- 7-3 Integrated Communications and Radar Equipment, Ku-Band. (Ku-Band/ Rendezvous Radar Subsystem Procurement Specification), Rockwell International (Downey), March 15, 1976.
- 7-4 Space Shuttle OFT Level C FSSR GN&C Part B, Navigation, On-Orbit. Rockwell International (Downey), October 1977.

8.0 RADAR ALTIMETER

8.1 GENERAL DESCRIPTION

The radar altimeter (RA) is a C-band altimeter system that provides a measurement of ground-relative altitude of the antenna system of an airborne vehicle from 5480 feet altitude to touchdown. The RA requires no ground station information as is the case with the other navigation sensors. The user simply applies power to the RA and the system provides altitude from the antenna to the nearest point on the terrain. Thus, the RA reads 4 ± 0.5 feet when the Orbiter's wheels are on the ground.

To obtain altitude information the airborne transmitter illuminates the terrain below the aircraft with periodic 4.3-GHz pulses. The airborne receiver then measures the time delay between transmission and the first echo received (denoted leading edge detection). The two-way propagation time is then multiplied by one-half the propagation velocity to compute the aircraft's altitude above the nearest terrain point. The altitude measurement is then sent to the onboard computer at a 6.25-Hz rate for use in guidance computations and attitude vertical velocity indicator (AVVI) processing. A repetition rate of 8.5 kHz for the transmit-receiver sequence allows the RA to track altitude change rates of up to 2000 ft/sec.

The radar altimeter will operate accurately over any terrain type that exhibits a coefficient of reflection of 0.05 or greater. The RA may, therefore, be used over water or ice as well as land. The RA may be used in heavy rainfall of up to 40 mm/hour.

~~PRECEDING PAGE BLANK NOT FILLED~~

8.2 SIMULATION APPROACH

The Shuttle radar altimeters lock on and yield valid altitude measurements at an altitude of 5480 feet. Altimeter data are not utilized, however, until the sub-Orbiter point is within a specified distance from the runway threshold. This limit, denoted R_GO_RAMP, may be found in the navigation I-load (ref. 8-6). The current value for R_GO_RAMP is 4000 feet. Assuming a 1.5-degree glide-slope after final flare, and an aim point 1500 feet beyond the runway threshold, radar altimeter data will first be incorporated in the nav. state vector sent to guidance at a nominal altitude of 144 feet ($= (1500+4000) \sin 1.5 \text{ deg}$).

After RA lockon, altitude measurements are simulated via the altitude-dependent error model (sec. 8.3).

8.3 ERROR MODEL

Radar altimeters are, in general, subject to the following four potential error sources:^a

- a. Averaging of the terrain illuminated by the EM beam
- b. Multipath effects
- c. Error in pointing of the altimeter EM beam or terrain slope
- d. Errors inherent in the altimeter measurement equipment

The technique of leading edge detection (utilized by the Space Shuttle radar altimeters) effectively eliminates the second error source. Leading edge detection yields altitude above the highest or nearest terrain point. The first and third error sources (terrain averaging and terrain slope) are not significant near airstrips where the Shuttle is likely to land. In special cases when the Orbiter makes its final approach over uneven terrain (as is the case for certain approaches to Vandenberg) it is likely that the threshold point at which RA measurements are incorporated will be moved closer to the runway threshold so that altimeter data over rough terrain will not be used.

Measurement equipment error constitutes the most significant error in the Shuttle RA system. Limited flight-test data gathered by the manufacturer

^aA fifth RA error source has emerged during the Approach and Landing Test (ALT) program. ALT free-flight test data have indicated erroneous altitude transients (from RA #1) of 45 feet when the Orbiter is below 100 feet altitude on final approach. To correct this problem for the orbital flight tests (OFT), the RA antennas will be repositioned so that interference between the two RA's and the landing gear is minimized. The error model presented here assumes that this RA altitude transient problem will be corrected for OFT.

From two altimeters flown in a C141A aircraft indicate that bias accounts for approximately 97 percent of the total RMS system error. The residual RMS system error of 25 percent ($= (100 \text{ percent}^2 - 97 \text{ percent}^2)^{1/2}$) is attributed to random noise. Radar altimeter error is modeled as follows:

$$h_c = h + b_h u_1 + \sigma_h u_2$$

where h_c is the corrupted altitude measurement

h is the true altitude of the radar altimeter antennas above the local terrain

b_h, σ_h are the 1σ bias and noise figures given in section 8.4

u_1 is a unity variance, zero-mean Gaussian random number, sampled once per flight for each altimeter

u_2 is the same as u_1 , but sampled once per measurement for each altimeter.

Finally, the altitude measurement is quantized to the nearest foot via:

$$h = 0.5 \text{ ft} + q(h_c)$$

where $q()$ is the quantization operator that truncates the argument to the least significant bit for the RA altitude word.

8.4 ERROR SOURCE VALUES

The Orbiter carries two Honeywell model HG7193C1 radar altimeters: one each in the 1 and 2 forward avionics bays. The following error model statistics are based on the Shuttle RA procurement specification (ref. 8-3).

<u>Bias (1σ):</u>	<u>Value</u>
$0 \leq h < 10$ ft	1.552 ft
$10 \leq h < 66$ ft	2.522 ft
$66 \leq h < 5476$ ft	.0291 h
<u>Noise (1σ):</u>	
$0 \leq h < 10$ ft	0.389 ft
$10 \leq h < 66$ ft	.632 ft
$66 \leq h < 5476$ ft	.0075 h
<u>Quantization</u>	
1 ft	--

8.5 REFERENCES

- 8-1 Minimum Performance Standards - Airborne Low-Range Radar Altimeters. RICA SC-102 paper 96-63/DO-123, August 15, 1963.
- 8-2 Shuttle Tracking Systems Data Packages. MSC/TCSD Document No. 1902, November 1971.
- 8-3 Altimeter, Radar. Procurement Specification #MC409-0015, January 31, 1974.
- 8-4 Space Shuttle Orbiter Radar Altimeter Handbook. Honeywell Document No. W0075-TG01-001, January 16, 1975.
- 8-5 Space Shuttle Orbital Flight Test Level C Functional Subsystem Software Requirements; Guidance, Navigation, and Control, Part E, Subsystem Operating Programs, Radar Altimeter.
- 8-6 Space Shuttle Orbital Flight Test Level C Functional Subsystem Software Requirements; Guidance, Navigation, and Control, Part B, Entry Through Landing Navigation.
- 8-7 Eckelkamp, R. E.: Test Case for OFT 1 Nominal Entry-Landing Study. NASA Memorandum FM83 (76-112), April 7, 1976.
- 8-8 Speir, R. E.: ALT Navaid Performance Vs. Expected Performance. MDTSCO TM No. 1.2-TM-C0814-117, October 6, 1977.

9.0 TACAN

9.1 GENERAL DESCRIPTION

Tacan (tactical air navigation) is a military L-band air navigation system that provides slant range and magnetic bearing from user aircraft to the ground beacon. Tacan is an internationally accepted system with over 1300 ground stations worldwide, of which over 800 are within the United States.

The user selects a desired ground beacon by tuning to one of the 126 channels in the frequency band from 1025 MHz to 1150 MHz (ref. 9-1). At intervals of 30 seconds each ground beacon broadcasts its unique station ID in audible Morse code tones to allow positive station identification by the crew of the user aircraft.

To obtain slant range information an airborne interrogator transmits a pair of pulses omnidirectionally on a specific frequency appropriate to a selected ground station, then searches for a returning pair of pulses from the ground station transponder (receiver, retransmitter) on a frequency ± 63 MHz from the interrogation frequency. The airborne unit then determines slant range distance by measuring the two-way propagation time, subtracting 50 μ sec to account for ground transponder delay, and multiplying by one-half the propagation velocity. This one-way distance is then provided to the onboard computer in units of nautical miles. The slant range function of the Tacan system is often called distance measuring equipment (DME). Each Tacan ground station can provide DME service to as many as 100 aircraft simultaneously.

Bearing information is transmitted from the ground station whether or not DME interrogation pulses are being received. The transmitted signal is a nine-lobe cardioid radiation pattern at a fixed 15 revolution/second rate. As one

~~PRECEDING PAGE BLANK NOT FILLED~~

particular lobe passes through magnetic north, a particular string of pulses (code) is transmitted. A different string is transmitted for each of the other eight lobes. Bearing is determined by the receiver by measuring the time difference between the most recent reference pulses and a signal strength maximum on the rotating cardioid of known rate. The mechanization permits a 360° bearing sector to be divided into 9 identifiable 40° sectors, for a nine-fold increase in accuracy in determining bearing as compared to single lobe systems.^a

^aIt has been shown during the Approach and Landing Test program that Tacan bearing data are subject to transitory 40° spikes. Navigation designers should know that such transients may occur during OFT entry, and should be aware of their effects on the navigated state vector.

9.2 SIMULATION APPROACH

Tacan provides a slant range measurement (ρ) from the Orbiter to the ground station, as well as a measurement of magnetic bearing (θ) from the Orbiter to the ground station (w.r.t. magnetic north at the ground station). Signal strength and low elevation constraints are reflected in the range and bearing lockon flags (ρ_{lock} , θ_{lock}), which are provided by the Tacan simulation. (Note: the user program must test for the high elevation constraint (elevation angle $> 45^\circ$) or the cone of confusion, in which Tacan bearing data becomes unreliable.) This Tacan simulation includes the automatic antenna selection logic between upper and lower antennas for each navset that is found in the TACAN SOP (ref. 9-2).

An environment simulation provides the true Orbiter position and velocity, \underline{R}_{ORB} and \underline{V}_{ORB} , as well as the Orbiter's attitude as described by the transformation from Earth-centered inertial (ECI) to body coordinates, T_{ECI}^{BODY}

This Tacan simulation requires the following data for each ground station.

- a. Ground station position, R_{GND}
- b. Magnetic variation at ground station, θ_{VAR}
- c. Ground station equipment type

These data are available from the Environmental File, which is prepared and maintained by the Department of Defense Electromagnetic Compatibility Analysis Center (ECAC) in Annapolis, Maryland. Limited data concerning Tacan's in the KSC and Edwards areas are available from references 9-3 and 9-4.

It is assumed here that the Tacan tuning schedule has been chosen to avoid the following conditions:

- a. Ground stations obstructed by surroundings (mountains, buildings, etc.)
- b. Cochannel interference caused by simultaneously receiving two ground stations on the same channel (ref. 9-3, and 9-5).

Figure 9-1 presents a block diagram for a Tacan simulation. The functions of each block are as follows:

- a. Block 1 - computes five parameters specifying the Orbiter/ground station geometry. Equations used to derive each of the five parameters are as follows:

Slant range (ρ)

$$\rho = |\underline{R}_{ORB} - \underline{R}_{GND}|$$

Line of sight vector (\underline{u}_{LOS}), Orbiter to ground station

$$\underline{u}_{LOS} = (\underline{R}_{GND} - \underline{R}_{ORB})/\rho$$

Note: Using knowledge of the Orbiter's attitude (i.e., T_{ECI}^{BODY}), \underline{u}_{LOS} is expressed in body coordinates for use in block 2.

Orbiter elevation (EL)

$$EL = 90^\circ - \cos^{-1} (\underline{u}_{LOS} \cdot \underline{u}_{V,GND})$$

where $\underline{u}_{V,GND}$ is the unit vector describing geodetic vertical at the ground station

Magnetic bearing (θ), Orbiter to ground station

$$\theta = \tan^{-1}((\underline{u}_{LOS} \cdot \underline{u}_{E,GND})/(\underline{u}_{LOS} \cdot \underline{u}_{N,GND})) - \theta_{VAR}$$

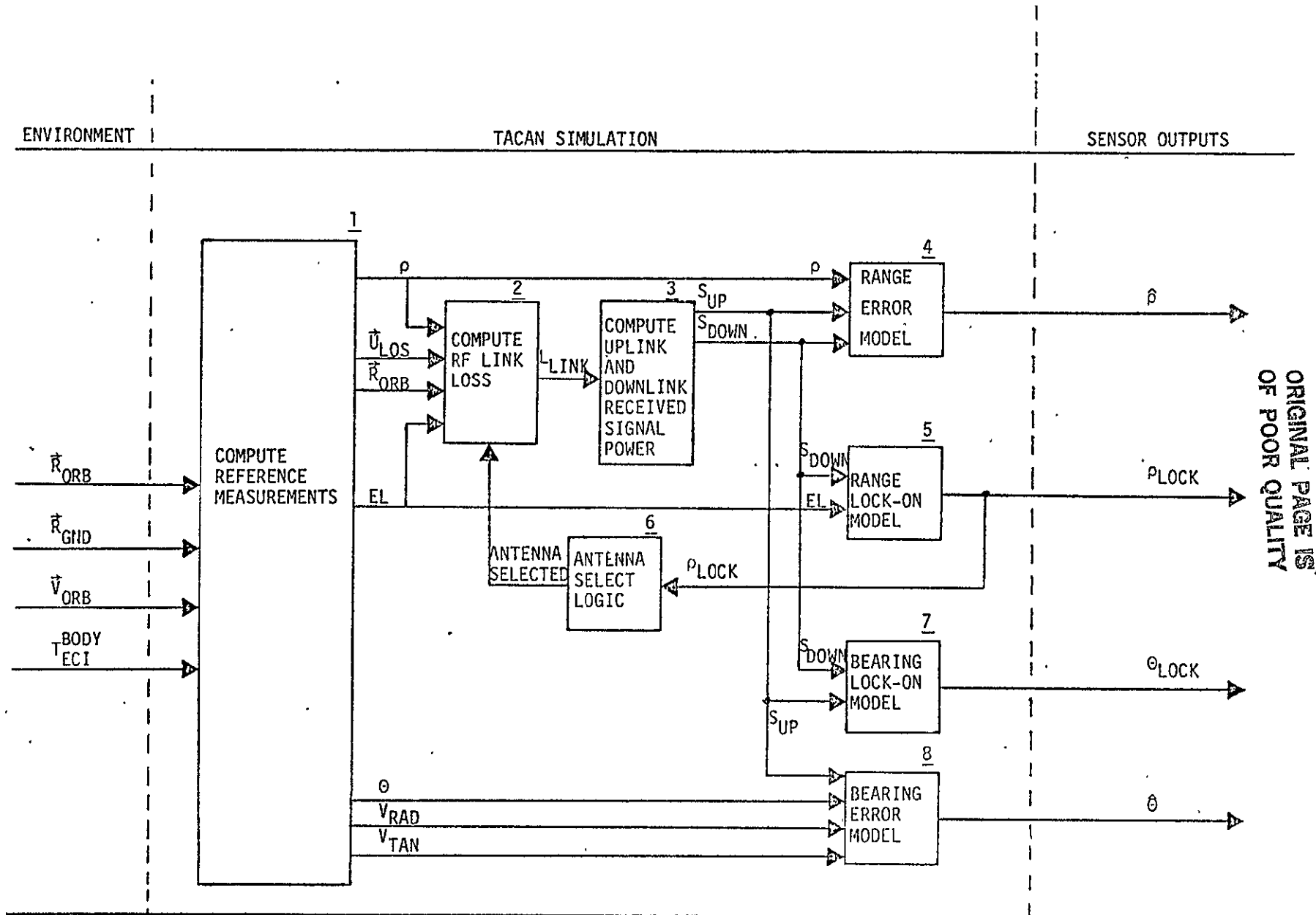


Figure 9-1.- TACAN simulation functional block diagram.

where $\underline{u}_{E,GND}$ is the unit vector pointing east at the ground station
 $\underline{u}_{N,GND}$ is the unit vector pointing true north at the ground station
 θ_{VAR} is the angle variation from true to magnetic north at the ground station

Radial velocity, V_{RAD} , along line-of-sight vector

$$V_{RAD} = |\underline{V}_{ORB} \cdot \underline{u}_{LOS}|$$

Tangential velocity, V_{TAN} , relative to the ground station

$$V_{TAN} = |\underline{V}_{ORB} \cdot \underline{u}_{TAN}|$$

where \underline{u}_{TAN} is the horizontal unit vector perpendicular to the line of sight

- b. Block 2 - computes the radio frequency (RF) link loss (L_{LINK}) using the following equations extracted from reference 9-6:

$$L_{LINK} = G_{ORB} + G_{GND} + L_C + L_F + L_P + FSPL$$

Each of the individual terms in this equation are computed as follows:

G_{ORB} : Orbiter antenna gain

First compute the look angles from the Orbiter antennas to the ground station:

$$\alpha = \cos^{-1} (\underline{u}_{ANT} \cdot \underline{u}_{LOS})$$

where \underline{u}_{ANT} is the antenna pointing direction given in section 9.4.1. The particular antenna is specified by the antenna auto-select logic (block 6) and the navset being used.

\underline{u}_{LOS} is the line of sight vector in body coordinates from block 1.

G_{ORB} is then computed as:

$$* \quad \text{If } \alpha < 100^\circ, P8(\alpha) = \sum_{n=0}^8 C_n \alpha^n \text{ dBi}$$

where the C_n 's are given in section 9.4.2.

* After the eight-order polynomial $P8(\alpha)$ has been evaluated, the onboard gain
* is computed depending on which region the look angle lies.

* Region 1: ($\alpha \leq 10^\circ$)

$$* \quad G_{ORB} = P8(\alpha) + | 2 \sin(0.4\pi\alpha) |$$

* Region 2: ($10^\circ < \alpha \leq 40^\circ$)

$$* \quad G_{ORB} = P8(\alpha) - 1.5 \sin(0.15\pi\alpha)$$

* Region 3: ($40^\circ < \alpha \leq 100^\circ$)

$$* \quad G_{ORB} = P8(\alpha) - A3(\alpha) \sin(F3(\alpha) \pi\alpha),$$

$$* \quad \text{where } A3(\alpha) = 2 - 0.0333(\alpha - 40)$$

$$* \quad F3(\alpha) = 0.15 - 0.000833(\alpha - 40)$$

* Region 4: ($100^\circ < \alpha \leq 180^\circ$)

$$* \quad G_{ORB} = G4(\alpha) + | A4(\alpha) \sin(F4(\alpha) \pi\alpha) |;$$

$$* \quad \text{where } G4(\alpha) = -10 - 0.375(\alpha - 100)$$

$$* \quad A4(\alpha) = 0.25(\alpha - 100)$$

$$* \quad F4(\alpha) = 0.1 + 0.000625(\alpha - 100)$$

* If the user desires to simulate the effects of variations in the on-board antenna patterns, then a random shift may be introduced in the sinusoidal scalloping of the gain pattern by adding a uniformly distributed random (on $[0, 2\pi)$) phase shift to the argument of the sine function in each region. The random phase shift is intended to be chosen only once for each onboard antenna thereby introducing a pseudorealistic pattern variation.

G_{GND}: Ground station antenna gain

$$G_{GND} = 20 \log (G_E) + G_{TYPE} \text{ dBi}$$

* where G_E is the normalized antenna gain, specified by the function of the elevation angle EL, as given in section 9.4.3.

G_{TYPE} is equal to 2 dB for the older ground station antenna design (utilized by the military) and is equal to 5 dB for the new equipment types (RTB or RTC). Reference 9-2 gives equipment types for Tacan's in the Edwards AFB area. Reference 9-3 gives similar information for Tacan's close to KSC.

L_C: Cable losses

$$L_C = -4.8 \text{ dB (based on the Orbiter acceptance criterion)}$$

L_F: Fading loss (multipath)

$$\text{If } EL \geq 15^\circ, L_F = 0 \text{ dB}$$

$$\text{If } EL < 15^\circ, L_F = -(4.5 - .6 EL + .02 EL^2) \text{ dB}$$

This page intentionally left blank

L_p : Polarization loss

First, compute the mismatch angle (ϕ) between the Orbiter and ground station polarization directions:

$$\phi = \cos^{-1} (\underline{P}_R \cdot \underline{u}_I / |\underline{P}_R|)$$

where $\underline{P}_R = \underline{u}_{ANT} - \underline{u}_{LOS} \cos \alpha$

$$\underline{u}_I = (\underline{R}_{ORB} \times \underline{u}_{LOS}) \times \underline{u}_{LOS} / |\underline{R}_{ORB} \times \underline{u}_{LOS}|$$

Polarization loss is then computed from the mismatch angle via:

$$L_p = 10 \log (.5 + .49373 \cos 2\phi) \text{ (dB)}$$

FSPL: Free space path loss

$$FSPL = 20 \log (\lambda / 4\pi\rho) \text{ dB}$$

Assuming a λ corresponding to $f = 1.213$ GHz (the shortest Tacan wavelength), we have:

$$FSPL = -99.48 - 20 \log \rho \text{ (dB)}$$

where ρ is in units of nautical miles

- c. Block 3 - computes received signal powers at the ground station for the downlink (S_{DOWN}) and at the Orbiter for the uplink (S_{UP}).

$$S_{DOWN} = P_{ORB} + L_{LINK} \text{ (dBm)}$$

where P_{ORB} is the radiated power from the Orbiter navset, assumed to be 60 dBm (1000 watts)

\underline{u}_{LOS} is the line of sight vector in body coordinates from block 1.

G_{ORB} is then computed as:

If $\alpha \geq 120^\circ$, $G_{ORB} = -40$ dBi

If $\alpha < 120^\circ$, $G_{ORB} = \sum_{n=0}^8 C_n \alpha^n$ dBi

where the C_n 's are given in section 9.4.2.

G_{GND} : Ground station antenna gain

$G_{GND} = 20 \log (G_E) + G_{TYPE}$ dBi

where G_E is the normalized antenna gain, specified by a tabular function of the elevation angle EL, as given in section 9.4.3.

G_{TYPE} is equal to 2 dB for the older ground station antenna design (utilized by the military) and is equal to 5 dB for the new equipment types (RTB or RTC). Reference 9-2 gives equipment types for Tacan's in the Edwards AFB area. Reference 9-3 gives similar information for Tacan's close to KSC.

L_C : Cable losses

$L_C = -4.8$ dB (based on the Orbiter acceptance criterion)

L_F : Fading loss (multipath)

If $EL \geq 15^\circ$, $L_F = 0$ dB

If $EL < 15^\circ$, $L_F = -(4.5 - .6 EL + .02 EL^2)$ dB

L_p : Polarization loss

First, compute the mismatch angle (ϕ) between the Orbiter and ground station polarization directions:

$$\phi = \cos^{-1} \left(\frac{\underline{P}_R \cdot \underline{u}_I}{|\underline{P}_R|} \right)$$

where $\underline{P}_R = \underline{u}_{ANT} - \underline{u}_{LOS} \cos \alpha$

$$\underline{u}_I = (\underline{R}_{ORB} \times \underline{u}_{LOS}) \times \underline{u}_{LOS} / |\underline{R}_{ORB} \times \underline{u}_{LOS}|$$

Polarization loss is then computed from the mismatch angle via:

$$L_p = 10 \log (.5 + .49373 \cos 2\phi) \text{ (dB)}$$

FSPL: Free space path loss

$$FSPL = 20 \log (\lambda / 4\pi\rho) \text{ dB}$$

Assuming a λ corresponding to $f = 1.213$ GHz (the shortest Tacan wavelength), we have:

$$FSPL = -99.48 - 20 \log \rho \text{ (dB)}$$

where ρ is in units of nautical miles

- c. Block 3 - computes received signal powers at the ground station for the downlink (S_{DOWN}) and at the Orbiter for the uplink (S_{UP}).

$$S_{DOWN} = P_{ORB} + L_{LINK} \text{ (dBm)}$$

where P_{ORB} is the radiated power from the Orbiter navset, assumed to be 60 dBm (1000 watts)

L_{LINK} is the RF link loss computed in block 2

$$S_{UP} = P_{GND} + L_{LINK} \text{ (dBm)}$$

where P_{GND} is the power radiated by the ground station in dBm. This is assumed to be 67 dBm (5kW) for permanent Tacans and 58.45 dBm (700 W) mobile ones.

- i. Block 4 - computes the corrupted range measurement, ρ , using the range error model equations presented in section 9.3.1.
- e. Block 5 - determines range data lockon as a function of downlink received signal strength, S_{DOWN} , and the elevation angle, EL , as follows:

If $EL \geq 1^\circ$ and $S_{DOWN} \geq -90$ dBm, then $\rho_{LOCK} = TRUE$

Otherwise

$$\rho_{LOCK} = FALSE$$

After the range threshold criterion has been met, a period of time is required for the Orbiter navset to lock on to the ground station replies. This time increases as range rate increases, but 2 seconds may be assumed at range rates less than 4500 knots (ref. 9-8).

In addition to lockon delay a memory feature exists in the hardware that causes the lockon indication to remain for about three-quarters of a second after the signal falls below threshold.

The 1° constraint on elevation angle accounts for atmospheric effects such as tropospheric scatter. This is felt to be a conservative limit since the

hardware may actually achieve lockon below 1° elevation, but will not dependably do so all the time.

The -90 dBm constraint on the received power at the ground station is due to the receiver threshold in the ground equipment that causes all interrogations with less than -90 dBm received power to be ignored. Uplink signal power is not a range acquisition constraint since (1) ground stations are generally more powerful than the Orbiter transmitters (mobile Tacan ground stations are less powerful, transmitting only 700 watts), and (2) airborne receivers are more sensitive than ground receivers, with a DME acquisition threshold of -94 dBm.

- f. Block 6 - selects between the two antennas (upper and lower) associated with each Tacan navset.

Since range data yields more accurate position updates than bearing, it is desirable to switch antennas when DME is not locked-on, even though bearing lock might be present. The Tacan Subsystem Operating Program (SOP) performs this antenna selection automatically, independently for each navset, in the following manner:

- (1) The SOP will initially select the bottom antenna when a new station is tuned.
- (2) If, after 10 seconds (I-load), range lockon has not occurred the top antenna is selected.
- (3) If, after an additional 10 seconds, range lockon still has not occurred the bottom antenna is reselected.

This switching sequence continues until range lockon has occurred, at which time the SOP freezes to the lockon antenna. Should range lock disappear for a 10-second period the acquisition switching sequence is resumed.

- g. Block 7 - determines bearing data lockon as a function of uplink received signal strength, S_{UP} , and the elevation angle, EL , as follows:

If $EL \geq 1^\circ$ and $S_{UP} \geq -90$ dBm, then $\theta_{LOCK} = TRUE$

Else $\theta_{LOCK} = FALSE$

Similar to range, bearing lockon is delayed by a constant 3 seconds (regardless of range rate) (ref. 9-8). Also, the data value and lockon indication is held for 3 seconds after loss of adequate signal.

- h. Block 8 - computes the corrupted bearing measurement, θ , using the bearing error model equations presented in section 9.3.2.

9.3 ERROR MODELS

Tacan range and bearing errors are modeled using knowledge of the uplink and downlink received signal strengths, S_{UP} and S_{DOWN} , which are computed in block 3.

9.3.1 Range Error Model - Block 4

Tacan range measurements are subject to biases; bias shift, noise, and scale factor errors as related in the following equation:

$$\rho_c = (1 + SFE)\rho + b_{GND} + b_{ORB} + b_{LOC} + b_{SHIFT} + n_{GND} + n_O$$

where ρ_c is the corrupted range measurement
 SFE is the scale factor error
 ρ is the true slant range
 b_{GND} is the range bias induced by the ground station electronics
 b_{ORB} is the range bias induced by the Orbiter navset electronics
 b_{LOC} is the range bias induced by ground station survey errors
 b_{SHIFT} is the ground station bias shift
 n_{GND} is the ground station random noise
 n_{ORB} is the Orbiter navset random noise

The range errors are modeled as independent zero-mean Gaussian random variates with the 1σ values given in section 9.4.4.

* Finally, the range is quantized to the nearest 0.05 nautical mile via:

$$* \quad \text{RNGQUANT.} = \text{INT} \left[\frac{\rho + 0.025}{0.05} \right] \quad 0.05 \text{ (nm)}$$

* where INT = the greatest integer function and ρ = raw RNG data.

9.3.2 Bearing Error Model - Block 8

Tacan bearing measurements are subject to bias, path errors, and noise as described in 'th

$$\hat{\theta} = \theta + b_{\text{GND}} + b_{\text{ORB}} + n_{\text{GND}} + n_{\text{ORB}} + n_{\text{ROUGH}} + b_{\text{BS}}$$

where $\hat{\theta}$ is the corrupted magnetic bearing measurement
 θ is the true magnetic bearing
 b_{GND} is the ground station bearing bias
 b_{ORB} is the Orbiter navset bearing bias
 n_{GND} is the random bearing error induced by the ground station
 n_{ORB} is the signal strength dependent random error induced by the Orbiter receiver
 n_{ROUGH} is the random error due to roughness of the bearing beam
 b_{BS} is the exponentially correlated bias due to bending and scalloping of the bearing beam. The time constant (τ_{BS}) of this ECRV is computed via:

$$\tau_{\text{BS}} = \left((V_{\text{RAD}}/D_{\text{RAD}}) + (V_{\text{TAN}}/D_{\text{TAN}}) \right)^{-1}$$

where D_{RAD} is the radial correlation distance
 V_{RAD} is the Orbiter's velocity component along the line-of-sight vector
 D_{TAN} is the tangential correlation distance
 V_{TAN} is the Orbiter's ground relative velocity perpendicular to the line of sight

b_{BS} is computed sequentially in the following manner:

Initialization: $b_{BS}(t=0) = \sigma_{BS} u$

Iteration: $b_{BS}(t) = a \cdot b_{BS}(t - \Delta t) + \sigma_{BS} \sqrt{1-a^2} u$

where $a = e^{-\Delta t / \tau_{BS}}$

u is a unit variance, zero-mean Gaussian random number

1σ values for all the above error sources are given in section 9.4.5.

* Finally, the bearing is quantized to the nearest 0.1759 degree via;

$$* \quad BRG_{QUANT.} = INT \left[\frac{\theta + 0.0879}{0.1759} \right] \cdot 0.1759 \text{ (deg)}$$

* where INT = the greatest integer function and θ = raw BRG data.

ORIGINAL PAGE IS
OF POOR QUALITY

9.4 ERROR SOURCE VALUES

The Orbiter carries three Hoffman ARN-84 Tacan navsets, one each in the 1, 2, and 3A forward avionics bays. Each receiver is fed by two L-band antennas, one mounted on the upper and one on the lower portion of the Orbiter's outer structure. Error modeling data specific to the Shuttle Tacan system follow.

9.4.1 Orbiter Antenna Pointing Directions

Tacan antenna pointing vectors are given below in body coordinates.

<u>Antenna number</u>	<u>Antenna location</u>	<u>Tacan number</u>	<u>X</u>	<u>Y</u>	<u>Z</u>
1	Upper left	1	+0.41742	-0.15643	-0.89515
2	Lower left	1	+0.04532	-.49931	+0.86484
3	Upper center	2	+0.42262	0	-.90631
4	Lower right	2	+0.04532	+0.49931	+0.86484
5	Upper right	3	+0.41742	+0.15643	-.89515
6	Lower center	3	+0.03490	0	+0.99939

9.4.2 Orbiter Antenna Gain Pattern

The Tacan antenna gain patterns are approximated by an eighth-order curve fit to the angle of offset between the ground beacon and the Orbiter antenna boresight.

The nine coefficients specifying the curve fit are:

$$C_0 = -2.442764458 \text{ E}1$$

$$C_1 = 4.219265311 \text{ E}0$$

$$C_2 = -4.327836256 \text{ E-}1$$

$$C_3 = 2.344000307 \text{ E-}2$$

$$C_4 = -6.865056346 \text{ E-}4$$

$$C_5 = 1.138519773 \text{ E-}5$$

$$C_6 = -1.069845253 \text{ E-7}$$

$$C_7 = 5.303361563 \text{ E-10}$$

$$C_8 = -1.077010598 \text{ E-12}$$

9.4.3 Ground Station Antenna Gain

Ground beacon normalized antenna gain is specified by the following function of elevation angle (EL).

* a. If $EL \leq 29$

$$* \quad G_E = 0.6725 + 0.2975 \sin(\delta)$$

$$* \quad \text{where } \delta = 0.05265 * \pi * (EL)$$

* b. If $29^\circ < EL \leq 90^\circ$

$$* \quad G_E = 0.212 + A2 \sin(\delta)$$

$$* \quad \text{where } A2 = 0.22 - 0.0022 (EL - 22^\circ)$$

$$* \quad F2 = 0.03125 + 0.0002367 (EL - 29^\circ)$$

$$* \quad \text{and } \delta = F2 * \pi * (EL - 22^\circ)$$

* If the user desires to introduce a random shift and a random amplitude variation

† the expression

$$† \quad V(EL) = 0.05 \sin(0.1 * \pi * EL + \phi)$$

† should be added to the normalized gain G_E computed above. The phase angle ϕ

† is a uniformly distributed random variable on the interval $[0, 2\pi)$ and is in-

† tended to be chosen only once for each ground sta

9.4.4 Range Error Values

Bias (1σ):

Ground station: 300 ft

Orbiter transceiver: 100 ft

Ground station bias shift: 15.8×10^{-115} (SDOWN + 60) ft

Noise (1σ):

This page intentionally left blank

Ground station:

If $S_{\text{DOWN}} \geq -55$ dBm: 20 ft

If $S_{\text{DOWN}} < -55$ dBm: $20 - 2.33 (55 + S_{\text{DOWN}})$ ft

Orbiter transceiver:

If $S_{\text{UP}} \geq -80$ dBm: 42 ft

If $S_{\text{UP}} < -80$ dBm: $42 - 4.2 (80 + S_{\text{UP}})$ ft

Station location uncertainty: 33 ft (1σ , per axis)

Quantization error: 304 ft (0.05 n. mi.)

Scale factor error: 100 ppm (1σ)

9.4.5 Bearing Error Values

Bias (1σ)

Ground station: 0.33°

Onboard receiver: 0.353°

Noise (1σ)

Ground station: 0.1°

Orbiter receiver: 0.353° ($S_{\text{UP}} \geq -82$ dBm)

1.458° ($S_{\text{UP}} < -82$ dBm)

Quantization error: 0.1758° (ref. 9-11)

Path errors

Roughness 0.3° (1σ)

Bending and scalloping 0.4° (1σ)

Radial correlation 10 000 ft
distance

Tangential 5 000 ft
Correlation distance

9.5 REFERENCES

- 9-1 Shuttle Operational Data Book, Vol. I, Shuttle Systems Performance and Constraints Data. JSC-08934, vol. I, rev. A, October 1976.
- 9-2 Space Shuttle Orbital Flight Test Level C Functional Subsystem Software Requirements; Guidance, Navigation, and Control, Part E, Subsystem Operating Programs, TACAN.
- 9-3 Lequieu, C. M.: TACAN Coverage for Shuttle Approach for KSC. Lockheed LEC-7176, October 1975.
- 9-4 Speir, R. E.: TACAN RF Considerations on Data Availability and Redundancy Management. MDTSCO TM No. 1.3-TM-C0603-320, November 1, 1976.
- 9-5 O'Herren, D. H.: Shuttle TACAN Limits Due to Co-Channel/Adjacent Channel Interference and Signal Adequacy. Lockheed Electronics Co., LEC-0200, June 1973.
- 9-6 Speir, R. E.: TACAN RF Link Simulation. MDTSCO Design Note 1.2-DN-C0714-006, August 31, 1977.
- 9-7 Speir, R. E.: TACAN DME Error Model. MDTSCO Working Paper 1.2-WP-C0614-22, March 8, 1977.
- 9-8 Specification for TACAN Receiver - Transmitter. Rockwell International, MC409-0014 rev. A, May 20, 1974.
- 9-9 Madni, A. Z.: Simulation Error Models for RF Nav Sensors. Rockwell International Internal Letter 383-350-RCS-77-003, January 21, 1977.

9-10 Gustafson, D. E.: A VOR/DME Error Model for SSV Navigation Analysis. MIT
STS Memo No. 17-70, June 23, 1970.

9-11 Speir, R. E.: TACAN Measurement Quantization. MDTSCO TM 1.2-TMC0814-141,
December 21, 1977.

10.0 MSBLS

10.1 GENERAL DESCRIPTION

The microwave scanning beam landing system (MSBLS) provides information representing azimuth angle, elevation angle, and distance of user aircraft with respect to a ground installation located beside the runway. The ground installation consists of two main elements: (1) an elevation station located just beyond the nominal touchdown point providing good geometry for altitude measurement prior to touchdown, and (2) an azimuth/DME station located beyond the far end of the runway to provide data through rollout. Using knowledge of the ground station locations, these data are transformed into the runway coordinate system yielding positional information for CRT and dedicated displays, and for incorporation into the Orbiter navigated state estimate. The MSBLS is a precision navigation sensor used during final approach through rollout at landing sites so equipped (ref. 10-1).

The crew selects a ground installation corresponding to the desired runway by tuning to 1 of 10 channels via the cockpit control head. Upon reception of ground station solicit pulses, the onboard navsets transmit DME interrogations on 15.47 GHz with a pulse pair spacing based on the channel number. Solicit pulses and all three information channels (Az, El, and DME) are transmitted from the ground stations on 1 of 10 frequency channels between 15.4 and 15.7 GHz. The pulse pair spacing is different for the solicits, DME replies, elevation, azimuth-fly-left, and azimuth-fly-right signals facilitating navset identification of the data type being received.

~~PRECEDING PAGE BLANK NOT FILLED~~

DME data are decoded by the navset using conventional transponding techniques. The round trip time is measured, ground station delay is subtracted, and then it is scaled by half the speed of light to be output in units of nautical miles. The ground DME antenna radiates into the entire coverage volume without scanning (ref. 10-1).

The azimuth and elevation antennas are designed such that the power radiated is focused nearly into a plane. The azimuth antenna is oriented with this plane vertical and is mechanically scanned horizontally. The opposite situation exists for the elevation antenna. The scans result from 2.5 Hz sinusoidal oscillations, whose angular extremes are in excess of the coverage volume, but RF transmissions occur only during the central portion of the scan where the angular rate is approximately constant. The sector of transmissions is plus or minus 15 degrees (from parallel to runway centerline) for azimuth, and zero to 30 degrees (from the horizontal) for elevation. The solicits, DME operations, and angle scans are electronically synchronized for time-shared transmissions at 200 milliseconds per complete cycle. The spacing between pulse pairs fed to the angle antennas is proportional to the pointing angle of the antenna at that instant. The navset tracks the amplitude modulation caused by antenna scanning and averages the spacing of pulse pairs received between two points of equal power on either side of the symmetrical antenna beam. The average spacing is scaled to degrees for output. Although the antenna beamwidth may be 1 degree (Az) and the spacing of pulse pairs is incremented only every one-eighth degree, angular accuracies in excess of 0.05 degree (system spec) are obtainable with this approach. This represents less than 1 foot error per thousand feet of distance to the ground station.

10.2 SIMULATION APPROACH

Each of the triple redundant navsets aboard the Orbiter make three data words available to the data processing system at a 5-Hz rate. This subsystem simulation defines the algorithms necessary to model Az, El, and DME measurements histories with respect to various error mechanisms and the behavior of the data validity flags. The lockon and error models utilize parameters normally available in an environmental simulation in order to produce measurement and lockon histories to a relatively high degree of fidelity (subject to the accuracy to which these dependences are known and can be simply modeled).

10.2.1 Block Diagram Description

Figure 10-1 is a functional block diagram of the MSBLS subsystem simulation.

- a. Block 1 - the first task is to take the vehicle position and attitude and, utilizing knowledge of the Orbiter antenna and ground station locations, compute the desired line-of-sight vectors. This is done both from the ground stations to the Orbiter in runway coordinates and from the Orbiter to the ground stations in body coordinates. Slant ranges and look angles are then determined (sec. 10.2.2).
- b. Block 2 - the slant range from the DME site to the Orbiter and the ground station look angles are then checked against geometrical limits to ascertain whether the ground station is radiating valid data in this region (sec. 10.3.1). This alone does not determine validity because adequate signal levels may not be present.
- c. Block 3 - the slant ranges and look angles are then used to compute expected signal levels via antenna pattern curve fits and other formulations to be compared to an assumed threshold for lockon determination (sec. 10.3.2).

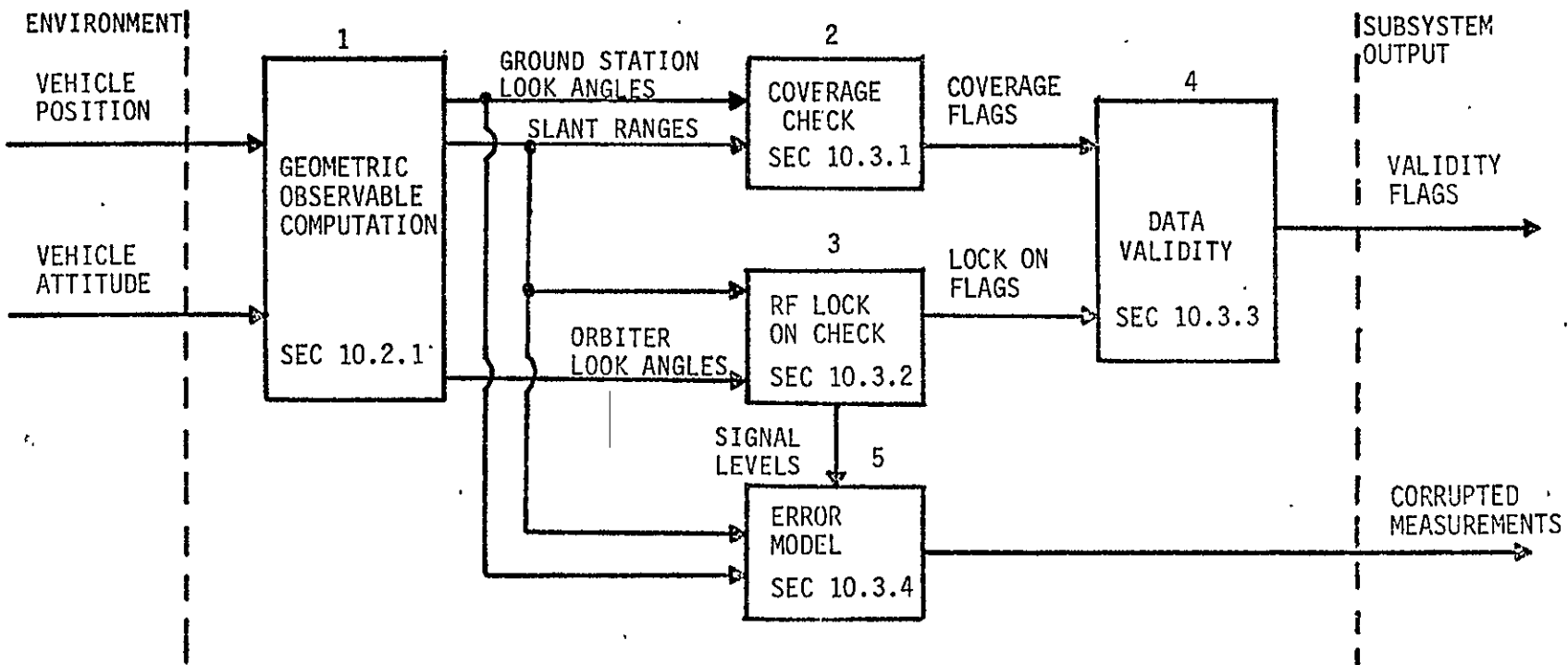


Figure 10-1.- MSBLS subsystem model functional block diagram.

- d. Block 4 - the presence of adequate RF signal and ground station coverage is required for each information channel validity flag. All three onboard navsets are assumed to behave in a parallel fashion with respect to data validity (sec. 10.3.3).
- e. Block 5 - the look angles and signal levels are then applied to the error model that contains known error dependences for the ground stations, path, and each onboard navset (sec. 10.3.4). The three corrupted measurements for each data type are assumed to be representative of the performance of a non-failed system in the configuration experienced during the approach and landing tests (with the exceptions listed in sec. 10.3.5).

10.2.2 Geometric Observables Computation.

The Orbiter c.g. position ($\overset{RW}{R}_{CG}$) is assumed in units of feet in runway coordinates, and an Orbiter attitude transformation matrix (T) is assumed to convert a vector in runway coordinates to body coordinates by multiplication. Values to be used as the Orbiter antenna location ($\overset{BODY}{R}_{ORBANT}$) and ground station locations ($\overset{RW}{R}_{AZ/DME}$ and $\overset{RW}{R}_{EL}$) are given in section 10.4.1. Lines-of-sight (U) from the ground stations to the Orbiter antenna are:

$$\overset{RW}{U}_{AZ/DME} = T^{-1} \left(\overset{BODY}{R}_{ORBANT} \right) + \overset{RW}{R}_{CG} - \overset{RW}{R}_{AZ/DME}$$

$$\overset{RW}{U}_{EL} = T^{-1} \left(\overset{BODY}{R}_{ORBANT} \right) + \overset{RW}{R}_{CG} - \overset{RW}{R}_{EL}$$

Lines-of-sight from the Orbiter antenna to the ground stations are then:

$$\overset{BODY}{U}_{AZ/DME} = T \left(\overset{RW}{R}_{AZ/DME} - \overset{RW}{R}_{CG} \right) - \overset{BODY}{R}_{ORBANT}$$

$$\overset{BODY}{U}_{EL} = T \left(\overset{RW}{R}_{EL} - \overset{RW}{R}_{CG} \right) - \overset{BODY}{R}_{ORBANT}$$

Slant ranges from both ground stations to the Orbiter are:

$$SR_{AZ/DME} = \left| \underline{U}_{AZ/DME}^{RW} \right| \quad (ft)$$

$$SR_{EL} = \left| \underline{U}_{EL}^{RW} \right| \quad (ft)$$

Elevation (Θ) and azimuth (Ψ) look angles from the ground antennas to the Orbiter may be obtained as follows:

Assuming: $\underline{U} = u_1 \hat{x} + u_2 \hat{y} + u_3 \hat{z}$

$$\Psi_{AZ/DME}^{RW} = \arctan \left(-u_{AZ/DME 2}^{RW} / u_{AZ/DME 1}^{RW} \right) \quad (deg)$$

$$\Theta_{AZ/DME}^{RW} = \arctan \left(u_{AZ/DME 3}^{RW} / \sqrt{(u_{AZ/DME 1}^{RW})^2 + (u_{AZ/DME 2}^{RW})^2} \right) \quad (deg)$$

$$\Psi_{EL}^{RW} = \arctan \left(u_{EL 2}^{RW} / \sqrt{(u_{EL 1}^{RW})^2 + (u_{EL 3}^{RW})^2} \right) \quad (deg)$$

$$\Theta_{EL}^{RW} = \arctan \left(u_{EL 3}^{RW} / u_{EL 1}^{RW} \right) \quad (deg)$$

The Orbiter-to-ground station antennas look angles are similarly:

$$\Theta_{AZ/DME}^{BODY} = \arctan \left(-u_{AZ/DME 3}^{BODY} / u_{AZ/DME 1}^{BODY} \right) \quad (deg)$$

$$\Psi_{AZ/DME}^{BODY} = \arctan \left(u_{AZ/DME 2}^{BODY} / \sqrt{(u_{AZ/DME 1}^{BODY})^2 + (u_{AZ/DME 3}^{BODY})^2} \right) \quad (deg)$$

$$\theta_{EL}^{BODY} = \arctan \left(\frac{-u_{EL\ 3}^{BODY}}{u_{EL\ 1}^{BODY}} \right) \quad (\text{deg})$$

$$\psi_{EL}^{BODY} = \arctan \left(\frac{u_{EL\ 2}^{BODY}}{\sqrt{(u_{EL\ 1}^{BODY})^2 + (u_{EL\ 3}^{BODY})^2}} \right) \quad (\text{deg})$$

10.3 SUBSYSTEM MODELING FORMULATIONS

This section identifies (and briefly explains) the algorithms necessary to characterize MSBLS subsystem behavior under the assumptions listed in section 10.3.5.

The values to be used as constraints, or in detailed computation of a parameter, are tabulated in section 10.4.

10.3.1 Coverage Check

The noncorrupted, or ideal, azimuth, elevation, and DME measurements are the inputs to be checked against the geometrical constraint values listed in section 10.4.2.

$$DME \text{ TRUE} = SR \text{ AZ/DME} \quad (\text{ft})$$

$$AZ \text{ TRUE} = \Psi \frac{RW}{AZ/DME} \quad (\text{deg})$$

$$EL \text{ TRUE} = \Theta \frac{RW}{EL} \quad (\text{deg})$$

DME coverage is constrained by a maximum (19.6 n. mi.) slant-range value.

$$\text{If } DME \text{ TRUE} \leq DME \text{ SR MAX} \quad (\text{ft})$$

DME data may be valid.

Azimuth and elevation coverage angles where data may be flagged valid are not the same as the previously mentioned angles where power is applied to the scanning antennas or the ground station specified coverage volume.

The azimuth coverage is constrained by an azimuth limit a little in excess of $\pm 15^\circ$. The system sign convention is positive if the vehicle is right of centerline (fly left).

If $| AZ_{TRUE} | \leq AZ_{\Psi MAX}$ (deg)

azimuth data may be valid. Similarly for elevation coverage

If $EL_{TRUE} \leq EL_{\Theta MAX}$ (deg)

elevation data may be valid.

10.3.2 RF Lockon Check

As discussed, completion of five RF links is required for acquisition of all three data types. They are the solicit (uplink), DME interrogation (downlink), DME reply (uplink), azimuth (uplink), and elevation (uplink) (ref. 10-2). A reduction in model complexity is possible since the solicit and DME reply links are identical. Furthermore, they differ from the DME downlink only by a constant (different transmission powers). The DME downlink is the weaker of the three such that it alone must be checked against a threshold to determine DME lockon. The DME downlink received signal level is also the only power represented in the DME error model. Azimuth and elevation powers will also be computed, checked, and passed to the error model.

The RF link model approach will be to compute antenna gains, polarization loss, and path loss, then add a constant reflecting cable losses and transmission powers required for that link to get a received power. The Orbiter antenna gains for the azimuth and DME links are the same but a gain must be computed for the look angle to the elevation station. Curve fits of the four antenna gain contours yield gain as a function of elevation and azimuth look angles. Path losses are determined by the slant ranges. Polarization loss is computed by finding the mismatch angle between the transmitting and receiving antenna's

polarization sense. This angle is approximately the angle between the Orbiter Z-axis and the runway X-Z plane. Received powers for the RF links may be computed via the formulas

$$S_{DME\ DOWN} = G_T^{ORB\ AZ/DME} + G_R^{DME\ GS} + L_{POL} + L_{PATH}^{AZ/DME} + K_{DME} \quad (dBm)$$

$$S_{AZ} = G_T^{AZ\ GS} + G_R^{ORB\ AZ/DME} + L_{POL} + L_{PATH}^{AZ/DME} + K_{AZ} \quad (dBm)$$

$$S_{EL} = G_T^{EL\ GS} + G_R^{ORB\ EL} + L_{POL} + L_{PATH}^{EL} + K_{EL} \quad (dBm)$$

where

$S_{DME\ DOWN}$ - received power input to the ground receiver from the Orbiter
(dBm)

S_{AZ} - received power input to the Orbiter receiver from the azimuth
station (dBm)

S_{EL} - received power input to the Orbiter receiver from the elevation
station (dBm)

$G_T^{ORB\ AZ/DME}$ - Orbiter antenna gain computed as a function of the Orbiter to
Az/DME station look angles (dBi)

$G_R^{DME\ GS}$ - DME ground receiving antenna gain determined by the Az/DME to
Orbiter look angles

L POL - polarization loss is computed by first finding the polarization mismatch angle (ϕ_{POL}). The loss is then

$$L_{POL} = 20 * \text{LOG}_{10} (\cos (\phi_{POL})) \quad (\text{dB})$$

L ^{AZ/DME} PATH - simple spreading loss is a function of the wavelength (λ) and the slant range (SR):

$$L_{PATH}^{\text{AZ/DME}} = 20 * \text{LOG}_{10} (\lambda / 4\pi \text{SR}_{\text{AZ/DME}}) \quad (\text{dB})$$

K DME - constant that includes transmitter power and circuit losses for the DME downlink (dBm)

G ^{AZ GS} T - azimuth ground antenna gain computed as a function of

$$\Theta_{\text{AZ/DME}}^{\text{RW}} \quad (\text{dBi})$$

G ^{ORB AZ/DME} R - Orbiter antenna gain along Az/DME look angles (same

as $G_T^{\text{ORB AZ/DME}}$ and, hence, will be denoted by $G_{\text{ORB AZ/DME}}$) (dBi)

K AZ - constant that includes transmitter power and circuit losses for the azimuth uplink (dBm)

G ^{EL GS} T - elevation ground antenna gain computed as a function of

$$\Psi_{\text{EL}}^{\text{RW}} \quad (\text{dBi})$$

G ^{ORB EL} R - Orbiter antenna gain along the Orbiter to elevation look angles (dBi)

L_{PATH}^{EL} - same as $L_{PATH}^{AZ/DME}$ but using SR_{EL} as the slant range (dBm)

K_{EL} - constant from elevation transmitter power and elevation uplink circuit losses (dBm)

Equations for the above, and values to be used, are listed in section 10.4.3.

RF lockon flags are then generated for each measurement (Az, El, and DME) by comparison of the received signal levels to the assumed receiver thresholds in sec.

10.4.3:

If $S_{DME\ DOWN} \geq THRESHOLD_{DME}$

If $S_{AZ} \geq THRESHOLD_{AZ}$

If $S_{EL} \geq THRESHOLD_{EL}$

Then RF lock on is present for DME, azimuth, and/or elevation, respectively.

10.3.3 Data Validity

It must be ascertained that both coverage constraints are met and RF lockon is present for each information channel before the data are flagged valid.

10.3.4 Error Modeling

Azimuth, elevation, and DME corrupted measurement formulations will be discussed separately. The dominant error sources are identified, briefly explained, and assigned to either the ground station, path, or navset. Those due to the ground station and path are assumed to be seen equally by all navsets. A particular hardware configuration has been assumed and is defined in the section on special notes.

Bias and noise errors are identified separately. Due to the different types of biases present in each measurement, different bias dependences are explained. Noise errors are assumed to be purely random with a normal distribution; however, the variance may change as a function of known parameters. Different additive bias formulations are suggested to account for the following types of bias mechanisms:

- a. Purely deterministic biases whose values would be the same the next time that trajectory is flown
- b. Calibration uncertainties whose magnitudes may change from flight to flight but, having been randomly sampled, behave deterministically on that flight (ref. 10-3)
- c. Correlated biases whose exact values are unknown but whose effect may be modeled via an exponentially correlated random variable (ECRV) whose time constant may change (ref. 10-4).

10.3.4.1 Azimuth Angle Errors

The dominant bias sources are azimuth boresight error, angle pickoff bias, sidelobe multipath, and beam truncation. Azimuth boresight error and angle pickoff bias are due to ground station alignment uncertainties. Therefore, a random number is chosen from a unit variance, zero mean, normal distribution to be multiplied by the formulation described in section 10.4.4.

Multipath cannot be modeled deterministically due to lack of knowledge about reflecting surface locations and sidelobes. The magnitude and rate of change of error is inferred from flight test data and modeled as an ECRV.

Beam truncation is purely deterministic and results from receiving only a portion of the scanning beam near the edge of the coverage volume. This effect begins at a true azimuth angle (Ψ_{TRUNC}) typically about $\pm 13.5^\circ$ and continues out to the edge of the coverage volume (about $\pm 17^\circ$). An error is introduced equal to half the difference between AZ_{TRUE} and Ψ_{TRUNC} , always in the direction yielding a smaller corrupted azimuth angle.

Of all the azimuth random noise sources considered (ref. 10-3) beam pulse resolution error is the largest when signal levels are high, but at lower levels receiver noise beamshape error causes quite erratic measurements. A random number is sampled from each measurement to be multiplied by the one-sigma random noise value computed as a function of signal level and geometry.

All the bias may be assumed attributable to the ground station and path, but random noise is inserted on transmission and detection.

The corrupted measurement formulation for azimuth becomes

$$AZ_{CORRUPTED} = AZ_{TRUE} + \Psi_{BIAS}^{CAL} + \Psi_{BIAS}^{TRUNC} + \Psi_{BIAS}^{MP} + \Psi_{NOISE}^{GRND} + \Psi_{NOISE}^{NAVSET}$$

where

Ψ_{BIAS}^{CAL} - Calibration accuracy bias

Ψ_{BIAS}^{TRUNC} - Beam truncation bias

Ψ_{BIAS}^{MP} - Multipath

Ψ_{NOISE}^{GRND} - Random noise due to the ground station

Ψ_{NOISE}^{NAVSET} - Random noise due to the navset

10.3.4.2 Elevation Angle Errors

Elevation angle bias sources are the same as for azimuth, but initial alinement uncertainties yield elevation axis level errors instead of azimuth boresight errors. Angle pickoff bias, multipath from sidelobes, and beam truncation all have similar contributions as with azimuth. However, main lobe multipath occurs at true elevation angles below about 2 degrees, and will be assumed to behave in a purely deterministic fashion (ref. 10-5).

Elevation angle random noise sources and dependences on signal level are about the same as with azimuth (slightly smaller in magnitude). It may again be assumed that biases would be seen the same in all navsets, but that random noise is inserted upon transmission and detection.

$$EL_{CORRUPTED} = EL_{TRUE} + \theta_{BIAS}^{CAL} + \theta_{BIAS}^{TRUNC} + \theta_{BIAS}^{SLMP} + \theta_{BIAS}^{MLMP} + \theta_{NOISE}^{GRND} + \theta_{NOISE}^{NAVSET}$$

where

- θ_{BIAS}^{CAL} - Calibration accuracy bias
- θ_{BIAS}^{TRUNC} - Beam truncation bias
- θ_{BIAS}^{SLMP} - Sidelobe multipath
- θ_{BIAS}^{MLMP} - Mainlobe multipath
- θ_{NOISE}^{GRND} - Random noise due to the station
- θ_{NOISE}^{NAVSET} - Random noise due to the navset

10.3.4.3 DME Errors

As was the case with angle errors, three types of bias are present. The largest is due to receiver threshold mean times, which are expected offsets that are a function of signal strength. Incoming interrogation and reply pulses have a finite rise time causing weaker signals to be detected later, resulting in a positive error. The system is calibrated to minimize this error at the closer ranges (higher signal levels). A calibration bias term is included where a random number is multiplied times a one-sigma formulation. The multipath may be modeled as an ECRV.

Considering DME random noise, at high-signal levels the ground and airborne clock resolutions and airborne output increment errors dominate with approximately equal error contributions. At low levels the airborne and ground thermal noise become the largest. The formulation for the corrupted DME measurement is then:

$$DME_{CORRUPTED} = DME_{TRUE} + DME_{BIAS}^{GRND\ OFFSET} + DME_{BIAS}^{NAVSET\ OFFSET} + DME_{BIAS}^{GRND\ CAL} + DME_{BIAS}^{NAVSET\ CAL} + DME_{BIAS}^{MP} + DME_{NOISE}^{GRND} + DME_{NOISE}^{NAVSET}$$

where

$DME_{BIAS}^{GRND\ OFFSET}$ - Ground expected bias

$DME_{BIAS}^{NAVSET\ OFFSET}$ - Airborne expected offset

$DME_{BIAS}^{GRND\ CAL}$ - Ground calibration uncertainty

$DME_{BIAS}^{NAVSET\ CAL}$ - Airborne calibration uncertainty

DME_{BIAS}^{MP} - Multipath

GRND
DME NOISE - Random noise due to the station

NAVSET
DME NOISE - Random noise due to the navset

10.3.5 Special Notes

The algorithms presented and values to be used are subject to the following configuration and other assumptions

- a. DME double computes, which results in erroneous DME measurements and a required user software fix for ALT is assumed fixed in the hardware.
- b. Signal attenuation due to rain is not modeled. It could be easily inserted reflecting either rain cell or widespread rain conditions (ref. 10-1). Rain attenuation (dB) values are proportional to the propagation distance through the rain and the rainfall rate.
- c. Azimuth polarization errors are not modeled as yet due to lack of knowledge of the Orbiter antenna polarization characteristics. Although error magnitudes are unknown, significant differences in the angle detected in different receivers are possible since three receiving antennas are used that may have differing polarization characteristics.
- d. Possible azimuth and DME dropouts due to not having RF multipath fences are not modeled.
- e. Multipath error magnitudes reflect performance without RF fences present.
- f. A somewhat idealized Orbiter antenna pattern unaffected by the Orbiter nose boom present on OV-101 is assumed.

- g. The effect of receiving only part of the scanning beam on signal levels at the edge of the angular coverage volume is neglected.
- h. Station location uncertainty, although traditionally modeled, is neglected due to expected survey accuracies.

10.4 MSBLS MODEL VALUES

The contingent values for Orbiter and ground antenna locations, coverage constraints, RF parameter computations, and error model formulations are listed below.

10.4.1 Geometric Observable Values (ref. 10-1)

$$\begin{matrix} \text{BODY} \\ \underline{R} \text{ ORB ANT} \end{matrix} = 67.9 \hat{x}_O - 1.3 \hat{z}_O \quad (\text{ft})$$

$$\begin{matrix} \text{RW} \\ \underline{R} \text{ AZ/DME} \end{matrix} = 16300 \hat{x}_{RW} \pm 300 \hat{y}_{RW} - 7.6 \hat{z}_{RW} \quad (\text{ft})$$

$$\begin{matrix} \text{RW} \\ \underline{R} \text{ EL} \end{matrix} = 3350 \hat{x}_{RW} \pm 300 \hat{y}_{RW} - 4.6 \hat{z}_{RW} \quad (\text{ft})$$

The plus or minus sign depends on whether the installation is on the left or right of runway centerline. The minus 7.6 and 4.6 feet represents the height of the antenna above ground (plus \hat{z}_{RW} is down).

10.4.2 Coverage Check Values

$$\text{DME SR MAX} = 119\ 090 \quad (\text{ft})$$

$$\text{AZ } \Psi_{\text{MAX}} = 17.0 \quad (\text{deg})$$

$$\text{EL } \Theta_{\text{MAX}} = 31.3 \quad (\text{deg})$$

10.4.3 RF Parameter Values

10.4.3.1 Ground Station Antenna Gains (ref. 10-2)

$$\begin{aligned} \underline{G}_R^{\text{DME GS}} &= 12 + 10 \sin(9(\theta_{\text{AZ/DME}}^{\text{RW}} - 3.5)) \\ &\quad - 20(1 - \cos(2.15 * \psi_{\text{AZ/DME}}^{\text{RW}})) - .15 * \theta_{\text{AZ/DME}}^{\text{RW}} \quad (\text{dBi}) \end{aligned}$$

$$\text{If } \left| \Psi_{\text{AZ/DME}}^{\text{RW}} \right| \geq 45^\circ; \quad G_{\text{R}}^{\text{DME GS}} = -10 \quad (\text{dBi})$$

$$G_{\text{T}}^{\text{AZ GS}} = \sum_{n=0}^5 C_n \left(\Theta_{\text{AZ/DME}}^{\text{RW}} \right)^n \quad (\text{dBi})$$

Where

$C_0 =$	2.10407996	E1
$C_1 =$	4.84938878	E0
$C_2 =$	-8.06039523	E-1
$C_3 =$	5.59289151	E-2
$C_4 =$	-1.91706739	E-3
$C_5 =$	2.64114983	E-5

$$G_{\text{T}}^{\text{EL GS}} = 27 \cos \left(1.336 * \Psi_{\text{EL}}^{\text{RW}} \right) \quad (\text{dBi})$$

$$\text{If } \left| \Psi_{\text{EL}}^{\text{RW}} \right| \geq 26^\circ; \quad G_{\text{T}}^{\text{EL GS}} = -100 \quad (\text{dBi})$$

10.4.3.2 Orbiter Antenna Gains

$G_{\text{ORB AZ/DME}}$ is a function of $\Theta_{\text{AZ/DME}}^{\text{BODY}}$ and $\Psi_{\text{AZ/DME}}^{\text{BODY}}$ while $G_{\text{R}}^{\text{ORB EL}}$ will

be computed using $\Theta_{\text{EL}}^{\text{BODY}}$ and $\Psi_{\text{EL}}^{\text{BODY}}$. Since the same antenna curve fit is used for both lines of sight the equation may be generalized to the form

$$\text{If } \left(2.56 \left(\Theta^{\text{BODY}} - 2 \right)^2 + \Psi^{\text{BODY}^2} \right)^{1/2} < 40$$

$$G_{\text{ORB}} = \sum_{n=0}^3 a_n * \left(2.56 \left(\Theta^{\text{BODY}} - 2 \right)^2 + \Psi^{\text{BODY}^2} \right)^{n/2} + 10 \quad (\text{dBi})$$

Where $a_0 = -5.578790329 \quad E-2$
 $a_1 = -1.916198777 \quad E-2$
 $a_2 = 8.122955059 \quad E-4$
 $a_3 = -1.066190991 \quad E-4$

Otherwise $G^{ORB} = -5 \quad (dBi)$

This low antenna gain represents exceeding the Orbiter antenna specified coverage volume.

10.4.3.3 Polarization Loss

The polarization mismatch angle (ϕ_{POL}) is assumed to be the angle between the Orbiter Z-axis and the runway X-Z plane. The orientation of the Orbiter Z-axis (\underline{Z}^{RW}_{ORB}) is contained in the last column of the body to runway transformation matrix (T^{-1}). ϕ_{POL} may be expressed as the complement

of the angle between \underline{Z}^{RW}_{ORB} and the runway Y-axis (\underline{Y}^{RW}).

$$\phi_{POL} = 90 - \cos^{-1} \left(\underline{Z}^{RW}_{ORB} \cdot \underline{Y}^{RW} / |\underline{Z}^{RW}_{ORB}| |\underline{Y}^{RW}| \right) \quad (deg)$$

The voltage interaction between the transmitted wave and receiving antenna, assuming linear polarization, is proportional to the cosine of ϕ_{POL} . The power loss in dB may be expressed as

$$L_{POL} = 20 * \text{LOG}_{10} | \cos \phi_{POL} | \quad (dB)$$

10.4.3.4 Path Loss

Assuming a wavelength (λ) corresponding to a frequency of 15.7 GHz, the equations for path loss reduce to

$$L_{\text{PATH}}^{\text{AZ/DME}} = -46 - 20 \cdot \text{LOG}_{10} (\text{SR}_{\text{AZ/DME}}) \quad (\text{dB})$$

$$L_{\text{PATH}}^{\text{EL}} = -46 - 20 \cdot \text{LOG}_{10} (\text{SR}_{\text{EL}}) \quad (\text{dB})$$

10.4.3.5 Constants

The following transmit power and cable loss assumptions lead to four constants that are summed with the computed parameters above yielding the received powers

<u>Link</u>	<u>Transmit power (dBm)</u>	<u>Transmit cable loss (dB)</u>	<u>Receive cable loss (dB)</u>
DME down	63	-3.8	-1.7
Azimuth up	62	-2.5	-3.8
Elevation up	62	-2.5	-3.8

$$K_{\text{DME DOWN}} = 57.5 \quad (\text{dBm})$$

$$K_{\text{AZ}} = 55.7 \quad (\text{dBm})$$

$$K_{\text{EL}} = 55.7 \quad (\text{dBm})$$

10.4.3.6 Receiver Thresholds (ref. 10.6)

$$\text{THRESHOLD}_{\text{DME}} = -77 \quad (\text{dBm})$$

$$\text{THRESHOLD}_{\text{AZ}} = -74 \quad (\text{dBm})$$

$$\text{THRESHOLD}_{\text{EL}} = -74 \quad (\text{dBm})$$

10.4.4 MSBLS Error Model Values

The majority of the error formulations presented are adapted from vendor (AIL) theoretical error analyses (ref. 10-9). Exceptions are referenced. Flight test

data indicate that real world measurement histories behave as theoretically predicted in general.

10.4.4.1 Azimuth Error Values

$$\Psi_{\text{BIAS}}^{\text{CAL}} = R_{N1}^{\Psi} * 10^{-3} * \left(202 + 113(1 + \cos(2 * \Psi_{\text{AZ/DME}}^{\text{RW}})) + 225 * \sin^2(2 * \Psi_{\text{AZ/DME}}^{\text{RW}}) * \tan^2(\theta_{\text{AZ/DME}}^{\text{RW}}) \right)^{1/2} \quad (\text{deg})$$

Where R_{N1}^{Ψ} = random number chosen from a unit variance, zero mean, normal distribution at the start of each approach and landing to remain constant through rollout

$\Psi_{\text{BIAS}}^{\text{CAL}}$ (1 σ) varies between 0.0142° and 0.017°. Modeling simplification is achievable by assuming the conservative 0.017° (1 σ) is constant (ref. 10-9).

If $\text{AZ}_{\text{TRUE}} > 13.5^{\circ}$

$$\Psi_{\text{BIAS}}^{\text{TRUNC}} = - (\text{AZ}_{\text{TRUE}} - 13.5) / 2 \quad (\text{deg})$$

If $\text{AZ}_{\text{TRUE}} < -13.5^{\circ}$

$$\Psi_{\text{BIAS}}^{\text{TRUNC}} = - (\text{AZ}_{\text{TRUE}} + 13.5) / 2 \quad (\text{deg})$$

Otherwise $\Psi_{\text{BIAS}}^{\text{TRUNC}} = 0^{\circ}$

The general formulation for an ECRV to model multipath for each measurement will be presented once. Thereafter, only correlation distance and one-sigma values to be used are listed (ref. 10-8).

First measurement:

$$\text{BIAS}_{MP}(t=0) = \sigma_{MP} * \text{RN}_2$$

Thereafter:

$$\text{BIAS}_{MP}(t) = a * \text{BIAS}_{MP}(t-\Delta t) + \sigma_{MP} (1 - a^2)^{1/2} * \text{RN}_2$$

Where σ_{MP} = one sigma value (deg or ft)

RN_2 = random number chosen each measurement

$$a = \exp(-\Delta t / \tau_{BS})$$

$$\tau_{BS} = D_{COR} * \Delta t / \{SR(t) - SR(T - \Delta t)\} \quad (\text{sec})$$

$$SR = SR_{AZ/DME} \text{ or } SR_{EL} \quad (\text{ft})$$

$$D_{COR} = \text{correlation distance} \quad (\text{ft})$$

SLMP

For Ψ BIAS -

$$\sigma_{SLMP} = .015 \quad (\text{deg})$$

$$D_{COR} = 6000 \quad (\text{ft})$$

$$\Psi_{GRND} \text{ NOISE} = \text{RN}_3 * 10^{-3} * (87 + 4.8 * \Psi_{RW} \text{ AZ/DME})^{1/2} \quad (\text{deg})$$

Where RN_3 - random number chosen each measurement

$$\Psi_{NAVSET} \text{ NOISE} = \text{RN}_4 * 10^{-3} * \{30 + 8.8 * 10^{(-4 - SAZ/10)}\}^{1/2} \quad (\text{deg})$$

Where RN_4^{Ψ} - random number chosen each measurement

10.4.4.2 Elevation Error Values

$$\Theta_{BIAS}^{CAL} = RN_1^{\Theta} 10^{-3} \{ 202 + (113(1 + \cos(2\Theta_{EL}^{RW})) + 169 \sin^2(2\Theta_{EL}^{RW})) \tan^2(\Psi_{EL}^{RW}) \}^{1/2} \quad (\text{deg})$$

Where RN_1^{Θ} - random number chosen at the first of each flight and to remain constant (different from RN_1^{Ψ}).

Note Θ_{BIAS}^{CAL} may be assumed a constant 0.017° (1σ) with little sacrifice in accuracy as with Ψ_{BIAS}^{CAL} (ref. 10-9).

If $EL_{TRUE} > 29.0^{\circ}$

$$\Theta_{BIAS}^{TRUNC} = - (EL_{TRUE} - 29.0) / 2 \quad (\text{deg})$$

Otherwise $\Theta_{BIAS}^{TRUNC} = 0^{\circ}$

(Note: Elevation beam truncation at the lower elevation angles is included in the main lobe multipath maximum value curve fits presented later.)

For Θ_{BIAS}^{SLMP} -

$$\sigma_{SLMP}^{\Theta} = .015 \quad (\text{deg})$$

$$D_{COR}^{\Theta} = 6000 \quad (\text{ft})$$

Θ_{BIAS}^{MLMP} (ref. 10-5) -

The path length traveled by the reflected ray (R_{REF}) must be computed for comparison with the direct ray path length (SR_{EL}^{RW}) in order to determine the phase difference between the two paths. θ_{BIAS}^{MLMP} is then assumed to vary sinusoidally as a function of this phase angle between upper and lower limits which change as a function of elevation angle (EL_{TRUE}). R_{REF}^{RW} may be computed similarly to SR_{EL}^{RW} but using +4.6 feet for the ground antenna location runway Z component. This represents the antenna image in the reflecting plane (the ground). The phase difference is then found by taking the fractional portion of the path difference divided by the number of feet per wavelength and multiplied by 360° :

$$\theta_{EL}^{MLML} = 360 * \text{FRAC} \{ (R_{REF}^{RW} - SR_{EL}^{RW}) / .06382 \} \quad (\text{deg})$$

Maximum and minimum error bounds are described by third order curve fits:

$$\theta_{MLMP}^{MAX} = \sum_{n=0}^3 a_n * (\theta_{EL}^{RW})^n \quad (\text{deg})$$

$$\theta_{MLMP}^{MIN} = \sum_{n=0}^3 -b_n * (\theta_{EL}^{RW})^n \quad (\text{deg})$$

where

$a_0 = 0.3786178992$	$b_0 = -0.5041173814$
$a_1 = -.5765868845$	$b_1 = 1.599867284$
$a_2 = .3409840709$	$b_2 = -1.231612944$
$a_3 = -.0700743883$	$b_3 = .2834967565$

The size of the mainlobe multipath error envelope (A) is then,

$$A = \theta_{\text{MLMP}}^{\text{MAX}} - \theta_{\text{MLMP}}^{\text{MIN}}$$

With a mean value (B) of

$$B = (\theta_{\text{MLMP}}^{\text{MAX}} + \theta_{\text{MLMP}}^{\text{MIN}})/2$$

The previously computed phase angle is used to determine $\theta_{\text{BIAS}}^{\text{MLMP}}$

If $\text{EL}_{\text{TRUE}} < 2^\circ$

$$\theta_{\text{BIAS}}^{\text{MLMP}} = \frac{A}{2} * \cos(\theta_{\text{EL}}^{\text{MLMP}}) + B \quad (\text{deg})$$

Otherwise $\theta_{\text{BIAS}}^{\text{MLMP}} = 0^\circ$

$$\theta_{\text{NOISE}}^{\text{GRND}} = \text{RN}_3 * 10^{-3} * \{ 30 + 1.6(\theta_{\text{EL}}^{\text{RW}}) \}^{1/2} \quad (\text{deg})$$

$$\theta_{\text{NOISE}}^{\text{NAVSET}} = \text{RN}_4 * 10^{-3} * \{ 30 + 3.3 * 10^{(-4 - S_{\text{EL}}/10)} \}^{1/2} \quad (\text{deg})$$

10.4.4.3 DME Error Values

$$\text{DME BIAS}^{\text{GRND OFFSET}} = 0.0068 * 10^{-(S_{\text{DMEDOWN}}/20)} - 3.7 \quad (\text{ft})$$

$$\text{DME BIAS}^{\text{NAVSET OFFSET}} = 18.0 \quad (\text{ft})$$

$$\text{DME BIAS}^{\text{GRND CAL}} = \text{RN}_1 * 5.0 \quad (\text{ft})$$

$$\text{DME NAVSET CAL BIAS} = \text{RN}_2^{\text{DME}} * \{ 71 + (1.97 + 0.00005 * \text{SR}_{\text{AZ/DME}}^{\text{RW}})^2 \}^{1/2}$$

For DME MP BIAS -

$$\sigma_{\text{MP}}^{\text{DME}} = 10 \quad (\text{ft})$$

$$D_{\text{COR}} = 6000 \quad (\text{ft})$$

$$\text{DME GRND NOISE} = \text{RN}_4^{\text{DME}} * \{ 25 + 0.15 * 10^{(-6 - S_{\text{DME DOWN}}/10)} \}^{1/2} \quad (\text{ft})$$

$$\text{DME NAVSET NOISE} = \text{RN}_5^{\text{DME}} * \{ 27 + 0.15 * 10^{(-6 - S_{\text{DME DOWN}}/10)} \}^{1/2} \quad (\text{ft})$$

Note: RN_1^{DME} and RN_2^{DME} are chosen once per flight while RN_3^{DME} (for ECRV), RN_4^{DME} , and RN_5^{DME} are sampled each DME measurement.

10.5 REFERENCES

- 10-1 Microwave Scanning Beam Landing System Handbook. Second Edition, JSC-09480, January 1976.
- 10-2 Chen, T. S.: MSBLS Signal Level Computations. Lockheed LEC 8635, March 1976.
- 10-3 Battle, Fred H.: MSBLS Error Analysis. AIL Technical Note A980-18, August 1975.
- 10-4 Space Shuttle Guidance, Navigation, and Flight Control Accuracy Control Document. RI/SD, June 1974.
- 10-5 Speir, R. E.: MSBLS Elevation Angle Errors. MDTSCO 1.2-TM-C0614-68, May 1977.
- 10-6 Microwave Scanning Beam Landing System Navigation Set Specification. RI/SD, MC409-0017, rev. A, July 1974.
- 10-7 MSBLS System Compatibility and Performance. Engineering Analysis 75-1, AIL Project A980, July 1976.
- 10-8 Eckelkamp, R. E.: Test Case for OFT 1 Nominal Entry-Landing Study. JSC FM83 (76-112), May 1976.
- 10-9 Hann, K.: MSBLS Error Model Simplification. Sperry Autoland Memo No. 32, March 1978.

~~PRECEDING PAGE BLANK NOT FILMED~~

APPENDIX A

REVIEW OF CONCEPTS

APPENDIX A
REVIEW OF CONCEPTS

A.1 RANDOM PROCESSES

A random, or stochastic process, is a set of random numbers each representing, in some way, the probabilistic outcome of a particular event. It is not necessary, in the understanding of the error models contained in this document, that one mathematically perceives the meaning of random processes since only a few simple types are used. The most simple, random noise and fixed bias, involve the multiplication of a representative standard deviation and a random number chosen from a given distribution. This section will discuss the methods by which a digital computer is utilized in generating random samples from two such distributions: (1) uniform over the interval zero to one, and (2) Gaussian (normal) with zero mean and unit variance.

A.1.1 PSEUDORANDOM NUMBERS

Chambers (ref. A-1) presents an excellent treatise on the generation of random numbers on digital computers. The reader is referred to this paper for more complete detail of the following description of the particular technique being presently used for error analysis studies.

The general form of the random number generating function used on digital machines is

$$x_{i+1} = ax_i + c \pmod{m}$$

where $x_j = j^{\text{th}}$ random number

$a =$ a multiplicative factor

~~PRECEDING PAGE BLANK NOT FILMED~~

c = an additive factor

m = a positive integer larger than x_j

This form is called the mixed congruential method. The special case where $c = 0$ is called the multiplicative congruential method. The behavior of the technique in terms of its period (quantity of random numbers before repetition) and its randomness (uniformity of distribution of consecutive pairs) is determined by the choice of a and c . It has been shown that a multiplicative congruential method ($c = 0$) with the multiplier, a , on the order of \sqrt{m} provides excellent randomness. Note, also, that the recursion relationship is deterministic. That is, the sequence of random numbers is repeatable for a given starting number, x_0 ; hence the term pseudorandom numbers.

The technique used on the Univac 1108, as programed in subroutine RDM, is a multiplicative method with $a = 5^{15}$. The choice of this constant has been based on randomness, it would seem, since a number based on speed of execution would be an integer power of 2 (allowing the multiplication to be reduced to bit shifting). The modulus, m , is chosen as the largest positive integer possible in the 36-bit word (377,777,777,777₈). In practice, this is merely the least significant 35 bits of the word in question. Actually, the multiplication by a causes (eventually) the integer to overflow into the adjacent register. When this occurs, the less significant register (that containing the less significant numbers) is used to extract the random number. Once this occurs, the integer bit pattern is converted to a floating point number and the mantissa (least significant 27 bits) is taken to be a uniformly-distributed random number on the unit interval.

Mathematically, it looks like this.

$$x_{i+1} = 5^{15}x_i \pmod{377,777,777,7778}$$
$$u_{i+1} = x_{i+1}^* \pmod{1}$$

where u is a uniformly-distributed random number on the unit interval.

A.1.2 OTHER DISTRIBUTIONS

Relatively few random processes are uniformly distributed, and it therefore becomes necessary to convert a uniform distribution to one of another distribution. The procedure is as follows.

$$\text{let } p_u(u) = 1 \quad 0 \leq u \leq 1 \text{ (uniform)}$$

where p is the probability density function.

It is desired that $y = f(u)$ has a density of $p(y)$.

If we can calculate

$$U = f^{-1}(y)$$

then

$$dP = p_u(u)du = 1 du = p(y)dy$$

Therefore,

$$u = f^{-1}(y) = \int p(y)dy + c$$

(where c is a constant of integration) is the desired transformation.

*Note that the integer x_{i+1} has been correlated to a floating point number.

A.1.3 GAUSSIAN DISTRIBUTION

The Gaussian, or normal, distribution is most frequently used in error analysis and is generated, through an intermediate process, in the following manner.

$$\text{let } p_u(u) = 1 \quad 0 \leq u \leq 1 \text{ uniform}$$

Produce a Rayleigh-distributed variable r by

$$r = \sigma(-2 \ln u)^{1/2}$$

where the probability density function for this variable is

$$p(r) = \frac{r}{\sigma^2} e^{-\frac{r^2}{2\sigma^2}}$$

It is now possible to produce a pair of correlated Gaussian variables using r and a uniformly-distributed variable θ :

$$x_1 = r \cos\theta$$

$$x_2 = r \sin\theta$$

where θ is uniform over zero to 2π .

Substituting and constraining the distribution to have unit variance,

$$x_1 = (-2 \ln u_1)^{1/2} \cos 2\pi u_2$$

$$x_2 = (-2 \ln u_1)^{1/2} \sin 2\pi u_2$$

Proof of this method in its ability to produce Gaussian variables can be generated by an inverse procedure.

Assume x_1 and x_2 are independent Gaussian variables with densities $p(x_1)$ and $p(x_2)$. Then, the joint density is

$$\begin{aligned} p(x_1, x_2) &= p(x_1)p(x_2) \\ &= \frac{1}{2\pi\sigma^2} e^{-1/2(x_1^2 + x_2^2)/\sigma^2} \end{aligned}$$

$$p(x_1, x_2) = \frac{1}{2\pi\sigma^2} e^{-\frac{r^2}{2\sigma^2}}$$

where $r^2 = x_1^2 + x_2^2$

To complete the substitution of variables, assume the new probability density to be of independent variables r and θ . That is

$$\begin{aligned} f(r, \theta) &= \frac{1}{2\pi\sigma^2} e^{-\frac{r^2}{2\sigma^2}} & 0 \leq r \leq \infty \\ & & 0 \leq \theta \leq 2\pi \end{aligned}$$

By differential probability

$$dP(r, \theta) = f(r, \theta)r dr d\theta$$

where P = cumulative distribution function

$$P(r) = \int_0^{2\pi} r f(r, \theta) d\theta$$

$$P(r) = \frac{r}{\sigma^2} e^{-\frac{r^2}{2\sigma^2}} \quad \text{Rayleigh distribution}$$

and

$$P(\theta) = \int_0^{\infty} r f(r, \theta) dr$$

$$P(\theta) = \frac{1}{2\pi} \quad \text{uniform over } 0 \rightarrow 2\pi.$$

This process is programed in subroutine RN2S.

A.2 GAUSS-MARKOV PROCESSES

A Markov process may best be explained by conditional probabilities through a simple example (ref. A-2). Let E_1, E_2, \dots, E_j be a complete system of events. Consider the outcome of a sequence of consecutive statistical trials (flipping a coin, rolling a die, etc.) from the view of the occurrence of the events E_j ($j = 1, 2, \dots$) and define the random variable ξ_n ($n = 1, 2, \dots$) as follows: $\xi_n = j$ if E_j is the outcome of the n^{th} trial.

When all trials are statistically independent

$$P\{\xi_n = j | \xi_0 = i_0, \xi_1 = i_1 \dots \xi_{n-1} = i_{n-1}\} = P\{\xi_n = j\}$$

That is, the probability that the j^{th} event will occur on the n^{th} trial is independent of the outcome of all previous trials.

If we define a sequence where the outcome of the n^{th} trial depends only on the preceding outcome ($n-1$), we have defined a first-order Markov process.

That is,

$$P\{\xi_n = j | \xi_0 = i_0, \xi_1 = i_1, \dots, \xi_{n-1} = i_{n-1}\} = P\{\xi_n = j | \xi_{n-1} = i_{n-1}\}$$

Extension of this definition to dependence on p prior realizations defines a p^{th} -order Markov process. The remainder of this discussion will concern itself with processes of order one.

It is reasonable to assume

$$E\{w(k)\} = 0$$

$$E\{w(k) w(j)\} = \begin{cases} q & k=j \\ 0 & k \neq j \end{cases} \quad (\text{pure noise})$$

$$E\{X(o)\} = X(o) \quad (\text{unbiased})$$

$$E\{(X(o) - \mu_x)^2\} = P_o$$

$$E\{X(o) - \mu_x\} w(k) = 0 \text{ for all } k$$

If the statistics of the random variables are Gaussian, the process is called Gauss-Markov. A scalar Gauss-Markov sequence and the variance of that sequence may be represented as (ref. A-3).

$$X(k+1) = \alpha(k+1, k) X(k) + w(k)$$

$$P(k+1) = \alpha^2(k+1, k) P(k) + q$$

where $X(i)$ = random variable at i
 α = correlation coefficient.
 $w(k)$ = purely random noise at k
 $P(j)$ = variance of $X(j)$
 q = variance of w

A solution for $X(k+1)$ and $P(k+1)$ in terms of $X(o)$ and $P(o)$ may be found through their recursion relationships by

$$X(k+1) = \alpha^{k+1} X(o) + \alpha^k w(o) + \alpha^{k-1} w(1) + \dots + w(k)$$

or

$$X(k+1) = \alpha^{k+1} X(o) + \sum_{j=0}^k \alpha^{k-j} w(j)$$

and

$$P(k+1) = \alpha^{2k} P(o) + \alpha^{2k-2} q(o) + \alpha^{2k-4} q(1) + \dots q(k)$$

but for q constant

$$P(k+1) = \alpha^{2k} P(o) + q \sum_{j=1}^k \alpha^{2j-2}$$

If $\alpha^2 < 1$,

$$P(k+1) = \alpha^{2k} P(o) + q \left(\frac{1 - \alpha^{2k}}{1 - \alpha^2} \right)$$

For the process to be stationary, P will approach a limit for $k \rightarrow \infty$, which can be satisfied for $\alpha^2 < 1$. Taking the limit,

$$\lim_{k \rightarrow \infty} P(k+1) = \lim_{k \rightarrow \infty} \left[\alpha^{2k} P(0) + q \frac{1 - \alpha^{2k}}{1 - \alpha^2} \right] = \frac{q}{1 - \alpha^2}$$

and

$$P(k) \rightarrow \frac{q}{1 - \alpha^2}$$

The standard deviation of $w(k) = \sqrt{q}$ allowing $w(k) = \sqrt{q} u(k)$ where $u(k)$ is a unit-variance, zero-mean Gaussian random variable

Now,

$$X(k+1) = \alpha X(k) + \sqrt{1 - \alpha^2} \sqrt{P(k)}$$

or

$$X(k+1) = \alpha X(k) + \sigma_x \sqrt{1 - \alpha^2} u(k)$$

where σ_x = standard deviation of $X(k)$,

which is the desired form.

For exponentially-correlated, time-related variables

$$\alpha = e^{-\Delta T / \tau}$$

ΔT = the time between k and $k+1$

τ = correlation time constant

causing the form of the process to become

$$X(t_{k+1}) = e^{-\Delta T / \tau} X(t_k) + \sqrt{1 - e^{-2\Delta T / \tau}} \sigma_x u(x)$$

A.3 QUANTIZATION ERRORS

Quantization, as the name implies, connotes the value of parameter being truncated or otherwise rounded off to some level of significance. A simple example of this concept is the digital computer where word length constrains the internal numerical significance and transformations between internal and I/O number bases cause further numerical inaccuracies.

For navigation systems the quantization of data due to the physical devices (both hardware and software) may have one of two effects. The first, which we might call destructive quantization, truncates or rounds the data to a certain level of significance and forever loses the knowledge of the remainder. Mathematically this appears as

$$X_{\text{actual}} \equiv X_{\text{actual}} - X_{\text{actual}} \bmod q$$

where q is the quantization level

A second type of quantization occurs when the actual system is retaining the complete significance of the data but the device utilized to read or sense the data is passive (does not disturb the data) and has a higher quantization level than the raw data. A simple example of this is a time clock used for punching times on cards, letters, etc. Although the time appears in truncated form (nearest minute, nearest second, or whatever) the internal clock is keeping time to a much higher degree. That is, the data not shown in a given output will be retained and manifested in the next output.

An example of this nondestructive quantization in navigation systems is a pulse accelerometer. This device accumulates sensed delta-velocity until a particular

threshold is reached where the accelerometer sends a pulse representing a particular quantum of output. So at any one time the observer has only the largest integer pulses available to him, but the device has retained the remainder. This remainder, of course, is used as the initial accumulation for the next pulse. Mathematically,

$$X_{\text{sensed}} \equiv X_{\text{actual}} - X_{\text{actual}} \bmod q$$

Note that the actual value has remained unperturbed.

Nondestruct quantization results in a correlation of the error in a given quantity. That is, the error or uncertainty in $X(i)$ is dependent on the error in $X(i-1)$. To return to our time clock example, if A punches in at 8:00:59 on a clock that truncates to the last minute, his card will read 8:00 and will be 59 seconds in error. B punches in 2 seconds later at 8:01:01. His card reads 8:01, which is only 1 second in error, but he gets his pay docked anyway. Even though they arrived 2 seconds apart, they appear to have arrived 1 minute apart.

Let's look at the pulse accelerometer again to determine the error for destruct and nondestruct quantization. Lear (ref. A-4) presents the following example. Assuming a gravity-free environment and linear motion, consider nondestruct data.

$$\hat{R}_i = \hat{R}_{i-1} + \delta V_i$$

where $\delta V_i = V_i + q_i - V_{i-1} - q_{i-1}$

At the end of the first sample period the velocity estimate, \hat{R}_1 , is

$$\begin{aligned}\hat{R}_1 &= \dot{R}_0 + (V_1 + q_1 - V_0 - q_0) \\ &= \dot{R}_1 + q_1 - q_0\end{aligned}$$

for \dot{R}_1 = true velocity at time 1.

At the end of the second period,

$$\hat{R}_2 = \dot{R}_2 + q_2 - q_0$$

and expanding to the i^{th} period,

$$\hat{R}_i = \dot{R}_i + q_i - q_0$$

The standard deviation, then, of the velocity error due to nondestruct quantization is

$$\sigma_{\hat{R}} = \sqrt{2} \sigma_q = \text{constant}$$

For the case of destruct accelerometer data the change in velocity over the interval $i-1 \rightarrow i$ is

$$\delta V_i = V_i - V_{i-1} + q_i$$

Note that the error in δV_i is uncorrelated (dependent only on the quantization error at i , q_i). Performing a similar analysis as for the nondestruct case

$$\hat{R}_i = R_i + (q_i + q_{i-1} + \dots + q_1)$$

Calculating the standard deviation,

$$\sigma_R = \sqrt{i} \sigma_q$$

where i is the total number of samples.

Note that the error statistics are not constant and represent a larger error than nondestructive data for $i > 2$.

A.4 COVARIANCE MATRIX

Most error analyses, linear or Monte Carlo, utilize covariance matrices in several ways. Those most important to our discussion are the input and output matrices used for initializing and displaying results, respectively. The following discussion will assume a basic knowledge of statistics with respect to multivariate distributions, statistical moments, etc.

Given the n -dimensional vector random variable \bar{x} with joint density function $f(\bar{x})$ we can define the mean and variance of each component as well as joint or mixed moments in the following manner.

A.4.1 MEAN OF i^{th} COMPONENT

$$\mu_i = E(x_i) = \int_{-\infty}^{\infty} x_i f_i(\bar{x}) dx_i$$

where f_i = marginal density function of x_i

E = expected value operator

A.4.2 VARIANCE OF i^{th} COMPONENT

$$\sigma^2_{x_i} = E((x_i - \mu_i)^2) = \int_{-\infty}^{\infty} (x_i - \mu_i)^2 f_i(\bar{x}) dx_i$$

A.4.3 FIRST MIXED MOMENT ABOUT THE MEAN

$$\sigma_{ij} = E\{(x_i - \mu_i)(x_j - \mu_j)\} = \int_{-\infty}^{\infty} \int_{-\infty}^{\infty} (x_i - \mu_i)(x_j - \mu_j) f_{ij}(\bar{x}) dx_i dx_j$$

The mixed moment, σ_{ij} is sometimes called the covariant term and is actually composed of the following elements.

$$\sigma_{ij} = \rho_{ij} \sigma_i \sigma_j$$

where ρ_{ij} = correlation coefficient (linear)

σ_k = standard deviation of the k^{th} variable, x_k

A.4.4 CORRELATION COEFFICIENT

The variable ρ_{ij} above is shown to obtain the values

$$-1 \leq \rho_{ij} \leq 1$$

by proving the following inequality

$$|\sigma_{ij}| \leq \sigma_i \sigma_j$$

utilizing a technique outlined in reference A-5.

Consider the real variable λ and the function of λ

$$f(\lambda) = E\{(x_i - \mu_i) - \lambda(x_j - \mu_j)\}^2 \geq 0.$$

It must be true that $f(\lambda) \geq 0$ since it represents the variance (by definition) of a zero-mean, random variable for all λ . Expanding

$$f(\lambda) = \sigma_i^2 - 2\sigma_{ij} \lambda + \sigma_j^2 \lambda^2 \geq 0$$

It follows that the quadratic $f(\lambda)$ has either no real roots or two equal real roots. The conditions for this is that the discriminant satisfies the inequality

$$\sigma_{ij}^2 - \sigma_i^2 \sigma_j^2 \leq 0$$

or

$$\sigma_{ij}^2 \leq \sigma_i^2 \sigma_j^2$$

If there are no real roots, $f(\lambda) > 0$ and we have

$$\sigma_{ij}^2 < \sigma_i^2 \sigma_j^2$$

Suppose there is a real number of λ_0 such that $f(\lambda_0) = 0$, it would follow that $\lambda_0 = \sigma_{ij}^2 / \sigma_j^2$ and for that value of λ_0 we would have

$$z = (x_i - \mu_i) - \lambda_0(x_j - \mu_j) = 0$$

for $f(\lambda_0) = E(z^2) = 0$

since the variance of a random variable is zero if (and only if) that variable is equal to its mean with probability one. Therefore, for the following equality

$$\sigma_{ij}^2 = \sigma_i^2 \sigma_j^2$$

holds only if there exists a linear functional relationship between x_i and x_j as defined as z above. We define this relationship to be

$$\sigma_{ij} = \rho_{ij} \sigma_i \sigma_j$$

such that

$$-1 \leq \rho_{ij} \leq 1$$

The linear functional relation is, of course,

$$x_i - \mu_i = \frac{\rho\sigma_i}{\sigma_j} (x_j - \mu_j) \quad \rho = \pm 1.$$

We may loosely presume the correlation coefficient, ρ_{ij} , to be some measure of the tendency of the two variables to be linearly related (that is, the tendency of samples of the variables to cluster about a line). This would imply, in estimation theory, the observability of certain parameters; that is, the separability of the effects of each within the observations. This knowledge could be very useful in predicting the outcome of a given experiment. We will use, as an example, a simple least-squares problem.

Given that we are trying to predict a value for x , namely \hat{x} , that minimizes the sum of the squared deviations, $\min E[(x - \hat{x})^2]$, we note that this yields $\hat{x} = \mu_x$. Suppose we have joint random variables (x, y) and we wish to again predict \hat{x} by observing y (linearly).

We therefore seek

$$\hat{x} = ay + b$$

which will minimize

$$E[(x - \hat{x})^2] = E[(x - ay - b)^2]$$

This equation may be written as

$$\begin{aligned} E[(x - \mu_x) - a(y - \mu_y) - b + \mu_x - a\mu_y]^2 \\ = \sigma_x^2 - 2a\sigma_{xy} + a^2\sigma_y^2 + (b - \mu_x + a\mu_y)^2 \end{aligned}$$

and is minimized by

$$b = \mu_x - a\mu_y$$

$$a = \frac{\sigma_{xy}}{\sigma_y^2} = \frac{\rho\sigma_x}{\sigma_y}$$

The best estimate becomes

$$\hat{x} = \frac{\rho\sigma_x}{\sigma_y} (y - \mu_y) + \mu_x$$

Note that for zero correlation, $\rho = 0$, the best estimate is the mean,

$$\hat{x} = \mu_x.$$

A.4.5 COVARIANCE MATRICES

Alluding again to our vector random variable $\bar{x} = (x_1, x_2, \dots, x_n)$ with joint density function $f(\bar{x}) = f(x_1, x_2, \dots, x_n)$, we may recall the following quantities

$$\mu_i = E(x_i) = \text{mean of } x_i$$

$$\sigma_i^2 = E((x_i - \mu_i)^2) = \text{variance of } x_i$$

$$\sigma_{ij} = \rho_{ij} \sigma_i \sigma_j = E((x_i - \mu_i)(x_j - \mu_j)) =$$

covariance of x_i and x_j

$$\rho_{ij} = \text{correlation coefficient between } x_i \text{ and } x_j$$

It follows that

$$E(\bar{x}) = \bar{\mu} = \begin{pmatrix} \mu_1 \\ \mu_2 \\ \vdots \\ \mu_n \end{pmatrix} = \text{vector mean}$$

$$E(\bar{x} - \bar{\mu})(\bar{x} - \bar{\mu})^T = \Lambda_x = \begin{bmatrix} \sigma_1^2 & \rho_{12} \sigma_1 \sigma_2 & \dots & \rho_{1n} \sigma_1 \sigma_n \\ \text{symmetric} & & & \sigma_n^2 \end{bmatrix} = \text{covariance matrix}$$

$$R_x = \begin{bmatrix} 1 & \rho_{12} & \dots & \rho_{1n} \\ & 1 & & \rho_{2n} \\ \text{symmetric} & & & 1 \end{bmatrix} = \text{correlation matrix}$$

Another convenient form of the correlation matrix is

$$R_x = \begin{bmatrix} \sigma_1 & \rho_{12} & \dots & \rho_{1n} \\ & \sigma_2 & & \\ & & & \\ & & & \sigma_n \end{bmatrix}$$

The relationship of the statistics, σ_x and σ_y , through use of the eigenvectors and eigenvalues, is developed in figure A-1 geometrically and for two dimensions. The extension to higher dimensions should be trivial since we only consider two variables at a time.

The covariance matrix shown above (Λ) as an equiprobability ellipse can be represented as the covariance matrix Λ_ϵ in its eigenspace (ϵ_1, ϵ_2), in which case it would be diagonal, and as the matrix Λ_x in the space (x_1, x_2). The characteristic equation for the surface may be computed as (ref. A-6).

ORIGINAL PAGE IS
OF POOR QUALITY

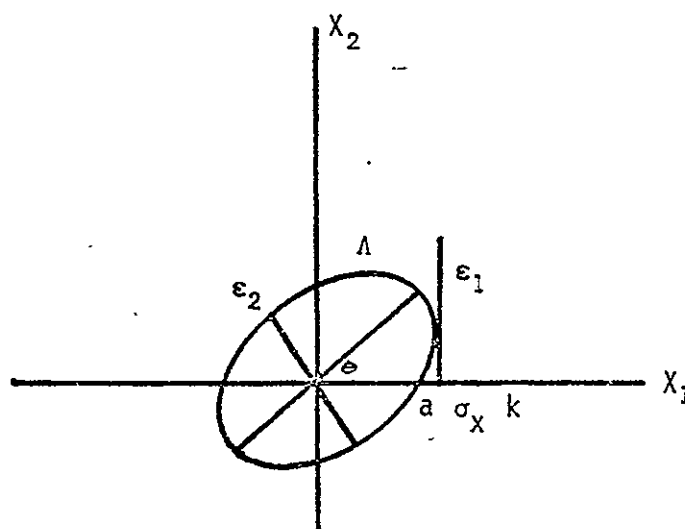


Figure A-1.- Equiprobability ellipse.

$$k^2 = \bar{X}^T \Lambda^{-1} \bar{X}$$

where \bar{X} is any arbitrary vector.

If we chose to represent the matrix as Λ_{ϵ} and chose an eigenvector of length ϵ_2 as \bar{X} , then the above equation reduces to

$$k^2 = 1$$

Since this must hold true over all orthogonal transforms,

$$k^2 = \bar{z}^T \Lambda_x^{-1} \bar{z}$$

then

$$k^2 = 1 \text{ for all } \bar{z} \text{ that intersect the ellipse}$$

and we will choose the vector a , o in x -space, which represents the intersect of the ellipse and the x_1 -axis. The above calculation results in

$$k^2 = a^2 / (\sigma_{x_1}^2 (1 - \rho^2)) = 1$$

or

$$a = \sigma_{x_1} (1 - \rho^2)^{1/2}$$

where it can be shown that σ_{x_1} is the intersect of a perpendicular to the extreme point of the ellipse with the x_1 -axis (fig. A-1). Inspection shows that $\rho\sigma_x$ completes the right triangle of side a and hypotenuse σ_x . The direction of that side depends on σ_{ϵ_1} and σ_{ϵ_2} (the eigenvalues of a one-sigma ellipse) and θ , the angle between ϵ_1 and x_1 .

If we consider the Λ_ϵ matrix and rotate to x-space, and get

$$\begin{bmatrix} \cos\theta & \sin\theta \\ -\sin\theta & \cos\theta \end{bmatrix} \begin{bmatrix} \sigma_{\epsilon_1}^2 & 0 \\ 0 & \sigma_{\epsilon_2}^2 \end{bmatrix} \begin{bmatrix} \cos\theta & -\sin\theta \\ \sin\theta & \cos\theta \end{bmatrix} = \begin{bmatrix} \sigma_{\epsilon_1}^2 \cos^2\theta + \sigma_{\epsilon_2}^2 \sin^2\theta & \sin\theta \cos\theta (\sigma_{\epsilon_2}^2 - \sigma_{\epsilon_1}^2) \\ \sin\theta \cos\theta (\sigma_{\epsilon_2}^2 - \sigma_{\epsilon_1}^2) & \sigma_{\epsilon_1}^2 \sin^2\theta + \sigma_{\epsilon_2}^2 \cos^2\theta \end{bmatrix}$$

The off-diagonal term may be equated to its x-space notation

$$\frac{1}{2} \sin 2\theta (\sigma_{\epsilon_2}^2 - \sigma_{\epsilon_1}^2) = \rho_{xy} \sigma_x \sigma_y$$

resulting in

$$\rho_{xy} \sigma_x = \frac{\sin 2\theta (\sigma_{\epsilon_2}^2 - \sigma_{\epsilon_1}^2)}{2\sigma_y}$$

The parameter σ_y has the same geometric interpretation as σ_x , the extreme value of the ellipse.

A.4.6 ADDITIONAL PROPERTIES

The covariance matrix is symmetric by its definition. It is also positive semidefinite, as is shown by the following proof.

Consider the vector constant \bar{a} and construct the scalar random variable

$$z = \bar{a}^t (\bar{X} - \bar{\mu}_x)$$

Then

$$E(z) = E(\bar{a}^T (\bar{x} - \bar{\mu}_x)) = \bar{a}^T E(\bar{x} - \bar{\mu}_x) = 0$$

and

$$\begin{aligned}
\sigma_z^2 &= E(z^2) = E(\bar{a}^T(\bar{x} - \bar{\mu}_x)(\bar{x} - \bar{\mu}_x)^T\bar{a}) \\
&= \bar{a}^T E((\bar{x} - \bar{\mu}_x)(\bar{x} - \bar{\mu}_x)^T)\bar{a} \\
&= \bar{a}^T \Lambda_x \bar{a} \geq 0 \text{ for all } \bar{a}
\end{aligned}$$

since variances are always nonnegative. Λ_x is positive semidefinite. For $z=0$ there exists a nonzero vector \bar{a}_0 such that

$$z_0 = \bar{a}_0^T (\bar{x} - \bar{\mu}_x) = 0$$

$$\bar{a}_0^T \Lambda_x \bar{a}_0 = 0$$

indicating that there exists a linear functional relationship between the components of \bar{x} (analogous to $|\rho| = 1$). There are $(n - k)$ such linear relationships where k is the rank of Λ_x .

Diamant (ref. A-7) has produced a parameter that is indicative of the elongation, or eccentricity, of an n -dimensional ellipsoid (representing an n -dimensional covariance matrix), which is called asphericity, and is computed as

The correlated random vector is computed from the mean and covariance matrix by

$$\bar{X} = \bar{\mu} + C \bar{U}$$

where C = a lower triangular matrix such that $CC^T = \Lambda$

\bar{U} = a vector of zero-mean, unit-variance random numbers generated by the technique described in section A.1.

This method is shown to provide the correct statistics by generating the covariance matrix for \bar{X} and comparing that to Λ by (ref. A-8).

$$(\bar{x} - \bar{\mu})(\bar{x} - \bar{\mu})^T = C \bar{U} \bar{U}^T C^T$$

Taking the expected value of both sides

$$E[(\bar{x} - \bar{\mu})(\bar{x} - \bar{\mu})^T] = C E(\bar{U} \bar{U}^T) C^T$$

but since

$$E(\bar{U} \bar{U}^T) = I$$

$$\Lambda_x = E[(\bar{x} - \bar{\mu})(\bar{x} - \bar{\mu})^T] = C C^T = \Lambda$$

The matrix C is determined from Λ by the square root method (ref. A-9) as follows.

$$c_{11} = \sqrt{\lambda_{11}} \quad , \quad c_{i1} = \lambda_{i1}/c_{11}$$

$$c_{ii} = \left(\lambda_{ii} - \sum_{k=1}^{i-1} c_{ik}^2 \right)^{1/2} \quad i > 1$$

$$c_{ij} = \left(\lambda_{ij} - \sum_{k=1}^{j-1} c_{ik} c_{jk} \right) / c_{jj} \quad i \geq j \geq 1$$

$$c_{ij} = 0 \quad i < j$$

The distribution of the output vector will, of course, depend on the distribution of the random vector \bar{U} . Computation of the elements c_{ij} is carried out successively by columns.

A.4.8 OUTPUT COVARIANCE MATRICES

Traditional output of error analyses is the mean and covariance matrix of the output vector random variable $y - \mu_y$ and Λ_y , respectively. An alternative method of interpreting error analyses results is presented below.

A.4.9 DIAGONAL ELEMENTS

Since we are all now experts on the properties of a covariance matrix, we immediately are drawn to the diagonal elements that we know represent variances of the individual components of the random vector. We are aware, however, that they represent marginal variances. That is, the variance of the i^{th} component of \bar{x} is:

$$\sigma_i^2 = \int_{-\infty}^{\infty} \int_{-\infty}^{\infty} \dots \int_{-\infty}^{\infty} (x_i - \mu_i)^2 f(x_1, x_2, \dots, x_n) dx_1 dx_2 \dots dx_n$$

It may be interpreted as the variance in the i^{th} component given the statistics of the other $n-1$ components and the dynamics of the system.

We may perform a similar analysis on several components at once when we realize that most of the vector variables we deal with contain components of different units (position, velocity, angles, etc.). The adding of variances with similar units produces a variance of the vector uncertainty magnitude in a multi-dimensional quantity. That is, the uncertainty in the magnitude of the error, not the uncertainty in the magnitude of the quantity. Since elements with like units are generally grouped together, the added variances constitute a semi-trace of the matrix. The square root of this quantity is called the root semi-trace (RST) and represents the standard deviation of the quantity. Note that this produces the same number as the root sum square (RSS) of the standard deviations of the same parameters (a very popular quantity).

A.4.10 OFF-DIAGONAL ELEMENTS

Recall that an off-diagonal element of a covariance matrix is composed of a linear correlation coefficient and two standard deviations

$$\lambda_{ij} = \rho_{ij} \sigma_i \sigma_j$$

Correlation coefficients, as we have noted above, indicate the tendency toward linear relationships between the variables. Even though it may not appear so at first glance, a correlation coefficient of one indicates a functional linear relationship between two variables independent of their units. This implies that such a coefficient appearing anywhere in the matrix denotes a singular matrix. A simple proof of this is offered by W. W. Ferry. Given that

$$\rho_{ij} = \pm 1$$

then the ratio of terms in the i^{th} and j^{th} rows is

$$\frac{\sigma_{ik}}{\sigma_{jk}} = \frac{\rho_{ik} \sigma_i \sigma_k}{\rho_{jk} \sigma_j \sigma_k} = \frac{\rho_{ik} \sigma_i}{\rho_{jk} \sigma_j}$$

Now, it follows that if $\rho_{ij} = \pm 1$, then

$$x_i - \mu_i = c(x_j - \mu_j) \text{ (linear dependence)}$$

and c is found by

$$\rho_{ij} = \frac{E((x_i - \mu_i)(x_j - \mu_j))}{\sigma_i \sigma_j} = 1$$

$$\frac{c E((x_j - \mu_j)^2)}{\sigma_i \sigma_j} = \frac{c \sigma_j^2}{\sigma_i \sigma_j} = 1$$

$$c = \frac{\sigma_i}{\sigma_j}$$

Again, constructing the ratio terms,

$$\frac{\sigma_{ik}}{\sigma_{jk}} = \frac{\rho_{ik} \sigma_i}{\rho_{jk} \sigma_j} = \frac{c E((x_j - \mu_j)(x_k - \mu_k)) \sigma_i}{E((x_j - \mu_j)(x_k - \mu_k)) \sigma_j}$$

$$\frac{\sigma_{ik}}{\sigma_{jk}} = \frac{\sigma_i^2}{\sigma_j^2} = \text{constant}$$

The above proof implies that now j is a constant times row i ; a sufficient condition for singularity.

The implication of a singular matrix depends on the problem being analyzed. In estimation problems singularity suggests nonobservability or ill-conditioning due to the dynamics of the system.

A.4.11 EIGENVECTORS AND EIGENVALUES

Since a nonsingular covariance matrix is symmetric and positive definite, it will have a set of n-positive eigenvalues λ_i and corresponding eigenvectors \bar{U}_i . The eigenvectors describe the direction of the principal axes of an n-dimensional ellipsoid and are an orthonormal set. The corresponding eigenvalues are the dimensions of these axes and may be used to represent the standard deviations of a set of independent random variables whose statistics are depicted in the original matrix (rotated into the x-space). That is,

$$\begin{bmatrix} \bar{U}_1 & \bar{U}_2 & \dots & \bar{U}_n \end{bmatrix} \begin{bmatrix} \lambda_1^2 & & & 0 \\ & \lambda_2^2 & & \\ & & \dots & \\ 0 & & & \lambda_n^2 \end{bmatrix} \begin{bmatrix} \bar{U} \\ \bar{U} \\ \cdot \\ \cdot \\ \bar{U}_n \end{bmatrix} = \Lambda_x$$

Insight into many problems may be gained by inspection of eigenvalues. A discussion of this subject is necessarily waived except for a simple example (ref. A-10). Consider the covariance matrix P associated with the particular estimation process.

$$\bar{y} = A\bar{x} + \bar{\eta}$$

where \bar{y} is a vector of independent observables

\bar{x} is the true state

$\bar{\eta}$ is a vector of noise

A is a linear matrix operator

where the best estimate of \bar{x} , \hat{x} may be

$$\hat{x} = (A^T W A)^{-1} A^T W \bar{y}$$

for $W =$ a weighting matrix

The covariance matrix associated with the error in the estimate is

$$P = (A^T W A)^{-1}$$

Suppose that we cannot invert $A^T W A$ for some reason (a criterion for deciding this ahead of time will be discussed later) and we wish to know what is wrong.

We generate the eigenvectors \bar{u}_i and their corresponding eigenvalues λ_i , which we know satisfy the equation

$$P^{-1} \bar{U} = U \Lambda$$

where $U =$ a matrix of eigenvectors $(\bar{u}_1 \bar{u}_2 \dots \bar{u}_n)$

$\Lambda =$ diagonal matrix of eigenvalues

We may diagonalize P^{-1} by

$$U P^{-1} U^T = D$$

where the components of D , d_{ii} represent statistics of n -independent random variables and represent the information in this variable gained by observing the y -vector.

Suppose d_{jj} is small. This means that little information can be gained about this parameter from our choice of observables and it would be best to ignore it or consider it another way.

On the other hand, say d_{kk} is large, implying good determination of this variable. Now, if \bar{u}_k (the eigenvector associated with the k^{th} parameter) had two large components (about equal) and the rest negligible, it is possible to determine a linear combination of the large components even if they are nonseparable. Insight into many similar problems may be gained by inspection of the eigenvalues and vectors of an information or covariance matrix.

Pace has pointed out that one criterion for inversion of a matrix on a digital computer is that the exponent of 10 in the ratio of the determinant to the trace have an absolute value less than the number of significant decimal digits contained in the machine word. That is, for

$$\frac{\text{DET}(\Sigma)}{\text{TR}(\Sigma)} = 10^m$$

$$|m| < \text{number of decimal digits}$$

is a necessary condition for invertability.

A.4.12 ONE-SIGMA VECTORS

By this time we should be familiar enough with scalar random variables to realize that their standard deviations represent a measure of the probability that a sample of one-sigma or less will occur. Similarly, we can assess probabilities to this many or that many sigma events. There does not appear, however, to be a simple extension to multidimensional random variables (random

vectors) of this concept. Detchmندی (ref. A-6) with reference to Cramer (ref. A-11), treats this subject excellently in a manner that is summarized below.

Let \bar{x} be a zero-mean, Gaussian random vector with covariance matrix Λ . Surfaces of equal probability are defined by

$$\bar{x}^T \Lambda^{-1} \bar{x} = k^2$$

where $k = \text{constant}$. This may be interpreted as any vector sample taken from Λ that satisfies a particular value of k^2 is equally probable.

Now the probability that a sample vector of dimension m lies within the ellipsoid defined by k is

$$P(k) = \frac{m}{2^{m/2} \Gamma(\frac{m}{2} + 1)} \int_0^k r^{m-1} e^{-1/2 r^2} dr$$

where $\Gamma(l) = \int_0^\infty e^{-x} x^{l-1} dx = \text{gamma function}$

For the special cases of $m = 2, 3,$ and $6,$

$m=2$

$$P(k) = 1 - e^{-k^2/2}$$

$m=3$

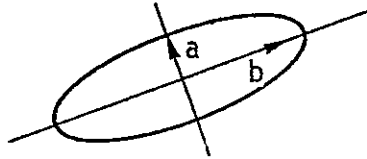
$$P(k) = \frac{2}{\pi} \int_0^k e^{-1/2 r^2} dr$$

m=6

$$P(k) = 1 - \frac{k^4}{8} + \frac{k^2}{2} + 1 e^{-1/2 k^2}$$

A plot of these functions is given in figure A-2.

We note two interesting points: (1) any eigenvector \bar{u}_i of length λ_i is a one-sigma vector ($k=1$), and (2) the length of a vector may not be representative of its probability of occurrence. That is, a short vector in the direction of the smallest principal axis may be less likely than a relatively long vector in the direction of the longest axis.



Even though b is longer than a , it is more likely to occur.

A.4.13 ACCURACIES OF SAMPLE COVARIANCE MATRICES

A question that necessarily arises when generating covariance matrices by Monte Carlo Analysis concerns the accuracy with which the sample variances and correlation coefficients have been constructed in N samples. In the discussion below we will note two features: (1) the accuracy in constructing variances is independent of the size of the variance whereas, (2) the accuracy in constructing a correlation coefficient depends on its sample value:

The accuracy with which the sample value of a variance S^2 is computed in N samples (when compared to its theoretical value σ^2) is given in figure A-3 (ref. A-12) for various levels of confidence. At 90 percent confidence we see that for

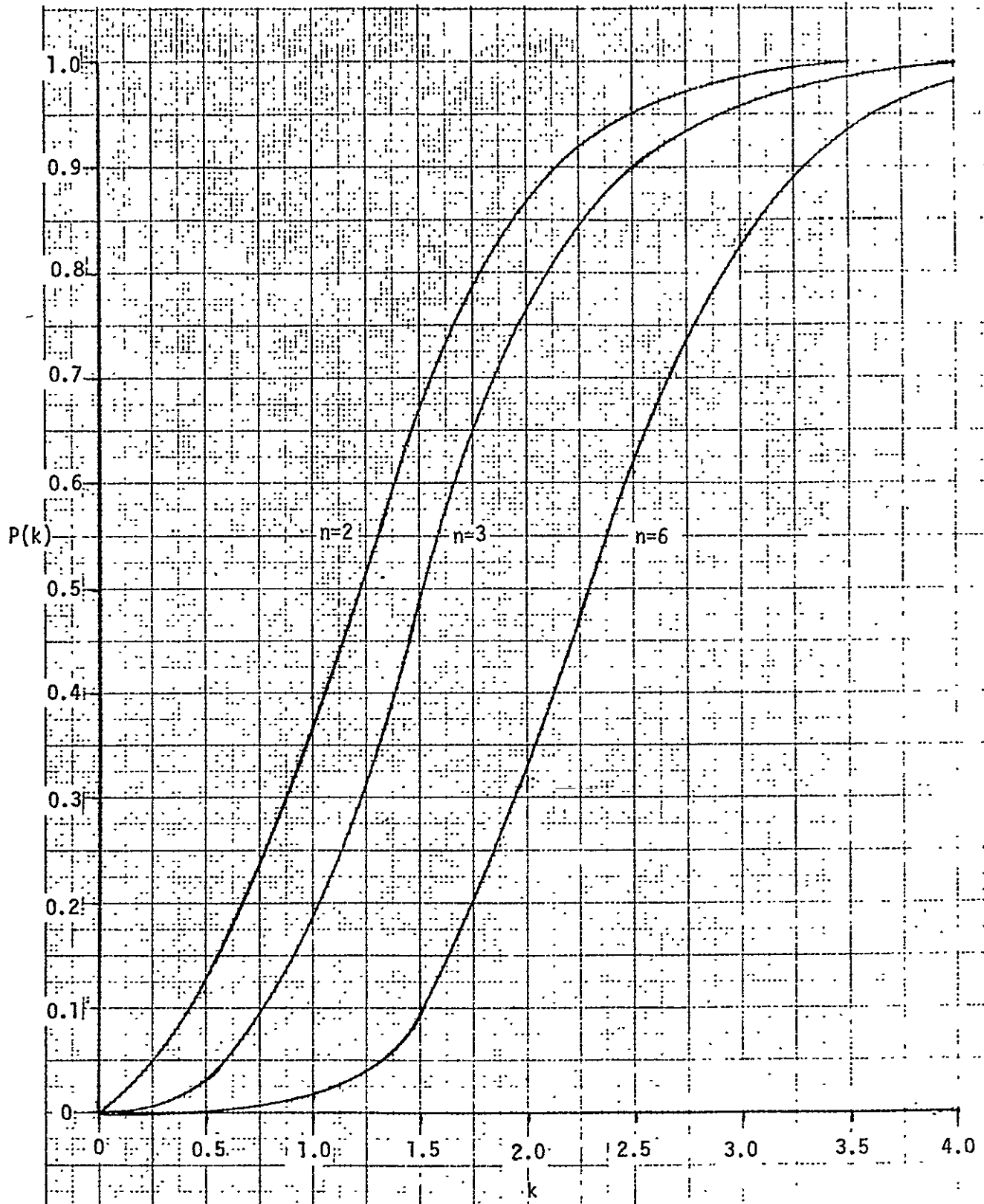
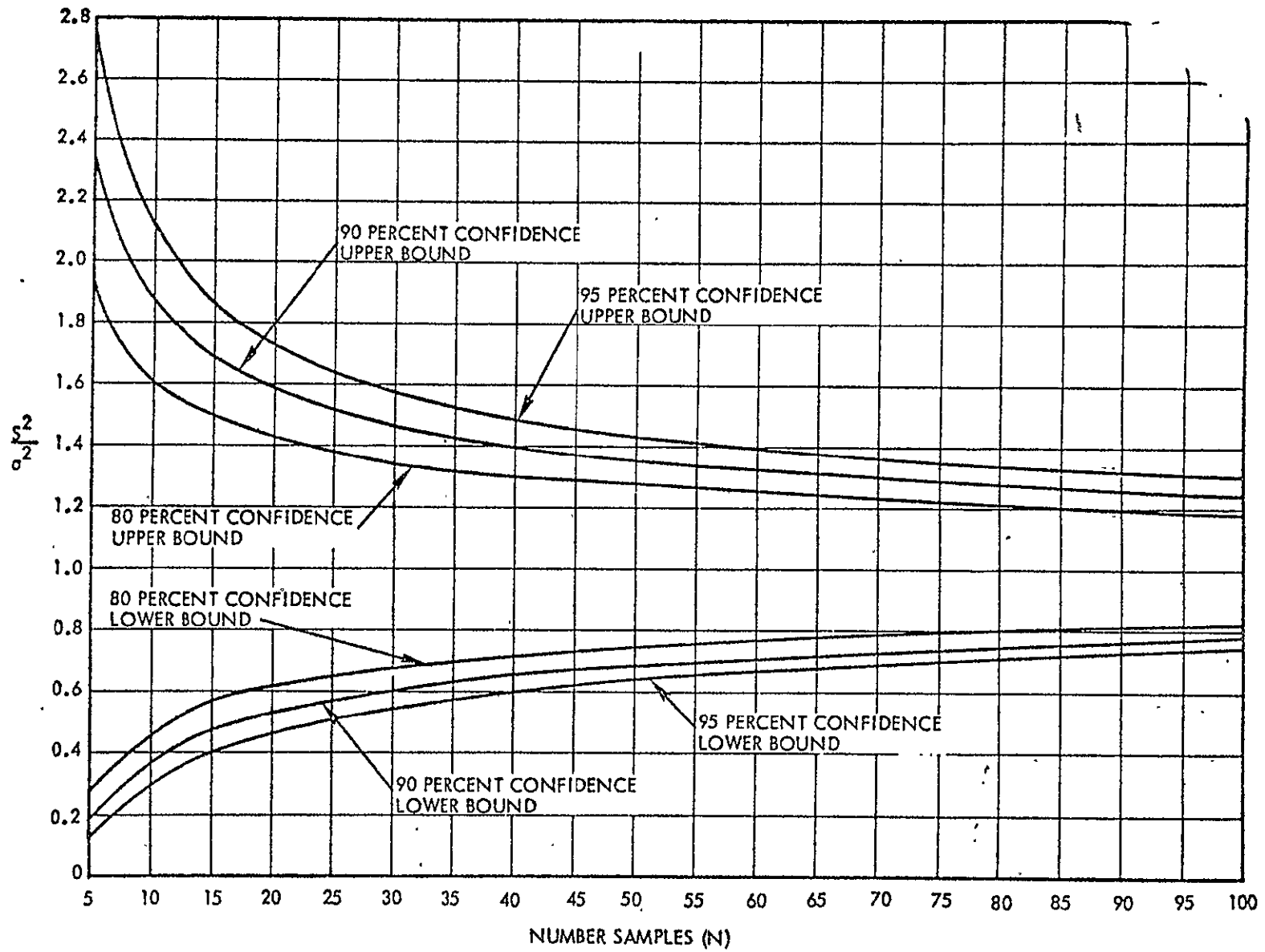


Figure A-2.- Likelihood of occurrence for multidimensional Stochastic variables.

A-35



ORIGINAL PAGE IS
OF POOR QUALITY

Figure A-3.- Accuracy of empirically-derived variances.

30 samples the true standard deviation will be within $\pm 0.23\sigma$ of the sample value S . If we up the sample size to 100, this difference becomes ± 0.12 ; not quite halving the error for more than tripling the sample size. Note the following.

- a. The value $\frac{S^2}{\sigma^2}$ is independent of S .
- b. Due to the flattening of the curves for increasing N , one must increase the sample size many-fold for lesser increases in accuracy.
- c. Extension of these curves will show that 1 percent accuracy in σ can be achieved at 90 percent confidence for N around 550.
- d. The sample size most appropriate for a given problem depends on what interpretation is placed on the answers. If one wishes to assign probabilities to these standard deviations, he must know the distribution of the results. Traditionally, we assume the results to be Gaussian (by the Central Limit Theorem) when they are only approaching a Gaussian distribution. Such an assumption may completely invalidate the use of large sample sizes.

Correlation coefficients behave a little differently (ref. A-13). Define the following terms.

r = computed value of correlation coefficient

ρ = theoretical value of correlation coefficient

N = number samples to compute r

$$Z = \frac{1}{2} \ln \frac{1+\rho}{1-\rho}$$

If the distribution of the samples is Gaussian, then Z has a nearly Gaussian probability density function with

$$\text{mean} = \frac{1}{2} \ln \frac{1+\rho}{1-\rho}$$

$$\text{variance} = \frac{1}{N-3}$$

The confidence limits for r may be determined by the following examples.

- a. Example 1.- Suppose for $N = 100$ observations a value of $r = 0.8$ is computed, then $Z = 1.098$ and the standard deviation is 0.101 . Since Z is nearly Gaussian, then it will be within $\pm 1.65 \sigma$ of its mean 90 percent of the time (i.e., the 90 percent confidence level). Thus, with 90 percent confidence $\frac{1}{2} \ln \frac{1+\rho}{1-\rho}$ is within $1.098, \pm 1.65 (0.101)$; i.e., within 0.931 to 1.265 . Translating this to the correlation coefficient, ρ , then, with 90 percent confidence is within $\rho_1 = 0.70$ to $\rho_2 = 0.852$.
- b. Example 2.- In order to illustrate the manner in which the confidence level values for ρ vary with the computed value of r , consider the identical case as above except with $r = 0.3$. For a 90 percent confidence level on ρ , the interval works out to be $\rho_1 = 0.143$ to $\rho_2 = 0.40$.

So we see that as the correlation coefficient estimate r gets smaller its accuracy becomes less. But, as the coefficient becomes smaller, the results are less influenced by its size and the two effects cancel each other.

A:6 REFERENCES

- A-1 Chambers, R. P.: Random Number Generation on Digital Computers. IEEE Spectrum, February 1967.
- A-2 Takacs, Lajos: Stochastic Processes. Science Paperbacks, Methuen and Co., Ltd. (London), 1966.
- A-3 Ingram, D. S.: The Standard Deviation of the Purely Random Component of a First-Order, Stationary, Gauss-Markov Sequence. TRW IOC 4922.7-71-114, June 11, 1971.
- A-4 Lear, W. M.: A Prototype, Real-Time Navigation Program for Multi-Phase Missions. TRW Report 17618-6003-TO-00, December 1, 1971.
- A-5 Solloway, C. B.: Elements of the Theory of Orbit Determination. JPL EPD-225, December 9, 1964.
- A-6 Detchmندی, D. M.: Good and Bad Error Vectors, or What's a Three-Sigma Vector? TRW IOC 5522.5-130, July 7, 1969.
- A-7 Diamant, L. S.: The Observability of Unforced Physical Systems by Linear Non-Sequential Estimators in the Validation of Linear Error Analysis. AIAA Guidance and Control Conference (Stanford), August 1972.
- A-8 Miller, A.: Monte Carlo Input - Correlated Random Vector Generator. TRW IOC 7221.5-127, January 13, 1967.
- A-9 Fadeeva, V. N.: Computational Methods of Linear Algebra. Dover Publications, Inc., 1959.

- A-10 Morrison, D. D.: The Use of Eigenvectors and Eigenvalues. TRW IOC
PA-2027-01/5, May 18, 1959.
- A-11 Cramer, H.: Mathematical Methods of Statistics. Princeton University
Press, 1966.
- A-12 Miller, A.: An Introduction to Monte Carlo Analysis. TRW IOC 3401.22-21,
April 11, 1968.
- A-13 Dixon, W. J.; and Massey, F. J., Jr.: Introduction to Statistical Analysis.
McGraw Hill (New York), 1957.

~~PRECEDING PAGE BLANK NOT FILLED~~

APPENDIX B

ENVIRONMENT PHENOMENOLOGY AND MODELING ERRORS

APPENDIX B.1

COORDINATE TRANSFORMATIONS

The coordinate transformation of primary interest is that between the reference inertial coordinate system and the (rotating) Earth-fixed geodetic coordinate system. For Space Shuttle work, the mean of 1950.0 coordinate system has been adopted as the reference inertial system.

Numerous subroutines that exactly perform this transformation based upon the adopted values of the relevant astronomical constants are available. These subroutines are consistent to 14 or more significant figures with the adopted constants. Two such subroutines are documented in the following reports: the Houston Operations Predictor/Estimator (HOPE) Engineering Manual (ref. B.1-1) and Description of a Self-Contained Subroutine which Analytically Generates Interplanetary Coordinate System Transformations Referenced to the Mean of 1950.0 Epoch (ref. B.1-2).

The exact subroutines are much too long for use in an onboard computer. A simpler subroutine more suitable for onboard use is documented in volume II of the Space Shuttle Navigation Software (ref. B.1-3) documentation.

This simpler subroutine is consistent with the more precise subroutines to about 7-8 significant digits, or about 1 foot at the surface of the Earth.

Errors in the transformation from the inertial system to the Earth-fixed system are generally ignored as a separate error source.

A second coordinate transformation of interest is that between the Earth-fixed coordinate system and the topocentric coordinate system at a point on the Earth's

~~PRECEDING PAGE BLANK NOT FILMED~~

surface. The topocentric system is oriented with its axes in the vertical, east, and north directions. Equations defining the transformation may be found in reference B.1-3.

Errors in this transformation are negligible compared to errors in quantities measured in this coordinate system (e.g., elevation angle).

The various coordinate systems that will be used during the Space Shuttle program are described in the Coordinate Systems for the Space Shuttle document (ref. B.1-4).

B.1.1 REFERENCES

- B.1-1 Houston Operations Predictor/Estimator (HOPE) Engineering Manual, Revision 1. TRW Note No. 70-FMT-792A, (11176-H408-RO-01) June 1970.
- B.1-2 Description of a Self-Contained Subroutine which Analytically Generates Interplanetary Coordinate System Transformations Referenced to the Mean of 1950.0 Epoch. TRW Note No. 70-FMT-853, September 30, 1970.
- B.1-3 Space Shuttle Navigation Software, Vol. II, Environment Subroutines. MSC IN 72-FM-132, June 1972.
- B.1-4 Coordinate Systems for the Space Shuttle. NASA TMX-58153 (JSC-09084), October 1974.

APPENDIX B.2
GRAVITY MODEL

B.2.1 GENERAL DESCRIPTION

The motion due to the gravitational interaction of two point masses is completely defined by the inverse square law of Newton. Newton's law also applies to radially homogeneous spheres. However, the gravitational potential of most physical masses found in the universe must be altered somewhat from the idealized two-point representation due to nonsphericity, nonhomogeneity, rotational dynamics, and nonrigid deformational effects. Methods of modeling the Earth's geopotential include spherical harmonic expansions, point mass representations, ellipsoidal harmonic expansions, density layer models, etc.

An Earth gravity model formulation due to Pines (ref. B.2-1 and B.2-2) requires that the orientation of a point in space be expressed in terms of direction cosines $s = x/r$, $t = y/r$, and $u = z/r$, where x , y , z are the Earth-fixed Cartesian components of the position vector of magnitude r . The formulation due to Pines is free of singularities (except at the origin) as the direction cosines are always well defined for any direction in space. Any formulation for the potential function and its derivatives is expressed in terms of an infinite series. However, it has been found that the gravity model obtained using the Pines formulation requires one-third the storage required for the classical formulation and that it executes at least 11 times faster due to the elimination of all trigonometric functions.

Earth gravity is modeled by the onboard software for all phases of a Space Shuttle flight. The degree and order of the gravity model used are varied

according to the flight phase and the availability of IMU velocity data. During the ascent, entry, and RTLS phases, a fourth degree by fourth order (4x4) gravity model is used during coasting periods (IMU delta velocities less than a given threshold); otherwise, for these phases, a 2x0 gravity model is used. During the onorbit and onorbit checkout phases a 2x0 gravity model is used during powered periods (IMU delta velocities greater than a given threshold); otherwise, for these phases, a 4x4 gravity model is used.

B.2.2 ENVIRONMENTAL MODEL

- a. Assumptions - in propagating the trajectory, the Shuttle vehicle is treated as if it were a point mass as far as gravitational forces are concerned.
- b. Equations - the expansion used to model the Earth's potential V is given by

$$V = \sum_{n=0}^{\infty} \rho_n \sum_{m=0}^n A_{n,m}(u) D_{n,m}(s,t)$$

where

n is the degree

m is the order

$$\rho_n = \mu a_e^n r^{-n-1} = a_e \rho_{n-1}/r$$

μ = Earth's gravitation constant

a_e = Earth's equatorial radius

$$A_{n,m}(u) = (n+m-1) A_{n-1,m-1}(u) + u A_{n-1,m}(u)$$

$$A_{1,0} = 0; \quad A_{1,1} = 1$$

$$D_{n,m} = C_{n,m} R_m(s,t) + S_{n,m} I_m(s,t)$$

$C_{n,m}$ and $S_{n,m}$ are the classical spherical harmonic coefficients

$R_m(s,t)$ and $I_m(s,t)$ are the real and imaginary parts, respectively, of the complex number $(s + it)^m$.

where $i = \sqrt{-1}$, and $s = x/r$, $t = y/r$, $u = z/r$.

x,y,z are the Earth-fixed Cartesian coordinates of the Shuttle vehicle

r is the distance from the center of the Earth to the Shuttle vehicle.

$R_m(s,t)$ and $I_m(s,t)$ are given by the recursive relations

$$R_m(s,t) = s R_{m-1}(s,t) - t I_{m-1}(s,t)$$

$$I_m(s,t) = s I_{m-1}(s,t) + t R_{m-1}(s,t)$$

where $R_0(s,t) = 1$, and $I_0(s,t) = 0$.

The gravitation acceleration of the Shuttle about the Earth is then given by the gradient of the potential function V . It can be shown that $\underline{\nabla}V$ is given by

$$\underline{\nabla}V = \sum_{m=0}^{\infty} \frac{\rho_{n+1}}{a_e} \sum_{m=0}^n (mA_{n,m}(u) (E_{n,m}(s,t)\underline{i} + F_{n,m}(s,t)\underline{j}) + A_{n,m+1}(u)D_{n,m}(s,t)\underline{k} - A_{n+1,m}(u)D_{n,m}(s,t) (\underline{si} + \underline{tj} + \underline{uk}))$$

where

$\underline{i}, \underline{j}, \underline{k}$ is a set of orthogonal unit base vectors along the coordinate axes x,y,z of the Earth-fixed system

$$E_{n,m}(s,t) = C_{n,m}R_{m-1}(s,t) + S_{n,m}I_{m-1}(s,t)$$

$$F_{n,m}(s,t) = S_{n,m}R_{m-1}(s,t) - C_{n,m}I_{m-1}(s,t).$$

Table B.2-I presents the recommended input gravity model coefficients that are baselined for the Space Shuttle software (refs. B.2-3, B.2-4, and B.2-5).

TABLE B.2-I GRAVITY MODEL COEFFICIENTS

Zonal harmonic coefficients

C(1,0)	=	0.0	C(5,0)	=	+2.1923000-07
C(2,0)	=	-1.0826283-03	C(6,0)	=	-5.2317000-07
C(3,0)	=	+2.5418000-06	C(7,0)	=	+3.7219000-07
C(4,0)	=	+1.6086000-06	C(8,0)	=	+1.7564000-07

Tesseral and sectorial coefficients

C(2,1)	=	-1.1619-09	S(2,1)	=	-4.1312-09
C(2,2)	=	1.5654-06	S(2,2)	=	-8.9614-07
C(3,1)	=	2.1625-06	S(3,1)	=	2.6809-07
C(3,2)	=	3.1875-07	S(3,2)	=	-2.1556-07
C(3,3)	=	9.7078-08	S(3,3)	=	1.9885-07
C(4,1)	=	-5.1257-07	S(4,1)	=	-4.4095-07
C(4,2)	=	7.7390-08	S(4,2)	=	1.4970-07
C(4,3)	=	5.7700-08	S(4,3)	=	-1.2389-08
C(4,4)	=	-3.4567-09	S(4,4)	=	6.4464-09
C(5,1)	=	-5.8574-08	S(5,1)	=	-7.2105-08
C(5,2)	=	1.0764-07	S(5,2)	=	5.0363-08
C(5,3)	=	-1.5381-08	S(5,3)	=	-6.4318-09
C(5,4)	=	-1.9349-09	S(5,4)	=	2.8031-10
C(5,5)	=	4.5428-10	S(5,5)	=	-1.7529-09
C(6,1)	=	-5.7751-08	S(6,1)	=	-1.1802-08
C(6,2)	=	7.991-09	S(6,2)	=	-4.6527-08
C(6,3)	=	2.3844-10	S(6,3)	=	2.0319-10

TABLE B.2-I.- Continued

Tesseral and sectorial coefficients

C(6,4)	=	-3.2820-12	S(6,4)	=	-1.7621-09
C(6,5)	=	-2.2170-10	S(6,5)	=	-4.4098-10
C(6,6)	=	4.0305-12	S(6,6)	=	-6.1204-11
C(7,1)	=	1.8305-07	S(7,1)	=	1.0137-07
C(7,2)	=	3.4492-08	S(7,2)	=	8.7152-08
C(7,3)	=	2.8003-09	S(7,3)	=	-2.5974-09
C(7,4)	=	-5.9607-10	S(7,4)	=	-2.9899-10
C(7,5)	=	9.3789-12	S(7,5)	=	8.0694-12
C(7,6)	=	-2.1337-11	S(7,6)	=	8.4194-12
C(7,7)	=	1.1576-12	S(7,7)	=	8.9043-14
C(8,1)	=	7.0093-09	S(8,1)	=	3.9788-08
C(8,2)	=	5.0102-09	S(8,2)	=	7.0635-09
C(8,3)	=	-3.8216-10	S(8,3)	=	-6.7434-10
C(8,4)	=	-3.0163-10	S(8,4)	=	3.7068-11
C(8,5)	=	-1.0317-11	S(8,5)	=	1.1258-11
C(8,6)	=	-2.6448-12	S(8,6)	=	7.0604-12
C(8,7)	=	3.3552-13	S(8,7)	=	4.1761-13
C(8,8)	=	-1.0606-13	S(8,8)	=	8.9361-14

Earth gravitational radius

$$a_e = 2.0925705+07 \text{ ft.}$$

Earth gravitational constant

$$\mu = 1.407645794+16 \text{ ft}^3/\text{sec}^2$$

B.2.3 ERROR SOURCES

As mentioned, the proposed formulation for modeling the gravity field of the Earth involves the use of an infinite series. Hence, one source of error is due to the truncation of the rather slowly convergent infinite series, the trade-off being numerical accuracy versus computation time and storage. Another source of error involves the numeric values of the coefficients used in the geopotential expansion. The values are based on a batch of observation data and, hence, must be consistent with the Earth gravitational constant and radius used in their calculation. Many of the higher-ordered coefficients are known to only a few significant digits.

B.2.4 REFERENCES

- B.2-1. Pines, S.: Uniform Representation of the Gravitational Potential and Its Derivatives. AIAA Journal, vol. II, no. 4, November 1973.
- B.2-2. Spencer, J. L.: Use of a Nonsingular Potential. JSC IN 75-FM-29, May 27, 1975.
- B.2-3. Space Shuttle OFT Level C Functional Subsystem Software Requirements Document GN&C, Part B, Navigation, On-Orbit. Rockwell International SD76-SH-0006, December 17, 1976.
- B.2-4. Lerch, F. J.; Richardson, J. A., and Brownd, J. E.: Goddard Earth Models: GEM5, GEM6. GSFC Report X-921-74-145.
- B.2-5. Kirkpatrick, J. C.: Zonal and Tesseral Harmonic Coefficients for the Geopotential Function, From Zero to 18th Order. JSC IN 75-FM-12, February 18, 1975.

APPENDIX B.3

ATMOSPHERE MODELS

B.3.1 GENERAL DESCRIPTION

The thermodynamic properties of the real-world atmosphere (temperature, pressure, density, and speed of sound) vary widely as functions of altitude, latitude, local weather conditions, time of day and year, and solar and geomagnetic activity. The following paragraphs describe the various types of atmospheric density models used for Space Shuttle development and operational support.

B.3.1.1 Standard Atmosphere Models

The properties of the Earth's atmosphere are described in references B.3-1, B.3-2, and B.3-3. Reference B.3-1 is the U.S. Standard Atmosphere, 1962, which is the result of a joint effort by NASA, the U.S. Air Force, and the U.S. Weather Bureau to depict idealized, middle latitude, year-round mean atmospheric conditions. Reference B.3-2, the U.S. Standard Atmosphere Supplements, 1966, was prepared in response to a need for atmospheric tables depicting conditions other than the midlatitude mean represented by the tables of the U.S. Standard Atmosphere, 1962. In September 1971 the Committee on Extension to the Standard Atmosphere (COESA) Working Group reviewed the temperature and density data derived from recent satellite and rocket observations. This review revealed a need to revise the 1962 Standard at altitudes above 50 kilometers. Data available for levels below 50 km were found to be in reasonably good agreement with the 1962 Standard. The U.S. Standard Atmosphere, 1976 (ref. B.3-3), with tables and graphs extending to 1000 km, was adopted by COESA in February 1975. These documents define the various standard atmosphere models, including

variation with latitude and season. Also given are tables of the atmospheric properties as a function of altitude, the equations and physical data from which the tables were generated, and polynomial approximations to the tabulated values.

B.3.1.2 Jacchia Atmosphere Model

Reference B.3-4 describes the Modified 1970 Jacchia Atmosphere Model, which replaces the 1968 and earlier Jacchia atmosphere models. The primary weakness of the 1968 and earlier models was the assumed constant boundary conditions at an altitude of 120 km. The 1970 Jacchia model assumes constant boundary conditions at 90 km, which closely corresponds to an observed layer of minimum variation in the global density distribution. The following characteristics of density are included in this model (ref. B.3-5):

- a. Variation with solar activity (daily and 3 month average)
- b. Diurnal variation
- c. Variation with geomagnetic activity (yearly mean and 3 hourly index)
- d. Semiannual variation
- e. Variation with height
- f. Seasonal-latitudinal variations of the lower thermosphere
- g. Seasonal-latitudinal variation of helium

To compute density at any point in the atmosphere, the Mission Control Center orbit prediction program will employ a model developed by Jacchia (ref. B.3-5) that corresponds to the 1970 Jacchia model in analytical structure but whose analytical formulation for the geomagnetic effect, semiannual, and helium variations have been updated. In the Jacchia model the first four variations are computed as changes in the exospheric temperature T_{∞} . One may then obtain

a rather complicated solution to the diffuse equilibrium equation, knowing T_{∞} and the height h . The density ρ may be determined from the solution of this equation for the different gas constituents. Also, the Jacchia model computes the last two variations, which becomes important for altitudes below 300 km. Although the model is accurate it requires a large amount of computer storage and execution time, thus making it ill-suited for the Shuttle's onboard computer program. However, the onboard program's atmospheric density model must be compatible with the Jacchia model that is used in the ground orbit prediction program.

B.3.1.3 B-M Density Model

The model described in section B.3.1.2 will be used by the Mission Control Center orbit prediction program. This model is quite accurate but it requires a large amount of storage and execution time. These undesirable features make it ill-suited for the Shuttle onboard program. It is desirable to have an onboard model with low storage and time requirements, but mission constraints require close agreement between onboard and ground programs. The Babb-Mueller (B-M) model was developed with this in mind.

The model employs a procedure by which coefficients in the model are calibrated so that it simulates the Jacchia model. The calibration is accomplished premission by direct use of the ground Jacchia model in the I-load program. The B-M model is sufficiently general that it can be used with no modifications to simulate any reference density model. Additional information about the model may be found in reference B.3-6.

B.3.2 ONBOARD FORMULATIONS FOR THE SPACE SHUTTLE

It is anticipated that calibrated models of atmospheric properties will be required in three cases

- a. Surface to 32 km (approx.) - An algorithm to convert sensed atmospheric pressure to an equivalent measurement of altitude is required to support the barometric altimeter (sec. 4.0).
- b. 30 km to 80 km (approx.) - An algorithm to compute density as a function of latitude and altitude will be required if the model presented in reference B.3-7 is used for entry analysis as discussed in appendix B.4.
- c. 125 km to 500 km (approx.) - An algorithm to compute density at orbital altitudes will be required to support state vector estimation.

B.3.2.1 Surface to 32 km

Measurements of the ambient atmospheric pressure by the barometric altimeter are converted to measurements of altitude for navigation updating. Section 4.0 discusses the accuracy with which this may be done. An algorithm for this problem is proposed in section 3.5.2 of reference B.3-8. In this algorithm the atmosphere is divided into several layers. In each layer the altitude is related to the pressure by a polynomial in the logarithm of the pressure ratio (p/p_b).

$$h = h_b - H_{p,b} \sum_{n=1}^N a_n (\ln(p/p_b))^n$$

where

p_b = base pressure of the layer

- a_n = polynomial coefficient
 $H_{p,b}$ = base pressure scale height
 h_b = geopotential altitude from the base of the layer
 p = measured pressure

The number of layers, and the parameters h_b , H_p , b , a_n , and p_b for each layer will be provided to the Shuttle. These are based upon ground reduction of meteorological observations.

For modeling barometric altimeter measurements in navigation simulations, it is both convenient and realistic to ignore the pressure algorithm and to model error sources directly as functions of altitude. (See sec. 4.0 for the error model and representative numerical values.)

B.3.2.2 30 kilometers to 80 kilometers

The altitude updating scheme discussed in reference B.3-7 requires an algorithm for computation of density as a function of latitude and altitude in the drag altitude region 30 km to 80 km. In this model the density is given by a four-layer, exponential function of altitude.

$$\rho = \rho_0 e^{-h/h_s}$$

where

- ρ_0 = base density
 h_s = scale height
 h = altitude above the Fischer's ellipsoid

In the above model, the base density (ρ_0) and scale height (h_s) are constants for each layer. Reference B.3-9 gives the following base density and scale

height constants used in modeling a four-layer density model for navigation error studies.

FOUR LAYER DRAG FORMULATION

<u>Altitude region, feet</u>	<u>Base density, kg/m³</u>	<u>Scale heights, meters</u>
85 200 to 155 348	1.6546565	6705.8
155 348 to 172 010	.47779728	8135.6
172 010 to 202 069	.42736363	8278.9
202 069 to higher	1.1927824	7274.9

However, it is possible to load a seasonal atmosphere where the base density and scale height are constants for each layer, but vary in value depending on the season and latitude of interest (ref. B.3-7). The following atmospheres have been specified for use

<u>Latitude</u>	<u>Season</u>
1962 Standard Atmosphere Model	All
60° N	Winter (January) Summer (July)
30° N	Winter (January) Summer (July) Spring (April)

These models were obtained from reference B.3-1 and exhibit an average curve fit error of 3 percent, with the maximum curve fits error never greater than 8 percent. Tables B.3-I through B.3-IV give the altitude regions, densities, base densities, and scale heights for each density model referenced above. The errors associated with the density model proposed for this altitude region can be grouped into two categories.

- a. Diurnal variation, which is a variation during a single day due to the heating of the atmosphere
- b. Variations from the model during any month of that season

These errors can be incorporated by varying ρ_0 and h_s or by specifying $\Delta\rho/\rho$ to account for the known excursions from the density model. The following tables present some recommended three-sigma error values for these error sources

Diurnal Variation	40 kilometers	65 kilometers
All latitudes	$\frac{\Delta\rho_0}{\rho_0} = 2.7\%; \frac{\Delta h_s}{h_s} = .05\%$	$\frac{\Delta\rho_0}{\rho_0} = 5.34\%; \frac{\Delta h_s}{h_s} = .10\%$

Variation from seasonal (for altitudes from 30 kilometers to 80 kilometers.

Latitude	Season	$\frac{\Delta\rho_0}{\rho_0}$, percent	$\frac{\Delta h_s}{h_s}$, percent
30° N	Winter (January)	12.01	1.39
	Summer (July)	9.90	.87
	Spring (April)	34.43	10.91
60° N	Winter (January)	4.32	2.31
	Summer (July)	7.92	1.68
1962 Standard Atmosphere Model - All		10.7	4.69

Table B.3-V presents the three-sigma density percentages versus altitude (30 to 80km) for the reference atmospheres. These two error sources are independent so that during any season the diurnal variations exist along with the predicted variation for that season. Also, it can be seen that the use of a seasonal atmosphere instead of the 1962 Standard Atmosphere reduces the predicted error (ref. B.3-7).

B.3.2.3 125 kilometers to 500 kilometers

In order to predict trajectories of orbiting vehicles, a model of the atmospheric density is required in the computation of aerodynamic forces.

Reference B.3-10 discusses the proposed replacement of the baselined Russian Atmospheric density model with the B-M density model for simulating the ground Jacchia model in the onboard software. The B-M density model, which computes density at orbital altitudes, uses the following equation for modeling density (ref. B.3-5).

$$\rho = \rho_0 \exp (A+B)$$

where A is the nighttime vertical profile

$$A = a_1 + a_2 h + a_3 / h$$

and B is the diurnal effect

$$B = (b_1 + b_2 h + b_3 / h) \left((1 + \cos \psi) / 2 \right)^{M/2}$$

where

ρ_0 = base density

h = altitude

$a_1, a_2, a_3, b_1, b_2, b_3$ = model parameters

M = power exponent of the diurnal term

$\cos \psi = [Z \sin \delta_s + \cos \delta_s (X \cos \gamma + Y \sin \gamma)] / R$

R = vehicle's distance from the center of the Earth

δ_s = declination of the Sun

γ = right ascension of the diurnal bulge

X, Y, Z = coordinates of the vehicle in M50 coordinates

The seasonal-latitudinal variation may be included in the B-M model. Since the Jacchia model computes this term as an explicit variation in the density, one may incorporate this in the B-M density model. The seasonal-latitudinal variation that is given by Jacchia is (ref. B.3-5)

$$\rho = \rho^* .10\epsilon$$

where

$$\epsilon = 0.02 (h-90)(\delta_v/|\delta_v|) \exp(-0.45(h-90)) \sin^2\delta_v \times \sin(360 (d+100)/Y)$$

where

- h = altitude in kilometers
- d = number of days into a year
- Y = number of days in a year
- δ_v = declination of the vehicle

This term may be rewritten so that the final form of the model is

$$\rho = \rho_0 \exp (A+B+C)$$

where

$$C = 0.04605 |Z| (Z/R^2)(h-90) \exp(-0.45(h-90)) \sin(360(d+100)/Y)$$

where

- Z = Z component of the vehicle's position vector
- h = altitude in kilometers
- Y = days in the year

d = initial day in the year

R = vehicle's distance from the center of the Earth

The sine term may be computed once with the initial day (d) and days in the year (Y) and then assumed constant. Reference B.3-5 discusses the calibration procedure for determining the nighttime vertical profile and diurnal coefficients through calibration to the Jacchia model. If one assumes that the power exponent of the diurnal term (M), ρ_0 and the bulge angle ϕ are known constants and unaffected by the solar activity or geomagnetic changes, the B-M density model has six coefficients to be determined. By careful study of the Jacchia model a value of $\phi = 37^\circ$, $M = 2.75$, and $\rho_0 = 1.22499 \text{ kg/m}^3$ has been adopted (ref. B.3-5).

However, all these values may be refined to obtain closer agreement with the Jacchia model. To compare the B-M density model to the Jacchia model, reference B.3-5 conducted several numerical experiments. Instead of comparing directly computed densities, predicted satellite positions are compared from a numerical orbit computation program. Several different orbits were chosen for the comparison; thus, the position difference is a good indication of the global difference between the density models used in the experiments. For each orbit the ballistic number was an average value for the Shuttle, $BN = 100 \text{ lb/ft}^2$, and the coefficient of drag, C_D was set to 2.2. Table B.3-VI displays the chosen orbits and table B.3-VII presents the results. The results in table B.3-VII are the differences in predicted position using the Jacchia model as compared to using the other three models or neglecting drag completely. It is apparent from the results of table B.3-VII that the B-M model gives better agreement to the Jacchia than either the U.S.S.R. or ADMB models.

TABLE B.3-I. DENSITY MODEL - 1962 STANDARD ATMOSPHERE

Altitude, m	ρ , kg/m ³	ρ_0 , kg/m ³	h_s , m
30480.0	0.01710		
32308.8	.01292		
34137.6	.00940		
35966.4	7.295 X 10 ⁻³	1.6724	6650.4
37795.2	5.533 X 10 ⁻³		
39624.0	4.221 X 10 ⁻³		
41452.8	3.239 X 10 ⁻³		
43281.6	2.498 X 10 ⁻³		
45110.4	1.937 X 10 ⁻³		
46939.2	1.439 X 10 ⁻³		
48768.0	1.142 X 10 ⁻³		
50596.8	9.066 X 10 ⁻⁴	.4811	8076.6
52435.6	7.219 X 10 ⁻⁴		
54254.4	5.796 X 10 ⁻⁴		
56083.2	4.640 X 10 ⁻⁴		
57912.0	3.702 X 10 ⁻⁴		
59740.8	2.945 X 10 ⁻⁴		
61569.6	2.345 X 10 ⁻⁴	.4938	8046.4
63398.4	1.875 X 10 ⁻⁴		
65227.2	1.489 X 10 ⁻⁴		
67056.0	1.174 X 10 ⁻⁴		
68884.8	9.186 X 10 ⁻⁵		
70713.6	7.128 X 10 ⁻⁵		
72542.4	5.482 X 10 ⁻⁵	4.596	6309.9
73761.6	4.578 X 10 ⁻⁵		
75590.4	3.464 X 10 ⁻⁵		
77419.2	2.593 X 10 ⁻⁵		
79248.0	1.909 X 10 ⁻⁵		
81076.8	1.351 X 10 ⁻⁵		
82905.6	9.561 X 10 ⁻⁶		
84734.4	6.766 X 10 ⁻⁶		

ORIGINAL PAGE IS
OF POOR QUALITY

ORIGINAL PAGE IS
OF POOR QUALITY

79FM5

TABLE B.3-II.- SEASONAL DENSITY MODEL - JANUARY 60° N AND JULY 60° N

JANUARY 60° N				JULY 60° N			
Altitude, km	ρ , kg/m ³	ρ_0 , kg/m ³	h_S , m	Altitude, km	ρ , kg/m ³	ρ_0 , kg/m ³	h_S , m
32	1.170 X 10 ⁻²			32	1.443 X 10 ⁻²		
34	8.487 X 10 ⁻³			34	1.061 X 10 ⁻²		
36	6.106 X 10 ⁻³	1.8898	6301.1	36	7.857 X 10 ⁻³	1.525	6881.0
38	4.424 X 10 ⁻³			38	5.861 X 10 ⁻³		
40	3.228 X 10 ⁻³			40	4.402 X 10 ⁻³		
42	2.371 X 10 ⁻³			42	3.328 X 10 ⁻³		
44	1.753 X 10 ⁻³			44	2.548 X 10 ⁻³		
46	1.303 X 10 ⁻³			46	1.969 X 10 ⁻³		
48	9.571 X 10 ⁻⁴			48	1.525 X 10 ⁻³		
50	7.336 X 10 ⁻⁴	.7351	7286.3	50	1.192 X 10 ⁻³	.5824	8100.4
52	5.641 X 10 ⁻⁴			52	9.315 X 10 ⁻⁴		
54	4.338 X 10 ⁻⁴			54	7.330 X 10 ⁻⁴		
56	3.377 X 10 ⁻⁴			56	5.792 X 10 ⁻⁴		
58	2.619 X 10 ⁻⁴			58	4.561 X 10 ⁻⁴		
60	2.014 X 10 ⁻⁴			60	3.613 X 10 ⁻⁴		
62	1.539 X 10 ⁻⁴	.5711	7533.7	62	2.869 X 10 ⁻⁴	.4554	8399.2
64	1.175 X 10 ⁻⁴			64	2.259 X 10 ⁻⁴		
66	8.955 X 10 ⁻⁵			66	1.761 X 10 ⁻⁴		
68	6.820 X 10 ⁻⁵			68	1.359 X 10 ⁻⁴		
70	5.221 X 10 ⁻⁵			70	1.038 X 10 ⁻⁴		
72	4.008 X 10 ⁻⁵			72	7.824 X 10 ⁻⁵		
74	3.062 X 10 ⁻⁵	.7367	7321.0	74	5.821 X 10 ⁻⁵	3.3202	6704.3
76	2.327 X 10 ⁻⁵			76	4.268 X 10 ⁻⁵		
78	1.759 X 10 ⁻⁵			78	3.080 X 10 ⁻⁵		
80	1.323 X 10 ⁻⁵			70	2.182 X 10 ⁻⁵		

TABLE B.3-III.- SEASONAL DENSITY MODEL - JANUARY 30° N AND JULY 30° N

JANUARY 60° N				JULY 60° N			
Altitude, km	ρ , kg/m ³	ρ_0 , kg/m ³	h_S , m	Altitude, km	ρ , kg/m ³	ρ_0 , kg/m ³	h_S , m
30	1.730 X 10 ⁻²			30	1.856 X 10 ⁻²		
32	1.265 X 10 ⁻²			32	1.362 X 10 ⁻²		
34	9.273 X 10 ⁻³			34	1.003 X 10 ⁻²		
36	6.840 X 10 ⁻³	1.5164	6706.4	36	7.425 X 10 ⁻³	1.5412	6778.4
38	5.076 X 10 ⁻³			38	5.530 X 10 ⁻³		
40	3.788 X 10 ⁻³			40	4.141 X 10 ⁻³		
42	2.843 X 10 ⁻³			42	3.118 X 10 ⁻³		
44	2.145 X 10 ⁻³			44	2.360 X 10 ⁻³		
46	1.627 X 10 ⁻³			46	1.795 X 10 ⁻³		
48	1.250 X 10 ⁻³			48	1.384 X 10 ⁻³		
50	9.697 X 10 ⁻⁴	.5853	7844.6	50	1.070 X 10 ⁻³	.6048	7933.4
52	7.576 X 10 ⁻⁴			52	8.433 X 10 ⁻⁴		
54	5.944 X 10 ⁻⁴			54	6.634 X 10 ⁻⁴		
56	4.646 X 10 ⁻⁴			56	5.20 X 10 ⁻⁴		
58	3.618 X 10 ⁻⁴			58	4.061 X 10 ⁻⁴		
60	2.818 X 10 ⁻⁴			60	3.180 X 10 ⁻⁴		
62	2.191 X 10 ⁻⁴	.5841	7846.8	62	2.491 X 10 ⁻⁴	.5656	8009.3
64	1.693 X 10 ⁻⁴			64	1.936 X 10 ⁻⁴		
66	1.299 X 10 ⁻⁴			66	1.492 X 10 ⁻⁴		
68	9.893 X 10 ⁻⁵			68	1.140 X 10 ⁻⁴		
70	7.479 X 10 ⁻⁵			70	8.632 X 10 ⁻⁵		
72	5.609 X 10 ⁻⁵			72	6.469 X 10 ⁻⁵		
74	4.171 X 10 ⁻⁵	2.5412	6679.2	74	4.796 X 10 ⁻⁵	3.0678	6645.7
76	3.074 X 10 ⁻⁵			76	3.514 X 10 ⁻⁵		
78	2.244 X 10 ⁻⁵			78	2.543 X 10 ⁻⁵		
80	1.597 X 10 ⁻⁵			80	1.815 X 10 ⁻⁵		

TABLE B.3-IV.- SEASONAL DENSITY MODEL - APRIL 30° N

Altitude, km	ρ , kg/m ³	ρ_o , kg/m ³	h_s , m
30	1.74 X 10 ⁻¹		
35	8.22 X 10 ⁻³	1.2536	7013.8
40	4.02 X 10 ⁻³		
45	2.05 X 10 ⁻³		
50	1.10 X 10 ⁻³	.4794	8249.9
55	6.10 X 10 ⁻⁴		
60	3.40 X 10 ⁻⁴	.5176	8156.1
65	1.79 X 10 ⁻⁴		
70	9.03 X 10 ⁻⁵		
75	4.35 X 10 ⁻⁵	2.6028	6781.6
80	1.96 X 10 ⁻⁵		

ORIGINAL PAGE IS
OF POOR QUALITY

TABLE B.3-V.- $3\sigma \frac{\Delta\delta}{\delta}$ VERSUS ALTITUDE FOR ENCLOSED ATMOSPHERES

Altitude (km)	1962 Standard atmosphere, percent	60° N January, percent	60° N July, percent	30° N January, percent	30° N July, percent	30° N April, percent
30	10.09	4.83	2.13	7.03	7.38	5.65
32	11.61	5.42	1.71	6.69	7.15	3.09
34	13.10	6.01	1.30	6.34	6.91	.60
36	14.57	6.60	.88	6.00	6.67	1.83
38	16.01	7.18	.47	5.65	6.44	4.21
40	17.42	7.76	.06	5.31	6.20	6.52
42	18.82	8.33	.35	4.96	5.97	8.78
44	20.18	8.90	.76	4.61	5.74	10.99
46	21.53	9.47	1.16	4.26	5.50	13.14
48	22.85	10.03	1.57	3.90	5.27	15.24
50	24.16	10.59	1.97	3.55	5.04	17.29
52	25.43	11.15	2.37	3.20	4.81	19.29
54	26.69	11.70	2.77	2.84	4.58	21.24
56	27.93	12.25	3.17	2.48	4.35	23.15
58	29.14	12.80	3.56	2.12	4.12	25.00
60	30.34	13.34	3.96	1.76	3.89	26.82
62	31.51	13.88	4.35	1.40	3.66	28.59
64	32.67	14.42	4.74	1.04	3.43	30.31
66	33.81	14.95	5.13	.67	3.20	32.00
68	34.92	15.48	5.52	.31	2.97	33.64
70	36.02	16.01	5.90	.06	2.75	35.25
72	37.10	16.53	6.29	.43	2.52	36.81
74	38.16	17.05	6.67	.80	2.30	38.34
76	39.20	17.57	7.05	1.17	2.07	39.83
78	40.23	18.08	7.43	1.54	1.85	41.29
80	41.24	18.59	7.81	1.91	1.62	42.71

TABLE B.3-VI.- ORBITS USED IN PREDICTION EXPERIMENTS

	A	B	C	D	E
perigee (km)	220	300	300	220	Same as
apogee (km)	380	600	600	380	A except
eccentricity	.012	.022	.022	.012	epoch
period (min)	90.5	93.6	93.6	90.5	is
argument of perigee	0	0	180°	0	12:00
ascending node	0	0	0	0	January 1,
inclination	30°	30°	30°	90°	1977
epoch	12:00		January 1, 1975		

ORIGINAL PAGE IS
OF POOR QUALITY

TABLE B.3-VII.- POSITION DEPENDENCE ON DENSITY MODEL

Orbit	time of integration, days	Position difference, km			
		No drag	U.S.S.R.	AMDB	B-M
A	0.5	8.9	0.2	0.3	0.005
	1.0	36.1	.8	1.5	.018
B	0.5	.83	.03	.07	.004
	1.0	3.16	.07	.28	.015
C	0.5	.5	<.001	.01	.004
	1.0	1.8	.02	.04	.018
D	0.5	8.6	.1	.3	.008
	1.0	34.4	.5	1.5	.027
E	0.5	13.9	3.4	0.4	.071
	1.0	56.0	19.2	1.9	.275

B.3.3 References

- B.3-1 U.S. Committee on Extension to the Standard Atmosphere: U.S. Standard Atmosphere, 1962. Government Printing Office (Wash., D.C.), 1962.
- B.3-2 U.S. Committee on Extension to the Standard Atmosphere: U.S. Standard Atmosphere Supplements, 1966. Government Printing Office, (Wash., D.C.) 1962.
- B.3-3 U.S. Committee on Extension to the Standard Atmosphere: U.S. Standard Atmosphere, 1976. Government Printing Office (Wash., D.C.), 1962.
- B.3-4 Lewis, J. R.; Sabayrac, R. B.; Austin, G. A.; Cockrell, B. F.: RTCC and MOPS Requirements for Modified 1970 Jacchia Atmosphere Model. MSC IN 70-FM-202, January 26, 1971.
- B.3-5 Mueller, A. C.: Atmosphere Density Models. Analytical and Computational Mathematics, Inc., June 1977.
- B.3-6 Mueller, A. C.: Atmospheric Density Models. Analytical and Computational Mathematics, Inc., January 25, 1977.
- B.3-7 Purifoy, D. D.: New Wind Bias, Density and Density Error Models for OFT-1 Simulation. JSC Memorandum FM83 (77-337), September 6, 1977.
- B.3-8 Clifford, J. B., Jr.; and Cockrell, B. F.: Space Shuttle Navigation Software, Volume II - Environment Routines. MSC IN 72-FM-132, June 1, 1972.

- B.3-9 McClain, C. R.: Comparison of Two-IMU Nominal Navigation Performance Between the Single and Four-Layer Atmospheric Density Models. MDTSCO Working Paper No. E914-8A/B-014, November 5, 1976.
- B.3-10 Lukaszewski, D. A.: Onorbit Navigation Software Atmospheric Density Model (Proposed Replacement for Baselined Russian Design). MDTSCO Transmittal Memo No. 1.4-MPB-804, August 30, 1977.

APPENDIX B.4

DRAG ALTITUDE PSEUDOMEASUREMENT

B.4.1 GENERAL DESCRIPTION

Vertical channel instability is an inherent problem with all unaided inertial navigation systems. The Shuttle navigation system experiences this problem during atmospheric reentry. External navigation aids, such as TACAN, are generally not available during the initial phase of entry due to blackout ionization of the air.

During entry only IMU data are available. Vehicle aerodynamic characteristics, an atmospheric density model, and IMU contact acceleration are used to compute altitude for processing with a Kalman filter to stabilize the vertical navigation channel. The measurement is referred to as pseudo since it is not directly measured. All the acceleration measured by the IMU accelerometers during entry is assumed to be attributed to aerodynamic forces. The following sections describe the drag altitude pseudomeasurement simulation approach and error model.

B.4.2 SIMULATION APPROACH

On nominal trajectories appreciable atmospheric drag is encountered at altitudes below 260 000 feet. Drag measurements begin when the accelerometers sense 11 ft/sec^2 and continue until the aerodynamic probe is extended and barometric altimeter data can be processed. This occurs at an altitude of approximately 100 000 feet. The drag updating technique is an effective method for reducing the error buildup during the blackout portion of entry. During the drag update period the altitude pseudomeasurement is calculated from accelerometer outputs, a model of air density as a function of altitude, and a model of drag as a function of the angle of attack. Figure B-1 presents a block diagram showing the computation of the drag altitude pseudomeasurement. A functional description of each block is as follows.

- a. Block 1 - computes the angle of attack (α) to be used in calculating the drag coefficient by the following equations

$$\underline{V}_R = \underline{V}_R - E_R (\underline{I}_P \times \underline{V})$$

$$\underline{V}_{RB} = T_{BM50}^T \underline{V}_R$$

$$\alpha = \arctan (V_{RB} (3)/V_{RB}(1))$$

where

\underline{V} = the Shuttle's velocity vector in M50 coordinates

E_R = Earth rate

\underline{I}_P = unit vector along the Earth's pole

T_{BM50} = transformation matrix from body to M50 coordinates

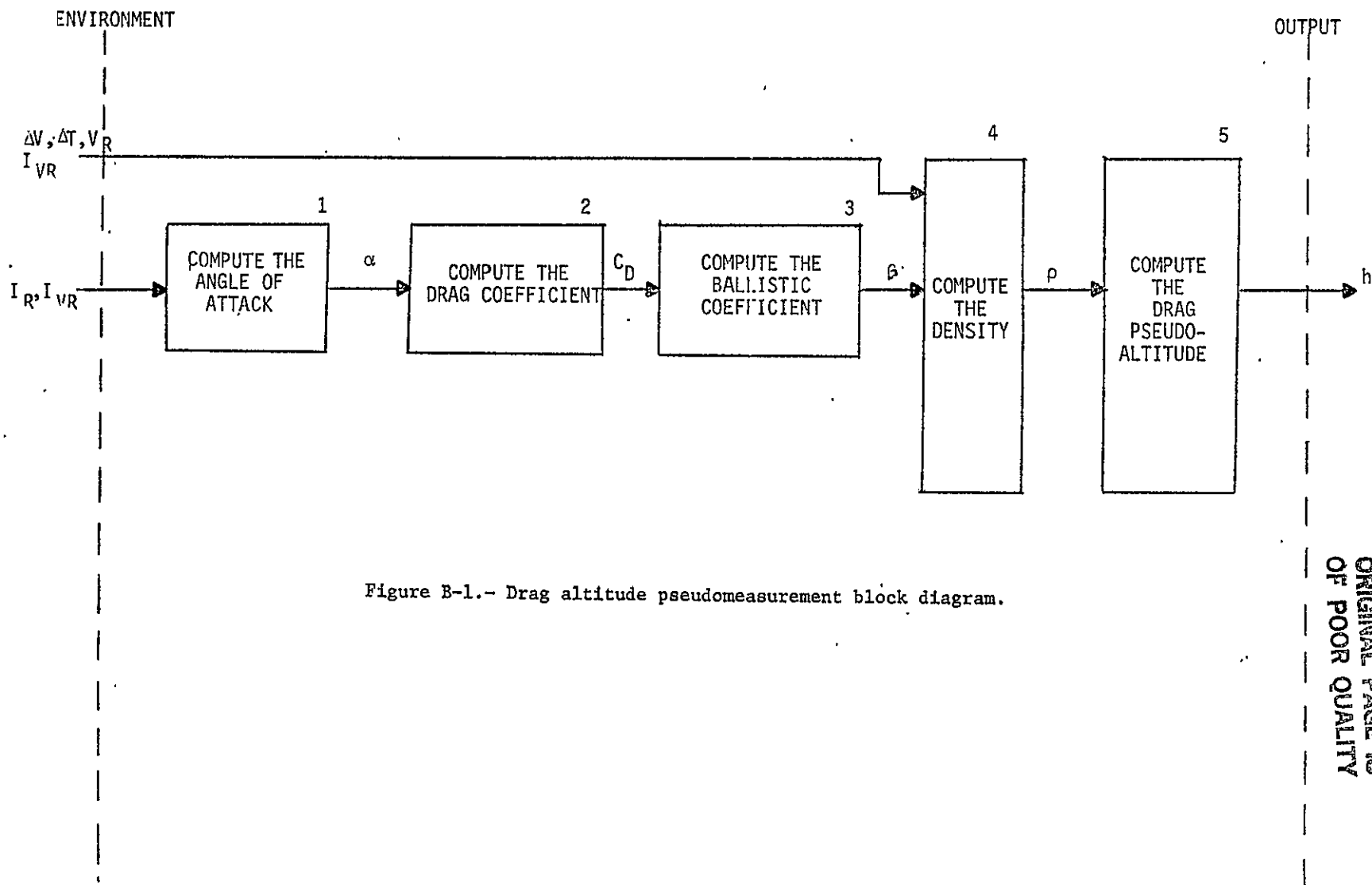


Figure B-1.- Drag altitude pseudomeasurement block diagram.

B-34

ORIGINAL PAGE IS
OF POOR QUALITY

Typical values for Earth rate and Earth's pole unit vector (ref. B.4-1) are

$$\underline{E}_R = 0.72921151 \text{ E-4 rad/sec}$$

$$0.28324166 \text{ E-2}$$

$$\underline{I}_P = -0.50463837 \text{ E-4}$$

$$0.99999598$$

- b. Block 2 - computes the drag coefficient (C_D) as a function of the angle of attack and premission determined coefficients (C_0 , C_1 , C_2) by the following equation:

$$C_D = C_0 + C_1 \alpha + C_2 \alpha^2$$

where

α = flight angle of attack in radians

C_0 , C_1 , C_2 = experimentally determined coefficients from wind tunnel tests for calculating the drag coefficients

The following typical values for calculating the drag coefficient are given in reference B.4-1.

$$C_0 = 0.2452220322$$

$$C_1 = -0.831161 \text{ rad}^{-1}$$

$$C_2 = 2.4092462 \text{ rad}^{-2}$$

- c. Block 3 - calculates the ballistic coefficient (β)

$$\beta = C_D A / W$$

where

A = frontal area of the Shuttle

W = mass

C_D = drag coefficient (unitless)

Due to the longitudinal center of gravity constraint the Orbiter's weight at entry will be kept constant at approximately 183 404 pounds (ref. B.4-2).

d. Block 4 - computes the density (ρ) by the following equation.

$$\rho = 2 \left| \underline{I}_{VR} \cdot \underline{\Delta V} \right| / (V_R^2 \beta \Delta T)$$

where

$$\underline{I}_{VR} = \underline{V}_R / V_R$$

$\underline{\Delta V}$ = the accelerometer sensed change in the velocity vector over the time interval ΔT

ΔT = time interval between accelerometer samples

\underline{V}_R = velocity vector of Shuttle relative to the atmosphere

$$V_R = \left| \underline{V}_R \right|$$

β = calculated in block 3

e. Block 5 - computes the drag pseudoaltitude as a function of density by the following equation.

$$h = h_s \ln(\rho_0 / \rho)$$

where

h_s = atmospheric density scale height

ρ_0 = base density

ρ = density of the atmosphere

Section B.3.2.2 of appendix B.3 discusses the baselined four-layer atmospheric density model. In this model the scale heights and base densities vary according to estimated altitude.

B.4.3 ERROR MODEL

In the navigation filter the error due to drag measurements is modeled as an ECRV. The atmospheric density and drag coefficient model errors comprise the bias error, while the accelerometer and atmospheric turbulence errors make up the random error seen in the estimate of drag altitude. The following error model (1-sigma values) presented in reference B.4-3 is used to corrupt the altitude calculated in block 5.

Drag altitude measurement bias	3750 ft
Drag altitude measurement random noise	250 ft
Drag altitude measurement bias time constant	720 sec

B.4.4 REFERENCES

- B.4-1 Space Shuttle Orbital Flight Test Level C Functional Subsystem Software Requirements Document; Guidance, Navigation, and Control, Part B, Entry Through Landing Navigation. SD-76-SH-0004C, October 1977.
- B.4-2 Telephone conversation with C. D. Eakman (MDTSCO), January 19, 1978.
- B.4-3 Bhatt J. K.: Implementation of the Latest New Drag Measurement Error Model into the ORACLE OPS 3 Bench Program. MDTSCO TM 1.4-MPB-1289, July 14, 1978.

B.5 REFRACTION CORRECTION MODELS

B.5.1 GENERAL DESCRIPTION

A complete refraction model would account for tropospheric and (for orbital altitudes) ionospheric refraction effects on the range, range rate, integrated Doppler, and elevation angle data for all ranges and elevation angles. These effects can be well modeled by a ray tracing program (ref. B.5-1) assuming that the physical parameters of the atmosphere are known. This is done by treating the atmosphere as a sequence of layers with the refractivity held constant in each layer. The refractivity of a given layer is determined from the single exponential refractivity profile. The spherical form of Snell's law is then used to trace the ray path through the atmosphere. The chief disadvantage of this method is that the computations require a considerable amount of computer time and are, therefore, unsuitable for general simulation programs or for onboard computer use. In these applications less complex and faster computational techniques are required.

A practical refraction model algorithm is discussed below, with estimates of the magnitudes of the effects and errors remaining after corrections have been applied. It is generally concluded that no matter how sophisticated the refraction correction model is, it should not be used for high-quality navigation work at elevation angles below 2 or 3 degrees when the vehicle is at large distances from the station. Because of diurnal, hourly, vertical, and horizontal variations of the index of refraction it is virtually impossible to construct an accurate, longrange, low-angle, refraction correction.

B.5.2 TROPOSPHERIC REFRACTION MODELS

The following discussion of tropospheric refraction is taken directly from reference B.5-2. Figure B-2 shows a simplified model of the atmospheric refraction of electromagnetic waves.

Two effects are involved. First, the electromagnetic waves travel more slowly through the atmosphere than they do through a vacuum. The ratio of the speeds is called the index of refraction, n . Due to the slower velocity in the atmosphere it takes longer for waves to travel from the tracking station to the vehicle than they would in a vacuum. This makes the measured distance appear greater than the actual distance. Secondly, the electromagnetic waves are bent at the outer edges of the atmosphere. This makes the path followed by the waves longer than the geometric, straight-line distance. This makes the measured distance appear to be greater than the actual distance ρ .

Before proceeding, let us precisely define a few of the terms shown in figure B-2.

n_S = the index of refraction for the electromagnetic wave at the tracking station antenna. $n_S - 1$ is called the refraction modulus, or refractivity.

H_S = Atmospheric decay constant, or atmospheric scale height. Looking straight up it is the equivalent height of a slab atmosphere whose index of refraction is n_S in every case.

H = altitude of the vehicle above the tracking station.

R_C = radius of curvature of the Earth in the vicinity of the tracking station.

If $R_E = 6\,378\,166$ meters is the equatorial radius, $e = 1/298.3$ is the ellipticity or flattening, of the Earth, and ϕ = geodetic latitude; then

$$R_C = \frac{(1 - e)^2 R_E}{(1 - (1 - (1 - e)^2) \sin^2 \phi)^{3/2}} + ALT_{\text{station}}$$

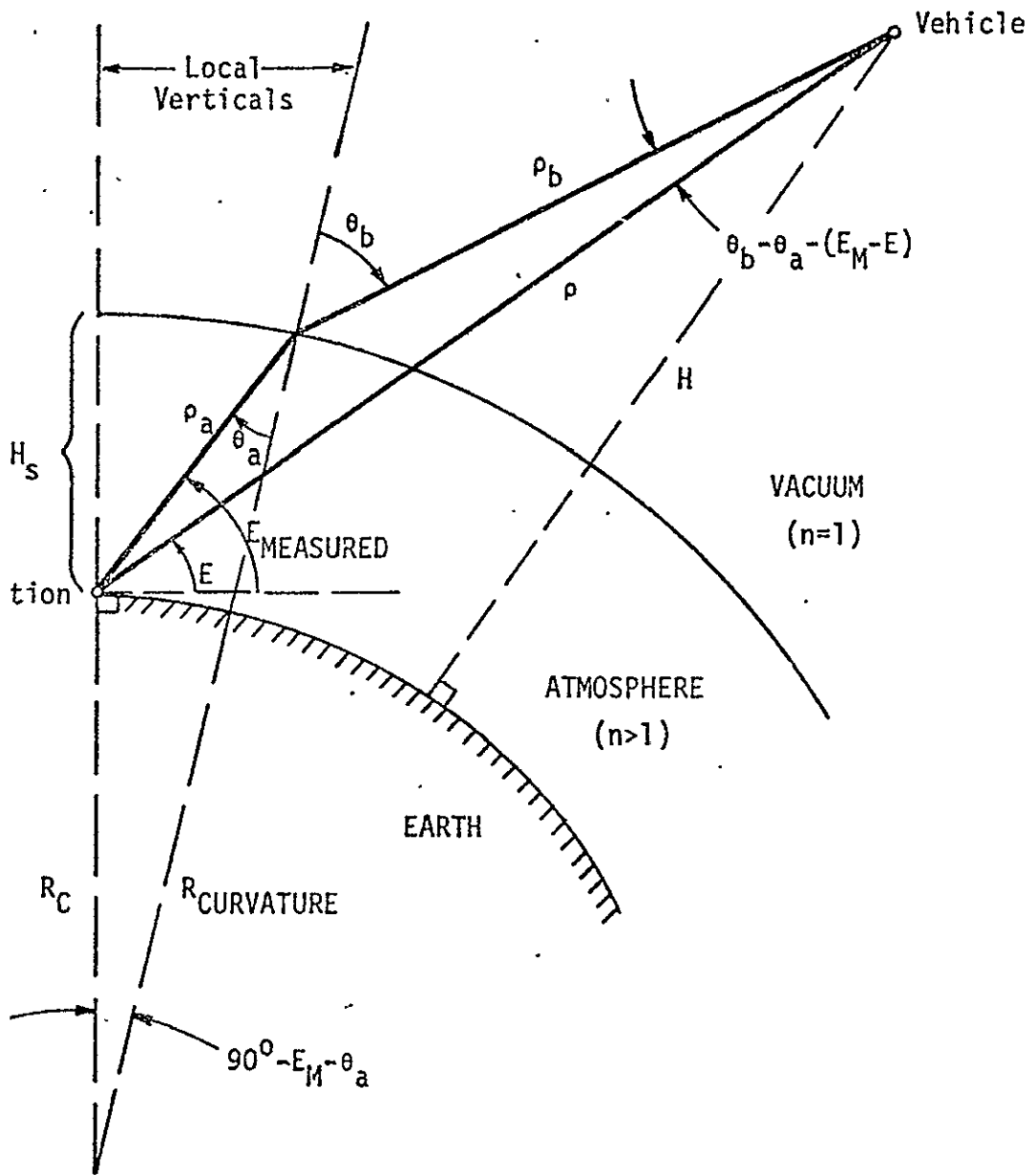


Figure B-2.- Refraction of electromagnetic waves by a slab atmosphere

From the R_C , ρ_a triangle and the law of sines, we see that

$$\frac{R_C}{\sin \theta_a} = \frac{R_C + H_S}{\sin(90^\circ + E_M)}$$

or

(1)

$$\sin \theta_a = \frac{1}{1 + H_S/R_C} \cos E_M$$

Also from this same triangle, using the law of cosines, we can show that

$$\rho_a = R_C \left[(1 + H_S/R_C)^2 - \cos E_M - \sin E_M \right] \quad (2)$$

or, alternatively

$$\rho_a = \frac{(2 + H_S/R_C)H_S}{\sin E_M + (1 + H_S/R_C)^2 - \cos^2 E_M}$$

If n_S is the index of refraction of the slab atmosphere, then from Snell's law of refraction

$$\sin \theta_b = n_S \sin \theta_a$$

Substituting equation (1) into the above gives

$$\sin \theta_b = \frac{n_S}{1 + H_S/R_C} \cos E_M \quad (3)$$

Note that for $n_S \geq 1 + H_S/R_C$ it is possible to have reflection rather than refraction.

From the ρ_a , ρ_b , ρ triangle we see that

$$\rho_a \sin(\theta_b - \theta_a) = \rho \sin(\theta_b - \theta_a - (E_M - E)) \quad (4)$$

$$\rho_b = \rho^2 + \rho_a^2 - 2\rho\rho_a \cos(E_M - E) \quad (5)$$

This now gives us five nonlinear equations in the five unknowns: E_M , θ_a , θ_b , ρ_a , and ρ_b . The quantities ρ and E are the independent variables or given in quantities. There is no analytic solution of these equations; however, an iterative solution is easily obtained as shown below.

$$E_M = E$$

$$D\phi \text{ a I} = 1,3$$

$$\theta_a = \arcsin \frac{\cos E_M}{1 + H_S/R_C}$$

$$\theta_b = \arcsin \frac{n_S \cos E_M}{1 + H_S/R_C}$$

$$\rho_a = R_C \left((1 + H_S/R_C)^2 - \cos^2 E_M - \sin E_M \right)$$

$$a \quad E_M = E + (\theta_b - \theta_a) - \arcsin \frac{\rho_a}{\rho} \sin(\theta_b - \theta_a)$$

$$\rho_b = \rho^2 + \rho_a^2 - 2\rho\rho_a \cos(E_M - E)$$

The refraction correction for range, $\Delta\rho$, is measured range, $n_S\rho_a + \rho_b$, minus computed range, ρ . Thus

$$\Delta\rho = n_S \rho_a + \rho_b + \rho$$

The previous refraction correction equations are only good for the vehicle well above the Earth's atmosphere. As the vehicle enters the atmosphere, part of the atmosphere will be above the vehicle, leaving a lesser quantity of atmosphere below the vehicle. Thus, for a vehicle in the atmosphere we would like to lower the scale height, H_S . This can be done by replacing H_S with H_S^* ,

$$H_S^* = (1 - \exp(-H/H_S)) H_S \quad (6)$$

where altitude above the tracking station is conveniently calculated from

$$H = \sqrt{R_C^2 + \rho^2 + 2\rho R_C \sin E} - R_C \quad (7)$$

Note that as H becomes small, $H_S^* \rightarrow H$. Except for $H = 0$, H_S^* is always less than H , for H positive. That is, the vehicle will always be above the slab atmosphere for H positive. Also note that as H becomes large, $H_S^* \rightarrow H_S$. As it turns out, to a first approximation the refraction modulus as a function of altitude is given by $(n_S - 1) \exp(-H/H_S)$. This being the case, we can show that eq. (6) is precisely the right equation to use to modify the scale height.

If we substitute H_S^* for H_S in our previous equations we encounter two difficulties. One is for negative altitudes and the other is the reflection problem. We can easily resolve the negative altitude problem by noting that when H is negative (station on a hill during landing) the range ρ will never be very large. Thus when H is negative we will use the approximate refraction corrections.

$$E_M \approx E$$

$$\Delta\rho \approx (n_S - 1)\rho \quad \text{for } H \leq 0$$

The other problem concerns eq. (3),

$$\theta_b = \arcsin \frac{n_S \cos E_M}{1 + H_S^*/R_C}$$

As mentioned earlier, for $1 + H_S^*/R_C \geq n_S$ it is possible to have reflection rather than refraction. This will occur when $H_S^* \approx 2000$ meters and $H \approx 2500$ meters. At this altitude we can obtain a reflection from the upper part of the slab atmosphere rather than a refraction. While this effect can occur in nature, and cause a mirage, it is not something that we desire to model here. In fact, it will not occur in an atmosphere whose refraction modulus is smoothly varying according to $(n_S - 1)\exp(-H/H_S)$. The reflection is due to the abrupt discontinuity in the refraction modulus at the top of the slab atmosphere. When reflection occurs, θ_b will be slightly greater than 90 degrees. We can not have $\theta_b > 90^\circ$ because in this case there will be regions in the sky where we would not be able to see the Shuttle. To resolve our difficulty we will limit $\theta_b \leq 90^\circ$. We can do this by checking

$$\frac{n_S \cos E_M}{1 + H_S^*/R_C}$$

Whenever this quantity is greater than 1, we will reset it equal to 1, causing θ_b be computed as 90 degrees.

Thus, the suggested algorithm for computing the range and elevation angle refraction corrections is summarized in figure B-3.

$$H = \sqrt{R_C^2 + \rho^2 + 2\rho R_C \sin E} - R_C$$

$$E_M = E$$

IF (H > 0) GO TO a

$$\Delta\rho = (n_S - 1)\rho$$

RETURN

a $H_S^* = (1 - \exp(-H/H_S))H_S$

DO b I = 1,3

$$\theta_a = \arcsin \frac{\cos E_M}{1 + H_S^*/R_C}$$

$$A = \frac{n_S \cos E_M}{1 + H_S^*/R_C}$$

IF (A > 1) A = 1

$$\theta_b = \arcsin (A)$$

$$\rho_a = R_C \left(\sqrt{(1 + H_S^*/R_C)^2 - \cos^2 E_M} - \sin E_M \right)$$

b $E_M = E + (\theta_b - \theta_a) - \arcsin \left[\frac{\rho_a}{\rho} \sin (\theta_b - \theta_a) \right]$

$$\rho_b = \sqrt{|\rho^2 + \rho_a^2 - 2\rho\rho_a \cos (E_M - E)|}$$

$$\Delta\rho = n\rho_a + \rho_b - \rho$$

RETURN

Figure B-3.- Suggested algorithm for computing refraction corrections for the Space Shuttle.

B.5.3 IONOSPHERIC REFRACTION MODELS

Ionospheric refraction affects signals between orbiting vehicles and the ground. It is a function of the electron density in the ionosphere. The electron density is, in turn, a function of the solar and geomagnetic activity parameters and the relative positions of the Sun, vehicle, and station.

A model for the density similar to that for the exospheric temperature (appendix B.3) might be available. If mean values for the electron density and the ionospheric limits are used instead, the correction for ionospheric refraction will not be more accurate than 20 percent.

The following equation, recommended by Cubic Corporation (refs. B.5-3 and B.5-4), may be used to compute the effect of ionospheric refraction on range measurements derived from frequency modulation.

$$\Delta\rho = \frac{1325 H_0 M_{F2}}{f^2 W (.05 \cos E_0 + \sin E_0)} \left\{ \tan^{-1} W - \tan^{-1} \left[W \left(\frac{H_0 - H}{H_0} \right) \right] \right\} \left(1 - e^{-H/160000} \right) \text{ (ft)}$$

where

H = the altitude of the vehicle (ft)

M_{F2} = the maximum electron density in the F_2 ionospheric layer (ft^{-3})

f = carrier frequency (Hz)

$W = 2H_0 / (H_H - H_L)$

E_0 = incident elevation angle

H_0 = height of M_{F2} layer (ft)

H_H, H_L = upper and lower heights of the half values of the electron density (ft)

Typical values are

$$M_{F2} = 13.4987 \times 10^9 \text{ ft}^{-3}$$

$$H_o = 725 \ 000 \quad \text{ft}$$

$$H_H = 1 \ 368 \ 600 \quad \text{ft}$$

$$H_L = 608 \ 266 \quad \text{ft}$$

The ionospheric refraction correction is typically about 75 to 80 percent of the tropospheric correction for a frequency of about 1.5 GHz. Because the correction is inversely proportional to the square of the frequency, it becomes small at the higher frequencies in the S-Band.

B.5.4 REFRACTION ERROR MODEL

The real atmosphere is, of course, vastly more complicated in its refractivity structure than the simple refractivity profile given above. One of the chief differences is that the model assumes horizontal homogeneity. That is, every place with the same height has the same refractivity. Clearly, this is not true in the real world.

The model for the effects of atmospheric variations on range and Doppler refraction corrections is modeled in the Navigation Analysis Program (ref. B.5-5) as a scaling error k , which is the sum of a random variable that is exponentially correlated over spacecraft position changes, and is common to all stations, and a statistically independent random variable. The modeled refraction correction is, therefore, given by the expression

$$\sqrt{\Delta\rho} = (1 + k) \Delta\rho$$

$$k = \epsilon + \eta$$

where

$\Delta\rho$ is the refraction correction computed from the simplified atmosphere model

k is the random scaling error to account for atmospheric variations

ϵ is an exponentially correlated random variable

η is white noise

The bias scale factor ϵ is computed as a first-order process in Δr .

$$\epsilon_{i+1} = \exp(-\Delta r/\tau)\epsilon_i + \sigma_{ATM}(1-\exp(-2\Delta r/\tau))^{1/2}$$

where

$$\Delta r = |R_{i+1} - R_i|$$

τ is the correlation distance constant

σ_{ATM} is the standard deviation for the random variable

Numerical values for τ and σ_{ATM} are difficult to obtain. A reasonable value for σ_{ATM} is probably on the order of 5 percent for elevation angles above 3 degrees and 10 to 20 percent below 3 degrees.

B.5.5 REFERENCES

- B.5-1 Miller, L. J.: A Study of Tropospheric Refraction. JSC IN 73-FM-98, June 25, 1973.
- B.5-2 Lear, W. M.: Suggested Refraction Correction Model for Space Shuttle Work. TRW Report 20029-6021-TO-00, April 6, 1973.
- B.5-3 Mathematics of Geodetic SECOR Data Processing. Cubic Corporation Final Technical Report, September 1964.
- B.5-4 Mathematics for Army Map Service Geodetic Satellite Processing System. Cubic Corporation Final Technical Report, July 1968.
- B.5-5 Engineering and Programming Guide for the Navigation Analysis Program (NAP). TRW Note No. 72-FMT-908, December 29, 1972.

B.6 LIGHT TIME ALGORITHM*

The Light Time Algorithm is necessary because the actual times of signal reception/transmission at the vehicle t_v and transmission from the ground based transmitting station t_t are not necessarily known. To calculate the range and range rate measurements it is necessary to compute the actual time required for the signal to travel to and from the vehicle. The times are obtained as follows.

A signal is transmitted from a ground based station at time t_t and travels to the vehicle at the speed of light. This signal is received and transmitted by the vehicle at time t_v to a ground based receiving station. The onboard processing time is assumed to be zero. The input range and range rate observation data is tagged only with the time of data reception t_r . In order to accurately compute the observations it is necessary to calculate the transmission times, $\Delta t_2 = t_r - t_v$ and $\Delta t_1 = t_v - t_t$, and in turn the times t_v and t_t . The transmission times are obtained from the Light Time Algorithm. This method determines the transmission times by successive approximations. It considers two transcendental equations

$$\Delta t_2 = \frac{\rho_2(t_v)}{c} = \frac{\rho_2(t_r - \Delta t_2)}{c} \quad (G1)$$

$$\Delta t_1 = \frac{\rho_1(t_t)}{c} = \frac{\rho_1(t_v - \Delta t_1)}{c} \quad (G2)$$

*This appendix is taken directly from the following document: "Houston Operations Predictor/Estimator (HOPE) Engineering Manual - Revision 01," TRW Report 11176-H408-RO-01, June 1970.

where

ρ_2 = magnitude of the downlink range vector $\vec{\rho}_2$

ρ_1 = magnitude of the uplink range vector $\vec{\rho}_1$

c = speed of light.

The equation for the downlink range vector $\vec{\rho}_2$ is

$$\vec{\rho}_2 = \vec{r} - \vec{r}_r$$

where

\vec{r} = position vector of the vehicle at time t_v

\vec{r}_r = position vector of the ground based receiving station at time t_r .

The equation for the uplink range vector $\vec{\rho}_1$ is

$$\vec{\rho}_1 = \vec{r}_t - \vec{r} \tag{G-4}$$

where

\vec{r} = position of the vehicle at time t_v

\vec{r}_t = position of the ground based transmitting station at time t_t .

Equations (G-1) and (G-2) must be solved by an iterative procedure, since they are transcendental equations. Equation (G-1) begins with the known time t_r and retraces the received signal backwards along the light path to solve for t_v . Equation (G-2) is then used to retrace the signal from the vehicle backwards to the ground based transmitting station to solve for t_t . The solution to these two equations is obtained as follows.

First, the solution to the downlink light time equation (Equation G-1) is determined. The function $\rho_2(t_r - \Delta t_2)$ is expanded into a first-order Taylor series. The Taylor series for the function $\rho(t_r - \Delta t_2)$ at $\Delta t_2 = \Delta t_2'$ is

$$\rho_2(t_r - \Delta t_2) = \rho_2(t_r - \Delta t_2') + \left. \frac{d\rho_2(t_r - \Delta t_2)}{d(\Delta t_2)} \right|_{\Delta t_2 = \Delta t_2'} (\Delta t_2 - \Delta t_2') + \dots \quad (G-5)$$

where

Δt_2 = signal transmission time to be determined

$\Delta t_2'$ = signal transmission time assumed

$$\left. \frac{d\rho_2(t_r - \Delta t_2)}{d(\Delta t_2)} \right|_{\Delta t_2 = \Delta t_2'} = \frac{\vec{\rho}_2 \cdot \vec{v}}{\rho_2}$$

\vec{v} = velocity vector of the vehicle at time $t_r - \Delta t_2'$.

Substituting the expression for ρ_2 from Equation (G-1) into Equation (G-5) yields with some manipulation

$$\Delta t_2 = \frac{\rho_2(t_r - \Delta t_2') + \frac{\vec{\rho}_2(t_r - \Delta t_2') \cdot \vec{v}(t_r - \Delta t_2')}{\rho_2(t_r - \Delta t_2')} \Delta t_2'}{c + \frac{\vec{\rho}_2(t_r - \Delta t_2') \cdot \vec{v}(t_r - \Delta t_2')}{\rho_2(t_r - \Delta t_2')}} \quad (G-6)$$

The scheme consists of iterating on Equation (G-6) until $|\Delta t_2 - \Delta t_2'|$ is sufficiently small:

Step 1: $\Delta t_2' = 0$. Obtain corresponding values of ρ_2 , \vec{r} , \vec{v} and $\vec{\rho}_2$.

$$\text{Step 2: } \Delta t_2 = \frac{\rho_2(t_r)}{c + \frac{\vec{\rho}_2(t_r) \cdot \vec{v}(t_r)}{\rho_2(t_r)}}$$

Step 3: $\Delta t_2' = \Delta t_2$, value obtained from previous step. Obtain corresponding values of ρ_2 , \vec{r} , \vec{v} and $\vec{\rho}_2$.

Step 4: Compute Δt_2 using Equation (G-6).

Step 5: Check if $|\Delta t_2 - \Delta t_2'| \leq \epsilon$. If it is sufficiently small, then the value of t_v is $t_r - \Delta t_2$. Final values of downlink range and range rate vectors plus their associated magnitudes are obtained from this corrected value of time.

Step 6: If the value is unacceptable Steps 3, 4 and 5 are repeated until convergence is obtained.

The uplink data is determined in a similar manner by iterating on the equation

$$\Delta t_1 = \frac{\rho_1(t_v - \Delta t_1') + \frac{\vec{\rho}_1(t_v - \Delta t_1') \cdot \vec{v}(t_v - \Delta t_1')}{\rho_1(t_v - \Delta t_1')} \Delta t_1'}{c + \frac{\vec{\rho}_1(t_v - \Delta t_1') \cdot \vec{v}(t_v - \Delta t_1')}{\rho_1(t_v - \Delta t_1')}} \quad (G7)$$

until $|\Delta t_1 - \Delta t_1'|$ is sufficiently small. Then the value for t_t is $t_v - \Delta t_1$.

APPENDIX B.7

VENT MODELS

B.7.1 GENERAL DESCRIPTION

There are well over 50 purge, vent, and relief ports located throughout the Shuttle (e.g., fuel cell O_2 , H_2 purge, avionics bay vents, H_2O boilers, freon coolant loop flash evaporators, H_2 gas separator vent, APU dumps, ammonia dumps, urine dump vents, RCS fuel purge vents, etc.), as well as several sources of unscheduled leaking (e.g., cabin leakage, payload bay venting, etc.). Figure B-4 shows the location of major ports and vents. Of these sources the APU and water spray boiler cause the largest perturbations to the Shuttle trajectory. During portions of ascent and deorbit, when the payload bay doors are closed, the topping flash evaporator and high load flash evaporator steam vents are also major sources of trajectory perturbation.

B.7.2 ENVIRONMENTAL SIMULATION

The following tables are from reference B.7-1. These tables list the vent source the location in Orbiter structural body coordinates (ref. B.7-2), the effluent, the magnitude of the thrust, the thrust direction in Orbiter body coordinates, and the duration of the vent. Table B.7-I lists scheduled vents. Most vents listed vary with respect to time. Reference B.7-1 includes plots of venting magnitudes versus time. The APU venting thrust is also a function of pump shaft horsepower, while the hydraulic water spray boiler venting thrust is a function of pump shaft horsepower, water temperature, and time. Moreover, plume impingement effects are negligible for all but the three APU and three water spray boiler vents. A series of tables are given in reference B.7-1 that detail

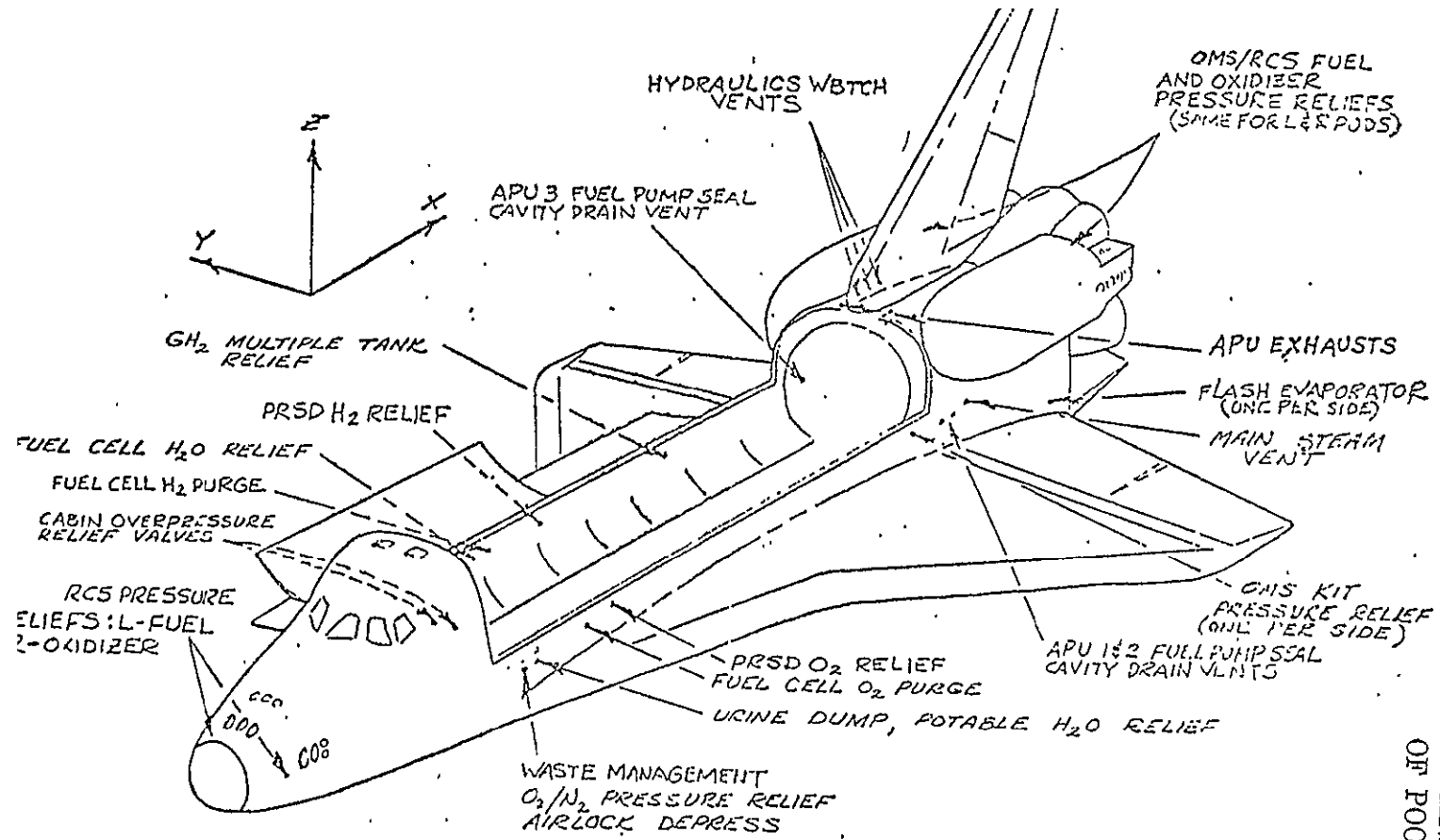


Figure B-4.- Locations of onorbit vents

ORIGINAL PAGE IS
OF POOR QUALITY

TABLE B.7-I.- SCHEDULED VENTS

Vent source	Location, in.			Effluent	Thrust, lbf	Vector			Duration	Remarks
	X _o	Y _o	Z _o			X	Y	Z		
ECLSS Cabin air (commode)	602.0	-105.5	336.0	Air	Negligible	0	1	0	2 seconds, 4 to 7 times per 24 hours	Depends on number of people
Water vapor from fecal material	602.0	-105.5	336.0	H ₂ O	Negligible	0	1	0	Same as above	Same as above
H ₂ separator (FCP water)	602.0	-105.5	336.0	H ₂	Negligible	0	1	0	Continuous	Flow rate 2x10 ⁻⁷ lbm/sec
Airlock depressur- ization	602.0	-105.5	336.0	Air	5.0 max.	0	1	0	5 minutes, three times per mission	
Topping flash evapor- ator steam vent No. 1	1505.7	-128.4	304.8	H ₂ O (steam)	0.5 max.	0	1	0	Intermittant for up to 10 hrs	Dependent on fuel cell H ₂ O production rate. Supplements radiators onorbit. Used in conjunction with high load evaporators during ascent and deorbit.
No. 2	1505.7	-128.4	304.8	H ₂ O (steam)	0.5 max.	0	1	0		
High load flash evap- orators steam vent	1390.3	-113.8	326.8	H ₂ O (steam)	2.0 max.	0	1	0	Operational during ascent above 140 000 ft and after pay- load bay door closure.	Used in conjunction with topping evap- orator during ascent.
Fuel Cell H ₂ purge	640.9	105.4	339.2	H ₂ (g)	0.05	0	-1	0	Normal mode - 2 minutes per FCP every 8 hrs	
O ₂ purge	640.9	-105.4	339.2	O ₂ (g)	0.05	0	1	0	Concurrent with H ₂ purge	

F-58

ORIGINAL PAGE IS
OF POOR QUALITY

TABLE B.7-I.- Concluded

Vent source	Location, in.			Effluent	Thrust, lbf	Vector			Duration	Remarks
	X ₀	Y ₀	Z ₀			X	Y	Z		
Hydraulic water boiler vent										Postboost MPS dump; onorbit APU checkout. Entry preparation.
No. 1	1375.7	16.3	508.1	H ₂ O (steam)	7 max.	0	0	-1	6 minutes	
No. 2	1395.7	16.3	510.5	H ₂ O (steam)	7 max.	0	0	-1	6 minutes	
No. 3	1355.7	16.4	505.8	H ₂ O (steam)	7 max.	0	0	-1	6 minutes	
APU exhausts										
Left 1	1327.9	-15.9	502.5	N ₂ (g)	9.0 lbf	0	0	-1	Same as above	Same as above
Left 2	1318.7	-15.7	501.3	N ₂ (g)	average per	0	0	-1		
Right 1	1327.9	15.9	502.5	NH ₃ (g)	vent, 30 lbf peak total.	0	0	-1		

the force vectors and moment vectors of these vents. Tables B.7-II and B.7-III list contingency and failure vents, respectively.

B.7.3 ERROR SOURCES

Thrust uncertainties of the quantities listed in the tables are ± 5 percent for all vent forces except

- a. Plume impingement forces, which are ± 10 percent
- b. RCS and OMS pressure relief vent forces, which are +zero to -10 percent.

These numbers are very optimistic and may be increased by a factor of 10 (ref. B.7-3).

B.7.4 REFERENCES

- B.7-1 Carminati, J. M.: Orbiter Vent/Thrust Reference Data For OFT Missions. MDTSCO Working Paper No. 1.4-7-204, January 4, 1978.
- B.7-2 Davis, L. P.: Coordinate Systems for the Space Shuttle Program. NASA TM X-58153, JSC-09084, October 1974.
- B.7-3 Osburn, R. K./FM8, Personal communication.

TABLE B.7-II.- CONTINGENCY VENTS

Vent source	Location, in.			Effluent	Thrust, lbf	Vector			Duration	Remarks
	X ₀	Y ₀	Z ₀			X	Y	Z		
ECLSS Urine dump	620.0	-105.4	336.0	Urine, sweat, biocide	1.275	0	1	0	4.5 hr/week-mission > 7 days	No dump for 7-day mission even with double failure
Potable water dump	620.0	-105.5	342.4	H ₂ O (l)	1.275	0	1	0	1.5 hr/day	Used if failure in flash evaporator or for thermal under- load
Fuel Cell Water relief	631.1	105.4	339.2	H ₂ O (l)	<0.01	0	-1	0	Can be continuous	Occurs only if ECLSS cannot accept FCP water
Reactant regulator Vent relief	640.9 640.9	-105.4 -105.4	339.2 339.2	O ₂ (g) H ₂ (g)	0.05 0.05	0 0	1 -1	0 0	Can be continuous	
Hydraulics water boiler vent										
No. 1	1375.7	16.3	508.1	H ₂ O (g)	7 max.	0	0	-1	6 minutes	Checkout of hydraulic system
No. 2	1395.7	16.3	510.5	H ₂ O (g)	7 max.	0	0	-1		
No. 3	1355.7	16.4	505.8	H ₂ O (g)	7 max.	0	0	-1		
APU exhausts										
Left 1	1327.9	-15.9	502.5	N ₂ (g)	9.0 lbf	0	0	-1	6 minutes	Checkout of hydraulic system
Left 2	1312.7	-15.7	501.3	H ₂ (g)	average per	0	0	-1		
Left 3	1327.9	15.9	502.5	NH ₃ (g)	vent 30.0 lbf peak total.	0	0	-1		

B-62

ORIGINAL PAGE IS
OF POOR QUALITY

TABLE B.7-III.- FAILURE VENTS

Vent source	Location, in.			Effluent	Thrust, lbf	Vector			Duration	Remarks
	X ₀	Y ₀	Z ₀			X	Y	Z		
RCS pressure relief				He+						
Fwd oxidizer	285.5	40.6	361.4	N ₂ O ₄	19.8 max.	See table			30 seconds	Occurs only if open failure of both primary and secondary regulators.
Fwd fuel	285.5	-40.6	361.4	MMH	19.8 max.	B.7-IV for				
Aft oxidizer (RHS)	1507.7	128.1	510.1	N ₂ O ₄	19.8 max.	flow direc-				
Aft fuel (RHS)	1509.4	65.7	529.9	MMH	19.8 max.	tion cosines.				
Aft oxidizer (LHS)	1507.7	-128.1	510.1	N ₂ O ₄	19.8 max.	Thrust is				
Aft fuel (LHS)	1509.4	-65.7	529.9	MMH	19.8 max.	in opposite direction				
OMS pressure relief				He+						
Oxidizer (RHS)	1507.7	128.1	510.1	N ₂ O ₄	24.7	See table			30 minutes max.	Occurs only if open failure of both primary and secondary regulators.
Fuel (RHS)	1509.4	65.7	529.9	MMH	24.7	B.7-IV for				
Oxidizer (LHS)	1507.7	-128.1	510.1	N ₂ O ₄	24.7	flow direc-				
Fuel (LHS)	1509.4	65.7	529.9	MMH	24.7	tion cosines. Thrust is in opposite direction				
OMS pressure relief (PLB)				He+						
Oxidizer	1295	105	331.2	N ₂ O ₄	24.7	0	-1	.0	3 minutes max.	1 kit
Fuel	1295	-105	331.2	MMH	24.7	0	1	0	6 minutes max.	2 kits
									9 minutes max.	3 kits
APU fuel pump seal vents										
APU 1	1343.3	-107.8	413.3	N ₂ H ₄	3.5	0	1	0	Leakage stops at	Failure of pump seal ring only
APU 2	1349.9	-108.3	413.6	N ₂ H ₄	3.5	0	1	0	crew initiated	
APU 3	1343.3	107.8	413.3	N ₂ H ₄	3.5	0	-1	0	shutdown	
ECLSS										
O ₂ vents	602.0	-105.5	336.0	O ₂ (g)	4.6	0	1	0	10 minutes max. (deplete one tank)	Single failure pressure regulator
N ₂ vent	602.0	-105.5	336.0	N ₂ (g)	4.9	0	1	0	16 minutes (deplete two of four tanks)	Single failure of pressure regulators.

B-63

ORIGINAL PAGE IS
OF POOR QUALITY

TABLE B.7-III.- Concluded

Vent source	Location, in.			Effluent	Thrust, lbf	Vector			Duration	Remarks
	X _o	Y _o	Z _o			X	Y	Z		
Cabin overpressure Relief valves ^b	571.0	-67.7	394.4	Air	53.0 ^{a,e}	-1	0	0	Flow stops at crew initiated shutdown.	Opens at 15.5 psia cabin pressure.
	576.0	-74.2	394.4	Air	53.0 ^{a,e}	-1	0	0		
Power reactant storage and distribution H ₂ relief vent	822.2	105.4	342.5	H ₂ (g)	60 ^b 130 ^c	0	-1	0	Total venting time (each tank) is 17 hrs; 20 min. in cycles ≤ 10 sec	Occurs due to tank overheating; heaters failed on most likely cause.
						0	-1	0		
H ₂ multiple-tank relief vents	990.0	105.4	352.2	H ₂ (g)	1071 ^c	0	-1	0	Same as above	Same as above
O ₂ relief vent	760.0	-105.4	355.5	O ₂ (g)	17 ^b	0	1	0	Total venting time (each tank) in 16 hrs; 2.4 hrs in cycles ≤ 100 sec	Occurs due to tank overheating; heaters failed on most likely cause.
O ₂ 12 tank relief	760.0	-105.4	355.5	O ₂ (g)	600 ^d	0	1	0	Same as above	Same as above
Fuel cell H ₂ purge	640.9	105.4	339.2	H ₂ (g)	0.3	0	-1	0	Flow stops at crew initiated isolation	Failure of FCP reactant regulator
O ₂ purge	640.9	-105.4	339.2	O ₂ (g)	0.5	0	1	0	Same as above	Same as above
Hydraulic water boiler vent										
No. 1	1375.7	16.3	508.1	H ₂ O (g)	7 max.	0	0	-1	No venting if hydraulic system fails	
No. 2	1395.7	16.3	510.5	H ₂ O (g)	7 max.	0	0	-1		
No. 3	1355.7	16.4	505.8	H ₂ O (g)	7 max.	0	0	-1		

^aPlume impingement within PLB will change magnitude and direction of thrust vector.

^bTwo tanks relieving simultaneously.

^cThree tanks relieving simultaneously through the forward vent (X_o 822.2) and nine relieving simultaneously through the multiple tank relief vents, 30 day mission only.

^dTwelve tanks relieving simultaneously, 30 day mission only.

^eRegulator on line failures resulting in flow through both valves.

TABLE B.7-IV.- RCS AND OMS PRESSURE RELIEF VENTS

RCS	Location, in.			Direction cosines		
	X_o	Y_o	Z_o	i	j	k
Fwd oxidizer	285.5	40.6	361.4	-0.4520	0.8103	0.3729
Fwd fuel	285.5	-40.6	361.4	-0.4520	-0.8103	0.3729
Aft oxidizer (RHS)	1507.7	128.3	510.1	0.9986	0.0379	0.0366
Aft fuel (RHS)	1509.4	65.7	529.9	0.9986	0.0379	0.0366
Aft oxidizer (LHS)	1507.2	-128.3	510.1	0.9986	-0.0379	0.0366
Aft fuel (LHS)	1509.4	-65.7	529.9	0.9986	-0.0379	0.0366

OMS	Location, in.			Direction cosines		
	X_o	Y_o	Z_o	i	j	k
Oxidizer (RHS)	1507.7	128.0	510.1	0.9986	0.0379	0.0366
Fuel (RHS)	1509.4	65.7	529.9	0.9986	0.0379	0.0366
Oxidizer (LHS)	1507.2	-128.1	510.1	0.9986	-0.0379	0.0366
Fuel (LHS)	1509.4	-65.7	529.9	0.9986	-0.0379	0.0366

APPENDIX B.8

VEHICLE BENDING

B.8.1 GENERAL DESCRIPTION

In most simulations the Space Shuttle is treated as a rigid body. In analyzing the effects of external navigation aids on the navigated state, this is a good approximation. However, when analyses of guidance, of flight control, or of the effects of internal navigation aids, such as the IMU's or RGA's, are desired vibration and bending modes of the vehicle are relevant for realistic modeling. This appendix gives a brief overview of the theory of elastic motion as employed by the space vehicle dynamics simulation (SVDS). For more detail see references B.8-1. and B.8-2.

It is assumed that the equations of motion of a system can be derived from a Lagrangian function defined by the kinetic energy function T , the virtual work of the external forces δW , the strain energy function U , and the Rayleigh dissipation function R . These can be written as

$$T = 1/2(\dot{q}_R^T \quad \dot{q}_B^T \quad \dot{q}_S^T) \begin{bmatrix} M_{RR} & M_{RB} & M_{RS} \\ M_{BR} & M_{BB} & M_{BS} \\ M_{SR} & M_{SB} & M_{SS} \end{bmatrix} \begin{bmatrix} \dot{q}_R \\ \dot{q}_B \\ \dot{q}_S \end{bmatrix}$$

$$\delta W = \delta q_B^T Q_B + \delta q_R^T Q_R$$

$$U = (q_B^T F_B q_B + q_S^T F_S q_S)/2$$

$$R = (\dot{q}_B^T R_B \dot{q}_B + \dot{q}_S^T R_S \dot{q}_S)/2$$

where q_R , q_B , and q_S are respective sets of pseudorigid body generalized

coordinates, elastic body generalized coordinates defined by a set of base modes, and linear springs mass generalized coordinates. M_{ij} is the modal coupling mass matrix, Q_i is the generalized force acting on the body, F_i is the modal stiffness matrix, and R_i is the Rayleigh dissipation function. The subscripts refer to pseudorigid body coordinates (R), elastic body coordinates (B), and linear spring coordinates (S). In terms of the above quantities Lagrange's equations can be written as

$$\frac{d}{dt} \left(\frac{\partial T}{\partial \dot{q}_i} \right) - \frac{\partial T}{\partial q_i} + \frac{\partial U}{\partial q_i} + \frac{\partial R}{\partial \dot{q}_i} = Q_i$$

subject to the constraint

$$M_{RR} \ddot{q}_R + M_{RB} \ddot{q}_B + M_{RS} \ddot{q}_S = 0. \quad (1)$$

The following set of equations result in

$$M_{RR} \ddot{q}_R + M_{RB} \ddot{q}_B + M_{RS} \ddot{q}_S = 0$$

$$M_{BR} \ddot{q}_R + M_{BB} \ddot{q}_B + M_{BS} \ddot{q}_S + R_B \dot{q}_B + F_B q_B = Q_B - M_{BR} M_{RR}^{-1} Q_R$$

$$M_{SR} \ddot{q}_R + M_{SB} \ddot{q}_B + M_{SS} \ddot{q}_S + R_S \dot{q}_S + F_S q_S = -M_{SR} M_{RR}^{-1} Q_R$$

These equations can be rewritten as

$$Q_B = G_{BB}^{-1} \left(Q_B - M_{BR} M_{RR}^{-1} Q_R - R_B \dot{q}_B - F_B q_B + G_{BS} G_{SS}^{-1} (M_{SR} M_{RR}^{-1} Q_R + R_S \dot{q}_S + F_S q_S) \right) \quad (2)$$

$$\ddot{q}_S = -G_{SS}^{-1} (M_{SR} M_{RR}^{-1} Q_R + R_S \dot{q}_S + F_S q_S + G_{SB} \ddot{q}_B) \quad (3)$$

$$\ddot{q}_R = -M_{RR}^{-1} (M_{RB} \ddot{q}_B + M_{RS} \ddot{q}_S) \quad (4)$$

where $G_{SB} = M_{SB} - M_{SR}M_{RR}^{-1} M_{RB}$

$$G_{BS} = G_{SB}^T$$

$$G_{SS} = M_{SS} - M_{SR}M_{RR}^{-1} M_{RS}$$

$$G_{BB} = M_{BB} - M_{BR}M_{RR}^{-1} M_{RB} - G_{BS}G_{SS}^{-1} G_{SB}$$

The constraint equation yields the following two equations that, with equations (2) through (4), completely define the pseudorigid body motion,

$$q_R = -M_{RR}^{-1} (M_{RB}q_B + M_{RS}q_S) \quad (5)$$

$$\dot{q}_R = -M_{RR}^{-1} (M_{RB}\dot{q}_B + M_{RS}\dot{q}_S) \quad (6)$$

The actual displacement of the point of interest is given by

$$p = \phi q = \phi_R q_R + \phi_e q_e$$

Where ϕ is the matrix of base mode shapes and can be broken down into two submatrices, ϕ_R , of rigid body base mode shapes, and ϕ_e , elastic body base mode shapes which include both elastic body and linear spring modes. The matrix, ϕ , has the properties that at some time, τ ,

$$\phi^T A(\tau) \phi = \begin{bmatrix} M_{RR} & 0 \\ 0 & I \end{bmatrix} = M(\tau)$$

$$\phi^T K \phi = \begin{bmatrix} 0 & 0 \\ 0 & \omega_\tau^2 \end{bmatrix} = F(\tau)$$

and $\phi^T B \phi = \begin{bmatrix} 0 & 0 \\ 0 & 2\zeta_\tau \omega_\tau \end{bmatrix} = R(\tau)$

Where $A(\tau)$ is the panel point inertial matrix; K , the panel point stiffness matrix; B , the panel point damping matrix. The notation, $[\quad]$, denotes a diagonal matrix. ω_τ are the natural frequencies corresponding to elastic base modes; ζ_τ is the critical damping ratio for the elastic base modes. The velocity and acceleration of the panel point are given by

$$\dot{p} = \phi \dot{q}$$

and

$$p = \phi q$$

Reference B.8-3 gives data for various vehicle configurations and various missions for use in studying vehicle bending.

Although the navigation principal function runs at a low rate of 0.25 Hz, there are other navigation related functions that run at higher frequencies; e.g., the user parameter processor at 6.25 Hz and the attitude processor at 12.5 Hz. The spectrum of vehicle bending frequencies starts at 2 Hz and continues to infinity. The higher rate functions, which employ IMU and RGA data, will be affected in a systematic way, whereas the lower rate functions, navigation and redundancy management, will be affected in a more or less random manner. Furthermore, modeling errors will occur due to the finite cutoff of the bending spectrum when using a digital simulation of this essentially analog process.

B.8.2 REFERENCES

- B.8-1 SVDS Program Subroutine Library, Vol. I, Subroutines A-C. JSC IN 73-FM-110, July 20, 1973.
- B.8-2 Flanders, H. A.: Flexible Body Capability in the SVDS Simulation. . TRW I.C. 6531.2-66, October 31, 1972.
- B.8-3 Space Shuttle Flight Control System Data Book, Vol. I, Integrated Vehicle. Rockwell International SD73-SH-0097-1E, April 1976.

APPENDIX B.9

CLOCK AND TIMING ERRORS

B.9.1 GENERAL DESCRIPTION

The Space Shuttle master timing unit (MTU) provides time and synchronization frequency to various users. Greenwich mean time (GMT) and mission elapsed time (MET) are provided to all computers, displays, recorders, and telemetry (PCM). The GMT that is provided is universal coordinated time (UCT) (see appendix B.10 for a discussion of UTC).

Synchronization frequencies are provided to one-way Doppler systems, PCM master units, static inverters, and the time display (event timer).

Power is supplied redundantly to the MTU through two separate circuit breakers from two separate essential power busses. A switch is provided to manually select one of two redundant oscillators or to enable the MTU to automatically select the oscillator based on internal BITE (built-in test equipment) information.

B.9.2 ERROR SOURCES

The master timing unit performance is as follows:

B.9.2.1 Master Timing Unit Performance (ref. B.9-1)

- a. Frequency accuracy (offset): $\pm 7 \times 10^{-8}$
(can be adjusted to within $\pm 1 \times 10^{-9}$)
- b. Frequency stability (drift): $\pm 1 \times 10^{-9}$ per day
- c. Time accuracy: ± 10 milliseconds bias
one-eighth millisecond quantization

Mission rules permit oscillator frequency offset to be as much as $\pm 7 \times 10^{-8}$ at the start of any 7-day mission. Greater offset will require that the oscillator be adjusted before flight. Periodic adjustments at the launch site are anticipated without removal of the MTU.

d. Time accuracy - GMT will be set before launch to within ± 1 millisecond referenced to U.S. Naval Observatory time. GMT can then drift off as much as ± 10 milliseconds at any time during the mission. A frequency offset of $\pm 8 \times 10^{-7}$ will result in a time error of approximately ± 10 milliseconds in 24 hours. It is anticipated that a GMT update every 24 hours may be required to keep the MTU within the 10 millisecond limit. GMT initialization is accomplished by the ground computer launch processing system (LPS) via the umbilical and onboard computer. In flight the time delta is determined by the MCC ground computers and the GMT is then corrected via the uplink. It can also be updated by voice to the crew who can then input it by the keyboard through the computer to the MTU.

B.9.3 REFERENCES

- B.9-1 Procurement Specification for Master Timing Unit. Rockwell International
No. MC 456-0051, rev. B, May 18, 1976.

APPENDIX B.10

TIME

B.10.1 GENERAL DESCRIPTION

B.10.1.1 Ephemeris Time

Ephemeris time is the fundamental unit of time and is based on the period of orbital motion of the Earth about the Sun; thus, the time unit is in years. An ephemeris second is a subdivision of a period, or, in exact terms, it is $31\,556\,925.9747^{-1}$ of the tropical year for 1900. A tropical year is the time required for the Earth to rotate one revolution about the Sun passing through the point of vernal equinox.

B.10.1.2 Atomic Time

Atomic time is based on the time required to accumulate a fixed number of vibrational periods of transition frequency of atoms under a prescribed condition. The frequency of the atomic transition and, thus, the period of the frequency or any multiple thereof is so constant that by comparison with the ephemeris time it takes at least a century to be certain of any atomic time variation.

The Twelfth General Conference of Weights and Measures, which met in October 1964, designated "an atomic or molecular frequency standard to be employed temporarily for the physical measurement of time" and further declared "that the standard to be employed is the transition between the hyperfine levels $F = f, m_f = 0$ and $F = 3, m_f = 0$ of the fundamental state $2S_{1/2}$ of the atom of Cesium 133, not perturbed by external fields and that the value $9\,192\,631\,770$ Hertz is assigned to the frequency of this transition." F , m_f , and $2S_{1/2}$ represent numbers that identify the quantum states and energy levels associated with a

particular atomic transition and hence, with a particular spectral line (or frequency) of emission.

B.10.1.3 Universal Time or Greenwich Mean Time

Universal time (UT) is based on the Earth's period of rotation about its axis; thus, the fundamental time unit is in solar days. Since apparent solar days vary in length with the season, mean solar time was devised, and the tabulation of the difference between the apparent value and the mean value is called the equation of time. Because of its definition, UT is dependent upon the observer's position; thus, a reference based on the prime meridian at Greenwich, England was established. UT is therefore synonymous with GMT. The following are important points concerning UT (ref. B.10-1).

- a. Different versions of universal time - The value of UT at a particular instant must be determined from astronomical observations. This observed universal time (UTO) is calculated by the USNO and is based on observations of star transits across the meridian line passing through Washington, D.C., and Richmond, Florida. This version of UT is subject to a number of irregularities caused by variations in the rotation rate of the Earth. A more uniform UT (UT2) is obtained by correcting UTO for the seasonal variation variation variation in the rotation rate of the Earth and for polar drift. The correction formula is

$$UT2 = UTO + S + P$$

where

S is correction for seasonal variation

P is correction for polar drift

The precise value of UT2 cannot be known until after the astronomical data have been processed. The coordinated universal time (UTC) system provides a measure of universal time that is not subject to this delay. It is a convenient, up-to-date approximation of UT2 that is based on an atomic clock constrained to be in close agreement with UT2.

- b. Time system maintained by USNO and NBS - The National Bureau of Standards (NBS), through its radio station, WWV, transmits time signals monitored by its UTC clock. The stations of the National Aeronautics and Space Administration (NASA) spaceflight tracking and data network (STDN) use the WWV signals to time tag the observed Doppler and range data, and the clocks onboard spacecraft are calibrated prelaunch with WWV. In addition, all time-dependent calculations, both onboard and on the ground, use UTC as the basic dependent variable.

Under the old UTC system the rate of the atomic clock was changed by offsetting its output frequency, which is based on the natural resonant frequency of Cesium atoms, by an amount that made the rate of the clock nearly identical with the average rate of rotation of the Earth with all known seasonal and polar variations removed (UT2). The amount of rate difference was the offset of the UTC with respect to atomic time. On occasion, whenever the adopted frequency offset would clearly allow the UTC to diverge from UT2 by more than 0.1 second, the UTC clock of NBS would make instantaneous step adjustments. These periodic time corrections are known as step-time adjustments. The offset and step-time adjustments were made at the same time and by the same amount throughout the world by international

coordination through the Bureau International de l'Heure (BIH); thus, the term coordinated universal time.

- c. Problems with the old system - The variable offset method used in the pre-1972 UTC system prevented frequent step-time adjustments and answered astronomical and navigation needs each time an offset change was introduced; however, the length of the broadcast time interval (the UTC second) changed. Although the pre-1972 system satisfied those who required time based on the rotation of the Earth, other users needed time intervals that did not change and that were more directly related to atomic standards.

In 1968 CCIR (International Radio Consultant Committee) recognized the need to make the broadcasted second conform to the international definition of the second (the duration of 9 192 631 770 periods of radiation corresponding to the transition between the hyperfine levels of the ground state of the Cesium 133 atom). A working group was established to study the problem and its recommendations were adopted in February 1971 and implemented in January 1972.

- d. The improved UTC system - The improved UTC system eliminates the changing frequency offset and increases the size of the step-time adjustments from 0.1 to 1 second, which is called a leap second. Therefore, the UTC clocks are driven at the atomic clock rate but, by making periodic leap second adjustments, are synchronous with UT to a tolerance of ± 0.7 second. Figure B-5 shows the difference between the old UTC system prior to 1968 and the new UTC system in use at that time. Station WWV changed its clock time from the old UTC system to the improved UTC system by a time step that occurred on December 31, 1971, at 23 hours 59 minutes 60.107600

seconds (old UTC). At that instant the date became January 1, 1972, 0 hours 0 minutes 0 seconds exactly (new UTC). To users such as navigators, surveyors, and geodesists who need UT1 (UT corrected for polar variation only), the time difference between UT1 and UTC is transmitted in code to a precision of 0.1 second.

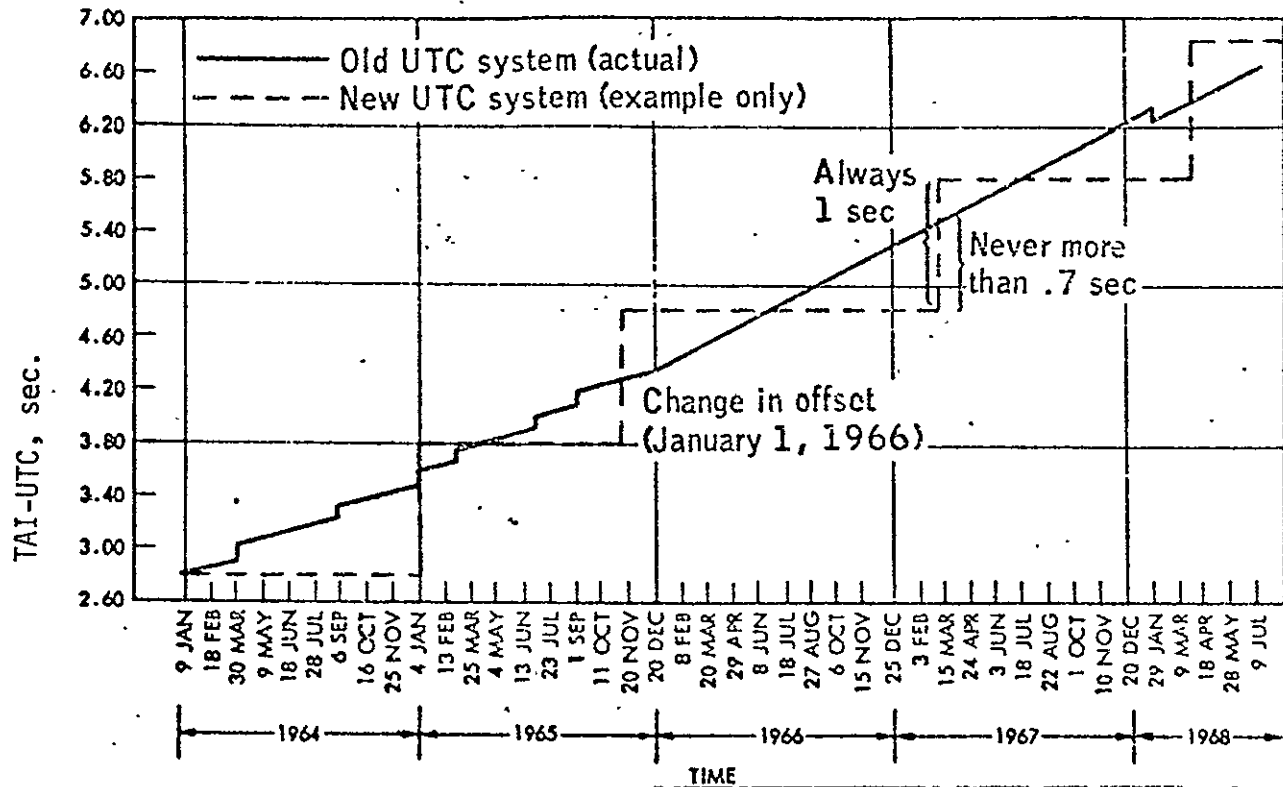


Figure B-5.- Recent behavior of TAI-UTC.

- e. Ephemeris time and its relation to UTC - The measure of ET is obtained by comparison of observed positions of the Sun, Moon, and planets with their corresponding ephemerides. The ephemerides of the Sun and Moon are needed for perturbation computations, targeting, and alignments and are maintained in ET. Since timekeeping, both onboard and on the ground, is in UTC the difference (Δt) between ET and UTC must be available. Since atomic clocks vary at the same constant rate as ephemeris time, and the relationship between atomic time and UTC is known, the Δt is easily computed. As of July 1977 the following formulae apply:

ORIGINAL PAGE IS
OF POOR QUALITY

Hence,

$$ET = TAI + 32.18 \text{ seconds} \quad (1)$$

$$TAI - UTC = 16.0 \text{ seconds} \quad (2)$$

$$\Delta t = ET - UTC = 48.18 \text{ seconds}$$

where TAI is International atomic time and UTC is National Bureau of Standards UTC. Equation (1) is constant.

B.10.2 Error Sources

The clocks associated with the ground tracking equipment are synchronized by time signals received via the LORAN-C networks. These networks are in turn synchronized to a master UTC clock of the United States Naval Observatory (USNO-MC) to an accuracy of 5 μ s. Some LORAN-C networks, such as the U.S. East Coast, North Atlantic, and Norwegian Sea chains are synchronized to the USNO-MC within 0.5 μ s, but the Central and Northwest Pacific may be off as much as 5 μ s of the USNO-MC.

The synchronization of ground station clocks to each other was calibrated during Apollo 16 by the use of interstation time synchronization tests. The results showed that the largest dispersion of any reference receiver combination was 5 μ s with an average dispersion of less than 2 μ s.

The use of portable clocks, and the complete implementation of the Defense Satellite Communication System (DSCS), known as Comm-Sat, will improve the synchronization of the LORAN-C network to the USNO-MC and the site-to-site synchronization to less than 1 μ s worldwide, but these systems are currently not fully operational and would require some changes in ground station synchronization procedures.

B.10.3 REFERENCES

B.10-1 Cockrell, B. F.: What Time Is It?. JSC IN 72-FM-59, March 7, 1972.

B.10-2 U.S. Naval Observatory Time Service Publications Series 3,4,17,11,14.

B.10-3 Metric Data Branch, GSFC: Apollo 16 STDN Metric Tracking Performance -
Final Report. GSFC document X-832-72-203, Sept. 1972.

APPENDIX B.11

ASTRODYNAMIC CONSTANTS

This section provides the basic astrodynamic constants for use in error analysis and mission simulations related to Space Shuttle development. The data included here are provided to facilitate the use of consistent numerical values throughout the Johnson Space Center (JSC).

The values of the constants presented here are taken primarily from reference B.11-1.

B.11.1 CONVERSION FACTORS

The conversion factors that are used to convert between systems of units are presented in the table B.11-I. These are the minimum number of factors required for conversion between the systems of units commonly in use at JSC.

TABLE B.11-I.- CONVERSION FACTORS

Original unit	Desired unit	Conversion factor
Earth radius	Meter	6.378160×10^6
Foot	Meter	3.048×10^{-1}
Nautical mile	Meter	1.852×10^3
Pound-mass (lbm)	Kilogram	4.5359237×10^{-1}
Hour (time)	Second (time)	3.600×10^3
Radian	Degree	$180/\pi$
Degree	Arc-second	3.600×10^3

B.11.2 CONSTANTS AND PARAMETERS

B.11.2.1 Earth Constants

B.11.2.1.1 Equatorial Earth radius (Gravitational)

$$1 \text{ e.r.} = 0.6378160000000000+007 \pm 0.5000000000000000+001 \text{ m (ref. B.11-1)}$$

$$1 \text{ e.r.} = .2092572178477690+008 \pm .1640419947506562+002 \text{ int. ft}$$

$$1 \text{ e.r.} = .1000000000000000+001 \pm .7839251445557967-006 \text{ E.r.}$$

$$1 \text{ e.r.} = .3443930885529158+004 \pm .2699784017278618-002 \text{ n. mi.}$$

B.11.2.1.2 Flattening

$$1/f = 0.2983500000000000+003 \pm 0.4000000000000000-001 \text{ (ref. B.11-1).}$$

$$f = 0.3352891869237217-002$$

B.11.2.1.3 Gravitational Parameter ($GM_e = \mu_e = \mu \text{ Earth}$):

$$\mu_e = 0.3986012000000000+015 \pm 0.4000000000000000+009 \text{ m}^3/\text{sec}^2 \text{ (ref. B.11-1)}$$

$$\mu_e = .1407646853278542+017 \pm .1412586668859544+011 \text{ (int. ft)}^3/\text{sec}^2$$

$$\mu_e = .1990936344044169+002 \pm .1997923081059631-004 \text{ (E.r.)}^3/\text{hr}^2$$

$$\mu_e = .6275027808522208+005 \pm .6297048587432459-001 \text{ (n. mi.)}^3/\text{sec}^2$$

B.11.2.1.4 Mass of the Earth

$$M_e = 0.5973343323842350+025 \text{ kg}$$

$$M_e = 0.1316896781981220+026 \text{ lbm}$$

B.11.2.1.5 Angular Velocity of the Earth's Rotation With Respect to the Vernal Equinox

By differentiating Newcomb's expression of the right ascension of the fictitious mean Sun (ref. B.11-2), one obtains

$$\dot{R}_U = 9856473354 + 2.1203 \times 10^{-8} T_U \text{ deg/d} \quad (1)$$

where T_U is Julian centuries of 36 525 days counted from 1900 January 0, 12h UT and R_U is the time rate of the right ascension.

Adding to this the time rate of the hour angle, 360 deg/d

$$\omega_p = 360.9856473354 + 2.1203 \times 10^{-8} T_U \text{ deg/d}$$

or

$$\omega_p = 7.292211585458 \times 10^{-5} + 4.283 \times 10^{-15} T_U \text{ rad/sec} \quad (2)$$

gives the rotation rate of the Earth with respect to a precessing vernal equinox. Tabular data for each year to the year 2000 is given in table B.11-II.

The motion defined in equation (2) is the result of the spin of the Earth and motion of the vernal equinox (precession). Because the latter motion takes place in the ecliptic, the equatorial component, or the general precession in the right ascension, m , must be used to compute the inertial (nonprecessing) Earth rate.

$$\omega_I = \omega_p - m .$$

From reference B.11-3

$$m = 0.00003505464 + 2.1253 \times 10^{-8} T_U + .92 \times 10^{-12} T_U^2 \text{ deg/d}$$

The angular velocity of the Earth's rotation with respect to an inertial coordinate system is therefore

$$\omega_I = 360.9856122808 - .0050 \times 10^{-8} T_U \text{ deg/d}$$

or

$$\omega_I = 7.29211514646 \times 10^{-5} - .010 \times 10^{-15} T_U \text{ rad/sec}$$

This rate is constant to 13 significant digits for the rest of this century.

Tabular values are given by year until the year 2000 in table B.11-II.

TABLE B.11-II.- THE EARTH'S ANGULAR ROTATIONAL VELOCITY WITH RESPECT TO
A PRECESSING EQUINOX (ω_p) AND INERTIAL EQUINOX (ω_I) VERSUS YEAR

Year	ω_p	ω_I
1960.	0.7292115854836980-004	0.7292115146459400-004
1961.	.7292115854841263-004	.7292115146459390-004
1962.	.7292115854845546-004	.7292115146459380-004
1963.	.7292115854849829-004	.7292115146459370-004
1964.	.7292115854854112-004	.7292115146459360-004
1965.	.7292115854858395-004	.7292115146459350-004
1966.	.7292115854862678-004	.7292115146459340-004
1967.	.7292115854866961-004	.7292115146459330-004
1968.	.7292115854871244-004	.7292115146459320-004
1969.	.7292115854875527-004	.7292115146459310-004
1970.	.7292115854879810-004	.7292115146459300-004
1971.	.7292115854884093-004	.7292115146459290-004
1972.	.7292115854888376-004	.7292115146459280-004
1973.	.7292115854892659-004	.7292115146459270-004
1974.	.7292115854896942-004	.7292115146459260-004
1975.	.7292115854901225-004	.7292115146459250-004
1976.	.7292115854905508-004	.7292115146459240-004
1977.	.7292115854909791-004	.7292115146459230-004
1978.	.7292115854914074-004	.7292115146459220-004
1979.	.7292115854918357-004	.7292115146459210-004
1980.	.7292115854922640-004	.7292115146459200-004
1981.	.7292115854926923-004	.7292115146459190-004
1982.	.7292115854931206-004	.7292115146459180-004
1983.	.7292115854935489-004	.7292115146459170-004
1984.	.7292115854939772-004	.7292115146459160-004
1985.	.7292115854944055-004	.7292115146459150-004
1986.	.7292115854948338-004	.7292115146459140-004
1987.	.7292115854952621-004	.7292115146459130-004
1988.	.7292115854956904-004	.7292115146459120-004
1989.	.7292115854961187-004	.7292115146459110-004
1990.	.7292115854965470-004	.7292115146459100-004
1991.	.7292115854969753-004	.7292115146459090-004
1992.	.7292115854974036-004	.7292115146459080-004
1993.	.7292115854978319-004	.7292115146459070-004
1994.	.7292115854982602-004	.7292115146459060-004
1995.	.7292115854986885-004	.7292115146459050-004
1996.	.7292115854991168-004	.7292115146459040-004
1997.	.7292115854995451-004	.7292115146459030-004
1998.	.7292115854999734-004	.7292115146459020-004
1999.	.7292115855004017-004	.7292115146459010-004
2000.	.7292115855008300-004	.7292115146459000-004

B.11.2.2 Fischer Earth Model

The following constants describe the Fischer Earth model (1960), which is used for the location of radar stations for the Space Shuttle.

B.11.2.2.1 Equatorial Earth radius

- a = 0.6378166000000000+007 m
- a = .2092574146981627+008 int. ft
- a = . 1000000940710173+001 E.r.
- a = .3443934125269978+04 n. mi.

B.11.2.2.2 Flattening

- f = flattening = 1 - b/a
- f = 1/298.30 = 0.3352329869259135 x 10⁻²

B.11.2.2.3 Polar Earth radius

- b = 0.635678428360717+007 m
- b = .2085559148165061+008 int. ft
- b = .9966486076873435+000 E.r.
- b = .3432388922034075+004 n. mi.

B.11.2.2.4 Eccentricity of Ellipsoid

- e = (a² - b²)/a²
- e = 0.8181333401693114-001
- e² = 2f - f²
- e = 0.6693421622965943-002

B.11.2.3 Basic Equivalents and Conversion Factors

- 1 int. ft = 0.3048000000000000+000 (exact) m (ref. B.11-1)
- 1 n. mi. = .1852000000000000+001 (exact) km (ref. B.11-1)
- 1 km = .5399568034557235+000 n. mi.
- 1 m = .3280839895013123+001 int. ft
- 1 m² = .1076391041670972+002 int. ft²
- 1 n. mi. = .6076115485564304+004 int. ft
- 1 rad = .5729577951308233+002 deg
- 1 deg = .1745329251994329-001 rad
- 1 lbm = .4535923700000000+000 kg (exact) (ref. B.11-1)
- 1 kg = .2204622621848776+001 lbm
- 1 km = .1567850289111593-003 E.r.
- 1 E.r. = .6378160000000000+004 km (exact for scaling)
- 1 U. S. Survey ft = 0.3048006096012192 m
- 1 int. stat. mi. = 5280 (exact) ft
- 1 lbf = 32.174048556 lbm int. ft/sec²
- π = 0.3141592653589793+001 (ref. B.11-1)
- 1 E.r./hr = 0.5812700495771362+004 int. ft/sec
- 1 int. ft/sec = 0.1720370765236369-003 E.r./hr
- 1 m/sec = 0.5644261040801736-003 E.r./hr
- 1 E.r./hr = 0.1771711111111111+004 m/sec

B.11.2.4 General Constants

B.11.2.4.1 Astronomical Unit

- AU = 0.1495978930000000+012 ± 0.5000000000000000+004 m (ref. B.11-1)
- AU = .4908067355643045+012 ± .1640419947506562+005 int. ft

$$\text{AU} = .2345470997905352+005 \pm .7839251445557967-003 \text{ E.r.}$$

$$\text{AU} = .8077640010799136+008 \pm .2699784017278618+001 \text{ n. mi.}$$

B.11.2.4.2 Velocity of Light in a Vacuum:

$$c = 0.2997925000000000+009 \pm 0.3000000000000000+003 \text{ m/sec (ref. B.11-1)}$$

$$c = .9835711942257218+009 \pm .9842519685039370+003 \text{ int. ft/sec}$$

$$c = .1692107128074554+006 \pm .1693278312240521+000 \text{ E.r./hr}$$

$$c = .1618750000000000+006 \pm .1619870410367171+000 \text{ n. mi./sec}$$

B.11.2.4.3 Gravitational Parameters for the Sun:

$$\mu_{\text{Sun}} = 0.1327124990000000+021 \pm 0.1500000000000000+014 \text{ m}^3/\text{sec}^2 \text{ (ref. B.11-1)}$$

$$\mu_{\text{Sun}} = .4686697671960888+022 \pm .5297200008223289+015 \text{ (int. ft)}^3/\text{sec}^2$$

$$\mu_{\text{Sun}} = .6628734122426762+007 \pm .7492211553969865+000 \text{ (E.r.)}^3/\text{hr}^2$$

$$\mu_{\text{Sun}} = .2089242635906454+011 \pm .2361393220287172+004 \text{ (n. mi.)}^3/\text{sec}^2$$

B.11.3 REFERENCES

- B.11-1. Natural Environment and Physical Standards for the Apollo Applications Program. NASA M-DE-8020.00C, SE 015-001-1B, July 10, 1969.
- B.11-2. Melbourne, William G., et al: Constants and Related Information for Astrodynamic Calculations, 1968. TR-32-1306, JPL, July 15, 1968.
- B.11-3. Krause, Hemut G. L: On a Consistent System of Astrodynamic Constants. NASA TN D-1642, July 1962.

APPENDIX C
SUBROUTINE LISTINGS AND DESCRIPTIONS

APPENDIX C.1

RANDOM NUMBER GENERATOR

The subroutines to be used for generation of random numbers in simulation programs are described in this appendix.

Two characteristics are desired. The numbers should be random in the sense that no patterns exist that affect the simulation, but they should follow a deterministic sequence in order to facilitate debugging any program modifications. These subroutines have the desired characteristics.

The subroutines described here use the congruential method, which is discussed in reference C-1.

The specific implementation described here is for the Univac 1108, but may be readily adapted for any similar machine.

The first step in the generation of the random numbers is to use subroutine RDM to generate a random number from a set uniformly distributed between zero and one. Let N be an (odd) integer, less than $2^{35}-1$; an initial value of unity is often used. The new value of N is given by the least significant 35 bits of the product of the old value and 5^{15} . The least significant 27 bits of N are then combined with an exponent and converted to a normalized floating point number, A . The output "A" is uniformly distributed over the interval zero to one.

The next step is conversion of the uniformly distributed random numbers to normally distributed random numbers. This transformation is accomplished by using two uniformly distributed numbers, A_1 and A_2 , in the following equations

~~ORIGINAL PAGE IS
OF POOR QUALITY~~

~~PRECEDING PAGE BLANK NOT FILMED~~

~~ORIGINAL PAGE
OF POOR QUALITY~~

$$X_1 = (-2 \ln A_1)^{1/2} \cos (2\pi A_2)$$
$$X_2 = (-2 \ln A_1)^{1/2} \sin (2\pi A_2)$$

These equations are implemented in subroutine RN2S. Every other call to RN2S results in two calls to RDM to generate A_1 and A_2 and the corresponding X_1 and X_2 ; then X_1 is returned. On alternate calls X_2 is returned. The particular version of RN2S, listed on page C-8, has several interesting features. By setting RNUM and X2 equal to zero the random numbers generated by RN2S are all zero; thus, a particular error model can be made perfect for checkout purposes. Secondly, use of the limit check value, SIGMA, will ensure that nominal systems, i.e., errors limited to 1σ or 3σ , will not be multiplied by large random numbers. If a number larger than SIGMA is chosen, it is thrown away and a new number is generated. In this manner the shape of the Gaussian curve is preserved; i.e., no spikes at the end points.

C.2 REFERENCE

C-1 Chambers, R. P.: Random-Number Generation. IEEE Spectrum, February 1967.

U.S. (L.P.C.) CARD
AS 1 14R1 RL/2R1 12/01/78 09:55:00 (0)

- 1.
- 2.
- 3.
- 4.
- 5.
- 6.
- 7.
- 8.
- 9.
- 10.
- 11.
- 12.
- 13.
- 14.
- 15.
- 16.
- 17.
- 18.
- 19.
- 20.
- 21.
- 22.
- 23.
- 24.
- 25.
- 26.
- 27.
- 28.
- 29.
- 30.
- 31.
- 32.
- 33.
- 34.
- 35.
- 36.
- 37.
- 38.
- 39.
- 40.
- 41.
- 42.
- 43.
- 44.
- 45.
- 46.
- 47.
- 48.
- 49.
- 50.
- 51.
- 52.
- 53.
- 54.
- 55.

```

. CD *****
. CD
. CD PROGRAMMER AND DATE
. CD T. P. KINNEY
. CD DOCUMENTATION
. CD J. R. BROWN
. CD OCTOBER, 1969
. CD
. CD PURPOSE
. CD TO GENERATE SAMPLES FROM A UNIFORM DISTRIBUTION ON THE
. CD INTERVAL FROM ZERO TO ONE.
. CD
. CD USAGE
. CD CALL RDM(I, A)
. CD
. CD DESCRIPTION OF PARAMETERS
. CD
. CD INPUT
. CD CALLING SEQUENCE
. CD I - INTEGER STARTER IS INPUT
. CD COMMON
. CD NONE
. CD CARD
. CD NONE
. CD TAPE
. CD NONE
. CD
. CD OUTPUT
. CD CALLING SEQUENCE
. CD I - RESULT IS OUTPUT
. CD A - NORMALIZED FLOATING POINT SINGLE PRECISION NUMBER,
. CD UNIFORMLY DISTRIBUTED ON INTERVAL FROM ZERO TO ONE
. CD COMMON
. CD NONE
. CD CARD
. CD NONE
. CD PRINT
. CD NONE
. CD TAPE
. CD NONE
. CD
. CD REMARKS AND RESTRICTIONS
. CD I .NE. 0 AND NOTE THAT VALUES DO REPEAT AFTER 2**32
. CD NUMBERS HAVE BEEN GENERATED AND THAT ANY GENERATED VALUE
. CD IS A FUNCTION OF THE NUMBERS USED TO INITIALIZE THE
. CD PROCEDURE
. CD
. CD SUBROUTINES REQUIRED
. CD NONE
. CD
. CD METHOD
. CD THE FIXED POINT NUMBER I IS MULTIPLIED BY 5**15 AND THE
. CD LEAST SIGNIFICANT 35 BITS ARE RETAINED AND REPLACE THE
. CD CONTENTS OF I. THE LEAST SIGNIFICANT 27 BITS ARE COM-
. CD BINED WITH AN EXPONENT AND CONVERTED TO A NORMALIZED

```

C-6

ORIGINAL PAGE IS
OF POOR QUALITY

```

56.
57.
58.
59.
60.
61.
62. 01 000000 12 00 00 13 1 000000
63. 000001 40 01 00 00 0 000011
64. 000002 30 00 01 00 0 000012
65. 000003 42 00 02 00 0 000013
66. 000004 01 00 03 13 1 000000
67. 000005 10 02 00 00 0 000011
68. 000006 76 05 00 00 0 000017
69. 000007 01 00 01 13 1 000001
70. 000010 74 04 00 13 0 000003
71. 000011 000170000001
72. 000012 343277244615
73. 000013 377777777777
74.

```

END ASH. ERRORS : NONE

```

. CD      FLOATING POINT NUMBER, A, WHICH HAS A UNIFORM DISTRIBUTION
. CD      ON THE INTERVAL FROM ZERO TO ONE.
. CD
. CD      *****
NBPR.
$(1)
RDM*  LM      AO,*0,B11 .      PICK UP ABS(I).
      OR      AO,CON,,1 .      SET BIT ZERO ON.
      HI      A1,CON1 .      GET NEW RANDOM NUMBER.
      AND     A2,MASK .      CLEAR BIT 35.
      SA      A3,*0,B11 .      STORE.
      LA      AO,CON,,2 .      PICK UP CHARACTERISTIC.
      LCF     AO,:3 .      FLOAT.
      SA      A1,*1,B11 .      STORE.
      J       3,B11 .      RETURN
CON      +0170000001
CON1     +30517578125
MASK     +037777777777.
END

```

ORIGINAL PAGE IS OF POOR QUALITY

00101 1*
 00101 2*
 00101 3*
 00101 4*
 00101 5*
 00101 6*
 00101 7*
 00101 8*
 00103 9*
 00103 10*
 00105 11*
 00105 12*
 00110 13*
 00111 14*
 00114 15*
 00116 16*
 00121 17*
 00122 18*
 00123 19*
 00124 20*
 00125 21*
 00126 22*
 00127 23*
 00130 24*
 00131 25*

```

C ***** SUBROUTINE RDM IS ENTERED TWICE IN SUCCESSION ON
C ***** ALTERNATE ENTRIES TO RN2S. RDM USES A FIXED POINT
C ***** RANDOM NUMBER TO GENERATE A NORMALIZED FLOATING POINT
C ***** RANDOM NUMBER HAVING A UNIFORM DISTRIBUTION ON THE
C ***** INTERVAL FROM ZERO TO ONE. A NEW VALUE FOR THE FIXED
C ***** POINT RANDOM NUMBER IS ALSO GENERATED AT EACH ENTRY TO
C ***** RDM
      DOUBLE PRECISION Q, SIGMA, X, X1, X2, X2B
      INTEGER ORNUM, RNUM, RNUM1
      COMMON/ RANDOM /SIGMA,X2,NSTART,X2B,NSTRTB
      1 IF (RNUM.EQ.0) GO TO 40
        RNUM1 = RNUM
        IF (X2) 20,60,20
      20 IF(NSTART.EQ.0) GO TO 40 @USE NON-ZERO X2 AS FIRST R.V.
        IF (RNUM1-ORNUM) 60,40,60
      40 X = X2
        X2 = 0.0
        GO TO 80
      60 CALL RDM(RNUM1,U1)
        CALL RDM(RNUM1,U2)
        NSTART=1
        ORNUM = RNUM1
        RNUM = RNUM1
        Q = 6.2831853071795864800 * U2
  
```

RN2S0001 000000
 RN2S0002 000000
 RN2S0003 000000
 RN2S0004 000000
 RN2S0005 000000
 RN2S0006 000000
 RN2S0007 000000
 RN2S0008 000000
 RN2S0009 000000
 RN2S0010 000000
 RN2S0011 000000
 RN2S0012 000000
 RN2S0013 000001
 RN2S0014 000003
 RN2S0015 000005
 RN2S0016 000007
 RN2S0017 000012
 RN2S0018 000013
 RN2S0019 000015
 RN2S0020 000017
 RN2S0021 000022
 RN2S0022 000026
 RN2S0023 000030
 RN2S0024 000032
 RN2S0025 000033

ORIGINAL PAGE IS
OF POOR QUALITY

C-8

RN2S *****

DATE 120178

PAGE 2

```

00132 26* X1 = DCOS(Q)
00133 27* X2 = DSIN(Q)
00134 28* Q = DSQRT(-2.00*DLOG(DBLE(U1)))
00135 29* X1 = Q * X1
00136 30* X2 = Q * X2
00137 31* X = X1
00140 32* 80 IF (DABS(X).GT.SIGMA) GO TO 1
00142 33* RETURN
00143 34* END
  
```

RN2S0026 000036
 RN2S0027 000042
 RN2S0028 000046
 RN2S0029 000062
 RN2S0030 000074
 RN2S0031 000067
 RN2S0032 000071
 RN2S0033 000074
 RN2S0034 000115

END OF COMPILATION: NO DIAGNOSTICS.